MECHANISM OF CATALYSIS AND INHIBITION OF MAMMALIAN PROTEIN FARNESYLTRANSFERASE

by

June E. Pais

A dissertation submitted in partial fulfillment
of the requirements for the degree of
Doctor of Philosophy
(Biological Chemistry)
in the University of Michigan
2007

Doctoral Committee:

Professor Carol A. Fierke, Chair
Professor Rowena G. Matthews
Professor William L. Smith
Associate Professor George A. Garcia
Assistant Professor Bruce A. Palfey

ACKNOWLEDGMENTS

I would like to express my deep appreciation and respect for my advisor, Professor Carol Fierke, for her creative and thoughtful insights, challenging ideas, and strong dedication to mentoring. Among other things, Carol has taught me unique approaches to solving problems, and her guidance has greatly assisted in both my personal and professional development.

I am very grateful to my mentor in the Fierke lab, Dr. Katherine Bowers, who patiently led me down all the paths that I have pursued in my graduate research. Thanks to the other fine researchers working on FTase in the Fierke lab before me, especially my rotation mentor Jenni Pickett, Heather Hartman and Katherine Hicks. Not only have they greatly contributed to our current understanding of the mechanism and substrate specificity of FTase, but they generously shared their expertise with me. Additionally, former lab members Marcy Hernick and Stephanie Gantt were ever willing teachers.

I would like to acknowledge my collaborators who contributed directly to this work. The inhibitor studies described in Chapter 4 are the result of a collaboration that was begun by Katherine Bowers, who performed all of the steady-state characterization. She was also instrumental in initiating the work described in Chapter 2, along with Andrea Stoddard who cloned the phosphate binding protein. Katherine also developed the methodology to prepare radiolabeled FPP and did preliminary kinetic isotope effects studies that led to the work described in Chapter 5. A rotation student in the lab, Yuta Suzuki, contributed significantly to the analog studies described in Chapter 3. These analogs were generously provided by Professor H. Peter Spielmann and Thangaiah Subramanian at the University of Kentucky. Heather Hartman aided in the development of the product dissociation assay described in Chapter 3 as well.

Thanks to my thesis committtee members, Professors George Garcia, Rowena Matthews, Bruce Palfey and Bill Smith. I would also like to thank Professor Anna Mapp,

who previously served on my committee. All have been helpful and supportive throughout the years. I am particularly indebted to Bruce Palfey, who not only taught me a great deal about kinetics but also assisted me in the data simulations and computational analysis described in Chapter 5.

I would like to thank all members of the Department of Biological Chemistry at the University of Michigan, for providing a stimulating environment in which to do science and form friendships. I especially thank Beth Goodwin for her good-natured patience and assistance throughout the years.

I also thank my previous mentors, Professor Paul Cook and Dr. Bill Karsten at the University of Oklahoma, both of who greatly influenced my decision to become a scientist. Dr. Cook provided me with the advice and confidence I needed to go to graduate school, and Bill inspired me with his unusual combination of enthusiasm and patience in the lab.

Thanks to all my friends, near and far, throughout my life. I would especially like to take this opportunity to thank those friends in Michigan who have been very dear to me during my graduate career. In particular, I thank Becky Haeusler, for sharing with me wonderful times, friends and even her family. I am also grateful for the friendships of Pam Wong and Qian Yang, as well as numerous companions in the Fierke lab and the Department of Biological Chemistry that I have no room to mention.

Finally, my love and appreciation to my family, especially my parents, Deryl and Pam Pais, for their unwavering support and devotion. Their hard work and sacrifice have enabled my achievements, and they taught me many important values that have provided the foundation for all my personal and academic accomplishments. I am also blessed to have three siblings, Mavis, Eve and Alex, and my niece Monica, who are tremendous sources of affection and encouragement. Last of all, I thank Andrew Waid, my best friend long before I became a scientist. Andrew asks me to think in new ways, gives me balance and provides endless understanding and comfort. He constantly challenges me to do the unusual, the unexpected and many times the "unpossible"...and for that I owe him my deepest love and gratitude.

TABLE OF CONTENTS

LIST OF FIGURES

LIST OF SCHEMES

LIST OF TABLES

LIST OF ABBREVIATIONS

βME, 2-mercaptoethanol

Biotin-TKCVIM, biotinylated peptide Thr-Lys-Cys-Val-Ile-Met

CaaX, tetrapeptide sequence cysteine-aliphatic amino acid-aliphatic amino acid-X

(serine, glutamine, or methionine for FTase; leucine or phenylalanine for GGTase I)

CPM, counts per minute

DMAPP, dimethylallyl diphosphate

DMSO, dimethylsulfoxide

Dns-GCVLS, dansylated pentapeptide Gly-Cys-Val-Leu-Ser

DPM, disintegrations per minute

DTT, dithiothreitol

EDTA, ethylenediaminetetraacetic acid

ER, endoplasmic reticulum

FPMP, farnesyl phosphonyl(methyl)phosphonate

FPP, farnesyl diphosphate

FSPP, (S)-farnesyl thiodiphosphate

FTase, protein farnesyltransferase

FTI, farnesyltransferase inhibitor

G protein, GTP-binding protein

GGPP, geranylgeranyl diphosphate

GGTase I, protein geranylgeranyltransferase type I

GGTase II, protein geranylgeranyltransferase type II

GPP, geranyl diphosphate

GSH, glutathione

Hepes, 4-(2-hydroxyethyl)-1-piperazineethanesulfonic acid

Heppso, *N*-[2-hydroxyethyl]-piperazine-*N'*-[hydroxypropanesulfonic acid]

I2, FPT Inhibitor II {(*E,E*)-2-[2-oxo-2-[[(3,7,11-trimethyl-2,6,10-dodecatrienyl)oxy]amino]ethyl] phosphonic acid, sodium}

IC_{50}, inhibitor concentration required to reduce enzyme activity to 50%

ICMT, isoprenylcysteine carboxyl methyltransferase

ICP-MS, inductively coupled plasma – mass spectrometry

IPP, isopentenyl diphosphate

IPTG, isopropyl-β-D-1-thiogalactopyranoside

KIE, kinetic isotope effect

LB, Luria-Bertani

MAP, mitogen-activated protein

MDCC, *N*-[2-(1-maleimidyl)ethyl]-7-(diethylamino)coumarin-3-carboxamide

MDCC-PBP, A197C mutant of PBP labeled with MDCC

MEG, 7-methylguanosine

MWCO, molecular weight cutoff

NAC, N-acetyl-cysteine GTP, guanosine triphosphate

Pi, phosphate

PBP, phosphate binding protein

PMSF, phenylmethylsulfonyl fluoride

PNPase, purine nucleoside phosphorylase

PPi, diphosphate

PPiase, inorganic pyrophosphatase

REP, Rab effector protein

SDS-PAGE, sodium dodecylsulfate polyacrylamide gel electrophoresis

SPA, Scintillation Proximity Assay^{TM}

TCEP, tris (2-carboxyethyl) phosphine hydrochloride

TLC, thin layer chromatography

Tris, tris(hydroxymethyl)-aminomethane

WT, wild-type

ABSTRACT

Mammalian protein farnesyltransferase (FTase) catalyzes the transfer of a 15-carbon prenyl group from farnesyl diphosphate (FPP) to a cysteine residue near the carboxyl terminus of many proteins, including several key molecules involved in signal transduction. Common substrates include oncogenic Ras proteins, and several FTase inhibitors are under development for the treatment of various cancers. FTase is a member of the newest class of zinc metalloenzymes that catalyze sulfur alkylation, and the work described here provides further insight into the mechanism of catalysis for this enzyme, which may lead to an increased understanding of the substrate specificity and inhibition of FTase.

The reaction catalyzed by FTase results in two products: diphosphate and farnesylated protein or peptide. To measure the rate constant for diphosphate dissociation, a coupled fluorescent assay was developed. This assay can also be used to measure FTase activity for mechanistic studies and for high throughput screening to identify FTase substrates and inhibitors. The dissociation of the farnesylated product bound to FTase is accelerated by binding FPP. This step is crucial for substrate selectivity, as measured by substrate analog studies, and inhibition studies demonstrate that some FPP-competitive inhibitors function by slowing product dissociation. Together, these studies suggest that the binding of a second substrate molecule to facilitate product release is an important determinant of the substrate specificity, and potentially of the physiological regulation of FTase.

To investigate the structure of the chemical transition state of FTase, the primary ^{14}C and α-secondary ^{3}H kinetic isotope effects (KIEs) were measured using transient kinetics. These data suggest that the FTase reaction proceeds via a concerted mechanism with dissociative character, facilitated by the zinc ion which coordinates the thiolate of the peptide substrate. The effects of the Mg^{2+} concentration and mutations of positively charged residues that interact with the diphosphate leaving group on the α-secondary KIE

suggest that Mg^{2+} and these side chains both stabilize the transition state for farnesylation and facilitate a conformational rearrangement of bound FPP that occurs prior to farnesylation. Finally, the dependence of the α-secondary KIE on peptide structure indicates that this FPP conformational change is important for substrate specificity.
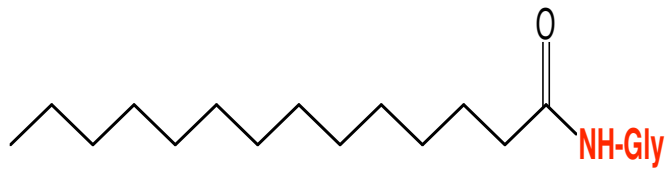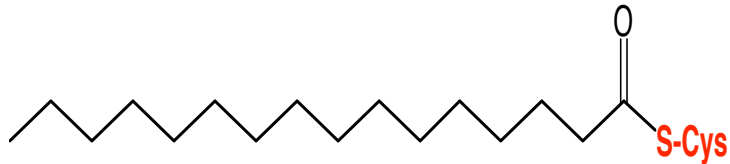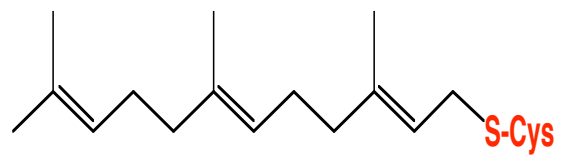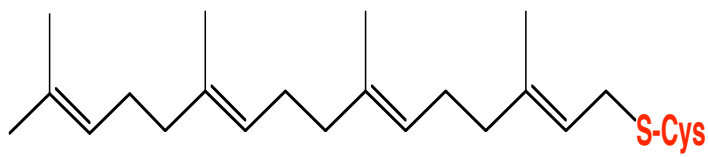
CHAPTER 1
MECHANISM, SPECIFICITY AND INHIBITION OF PROTEIN FARNESYLTRANSFERASE

Posttranslational protein lipidation

Following synthesis, many proteins undergo covalent modification of one or more amino acid residues. Posttranslational modification typically regulates the activity, stability, and/or cellular localization of proteins (*1*). Examples of common posttranslational modifications include phosphorylation, methylation, sulfation, biotinylation, ubiquitination, acetylation and lipidation. The covalent attachment of a lipid group increases the hydrophobicity of proteins, enhancing interactions with the hydrophobic tails of lipid molecules in the interior of the membrane bilayer. Lipidation enhances protein-protein interactions and localizes proteins to the plasma membrane, where they play crucial roles in the transduction of extracellular signals across the plasma membrane and into the nucleus (*2-4*) .

There are several types of protein lipidation, including myristoylation, palmitoylation and prenylation. Myristoylation occurs at the N-terminal glycine residues of proteins, while palmitoyl groups are linked to internal cysteine residues of proteins to form thioesters. In prenylation, an isoprenyl group (farnesyl or geranylgeranyl) is covalently attached to the cysteine residue near the C-terminus of a protein to form a thioether linkage (Table 1.1). Isoprenoid chains are unsaturated hydrocarbon chains consisting of repeating 5-carbon isoprene units, and are intermediates in cholesterol biosynthesis. The two isoprenoid chains used in protein prenylation are the 15-carbon farnesyl group and the 20-carbon geranylgeranyl group, which are derived from farnesyldiphosphate (FPP) and geranylgeranyldiphosphate (GGPP), respectively (Table 1.1). Farnesylation, catalyzed by protein farnesyltransferase (FTase), is the covalent transfer of a farnesyl group from FPP to the sulfur of an invariant cysteine residue located

Table 1.1 Types of posttranslational protein lipidation

Type of lipidation		Structure	Position
Myristoylation			NH$_2$-terminus
Palmitoylation			Internal; no defined sequence
Prenylation	Farnesylation		Near the COOH-terminus
	Geranylgeranylation		

four amino acids from the C-terminus, resulting in the formation of a thioether bond in the farnesylated protein (Scheme 1.1).   Geranylgeranylation is catalyzed by geranylgeranyltransferase type I (GGTase I) or geranylgeranyltransferase type II (GGTase II). Prenylation is thought to be required for the proper function of more than 300 proteins involved in cell growth, differentiation and morphology, and occurs in most, if not all, eukaryotic cells including mammalian cells, plant cells, yeast and pathogenic parasites (*5-7*).

Protein prenylation in the cell

Posttranslational protein prenylation is required for the localization and proper function of numerous proteins involved in key signaling pathways, e.g. Ras, Rho, and nuclear lamins. The processing of Ras is illustrated in Scheme 1.2, where "CaaX" represents the four terminal amino acids of the protein where prenylation occurs. Following prenylation at the cysteine residue, proteins are further processed in the endoplasmic reticulum (ER), where the three terminal amino acids are proteolytically cleaved by the membrane-bound CaaX protease Rce1 (Scheme 1.2) (*8*). The free carboxyl end of proteins is then methylated by isoprenylcysteine carboxyl methyltransferase (ICMT), which uses *S*-adenosylmethionine as its methyl donor (*2*).

After processing in the ER, proteins containing a C-terminal prenylated cysteine methyl ester are usually transported to the Golgi apparatus, where another lipid modification (termed a "second signal," often one or two palmitoyl groups) is added upstream of the C-terminal prenyl group that enhances plasma membrane association (e.g., H-Ras, N-Ras) (Scheme 1.2) (*9*). Other proteins contain an upstream "second signal" in their amino acid sequence, typically a stretch of positively charged polybasic residues that can interact directly with the acidic phospholipids on the inner leaflet of the plasma membrane (e.g., K-Ras) (Scheme 1.2) (*9*). These proteins do not require additional lipid modifications to localize to the membrane and may therefore transport directly to the cell membrane without transporting through the Golgi apparatus (*10*).

The most well-characterized prenylated proteins are guanosine triphosphate (GTP)-binding proteins (G proteins), which are involved in a variety of signaling

Farnesyldiphosphate (FPP)
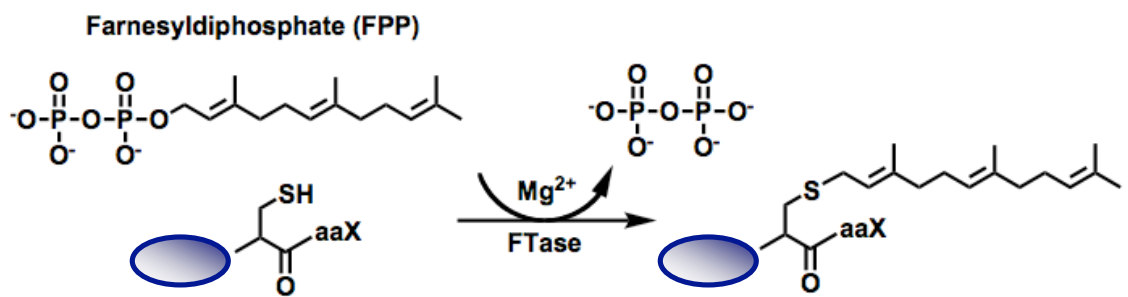
Scheme 1.1 Farnesyltransferase reaction
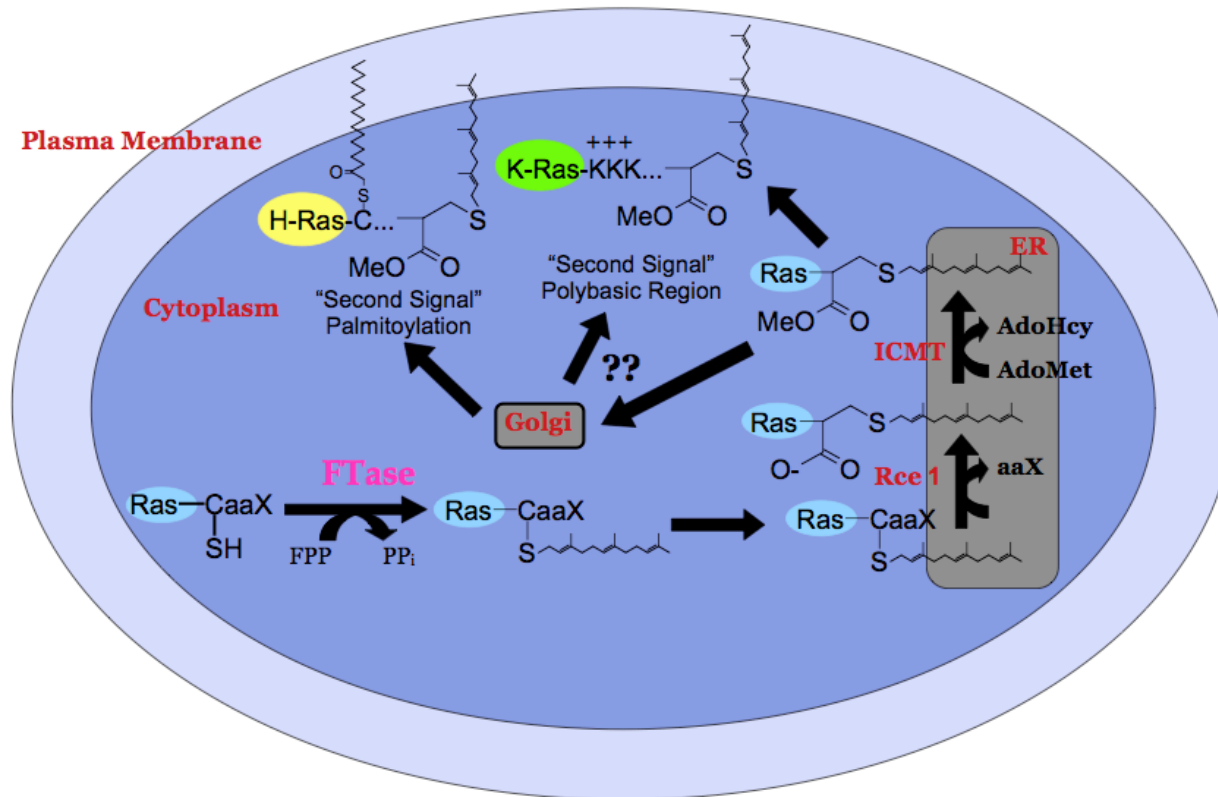
Scheme 1.2 Processing of prenylated proteins in the cell

Proteins, such as Ras, are posttranslationally farnesylated at the cysteine residue four amino acids from the C-terminus. They are further processed in the ER by Rce1 and ICMT to produce a prenylated cysteine methyl ester at the C-terminus. Proteins such as H-Ras are then palmitoylated in the Golgi apparatus, while proteins such as K-Ras contain an upstream polybasic region and may not be transported to the Golgi apparatus. These "second signals" enable association of the protein with the plasma membrane. Abbreviations: ER, endoplasmic reticulum; Rce1, CaaX protease; ICMT, isoprenylcysteine carboxyl methyltransferase; AdoHcy, adenosylhomocysteine; AdoMet, adenosylmethionine. Figure is adapted from ref. (*11*).

pathways in the cell (Scheme 1.3). These proteins require membrane association via a prenyl group to interact with downstream targets in their respective pathways. For example, the cytosolic protein Ras (H-, K-, and N-Ras) is farnesylated and localized to the plasma membrane, where it can be activated by a receptor tyrosine kinase through the adaptor proteins Grb2 and SOS, which act together as a guanine nucleotide exchange factor to exchange bound GDP for GTP (Scheme 1.3). Ras, in an activated GTP-bound form, initiates many signaling cascades, including the mitogen-activated protein (MAP) kinase, or Raf/MEK/Erk, pathway. The phosphorylation of downstream transcription factors of this pathway, such as Jun, Fos and Myc, leads to cellular growth and differentiation (Scheme 1.3). The γ subunits of heterotrimeric GTP-binding proteins also require prenylation for their normal physiological roles, which include cellular growth, differentiation, proliferation and apoptosis (*2*).

Three classes of prenyltransferases

There are three known classes of enzymes that catalyze the posttranslational prenylation of proteins in the cell: the CaaX prenyltransferases FTase and GGTase I, and GGTase II (also known as Rab GGTase). All three classes of prenyltransferases are heterodimers and contain a catalytic zinc ion that is essential for catalysis. FTase and GGTase II require Mg^{2+} for optimal activity, while the GGTase I-catalyzed reaction is Mg^{2+}-independent (*12-14*). The activity of all three prenyltransferases is highest in the brain, which was the original source of these enzymes (*2*). However, each of these enzymes have now been cloned and recombinantly expressed (*15*). FTase and GGTase I share many requirements in substrate specificity and are thought to proceed via similar kinetic and catalytic mechanisms, whereas the substrate specificity of GGTase II is quite distinct (*2*).

FTase and GGTase I are composed of identical α subunits and homologous but distinct β subunits (28% identity and 51% similarity for the rat enzymes) (*16-19*). A comparison of structures of substrate complexes captured along the reaction pathway for FTase and GGTase I reveal similar modes of catalysis (*20, 21*). Protein substrates for both FTase and GGTase typically contain a C-terminal Ca_1a_2X motif, where C is the
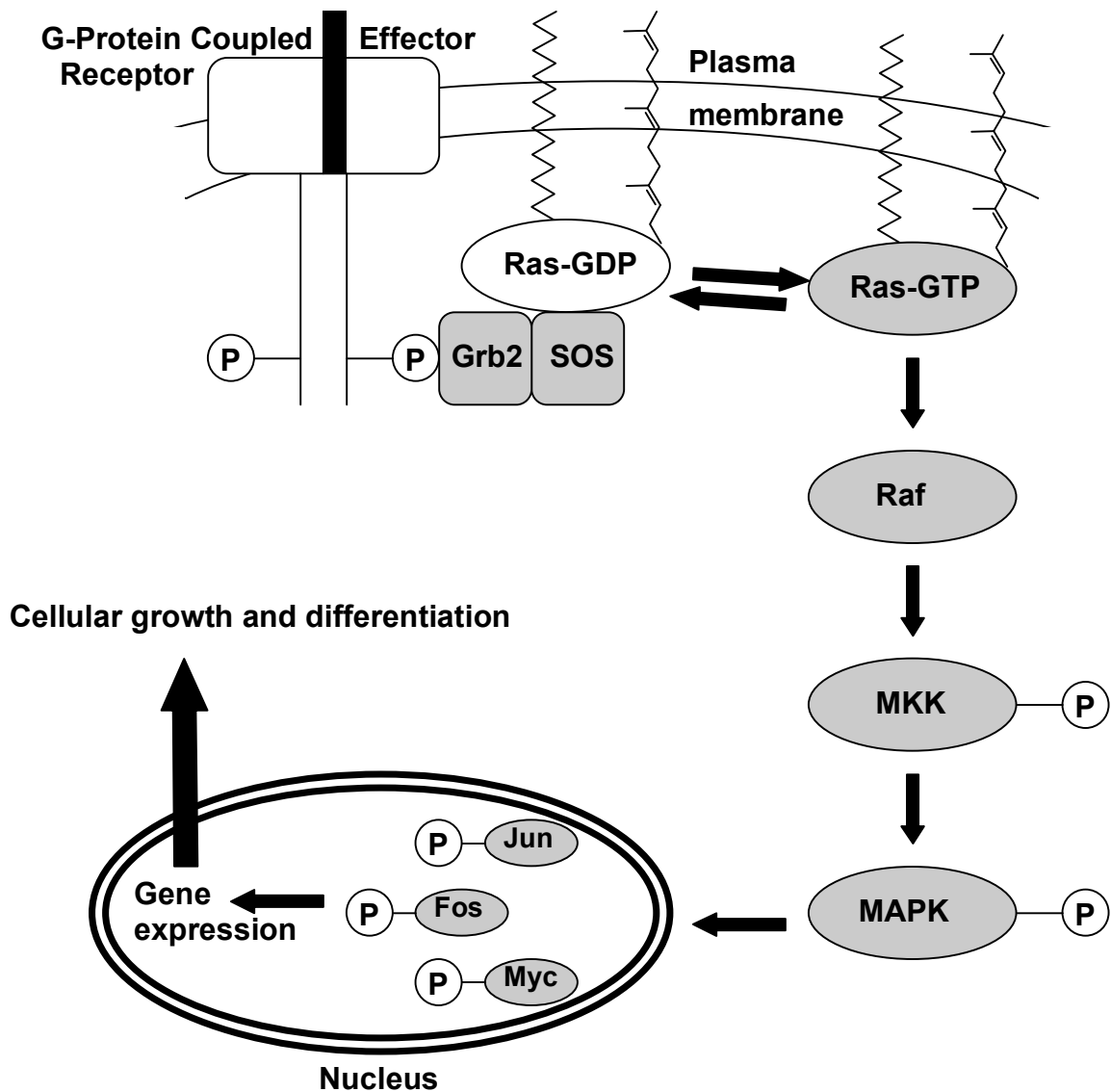
Scheme 1.3 GTP-binding proteins

Many signal transduction pathways involve GTP-binding proteins, which are activated by ligand (effector) binding to G-protein coupled receptors. The activation of Ras initiates the MAP kinase pathway, among others, leading to the upregulation of transcription factors involved in cellular growth and differentiation. Ras requires farnesylation and membrane localization for its proper biological function, as do other GTP-binding proteins which are similarly involved in a number of different signal transduction pathways regulating cellular growth, differentiation, proliferation and apoptosis.

reactive cysteine four amino acids from the C-terminus, a_1 and a_2 are proposed to contain small aliphatic residues, and X is typically serine, methionine, glutamine, threonine or alanine for FTase, and leucine or phenylalanine for GGTase I (*22*). It has been proposed that the identity of the X residue ultimately determines whether a protein is farnesylated or geranylgeranylated in the cell; however, there are many exceptions to this rule for prenyltransferase substrate specificity (*23, 24*). Similarly, exceptions to aliphatic residues at a_1 and a_2 have been observed (*25*).

While FTase and GGTase add one prenyl chain to protein substrates, GGTase II can catalyze the addition of one or two geranylgeranyl groups (*26, 27*). Known substrates of GGTase II are in the Rab protein family and are geranylgeranylated at one or both cysteine residues in the following motifs near their C-terminus: CC, CXC, CCX, or CCXX. The Rab substrate forms a complex with the Rab effector protein (REP) in order for GGTase II to catalyze geranylgeranylation (*28*). Despite these key differences in substrate recognition, the structure and proposed mechanism of GGTase II is quite similar to that of FTase and GGTase I (*29*).

GGTase I catalyzes the prenylation of most monomeric GTP-binding proteins in the Rho, Rac and Rap subfamilies, as well as most heterotrimeric G protein γ-subunits. However, most of the mechanistic and inhibition studies on prenyltransferases have focused on FTase, largely due to the farnesylation of members of the Ras superfamily of GTP-binding proteins. These proteins are not only essential for cellular growth and differentiation, but are also implicated in the progression of a variety of cancers. There has been great interest, therefore, in furthering our understanding of the mechanism, substrate specificity, and ultimately the inhibition of FTase.

Therapeutic inhibition of prenylation

Prenylation is essential for a number of important biological processes, and has been targeted in parasitic diseases, genetic disorders and, most notably, cancer. Pharmaceutical research has focused almost exclusively on the development of FTase inhibitors (FTIs), since many proteins essential in mediating the cell cycle are farnesylated. FTIs are cytotoxic to *Plasmodium falciparum* and *Trypanosoma brucei*, the

causative agents of malaria and African sleeping sickness, respectively, selectively killing these parasites over mammalian cells (*30, 31*). More recently, FTIs have shown promise in the treatment of genetic diseases such as Hutchinson-Gilford progeria syndrome, a disorder involving nuclear lamins (*32*). These drug discovery efforts are greatly aided by the considerable research over the last two decades toward the development of potent FTIs in the clinical treatment of cancer, and suggest that many other diseases may also be targeted by compounds that block prenylation of various proteins.

Oncogenic Ras proteins require farnesylation for their transforming activity and these proteins are mutated in approximately 30% of human cancers, most commonly pancreatic cancer, colon cancer and adenocarcinoma of the lung (*33, 34*). There are currently several FTIs in clinical trials for the treatment of various types of malignancies, including acute myeloid leukemia, myelodysplastic syndrome, glioma, metastatic breast cancer, and non-small cell lung cancer (*35*). These compounds also exhibit an additive or even synergistic growth suppression of cancer cells when used in combination with standard cytotoxic chemotherapeutic agents or radiation therapy (*36-39*). While most efforts have focused on FTase inhibition, GGTase I inhibitors are showing promise in pre-clinical models of tumor progression, as well as in the treatment of smooth muscle hyperplasia, multiple sclerosis, and malaria (*40-43*). It has also been recently shown that GGTase II is inhibited by some FTIs which leads to the induction of apoptosis, identifying this third prenyltransferase as another target for cancer chemotherapy (*7, 44*).

FTIs have been clearly shown to block the farnesylation of Ras, lamins and other farnesylated mammalian proteins and prevent the post-translational processing of Ras proteins (*45-47*). The physiological mechanisms responsible for the growth suppression by FTIs has been an area of intense investigation (*48*). In most cases, both *ras*-transformed rodent fibroblasts and human tumor cell lines undergo a cell cycle arrest during mitosis upon exposure to low micromolar concentrations of FTIs (*49-52*). FTIs have also been shown to induce apoptosis in transformed cell lines (*49, 53-55*). In transgenic mouse models, FTI treatment not only suppressed new tumor growth, but also inhibited the growth of existing tumors, in some cases even causing regression (*39, 56, 57*). These results point to the potential use of FTIs as chemopreventive agents, particularly after surgical removal of tumors of lung and breast cancer patients, where the

incidence of recurrence is high (*7*). Importantly, although a multitude of proteins may be farnesylated in the cell, many FTIs can shrink tumors in animals to an undetectable size without showing any toxicity to animals after weeks or even months of exposure, and have so far been well tolerated in patients at doses where clinical activity is observed (*58, 59*).

While these and other inhibitors were initially designed to block the farnesylation of Ras, it was subsequently discovered that FTI sensitivity does not correlate with oncogenic *ras* gene mutational status (*60*). It has been proposed that the farnesylation of RhoB is blocked instead, due to changes in cell morphology upon FTI treatment (*45, 61, 62*). RhoB can be either farnesylated or geranylgeranylated in the cell, and the prenylation status of RhoB may contribute to different subcellular localizations and therefore different cellular functions (*63, 64*). Additionally, when FTase activity is blocked, normally farnesylated proteins such as K-Ras can be geranylgeranylated, which is sufficient for the proper function of these proteins in many cases (*65*). This cross-prenylation may explain the low toxicity of FTIs; however, the mechanism of action has not yet been completely validated. Other targets of FTIs include RheB, a neural protein of unknown function in the brain, and the centromere proteins CENP-E and CENP-F, but direct proof that inhibition of farnesylation of these proteins is involved in the mechanism of antitumor activity of FTIs is lacking (*66, 67*).

Therefore, while FTIs clearly inhibit FTase and work well to treat cell hyperproliferation, the downstream targets of these inhibitors that inhibit cancer progression remain unclear. The full biological effects of inhibiting FTase may result from a cumulative effect of blocking the farnesylation of many proteins. Clinical studies of the therapeutic effects of FTIs have been hindered by a poor understanding of the substrate specificity of FTase. Since there are many potential prenylated proteins that may be responsible for the efficacy of FTIs, identification of the important targets is essential to further advances in specific drug treatments by FTIs.

Substrate specificity of prenyltransferases

The lack of knowledge regarding the substrate specificity of FTase presents a challenge both in the application of current FTase inhibitors as well as in the development of inhibitors that could potentially selectively block the farnesylation of specific proteins. There are approximately 30 known substrates of FTase, including proteins involved in cellular growth and differentiation, cytoskeletal function, vesicular trafficking, vision, and glycogen metabolism (Table 1.2) (*48, 68*). There are additionally many (>100) putative FTase substrates containing CaaX sequences, although the farnesylation of these substrates has not been fully characterized *in vivo* (*25, 69*).

While the "CaaX" paradigm is generally accepted, there are several key exceptions to this rule. As mentioned above, K-RasB, which has a classical FTase CaaX box (CVIM), can be geranylgeranylated by GGTase I when FTase is inhibited. Additionally RhoB, which contains a GGTase I CaaX box (CKVL), is farnesylated or geranylgeranylated by GGTase I (*70*). Recent studies using short peptides, which can substitute for full-length protein substrates in *in vitro* assays, suggest an even broader substrate specificity and cross-reactivity between FTase and GGTase I. Crystallographic and kinetic studies suggest that peptides terminating in C, F, L, N or H can also serve as FTase substrates, while peptides terminating in I or V are effective GGTase I substrates as well (*23, 24*). While a variety of amino acids are tolerated at the a_1 residue (termed "x" or "Z"), the identity of the a_2 residue appears to be more constrained than originally thought, with the majority (~85%) of the substrates tested containing V, I, L or T at the a_2 position (*25*).

Cross-specificity between FTase and GGTase I has been observed *in vivo* and *in vitro* for a variety of CaaX peptides (*71*). Alteration of the active site residues in the peptide-binding pocket of FTase to the corresponding residues in GGTase I changed the peptide specificity to more closely resemble that of GGTase I (*72, 73*). The van der Waals volume of the active site residues appear to be more important than the identity of the side chain, suggesting that the size and shape of the peptide binding pocket is more selective than the chemical properties of the active site side chains (*72, 73*). As mentioned above, some proteins contain a polybasic region upstream of the CaaX box which increases the affinity of the protein for FTase and aids in plasma membrane

Table 1.2 Known human substrates of FTase (*48, 68*)

Protein	GTPase	Protein Function	CaaX Sequence
H-Ras	Yes	Cell growth, differentiation	CVLS
K-RasA	Yes	Cell growth, differentiation	CIIM
K-RasB	Yes	Cell growth, differentiation	CVIM
N-Ras	Yes	Cell growth, differentiation	CVVM
RhoE	No	Regulation of actin cytoskeleton	CTVM
Rap2a	Yes	Unknown; localized in platelets and brain	CNIQ
RheB	Yes	Unknown; localized in brain	CSVM
Lamin A	No	Regulation of nuclear structure	CSIM
Lamin B	No	Regulation of nuclear structure	CYVM
Ptp4a1	No	Protein tyrosine phosphatase associated with cell proliferation	CCIQ
Transducin γ subunit	No	Retinal visual signal transduction	CVIS
cGMP phosphodiesterase α-subunit	No	Retinal visual signal transduction	CCIQ
Rhodopsin kinase	No	Retinal visual signal transduction	CVLS
Phosphorylase kinases	No	Muscle and liver glycogen metabolism	CAMQ, CQMQ, CLIS
PxF	No	Peroxisome assembly	CLIM
HDJ2	No	Protein import into mitochondria; cochaperone of Hsc70	CQTS
Interferon-induced guanylate binding protein-1	Yes	Binds GMP, GDP and GTP in macrophages	CTIS
CENP-F	No	Centromere (kinetochore) protein for G_2/M transition	CKVQ

localization (*74-76*). Bioinformatics data suggest that this region exhibits a tendency toward small, flexible hydrophilic amino acids (*69*). Polybasic residues in peptides can contribute to the substrate specificity of FTase and GGTase I, and are thought to be responsible for the altered substrate specificity for proteins such as K-RasB and RhoB (*77*).

Structure of FTase

FTase is a 93 kDa α/β heterodimer; the β subunit contains the binding site for the catalytically essential zinc ion and most of the active site residues (Figure 1.1) (*2, 78-80*). FTase contains double the number of normal hydrogen bonds and buried surface in the dimer interface, making the dimer extremely stable to dissociation in the absence of denaturant (*81*). The 48 kDa α subunit is a crescent-shaped seven-helical hairpin domain that envelops part of the β subunit (*80*). The 46 kDa β subunit is also predominantly α-helical, folded into an α-α barrel with six helices forming the inner barrel and six additional helices forming the outside of the barrel (*80*). One end of the barrel is closed by a loop, and the opposite end is solvent accessible. The catalytic zinc ion is bound at the top of the barrel of the β subunit, marking the active site. FPP binds in an extended conformation in a deep funnel-shaped hydrophobic cleft at the center of the α-α barrel lined with highly conserved aromatic residues. Bound FPP forms a substantial part of the binding surface for the peptide substrate, which also binds in an extended conformation and forms van der Waals interactions with the second and third isoprene units of FPP. The direct contact between FPP and peptide substrates can explain the observed synergy in binding affinity and apparent binding order for these substrates (*82, 83*).

X-ray crystal structures for the rat and human isoforms of FTase have been solved in a number of complexes, including the free enzyme (with and without zinc bound), binary substrate complexes, ternary complexes, and product complexes (*21, 80, 84-87*). The structure of the unliganded protein confirmed the identity of the active site zinc ligands as well as the overall protein structure (*80*). Binary complexes of FTase bound with FPP, as well as ternary complexes with an FPP analog and a peptide substrate, reveal that both substrates lie side by side in extended conformations (*86, 87*). The
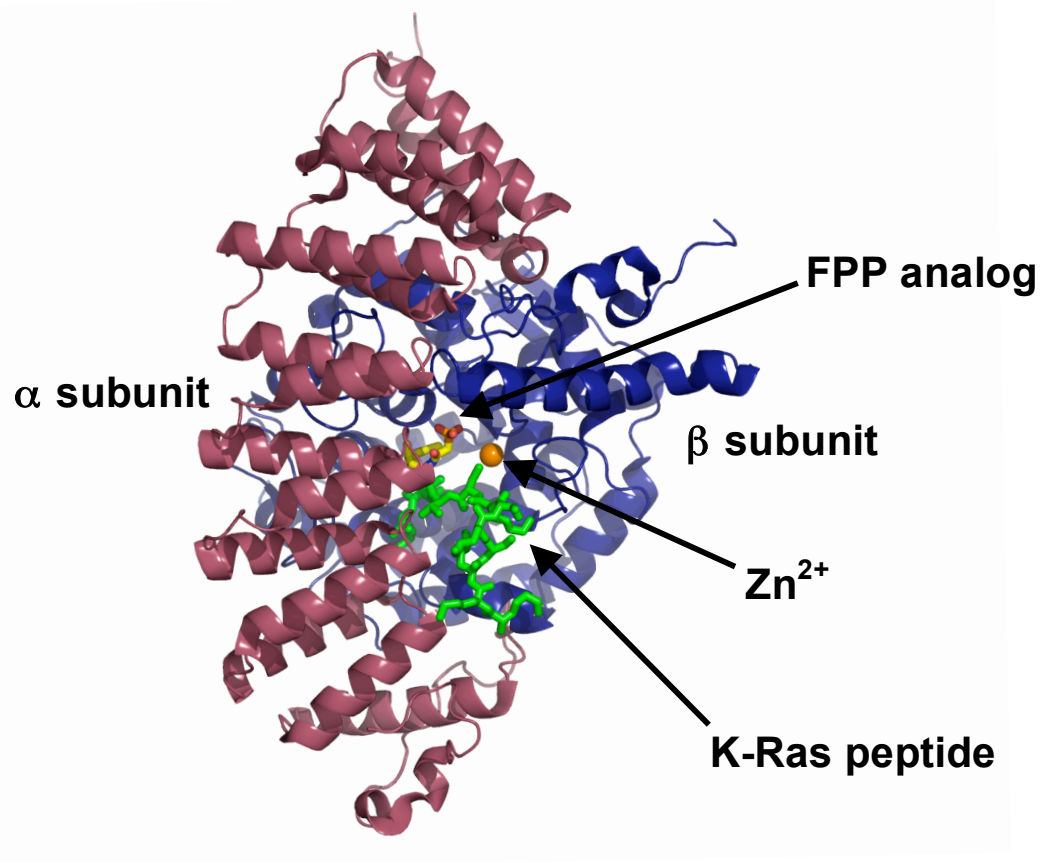
Figure 1.1 Crystal structure of FTase

X-ray crystal structure of FTase in a ternary complex, bound with the FPP analog FPT inhibitor II and the peptide KKKKKKSKTKCVIM, reflecting the C-terminus of K-Ras. Protein Data Bank code: 1D8D (*84*).

ternary complex structures, however, place the two reactive atoms, the sulfur of the peptide cysteine and the C1 of FPP, greater than 7 Å apart (Figure 1.2) (*84, 85, 87*). This is too far apart to be a reactive complex. In the structure of the farnesylated product bound to FTase, the prenylated peptide remains bound in an extended conformation with the sulfur near the zinc ion, but the first two groups of the farnesyl chain rotate such that the C1 of the farnesyl group forms a covalent bond with the sulfur of the peptide substrate (*21*). Therefore, in order for catalysis to occur, there must be a conformational rearrangement of FPP, since little change in the structures of either the peptide substrate or the active site of FTase itself is observed between the ternary and the product complexes (*21*). On the basis of structural and mutagenesis studies, a model has been proposed in which the first two isoprene units of FPP rotate to bring the C1 of FPP within reacting distance (2.4 Å) of the peptide thiolate (Figure 1.3) (*88*). However, a ternary complex in a reactive conformation has not yet been observed crystallographically.

A second major conformational rearrangement occurs upon binding of a second molecule of FPP to the FTase•product complex, a process which greatly accelerates the rate of dissociation of product from the enzyme (*21, 89*). In this structure, the CaaX peptide moves from its initial extended conformation to adopt a type I β-turn, and the prenyl chain swings out of the active site into the "exit groove," a shallow solvent-accessible groove that extends from the active site to the rim of the β subunit (Figure 1.4) (*21*). The incoming FPP molecule takes the place of the prenyl chain of the product, binding in the catalytic binding pocket (Figure 1.4) (*21*). This complex is quite stable under crystallographic conditions and may require additional peptide to release the farnesylated product from the enzyme. This mechanism of product dissociation suggests the possibility that additional cellular factors may be required for delivery and release of the farnesylated protein product *in vivo* (*21*).

Crystal structures of FTase bound with various different substrates provides structural information about substrate specificity. In the crystal structure of FTase with bound GGPP, the C1 of GGPP is in the same position as the C1 of FPP, due to a kink in the prenyl chain that allows the longer molecule to fit in the active site of FTase (*91*). It is this kink that slows turnover substantially for FTase with GGPP, potentially because either the rotation of the first two prenyl chains to form the active substrate conformation
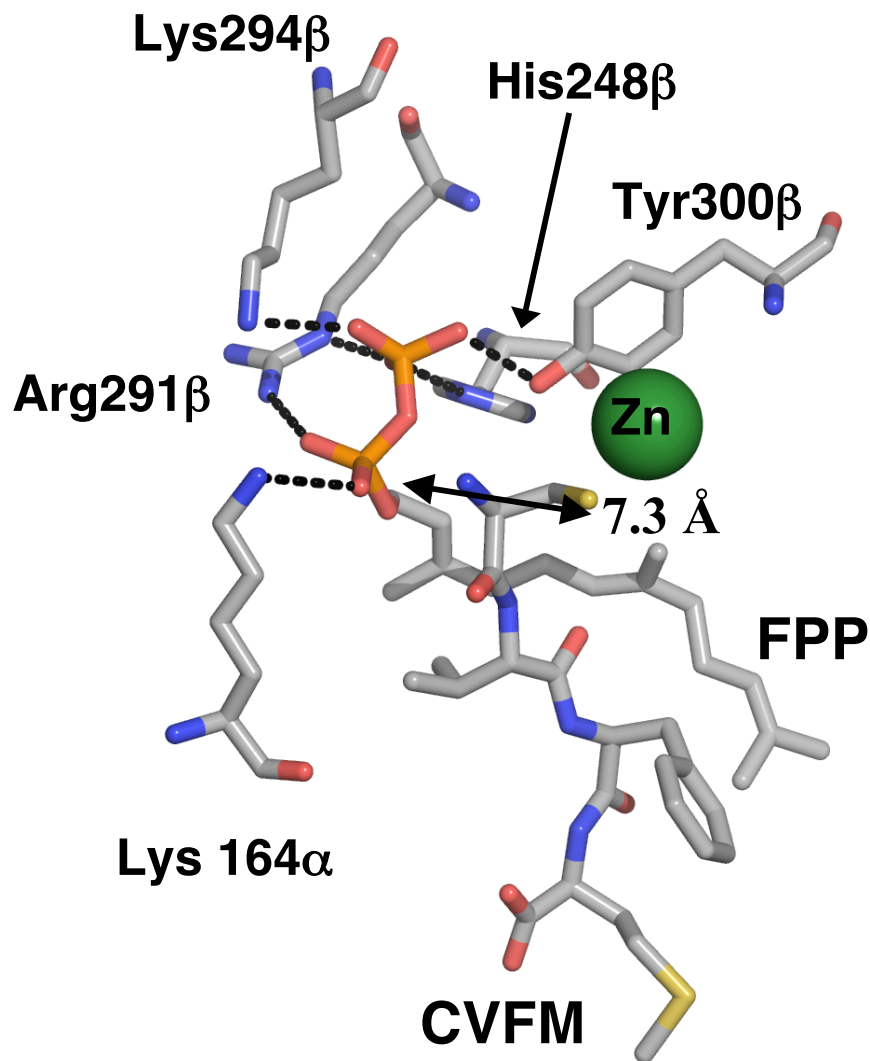
Figure 1.2 Ternary complex of FTase

X-ray crystal structure of the inactive ternary complex with a slow peptide substrate, FTase•FPP•CVFM. The conserved residues K164α, H248β, R291β, K294β and Y300β are shown interacting with the diphosphate moiety of FPP, and the zinc ion is coordinated to the peptide thiolate. Protein Data Bank code: 1JCR (*85*).
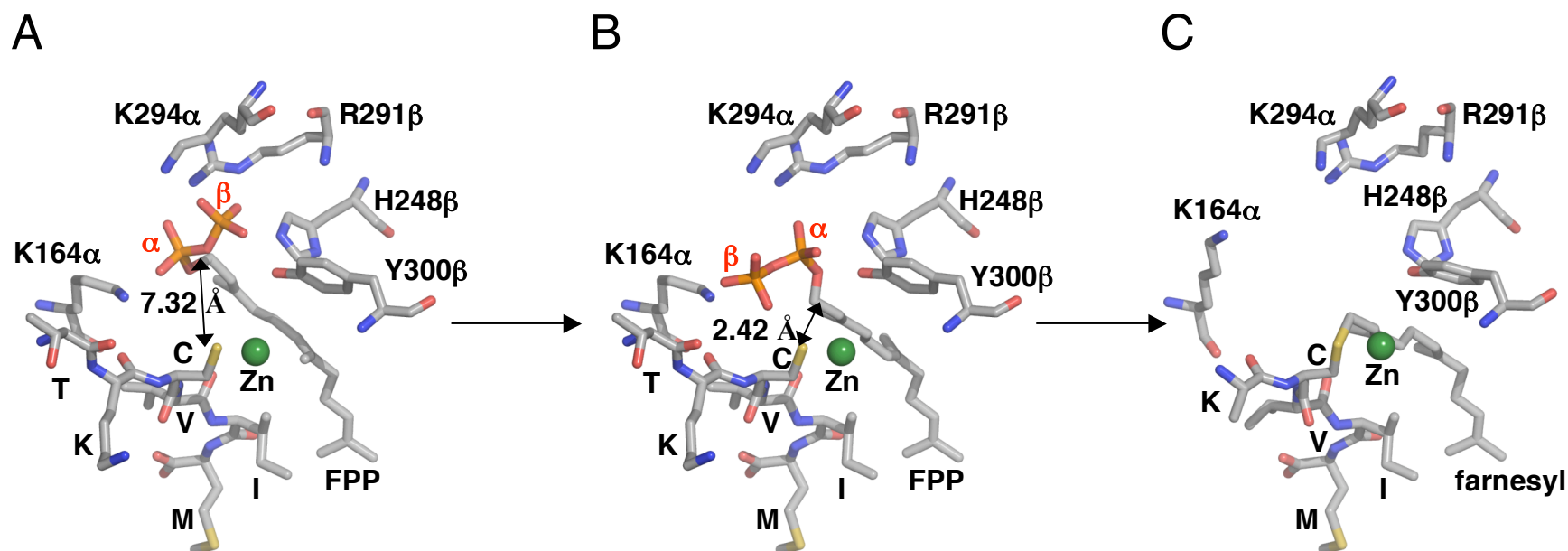
Figure 1.3 Model of active substrate conformation

Computational model of the proposed active substrate conformation for FTase (*88*). (A) Model of the inactive ternary complex, FTase•FPP•TKCVIM, where the C1 of FPP and the peptide thiolate are 7.32 Å apart (made from PDB ID 1JCQ (*85*) and PDB ID 1D8D (*84*)). (B) Proposed active substrate conformation, where the C1 of FPP is within reactive distance (2.42 Å) from the peptide thiolate (*88*). (C) Crystal structure of the FTase•product complex (Protein Data Bank code: 1KZP (*21*)). The coordinates of the threonine residue and the entire side chain of the lysine of farnesyl-TKCVIM were absent from the PDB and are therefore not shown.
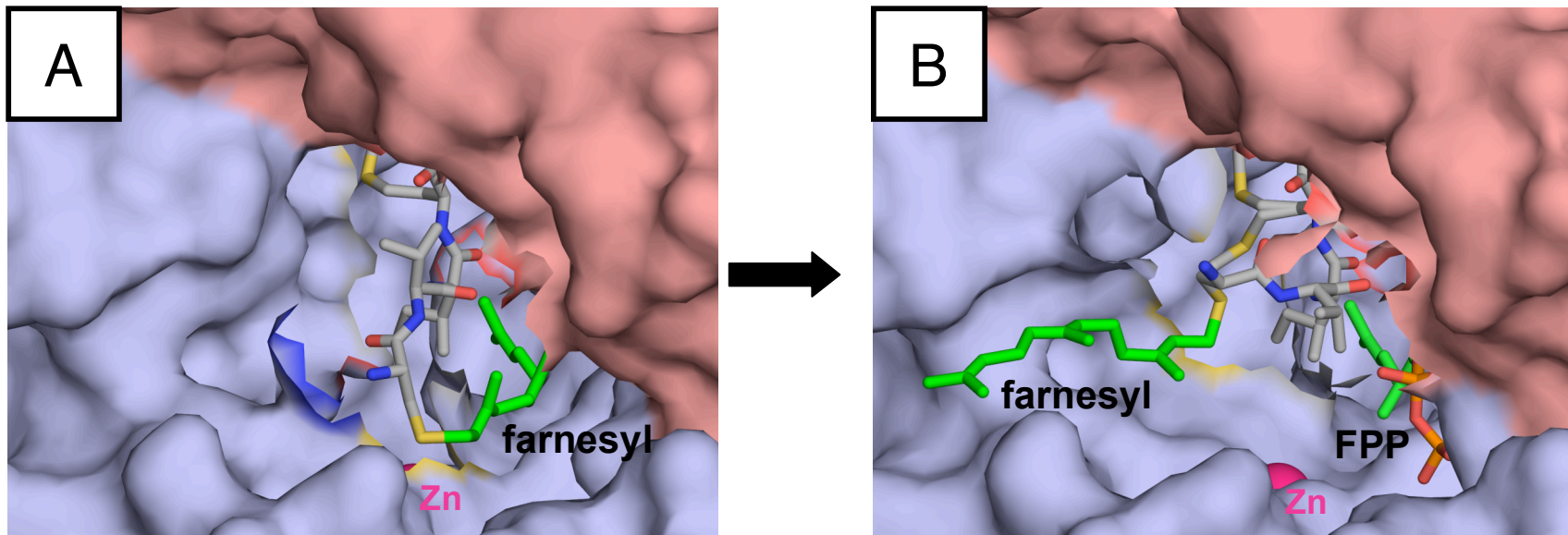
Figure 1.4 FPP-catalyzed product dissociation

X-ray crystal structure of the FTase active site for (A) the FTase•product complex, formed with FPP and KKKSKTKCVIM (Protein Data Bank code: 1KZP (*21*)); and (B) the FTase•product•FPP complex, where additional FPP has been added to the product complex formed in (A) (Protein Data Bank code: 1KZO (*21*)). For clarity, the FTase residue K164α is omitted, and only the four terminal amino acids of the peptide substrate are shown.

and/or the rotation to move the prenyl group into the exit groove is sterically hindered (*91*). The crystal structure of GGTase I with bound GGPP, on the other hand, reveals that the first three isoprene units are arranged along a straight line, while the fourth isoprene unit is turned $\sim 90^0$ relative to this axis (*20*). Interacting with this fourth isoprene unit is the amino acid residue T49β in GGTase I, which is replaced by a tryptophan residue in FTase and was shown by mutagenesis to account for the discrimination in isoprenoid length between the two enzymes (*20*).

A comparison of the ternary complex structures of FTase with bound peptides containing different CaaX sequences provides insight into the peptide specificities of FTase and GGTase I (*85*). A substrate binding mode, where the C and a_1 residues of the Ca_1a_2X box are positioned on the opposite side of the zinc ion, is sterically favored when the a_2 residue is isoleucine or valine, as was observed for TKCVIM. A non-substrate binding mode, in which the C and a_1 residues are rotated to a position between the zinc ion and FPP, is sterically favored when a hydrogen bond is formed between the N-terminus of the tetrapeptide and the α phosphate of FPP and the a_2 residue is phenylalanine, as was observed for CVFM (*85*). In this conformation, the rotation of FPP to form the active substrate conformation is proposed to be obstructed. Crystallographic data with a series of peptides varying in the X residue have led to the proposal that while GGTase I has one binding site for the X residue, FTase has two separate binding sites for the X residue: one which binds M, Q, S, A, T, and C and the other which binds F and possibly L, N, and H (*23*).

Kinetic mechanism of FTase

The kinetic mechanism of FTase is functionally ordered, meaning that either FPP or peptide can bind to the free enzyme, but the reaction only proceeds efficiently if FPP binds first (Scheme 1.4) (*83, 92*). The binding of substrates is synergistic, because the molecules are in direct contact in the active site of FTase; FPP binds FTase with a tight affinity (K_D = 6 nM), and the affinity of the peptide GCVLS is over 70-fold tighter for FTase in the presence of an FPP analog than for FTase alone (*82*). Both substrates bind to the enzyme with second order rate constants of 10^6 $M^{-1}s^{-1}$ at high pH (7.5-7.8) (Scheme

E + FPP $\underset{0.013 \text{ s}^{-1}}{\overset{2 \times 10^6 \text{ M}^{-1}\text{s}^{-1}}{\rightleftharpoons}}$ E•FPP + HSpep $\underset{0.06 \text{ s}^{-1}}{\overset{1 \times 10^6 \text{ M}^{-1}\text{s}^{-1}}{\rightleftharpoons}}$ E•FPP•Spep $\underset{k_{-1}}{\overset{k_1}{\rightleftharpoons}}$ [E•FPP•Spep]*

F-Spep

$1 \times 10^4 \text{ M}^{-1}\text{s}^{-1}$

0.01 s^{-1}

FPP

k_2

E•F-Spep•FPP $\rightleftharpoons$ E•F-Spep

PPi
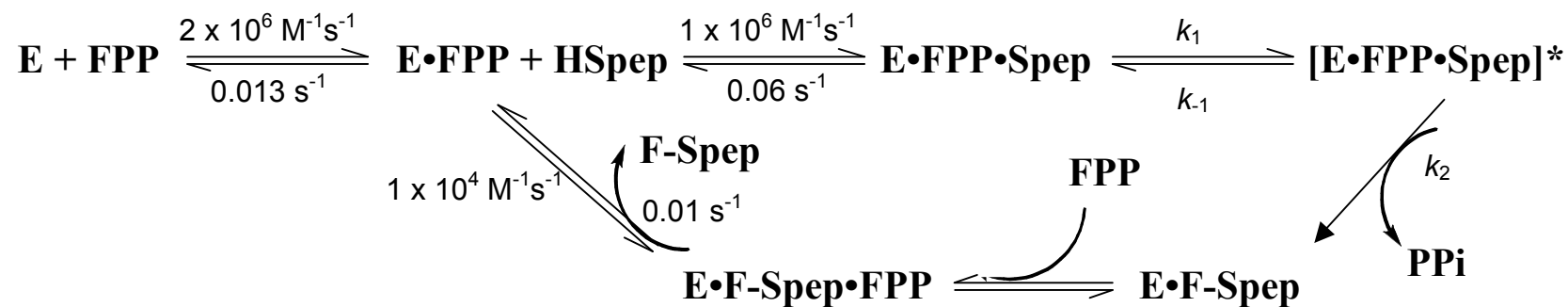
Scheme 1.4 Kinetic mechanism of mammalian FTase for farnesylation of the GCVLS peptide substrate at 25 ^{0}C (*83, 89, 92, 93*).

1.4).   The active site zinc ion directly coordinates the cysteine thiolate upon peptide binding, followed by a rotational movement of the FPP molecule to form the active substrate conformation, denoted as [E•FPP•Spep]* (*88, 94*).   The chemical or farnesylation step is the transfer of the farnesyl group to the cysteine sulfur of the peptide, and results in two products, diphosphate and the farnesylated peptide containing a thioether bond.

The binding affinity of the product for the enzyme is weaker than either of the substrates for FTase ($K_D \sim 1$ μM) (*89*).   However, the farnesylated product dissociates from the enzyme extremely slowly unless additional substrate is available to bind to the product complex (*89, 92*).   It is therefore thought that FTase does not exist as a free species during the course of the reaction pathway (Scheme 1.4).   Excess peptide or isoprenoid triggers product release, but FPP is more efficient with a maximum k_{off} value of 0.13 min^{-1} compared to 0.08 min^{-1} for the peptide CVIM at 10 ^{0}C (*89*).   FPP-stimulated product dissociation is observed for a farnesylated full-length Ras protein as well, and there is evidence suggesting that this phenomenon may be physiologically relevant (*89*).   Studies of FTase reactivity with a peptide library have identified ~60 peptides for which single turnover, but not multiple turnover, is observed.   For these peptides, no FPP-stimulated product dissociation is observed (*25*).   Three of these peptides correspond to full-length proteins that are known to be farnesylated *in vivo*, and may represent a class of proteins for which additional cellular factor(s) are required for product dissociation.   Some potential factors include intracellular membrane compartments, Mg^{2+} concentrations, other proteins, or contacts with upstream regions of the proteins.

The dissociation of farnesylated product is the slowest step in the overall reaction at 0.01 s^{-1}, so the steady-state rate constant (k_{cat}) reflects this step of catalysis (*92*). Therefore, transient kinetics are used to isolate the farnesylation step from the product release step, under conditions of limiting FPP with respect to FTase and a vast excess of peptide.   The observed first order rate constant of 5 s^{-1} is ~100-fold faster than the rate constant of peptide dissociation from the ternary complex, indicating that the reaction is essentially irreversible once the ternary complex is formed.   However, no kinetic information about the conformational rearrangement of FPP prior to farnesylation was

available prior to this work, and the observed rate constant measured under single turnover conditions includes both this conformational rearrangement and the farnesylation step (Scheme 1.4) (*95, 96*). The measurement of kinetic isotope effects, as described in Chapter 5, allows differentiation of the rate constants for these two steps for the first time.

Catalytic mechanism of FTase

FTase catalyzes a nucleophilic substitution reaction, which can proceed via an associative (also known as a nucleophilic, or S_N2-like) mechanism or a dissociative (also known as an electrophilic, or S_N1-like) mechanism (Scheme 1.5). In an associative mechanism, the thiolate nucleophile of the cysteine residue attacks the C1 of FPP at the same time as the cleavage of the diphosphate group occurs (Scheme 1.5A). The C1 atom in the transition state for an associative mechanism, therefore, is partially bonded to both the incoming nucleophile and the departing diphosphate group. In a dissociative mechanism, the diphosphate group leaves first, creating a carbocation at the C1 in the transition state which is then activated to react with the thiolate nucleophile (Scheme 1.5B).

A concerted, associative mechanism has been supported by direct zinc ion coordination which lowers the pK_a of the thiolate nucleophile, as well as inversion of configuration at C1 during the reaction for both human and yeast FTase (*82, 97, 98*). However, inversion of stereochemistry does not rule out a dissociative mechanism, due to potential steric constraints for an enzyme active site as well as possible rotational restriction around an allylic cation (*97*). Indeed, substitution of electron-withdrawing fluorine atoms at the C4 methyl position of FPP leads to a decrease in the rate constant for farnesylation proportional to the number of fluorines added, consistent with the formation of substantial positive charge in the transition state of FTase (*95, 99*). This effect is not as dramatic as was observed for FPP synthase which proceeds via a carbocation intermediate, and no carbocation intermediate in the FTase reaction has been successfully trapped by addition of other nucleophiles (*95, 100*). On the basis of these studies, an "exploded" transition state has been proposed, in which the bond between the
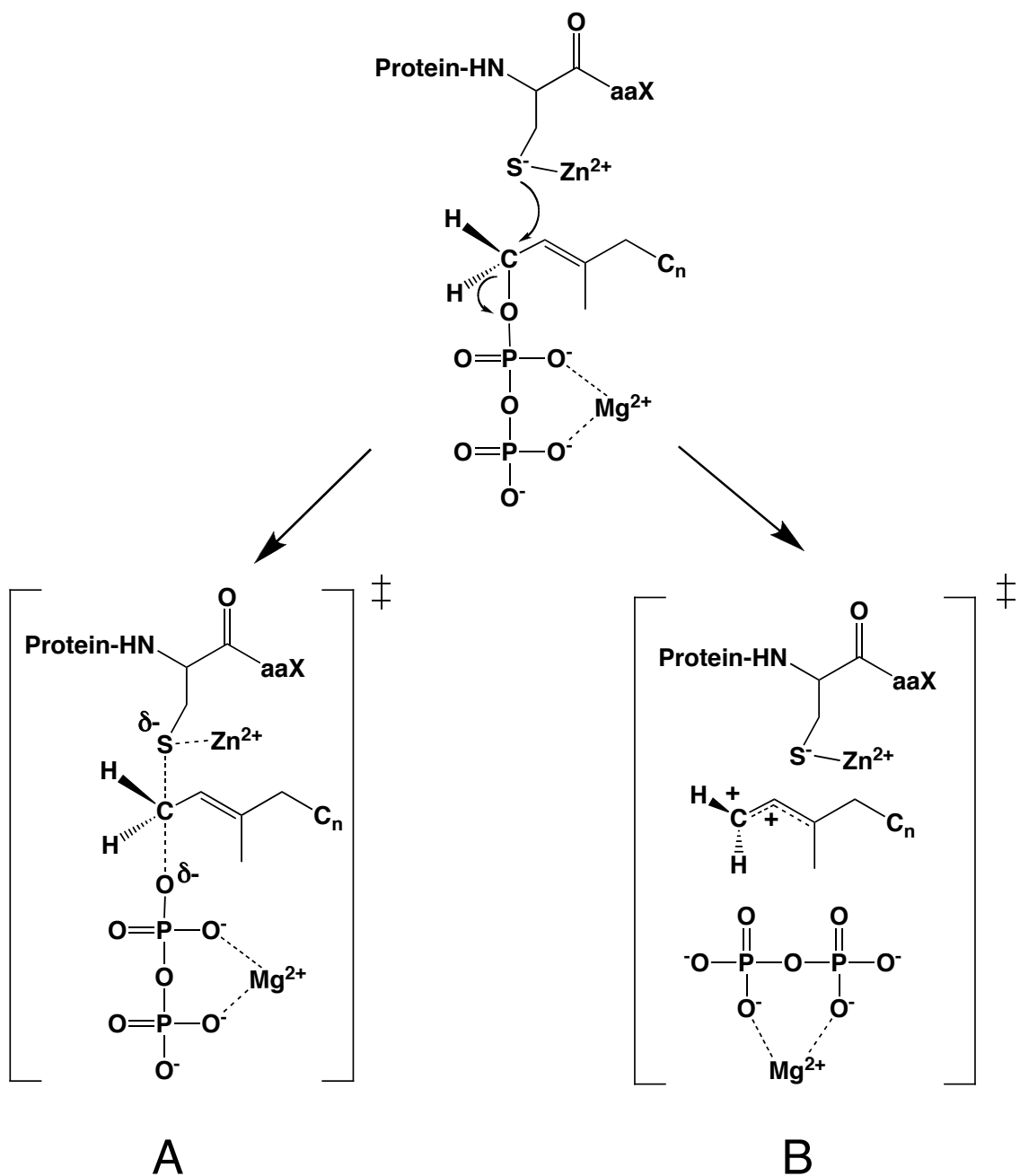
Scheme 1.5 Possible reaction mechansims for FTase

Two possible types of nucleophilic substitution mechanisms for FTase: (A) Associative (nucleophilic, or S_N2) mechanism, in which the thiolate nucleophile attacks C1 as the bond with the diphosphate leaving group is being cleaved in the transition state; and (B) Dissociative (electrophilic, or S_N1) mechanism, in which a carbocation is formed at the C1 of FPP in the transition state prior to nucleophilic attack.

C1 of FPP and the PPi group is nearly broken, and the bond with the incoming thiolate sulfur is barely formed (*95*). According to this model, the proposed transition state would comprise electrostatic and bonding character of both associative and dissociative transition states (Scheme 1.5). Importantly, the buildup of partial positive charge on C1 and partial negative charge on both the incoming thiolate nucleophile and departing diphosphate leaving group in the transition state is an important catalytic feature of this proposed mechanism.

Interestingly, the proposed mechanism for FTase represents an intermediate between two classes of enzymes closely related to FTase. The three prenyltransferases are members of the newest class of enzymes that catalyze zinc-mediated sulfur alkylation (*101*). Other members of this family of enzymes, including the DNA repair protein Ada, cobalamin-dependent (MetH) and cobalamin-independent (MetE) methionine synthase, betaine-homocysteine methyltransferase (BHMT), methylcobamide:coenzyme M methyltransferase (MT2-A and MT2-M), and epoxyalkane:CoM transferase, are proposed to proceed via associative mechanisms (*101*). The prenyltransferases are the only enzymes in this class for which dissociative character has been proposed, perhaps reflecting stabilization of the carbocation at C1 by resonance (*102*). Other enzymes involved in prenyl transfer, such as FPP synthase, proceed via purely dissociative, electrophilic mechanisms (*100*). However, these enzymes catalyze reactions with weaker nucleophiles. The catalytic roles of the zinc and magnesium ions, as well as the diphosphate leaving group, in the FTase mechanism shed further light on the similarities and differences between FTase and these two classes of enzymes.

Role of zinc in catalysis

A catalytic role for Zn^{2+} in the mechanism of FTase is supported by a great number of kinetic and structural studies. The protein structure of FTase crystallized in the absence of an active site zinc ion remains the same, indicating that Zn^{2+} does not play an essential structural role (*84, 95*). However, the peptide affinity of apo-FTase is significantly reduced, indicating that Zn^{2+} is important for binding the cysteine residue in the right position (*84, 95*). Direct interaction of the CaaX cysteine sulfur with the metal

ion was first observed from optical absorbance spectra of Co^{2+}-substituted FTase. An increase in absorbance at 340 nm, indicative of a Co^{2+}-sulfur charge transfer band, occurs upon addition of a CaaX peptide substrate to an FTase•isoprenoid complex (*82*). pH studies have subsequently shown that Zn^{2+} lowers the pK_a of the cysteine sulfur from 8.1 to 6.4, creating a reactive thiolate nucleophile at physiological pH (*82*).

A catalytic role for Zn^{2+} has been confirmed by X-ray crystallographic studies, in which Zn^{2+} is coordinated by D297β, C299β and H362β, with a water molecule or the second oxygen atom of D297β to potentially serve as a fourth and/or fifth ligand (*80*). This fourth ligand is replaced by the sulfur of the peptide substrate in the ternary and product complexes (*21, 87*). X-ray absorption spectroscopy has also been used to determine the structure of the zinc site in FTase, and while these data are consistent with the identity of the zinc ligands, they suggest a bidentate ligation with the D297β residue, which is also modeled to be a more stable interaction than a monodentate ligation with a water molecule (*103, 104*). Additionally, extended X-ray absorption fine structure data show zinc coordination to the peptide sulfur before, but not after, product formation (*103*). This is in contrast to the spectroscopic studies of Co^{2+}-substituted FTase, as well as crystallographic studies, which indicate that the zinc ion is coordinated with the sulfur cysteine in the product complex (*21, 94*).

As mentioned above, FTase belongs to a family of enzymes that catalyze zinc-dependent sulfur alkylation. While these enzymes all use a catalytic Zn^{2+} ion to coordinate directly to the substrate thiolate at the site of alkylation, the zinc ligand environments are quite different. In addition to the substrate cysteine ligand, the zinc is coordinated to two cysteine residues in MetE and MT2-A, and three cysteines in Ada, BHMT and MetH (*101*). The prenyltransferases are the only members of this class which only have one cysteine ligand (in addition to the substrate cysteine) (*103*). This likely results in the formation of a weaker zinc-thiolate nucleophile for the FTase-catalyzed reaction than other members of this class of enzymes. Given that the mechanism of FTase is proposed to proceed with some dissociative character, the enzyme may sacrifice the formation of a strong nucleophile in order to maintain zinc-sulfur coordination in the transition state to properly position the thiolate relative to the C1 of FPP.

Role of magnesium in catalysis

The free intracellular concentration of Mg^{2+} is approximately 1-2 mM (*105*). While Mg^{2+} is not strictly required for catalysis, millimolar concentrations greatly accelerate the rate of catalysis, enhancing a step at or before the chemical transition state with little effect on substrate binding (*95*). Like other diphosphate-utilizing enzymes, FTase has been proposed to use Mg^{2+} to stabilize the developing negative charge on the diphosphate leaving group (*95, 106*). The magnesium affinity of FTase increases with pH (pK_a = 7.4), reflecting the deprotonation of the FPP diphosphate to enhance Mg^{2+} coordination (*106*). The FTase-catalyzed reaction with farnesylmonophosphate is independent of Mg^{2+} ion concentration, indicating that both phosphates are needed to coordinate Mg^{2+} to accelerate the reaction (*106*). The magnesium ion dependence of the single turnover reaction has a $K_{1/2}$ of 2 mM, which is a weaker affinity than one would predict for a Mg^{2+}-diphosphate interaction (the K_D for FPP alone is 0.1 mM), indicating that the magnesium ion binding site in FTase consists of more than just the FPP diphosphate (*106*). Additionally, while both FTase and GGTase II require Mg^{2+} to achieve optimal catalytic activity, the reaction of GGTase I is not accelerated by Mg^{2+} (*12-14*). This suggests that catalysis by Mg^{2+} is more complex than just coordinating to the PPi group of FPP.

A ternary crystal structure of FTase with bound manganese identifies the two oxygens of the diphosphate as ligands, but crystallography does not reveal residues located near the PPi group that could coordinate Mg^{2+} (*84, 86, 87*). However, crystal structures represent inactive complexes, and may not observe the conformational rearrangement of FPP. Mutagenesis studies of D352β indicate that the carboxylate side chain coordinates to the Mg^{2+} ion. An octahedral Mg^{2+} binding site has been proposed in the active FPP conformation which includes two carboxylate oxygens of D352β, two oxygens from the diphosphate of FPP, one carbonyl oxygen of the the side chain of D297β (which also coordinates zinc), and a water molecule (Figure 1.5) (*107*). The D352β residue is conserved in FTase and GGTase II but is substituted with a lysine (K311β) in GGTase I, which is proposed to partially replace the catalytic function of Mg^{2+} (*20, 108*). Mutagenesis studies confirm that substitution of lysine for aspartate
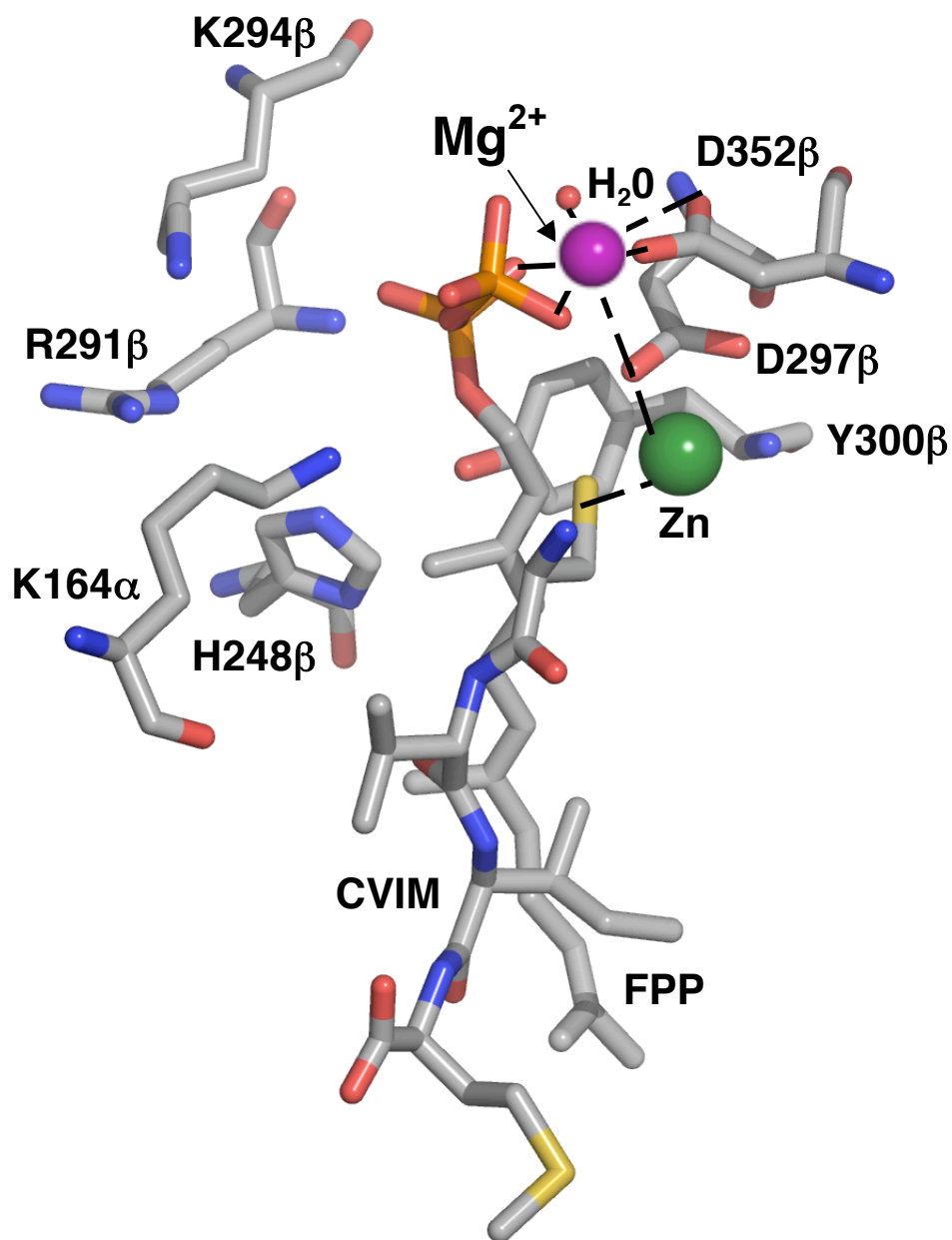
Figure 1.5 Proposed Mg^{2+} binding site in active substrate conformation

Model for the proposed Mg^{2+} binding site formed in the active ternary complex (*107*), based on mutagenesis and crystallographic data (PDB ID 1JCQ (*85*) and 1D8D (*84*)). The octahedral binding site consists of two nonbridging oxygens of the FPP diphosphate, two carboxylate oxygens of D352β, a water molecule, and one carboxylate oxygen of D297β.

27

at this position alters the Mg^{2+} dependence of both FTase and GGTase I (*107, 108*). The formation of this Mg^{2+} site requires rotation of the prenyl chain and is therefore proposed to be coupled to the formation of the active substrate conformation of FPP. Therefore, it was proposed that Mg^{2+} accelerates catalysis in FTase both by stabilizing developing negative charge in the transition state and by stabilizing the formation of the active site conformation prior to catalysis (*107*).

Role of conserved diphosphate binding pocket in catalysis

Typically, enzymes which utilize diphosphate contain a catalytic Mg^{2+} ion which is coordinated to the diphosphate group of the substrate as well as a group of negatively charged acidic side chains, usually a DDXXD motif, which bind the Mg^{2+} ion (*109-112*). The active site of FTase, on the other hand, contains a group of highly conserved positively charged residues, termed the "PPi binding pocket", with extensive hydrogen bonding interactions with the diphosphate oxygen atoms of FPP, illuminated in crystal structures of the inactive complex (Figure 1.2) (*85, 90*). The PPi binding pocket consists of the residues K164α, H248β, R291β, K294β and Y300β, and this binding pocket actually decreases the affinity of the FTase•FPP•peptide ternary complex for Mg^{2+} 10-fold when compared with the affinity of free FPP for Mg^{2+}, while enhancing the affinity of FTase for FPP (*90, 107*). Mutagenesis studies using steady-state and transient kinetics have also demonstrated that these residues, particularly Y300β, are important for catalysis (*88, 90, 113-116*). These data are consistent with stabilization of the developing negative charge on the PPi leaving group in the catalytic transition state. However, mutagenesis studies have also indicated that these residues are shifted in the active substrate conformation, and thereby may facilitate the conformational change of the FPP molecule (Figures 1.3 and 1.5) (*88, 90*). The position of the diphosphate in the active substrate conformation cannot be determined from crystal structures, but its position must accommodate the rotational movement of the FPP isoprene chains. It is thought that the PPi binding pocket residues may lower the affinity of the PPi moiety for Mg^{2+} prior to peptide binding, and is important for stabilizing the active substrate conformation (*88, 90*).

Inhibitors and substrate analogs of FTase

Small molecule inhibitors of FTase can be separated into three categories, based on different drug discovery strategies: (1) natural products; (2) peptidomimetics and other peptide-competitive inhibitors; and (3) FPP analogs and FPP-competitive inhibitors (*48, 117*). Additionally, bisubstrate FTIs have been developed (*117*). Natural products that inhibit FTase were discovered by random screening, and the molecules identified are for the most part structurally homologous to FPP (*48*). However, the evolution of non-substrate based FTIs identified from library hits presents the most promising area of inhibitor development currently, and has led to the development of potent peptide- and FPP-competitive compounds.

The most clinically successful FTIs to date are non-CaaX peptidomimetic inhibitors derived from library screening, but the development of CaaX peptidomimetic inhibitors has been an extremely active and successful area of research as well (*117*). These include mimics of the tetrapeptide CaaX sequence as well as compounds based on the conformation of the peptide substrate in the active site of FTase. It has been understood for quite some time that an aromatic substituent in a_2 of the Ca_1a_2X motif will lead to inhibition of farnesylation (e.g. CVFM). The a_2 region of the peptide has therefore been modified to allow for cell permeability, bioavailability and stability, in addition to potency and selectivity (*117*).

Many crystal structures of FTase bound with various peptide-competitive inhibitors have been determined (*85, 118-122*). These compounds, visualized in a ternary complex with bound FPP, make extensive van der Waals contacts with the lipid moiety of FPP, analogous to peptides. Interestingly, FTIs can mimic the extended conformation of the bound peptide in the ternary complex, as well as the displaced, type I β-turn conformation adopted by the farnesylated peptide product when an additional FPP molecule is bound in the active site (*21, 120*). Inhibitors that bind in an extended conformation frequently display rapid inhibition of FTase, while inhibitors that adopt a β-turn conformation often exhibit time-dependent inhibition, further suggesting that these compounds partially occupy the exit groove and overlap with the displaced product farnesyl moiety (*68, 119, 123*).

Less progress has been made toward the development of inhibitors that are FPP analogs, largely due to concerns about cell permeability and potential inhibition of other crucial FPP-utilizing enzymes (*117*). However, a series of farnesyl-derived FTIs has now been derived and shows considerable promise in potency (*117*). This includes FPP-mimetic compounds, in which the diphosphate group is altered, and FPP analogs, which maintain the diphosphate moiety and have alterations in one or more isoprenoid chains. Again, the most clinically successful FPP-competitive FTIs are non-isoprenoid and are derived from library-screening efforts (*117*). A hit identified during compound library screening discovered a potent and selective non-thiol peptidomimetic FTI, which turned out to be competitive with FPP (*124*). Inhibitors derived from this series of compounds are not structural analogs of FPP, so they do not inhibit other FPP-utilizing enzymes such as squalene synthase (*125*).

Many FPP-competitive inhibitors and FPP analogs have proven very useful in the study of the mechanism of FTI action. They have also been used to study the structure of the active site and the catalytic mechanism of FTase. Nonhydrolyzable FPP analogs have been used to determine several crystal structures of FTase in ternary complexes (*84, 85, 87*). Fluorinated FPP analogs and 3-desmethyl FPP have been studied as mechanistic probes with yeast and mammalian FTase to examine the dissociative character of the transition state of FTase (*95, 99*). Synthetic FPP derivatives have also been used to determine the stereochemical course of the FTase reaction (*97, 98*).

More recent work has led to the discovery of many classes of FPP analogs which are capable of modifying proteins in the cell (*126-129*). Excitingly, many groups have found that these compounds may alter the substrate specificity of FTase, thus providing additional tools to study the prenylation of specific proteins and potential substrate-specific inhibitors (*129-132*). Modulating the farnesylation of selected proteins would allow for a more precise determination of the functions of these individual proteins, as well as the roles of their lipid modifications. Combined with mechanistic studies, this approach may be used to determine the underlying mechanisms behind the substrate selectivity of FTase, which could be employed for the rational design of selective and potent inhibitors of prenylation.

Objectives of this work

There has been a great interest in studying prenylation over the last two decades, and the wealth of structural and kinetic data provides an emerging picture of the complexity of the FTase mechanism. Many of the pressing questions that remain unanswered center around the identification of the physiological substrates for FTase, as well as its *in vivo* regulation. An increased understanding of the cell biology of FTase will further advance work in developing FTase inhibitors than could more specifically target proteins in pathways that are implicated in particular diseases. To complement these studies, a biochemical approach to answering these questions provides detailed information that cannot be determined *in vivo*, and a better description of the catalytic mechanism of FTase should shed light on both the substrate specificity and the inhibition of prenylation.

This work addresses many key questions that remain regarding the mechanism of FTase. Following farnesylation, little was known about the dissociation of products from the enzyme. In particular, it was not clear whether the diphosphate product is released concomitantly with the formation of product, or remains bound in the active site until a second molecule of FPP binds to the enzyme to displace it. In Chapter 2, we report that the PPi product is released as fast as, or faster than, the farnesylation step. To answer this question, we developed a continuous, coupled fluorescent assay to measure the release of PPi, cleavage by inorganic pyrophosphatase, and subsequent binding of phosphate by a fluorescently labeled phosphate binding protein. Because PPi is released rapidly, this assay was further developed as a convenient assay to measure prenyltransferase activity under both multiple and single turnover conditions. This assay, which can also be used more generally for any reaction where diphosphate is a product, should aid greatly in the study of prenyltransferases by facilitating substrate specificity studies as well as high-throughput screens for inhibition studies.

The dissociation of the other product, the farnesylated protein or peptide, is accelerated by binding of a second molecule of substrate, either FPP or peptide (*89*). This step in the reaction pathway is quite unique, and may be important in the physiological regulation of farnesylation. In Chapter 3, we present a direct fluorescent assay to measure the dissociation of farnesylated product, and show that this process is

dependent on both the concentration of FPP and Mg^{2+}. We also report unexpected observations for a series of FPP analogs designed to alter the FPP conformational change and/or the chemical farnesylation step in the FTase reaction. While these compounds introduce major changes in the steric and electrostatic properties of the isoprene groups of FPP, no change in either of these catalytic steps is observed. Instead, the FPP-catalyzed product dissociation is affected, leading to a reduction in steady-state turnover. These studies implicate the binding of a second molecule of substrate to the E•product complex as an important determinant of the substrate specificity, and potentially the cellular regulation of FTase.

We further investigate the mechanism of farnesylated product dissociation in Chapter 4, where we have determined a novel inhibitory mechanism for a select group of FPP-competitive inhibitors. Deletion of positively charged residues in the diphosphate binding pocket ($K294\beta$ and $R291\beta$) of FTase enhances the potency of these inhibitors by as much as 400-fold, based upon changes in both IC_{50} and K_i values. For wild-type (WT) FTase, the potency of these inhibitors is enhanced by as much as 170-fold by the addition of exogenous phosphate ions. This phosphate synergy is almost completely lost in the $K294\beta$ and $R291\beta$ mutants, suggesting that phosphate ions enhance inhibitor potency in WT FTase by shielding the positive charge of these residues. The direct binding affinities of both FPP and the inhibitor to the free enzyme are not consistent with the K_i values measured under steady-state conditions. An inhibition constant for product dissociation is therefore measured for WT FTase, showing that a key and novel aspect of the inhibitory mechanism is to slow the dissociation of farnesylated product.

A clearer understanding of the chemical transition state of FTase would aid in the design of more potent, specific inhibitors, as well as provide a better mechanistic description of the class of enzymes that catalyze zinc-dependent sulfur alkylation. The best method for investigating the structure of the chemical transition state of FTase is heavy atom kinetic isotope effects (KIEs) (*133*). In Chapter 5, we measure the primary ^{14}C and α-secondary ^{3}H KIEs at the sensitive C1 position of FPP under single turnover conditions of limiting FPP and excess enzyme. These KIE studies are consistent with a concerted mechanism with dissociative character for mammalian FTase, and offer the first direct evidence of dissociative character for any member in the class of zinc-

dependent sulfur alkylating enzymes. We explore the contribution of the leaving group to catalysis by reporting the α-secondary KIEs at varying Mg^{2+} concentrations and for FTase mutants in the PPi binding pocket. The role of the nucleophile is addressed by determining the contribution of the Zn^{2+} metal ion, as measured by the α-secondary KIE for FTase substituted with cadmium.

Unexpectedly, the α-secondary KIE is masked for some peptides and indicates that the FPP conformational rearrangement, rather than the farnesylation step, is at least partially rate-limiting for these peptides. KIE measurements therefore allow the calculation of the individual rate constants for the conformational rearrangement and farnesylation, and provide the first kinetic information regarding these two steps in catalysis. The results presented in Chapter 5 implicate both Mg^{2+} as well as the PPi binding pocket residues in stabilizing both the conformational rearrangement of FPP and the transition state for farnesylation. In addition, we show that the structure of the peptide substrate has an effect on the equilibrium of the conformational rearrangement of the FPP substrate, as well as the chemical farnesylation step. These data provide intriguing information about the determinants for peptide substrate specificity in the FTase reaction pathway.

CHAPTER 2
A CONTINUOUS FLUORESCENT ASSAY FOR PROTEIN
PRENYLTRANSFERASES MEASURING DIPHOSPHATE RELEASE [1,2]

A convenient assay to measure FTase and GGTase I activity is needed to study inhibitors, determine the substrate specificities for these enzymes, and study their catalytic and kinetic mechanisms. Currently, methods to assay prenyltransferase activity are labor-intensive and depend on either radiolabeled isoprenyl substrate or modified peptides. Single turnover assays to measure the rate constant of prenylation are conducted using ^{3}H-labeled FPP or GGPP (*134*). Several multiple turnover assays have been developed, including a radioactive assay using ^{3}H-labeled FPP or GGPP (*93, 135-137*), a continuous fluorescent assay using a dansylated peptide (*138, 139*), and an assay using a biotinylated peptide and streptavidin-coated scintillation beads (*92*). A limitation to high-throughput fluorescence assays measuring prenyltransferase activity is that they use dansylated peptides which must be synthesized (*140*). In addition, the dansyl group may affect the binding of peptides to the enzyme, limiting the usefulness of this assay for determining the true values for k_{cat} and k_{cat}/K_M for peptides. Finally, farnesylation of native full-length proteins cannot be assayed using this method.

Webb and coworkers have developed a fluorescent assay to measure the kinetics of phosphate release from ATPases (*141*). They engineered the *E. coli* phosphate binding protein (PBP) by introducing a single cysteine residue, located at the edge of the phosphate-binding cleft, which was then covalently labeled with the fluorophore, *N*-[2-(1-maleimidyl)ethyl]-7-(diethylamino)coumarin-3-carboxamide (MDCC) (Figure 2.1). The fluorescence intensity of the labeled protein, MDCC-PBP, increases upon binding of

---
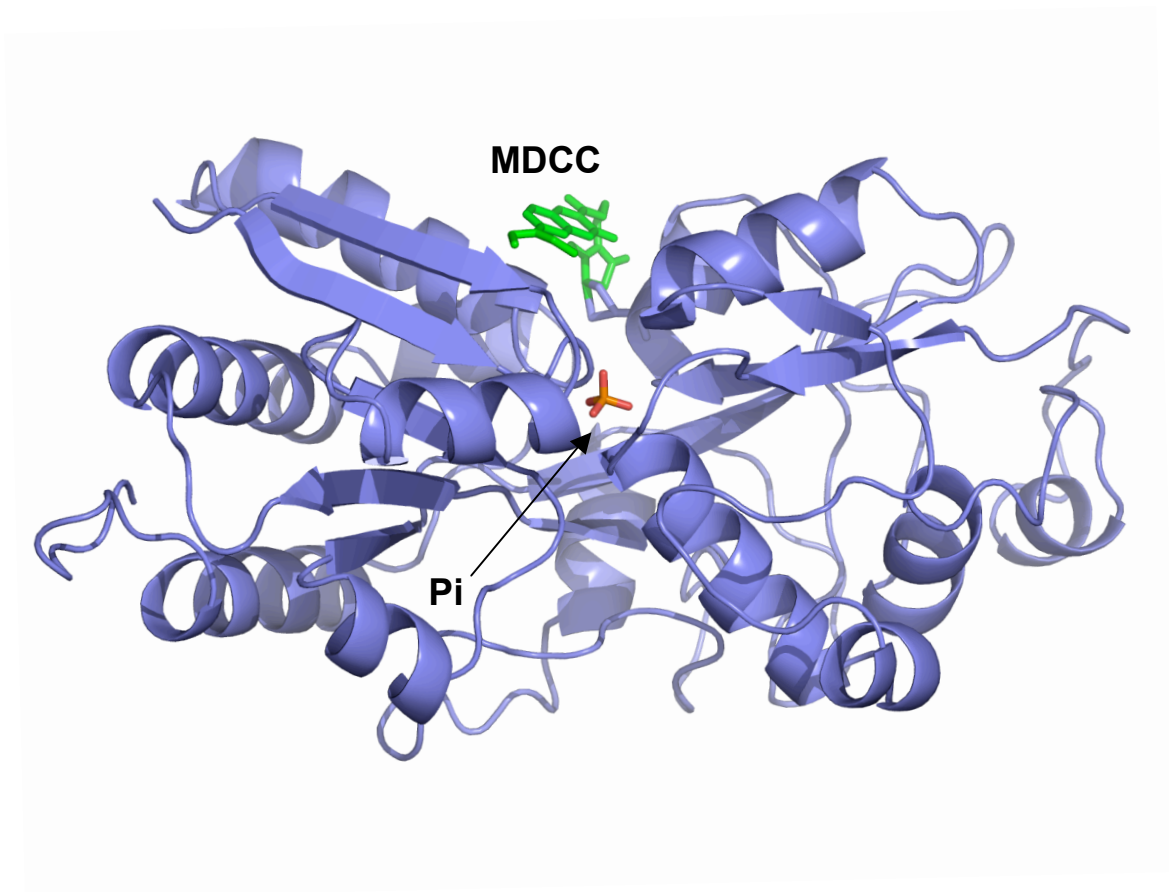
Figure 2.1 Crystal structure of MDCC-PBP

X-ray crystal structure of the A197C phosphate binding protein from *E. coli* covalently labeled with the coumarin fluorophore, MDCC. When Pi is bound, the protein undergoes a conformational change, leading to an increase in fluorescence (*141-143*). Protein Data Bank code: 1A54 (*143*).

inorganic phosphate (Pi), due to a significant change in the environment around the fluorophore (Figure 2.1) (*142, 143*). MDCC-PBP binds P_i tightly ($K_d \sim 0.1$ μM) and rapidly, with a second-order rate constant of 1.4×10^8 $M^{-1}s^{-1}$ (*141*). Measurement of the formation of a phosphate product using MDCC-PBP has been used to determine the single turnover kinetic rate constants of ATP hydrolysis catalyzed by actomyosin subfragment 1 from rabbit skeletal muscle (*141*), nucleoside triphosphate hydrolysis by actomyosin (*144*), and DNA-stimulated dTTP hydrolysis activity by T7 helicase (*145*).

Here we present a continuous, fluorescence-based assay which uses MDCC-PBP coupled to inorganic pyrophosphatase (PPiase) to measure the rate of diphosphate (PPi) formation and release during the FTase-catalyzed reaction. Studies of the single turnover kinetics of PPiase from *Saccharomyces cerevisiae* reveal that PPi is rapidly cleaved (800 s^{-1}) in the presence of Mg^{2+} (*146*). The release of the PPi product from the FTase•product complex is coupled to PPi cleavage catalyzed by PPiase, and the subsequent binding of Pi by MDCC-PBP is detected as an increase in fluorescent intensity (Scheme 2.1). Diphosphate release for both FTase and GGTase I equals the rate constant of the prenylation step, as measured by radiometric assays, indicating that diphosphate release occurs faster than, or concomitantly with, the formation of the prenylated peptide for both prenyltransferases. This assay can therefore be applied as a general method to measure prenyltransferase activity *in vitro*, as well as any reaction where diphosphate is a product. The reactivity of a variety of peptide substrates with a broad range of rate constants under both single turnover and multiple turnover conditions has been measured using this assay. Furthermore, this assay is useful for studying substrate analogs and inhibitors of prenyltransferases. This assay is the first non-radioactive assay developed which can be used to assay the reactivity of FTase with unmodified peptides as well as full-length proteins. A high throughput assay to measure steady state turnover for both FTase and GGTase I will greatly facilitate studies of prenyltransferases, including inhibitor studies.

$$\textbf{E•FPP•Spep} \xrightarrow{5 \text{ s}^{-1}} \textbf{E•F-Spep•PP}_i \xrightarrow{\gg 5 \text{ s}^{-1}} \textbf{E•F-Spep + PP}_i \xrightarrow[\text{PPiase}]{\gg 80 \text{ s}^{-1}} \textbf{2 P}_i \xrightarrow[\text{MDCC-PBP}]{80 \text{ s}^{-1}} \textbf{2 MDCC-PBP•P}_i$$

Scheme 2.1 Mechanism for MDCC-PBP/PPiase assay measuring FTase activity

Experimental Procedures

Materials

Tritium-labeled farnesyl diphosphate ([1-^{3}H]-FPP) was purchased from GE Healthcare (formerly Amersham Biosciences). Peptides were synthesized and purified by high-pressure liquid chromatography to > 90% purity, as follows: GCVLS and dansylated TKCVLA by Sigma-Genosys (The Woodlands, TX); TKCVIM and TKCVIS by Bethyl Laboratories (Montgomery, TX); and TKCVIF and TKCVIL by American Peptide Company (Sunnyvale, CA). The molecular masses of all peptides were confirmed by electrospray mass spectrometry. 7-Diethylamino-3-(((2-maleimidyl)ethyl)-amino)carbonyl) coumarin (MDCC) was purchased from Molecular Probes (Eugene, OR). All DNA primers were purchased from Invitrogen. Farnesyl diphosphate (FPP), purine nucleoside phosphorylase (PNPase), 7-methylguanosine (MEG), and inorganic pyrophosphatase from bakers' yeast (PPiase) were purchased from Sigma-Aldrich. Disodium hydrogen phosphate (NaPi) and sodium diphosphate (NaPPi) of the highest chemical purity available (Biochemika Ultra) were purchased from Fluka (Sigma-Aldrich). The concentrations of NaPi and NaPPi were determined by inductively coupled plasma-mass spectrometry (Keck Elemental Geochemistry Laboratory, University of Michigan, Ann Arbor, MI). All other chemicals used were reagent grade.

Cloning of *E. coli pstS* gene

DNA encoding the wild-type PBP gene, minus the periplasmic localization sequence, was generated by PCR amplification of the *pstS* gene from the *E. coli* strain DH5α genomic DNA with two sets of primers, 5'-CAGTAACGACATATGGAAGCAA GCCTGACAGGTGCAGG-3' and 5'-GAAGAGGTGGTGCTCGAGGTACAGC-3'. Each PCR amplification reaction was catalyzed by *pfu*-turbo DNA polymerase (Stratagene). The resulting fragments were purified using a 1% agarose gel and then cloned into a pCR-Blunt II-TOPO vector and transformed into OneShot TOP10 chemically competent *E. coli* cells (Invitrogen). The purified TOPO plasmid containing

the insert was then digested with NdeI and XhoI, and the fragments were gel purified and then ligated into the pET31b(+) vector (Novagen) digested with the same enzymes. The final gene contains a C-terminal 6X histidine tag and lacks the N-terminal periplasmic signal sequence. The plasmid pET31b-PBP was transformed into *E. coli* BL21(DE3) cells, and the cells were grown in LB medium containing 100 mg L^{-1} ampicillin. The plasmid was purified using a Plasmid Midi Kit (Qiagen, Valencia, CA). The sequence of the entire gene was confirmed by DNA sequencing (University of Michigan DNA Sequencing Core, Ann Arbor, MI).

Preparation of A197C PBP and MDCC-PBP

The A197C PBP mutant was prepared from the pET31b-PBP plasmid using the QuikChange site-directed mutagenesis kit (Stratagene, La Jolla, CA) with the codon change of GCT to TGT. The plasmid was transformed into SMART cells (Gene Therapy Systems, San Diego, CA), and the cells were grown in LB medium containing 100 mg L^{-1} ampicillin. The plasmid was purified and sequenced as described above.

The A197C PBP mutant is overexpressed in *E. coli* BL21(DE3) pET31b-PBP cells, grown at 37 ^{0}C to an OD_{600} of 0.6 in LB medium containing 100 mg L^{-1} ampicillin. Protein expression is induced by the addition of 1 mM isopropyl β-D-1-thiogalactopyranoside (IPTG) and incubated at 25 ^{0}C for 14-16 hours. The harvested cells are resuspended in 50 mM Hepes, pH 8.5, and 100 mM KCl, and lysed by a single pass through a microfluidizer (Microfluidics, Newton, MA). The supernatant is clarified by centrifugation and nucleic acids precipitated with 1% (w/v) streptomycin sulfate at 4 ^{0}C. The supernatant is loaded, 32 mg of total protein per run, onto a 7.8 mL Ni^{2+}-charged POROS Metal Chromatography Affinity column (Applied Biosystems, Foster City, CA), washed in 50 mM Hepes, pH 8.5, 100 mM KCl buffer, and eluted with a 0-150 mM imidazole gradient. The protein elutes at ~ 50 mM imidazole. Fractions containing pure A197C PBP are pooled and concentrated using Amicon Ultra centrifugal filter devices with a 10,000 molecular weight cutoff (MWCO) filter (Millipore, Billerica, MA), and then dialyzed at 4 ^{0}C against 20 mM Tris pH 8, 1 mM tris(2-carboxyethyl)phosphine hydrochloride (TCEP). Protein concentration and yield are

determined by absorbance at 280 nm using a molecular weight of 35276 g mol^{-1} and a calculated extinction coefficient of 64204 M^{-1}cm^{-1} (*147*).

The reaction of A197C PBP with MDCC is performed as described previously (*142*). Because MDCC-PBP binds nanomolar concentrations of Pi, a "Pi mop" consisting of purine nucleoside phosphorylase (PNPase) and its substrate, 7-methylguanosine (MEG), is used to irreversibly sequester Pi as ribose-1-phosphate (*141*). A197C PBP (85 μM) and MDCC (780 μM) are incubated in 20 mM Tris•HCl, pH 8, 1 mM TCEP, 200 μM MEG, and 0.2 units mL^{-1} PNPase at room temperature for 30 minutes, protected from light. Low molecular weight species are removed and the buffer exchanged to 50 mM Hepes, pH 8.5, 100 mM KCl using Amicon Ultra centrifugal filter devices (10,000 MWCO), followed by further purification on a POROS MC column exactly as described above. Pure, labeled fractions are pooled, concentrated, and dialysed against 50 mM Hepes, pH 7.8, 2 mM TCEP at 4 ^{0}C, followed by dialysis against 50 mM Hepes, pH 7.8, 2 mM TCEP, 0.5 units mL^{-1} PNPase, and 15 μM MEG to remove residual phosphate. The small molecules in the "Pi mop" are removed by exchanging the buffer to 50 mM Hepes, pH 7.8, and 2 mM TCEP using Amicon Ultra centrifugal filter devices (10,000 MWCO). The purity of the labeled protein was confirmed by SDS-PAGE. Protein concentration was determined as described above, and stocks were stored at −80 ^{0}C.

Preparation of FTase

Protein FTase expression and purification were carried out in *E. coli* BL21(DE3) FPT/pET23a cells as described previously (*90, 148*). The purified FTase was determined by SDS-PAGE to be >90% pure. The protein was dialyzed at 4 ^{0}C against 50 mM Hepes, pH 7.8, and 2 mM TCEP, and stored at −80 °C. Protein concentration was determined by active site titration as previously described (*90*).

Fluorescence Measurement of Pi binding to MDCC-PBP

The fluorescence spectrum of MDCC-PBP was measured in the absence and presence of 15 μM NaPi, using an SLM-Aminco Bowman series 2 luminescence

spectrometer with a 1 cm path length, an excitation wavelength of 430 nm, and an emission wavelength varying from 430 nm to 550 nm (bandpass = 8 nm). The kinetics of Pi binding to MDCC-PBP were measured at 25 ^{0}C on a KinTek model SF-2001 stopped-flow apparatus (KinTek Corporation, Austin, TX) (Scheme 2.2). The sample was excited at 430 nm and fluorescence emission was measured at > 450 nm using a cutoff filter (Corion LL-450-F). Prior to each experiment, the stopped-flow syringes and mixing chamber were preincubated in buffer containing "Pi mop" (50 mM Heppso, pH 7.8, 5 mM MgCl$_2$, 2 mM TCEP, 0.5 units mL^{-1} PNPase, and 15 μM MEG). A solution containing MDCC-PBP in buffer (50 mM Heppso, pH 7.8, 5 mM MgCl$_2$, and 2 mM TCEP) was rapidly mixed (at a flow rate of 10 mL s^{-1}) with an equal volume of solution containing NaPi in the same buffer (Scheme 2.2). Final concentrations were 5 μM MDCC-PBP and 0.4-1 μM NaPi. Fluorescence emission was measured as a function of time, and at least five kinetic traces were averaged and Eq. 1 was fit to these data to determine the observed rate constant, k_{obs}, where Fl is the observed fluorescence at <450 nm at time t, ΔFl is the amplitude, and Fl$_{max}$ is the fluorescence endpoint.

$$Fl = \Delta Fl * e^{-k_{obs}t} + Fl_{max} \qquad\qquad Eq.\ (1)$$

PPi cleavage by PPiase

The rate of PPi cleavage catalyzed by PPiase was determined by coupling the reaction to the binding of Pi by MDCC-PBP. Assays were conducted at 25 ^{0}C on the stopped-flow spectrometer as described above, where a solution containing MDCC-PBP and PPiase in buffer (50 mM Heppso, pH 7.8, 5 mM MgCl$_2$, and 2 mM TCEP) was rapidly mixed with an equal volume of solution containing NaPPi in the same buffer (Scheme 2.2). Final concentrations were 5 μM MDCC-PBP, 34 units mL^{-1} PPiase, and 200 nM NaPPi. At least five kinetic traces were averaged and Eq. 1 was fit to these data to determine k_{obs}. In FTase assays, the PPiase concentration was adjusted so that both the cleavage of PPi by PPiase and the binding of Pi by MDCC-PBP were rapid ($k_{obs} > 70$ s^{-1}).
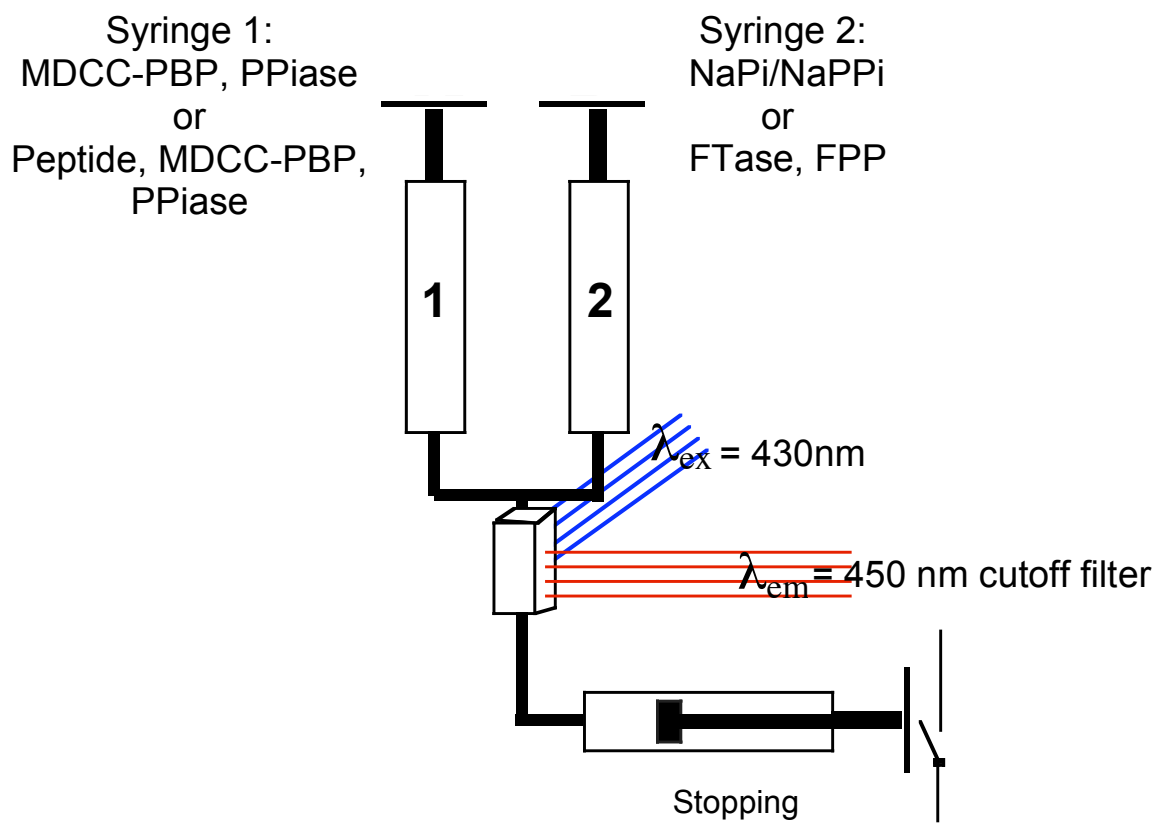
Scheme 2.2 Stopped-flow setup for measuring Pi binding by MDCC-PBP

Measurement of diphosphate release/single turnover assay on stopped-flow spectrophotometer

The rate of diphosphate release during a single turnover of FTase was determined using the following assay. The stopped-flow syringes and cell were washed and pre-incubated in buffer with "Pi mop" (50 mM Heppso, pH 7.8, 2 mM TCEP, 5 mM MgCl$_2$, 0.5 units mL^{-1} PNPase, and 15 μM MEG) prior to the experiment. FTase and FPP in buffer (50 mM Heppso, pH 7.8, 2 mM TCEP and 5 mM MgCl$_2$) were preincubated in one syringe at 25 ^{0}C, and then rapidly mixed with an equal volume of a solution containing peptide, MDCC-PBP, and PPiase in the same buffer (Scheme 2.2). The final concentrations were 800 nM FTase, 200 nM FPP, saturating (100 μM) peptide, 5 μM MDCC-PBP, and 34 units mL^{-1} PPiase. At least five kinetic traces were averaged and Eq. 1 was fit to these data to determine k_{obs}.

Steady-state assay for prenyltransferases

This assay was further adapted to measure steady-state turnover in a high throughput 96-well plate format. To measure k_{cat}/K_M, reactions were initiated by adding 50 nM FTase, 5 μM MDCC-PBP, and 34 units mL^{-1} PPiase in buffer (50 mM Heppso, pH 7.8, 2 mM TCEP, 5 mM MgCl$_2$) to solutions containing 10 μM FPP and varying concentrations (0-10 μM) of peptide in the same buffer. The change in fluorescence emission was monitored over time with an excitation wavelength of 430 nm and an emission filter of 450 nm, using a Polarstar Galaxy fluorescence platereader (BMG Lab Technologies, Durham, NC). Nonbinding, polystyrene plates (Corning Incorporated, Corning, NY) were used for these experiments. The fluorescence signal was converted to concentration of product using a standard curve measuring the change in fluorescence emission as a function of NaPPi concentration, in the presence of PPiase. This standard curve was comparable to a NaPi standard curve, as well as an FPP standard curve generated by repeating the experiment at a fixed peptide concentration (20 μM) and varying FPP concentrations (0-10 μM). Michaelis-Menten plots of product formed/time versus [peptide] were generated to calculate the k_{cat}/K_M value. Alternatively, the steady-

state turnover was measured from the change in fluorescence in a KinTek stopped-flow spectrometer under these conditions.

Measurement of single and multiple turnover rate constants for FTase using radiometric assay

As controls, the observed single turnover rate constant (k_{obs}) and the apparent second order rate constant for farnesylated peptide formation (k_{cat}/K_M) were measured using a radiometric assay with [1-^{3}H]-FPP in the presence of MDCC-PBP and PPiase to confirm that these components do not affect the catalytic rate constants of FTase. The single turnover rate constant for farnesylation of the peptide GCVLS was measured in a KinTek rapid quench apparatus (KinTek Corporation, Austin, TX) as previously described (*90, 95*). FTase and [1-^{3}H]-FPP in buffer (50 mM Heppso, pH 7.8, 5 mM MgCl$_2$, and 2 mM TCEP) were rapidly mixed with GCVLS in the same buffer to give final concentrations of 1 μM FTase, 500 nM [1-^{3}H]-FPP, 100 μM GCVLS, 5 μM MDCC-PBP, and 34 units mL^{-1} PPiase. The reaction was quenched at varying times using 80% 2-propanol and 20% acetic acid. Farnesylated product was separated from unreacted [1-^{3}H]-FPP on Whatman PE SIL G thin layer chromatography (TLC) plates in an 8:1:1 2-propanol/NH$_4$OH/H$_2$O mobile phase (*90*). Corresponding bands were cut from TLC plates and radioactivity was quantified by liquid scintillation counting using a Beckman LS 6500 liquid scintillation counter. The first order rate constant was calculated from a single exponential fit of the fraction product versus time (*90*).

The steady state kinetic rate constant k_{cat}/K_M was measured for the peptide TKCVIM on the benchtop, using final concentrations of 50 nM FTase, 1 μM [1-^{3}H]-FPP, and varying (0-10 μM) TKCVIM. At various times, the reaction was quenched by addition of 20% acetic acid, 80% 2-propanol and placed on ice. Samples were loaded directly onto TLC plates which were run as described above. The initial rate was calculated from a linear fit of product formation taken from the first 10% of the reaction.

<center>**Results**</center>

Preparation of MDCC-PBP

The preparation of MDCC-PBP has been described previously (*141, 142*). Here we overexpressed wild-type and A197C PBP as soluble, intracellular proteins in *E. coli* by removing the periplasmic localization sequence. The addition of a C-terminal histidine tag greatly facilitated the isolation and purification of PBP; a single Ni^{2+} column results in > 95% pure protein as determined by SDS-PAGE analysis. A typical yield of pure A197C PBP from a 1 L growth of cells was ~375 mg. After purification, the single cysteine residue was reacted with the coumarin fluorophore MDCC to yield the labeled protein, and the free fluorophore was then removed by ultrafiltration. Removal of any bound Pi by dialyzing the purified MDCC-PBP against the "Pi mop" circumvented the need to include the "Pi mop" in subsequent assays, which can remove Pi bound to MDCC-PBP at longer time intervals. Overall, this procedure allows the rapid preparation of MDCC-PBP in high yield. The purified, fluorescently labeled MDCC-PBP shows an increase in fluorescence upon binding of Pi, with an emission peak at ~465 nm (Figure 2.2).

Development of assay for PPi using PPiase and MDCC-PBP

The binding of Pi to MDCC-PBP was measured as an increase in fluorescence emission with an observed rate constant of 76 ± 1 s^{-1} at 400 nM Pi (Figure 2.3A), similar to previous measurements (*141, 142*). The cleavage of PPi by PPiase was also measured using a coupled assay with MDCC-PBP (Figure 2.3B). To investigate whether this assay could be adapted to measure the formation of PPi, PPi was mixed with MDCC-PBP in the presence of PPiase. The observed rate constant for the fluorescence increase is 77 ± 2 s^{-1} upon mixing MDCC-PBP and PPiase with 200 nM PPi, identical to the rate constant for binding 400 nM Pi. These data demonstrate that PPi cleavage by PPiase is rapid relative to Pi binding under these conditions. Indeed, kinetic studies of yeast PPiase have indicated that the cleavage of PPi in the presence of Mg^{2+} is 800 s^{-1} at pH 7.2 and 25 ^{0}C,

<div align="right">45</div>
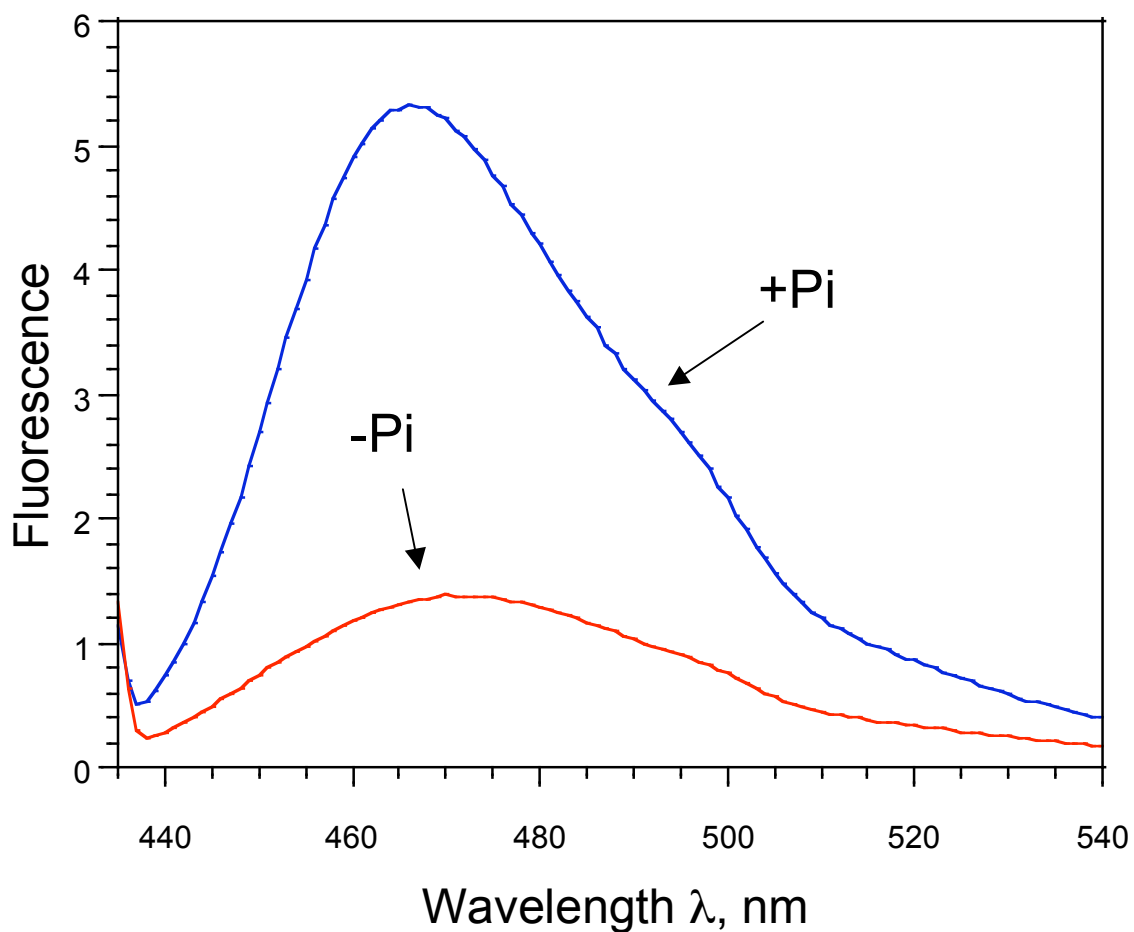
Figure 2.2 Fluorescence of MDCC-PBP

Fluorescence emission spectrum for 7 μM MDCC-PBP in 50 mM Heppso, pH 7.8, in the absence and presence of 15 μM NaPi.   Samples were excited at 430 nm, using an SLM-Aminco Bowman series 2 luminescence spectrometer with a 1 cm path length and a bandpass width of 8 nm.
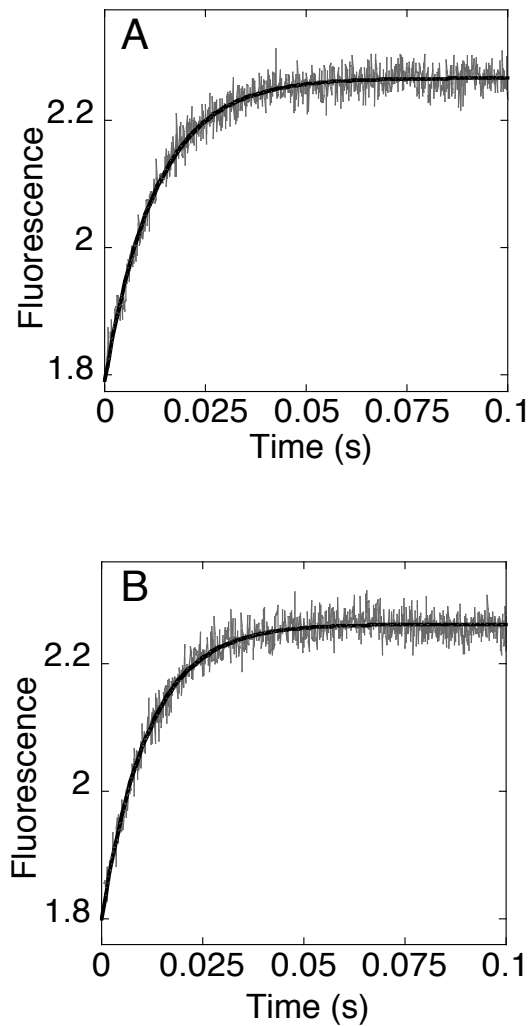
Figure 2.3 MDCC-PBP/PPiase assay

Stopped-flow fluorescence measurement of P_i binding by MDCC-PBP alone (A) and
coupled to cleavage of PPi by PPiase (B). Samples were excited at 430 nm, and
fluorescence emission was measured at wavelengths greater than 450 nm. Final solutions
contained 5 μM MDCC-PBP and 400 nM NaPi (A) or 200 nM NaPPi and 34 units ml^{-1}
PPiase (B) in 50 mM Heppso, pH 7.8, 5 mM MgCl$_2$, and 2 mM TCEP. Each trace
represents an average of five measurements. A single exponential is fit to the data.

and is too fast to measure over a broad pH and temperature range (*146, 149, 150*). In the absence of PPiase, a slow increase in fluorescence is observed when PPi is mixed with MDCC-PBP, most likely due to either the binding of PPi by MDCC-PBP or the slow hydrolysis of PPi (data not shown).

Measurement of FTase-catalyzed diphosphate release

GCVLS corresponds to the C-terminal sequence of the FTase substrate H-Ras, which has been well characterized mechanistically and kinetically. The single turnover rate constant for the formation of farnesylated GCVLS in 50 mM Heppso, pH 7.8, 2 mM TCEP, and 5 mM MgCl$_2$ has previously been measured as 4.6 ± 0.5 s^{-1} by a radioactive assay using [1-^{3}H]-FPP (*114*). The steady-state turnover rate constant is much slower than this at 0.01 s^{-1}, due to slow product dissociation (*89, 92*). To measure diphosphate dissociation from the FTase•product complex, the formation of "free" diphosphate was measured by a fluorescence change resulting from the formation of Pi catalyzed by PPiase and binding to MDCC-PBP, under conditions in which both PPi cleavage and Pi binding to PBP are rapid relative to the rate of PPi dissociation from the ternary complex (Scheme 2.1). Using this assay, the observed rate constant for formation of free PPi after reacting the peptide GCVLS with FTase•FPP under single turnover conditions is 4.7 ± 0.1 s^{-1} in the presence of 5 mM Mg^{2+} at 25 ^{0}C, pH 7.8 (Figure 2.4). This value is identical within experimental error to the rate constant measured by the radioactive assay (*114*). In addition, the farnesylation rate constant for GCVLS measured by the radioactive assay in the presence of MDCC-PBP, PPiase, PNPase, and MEG is unchanged, demonstrating that these components do not affect the rate constant for farnesylation or product release (data not shown). Using the MDCC-PBP assay, we demonstrated that varying the concentration of peptide (50-800 μM), MDCC-PBP (2-10 μM), or PPiase (17-102 units mL^{-1}) has no effect on the observed rate constant for PPi formation. Furthermore, the amplitude of the fluorescence change is dependent on the concentration of FPP. Finally, no fluorescence change is observed in the absence of FTase, FPP or peptide (data not shown). In the absence of PPiase, a slow increase in
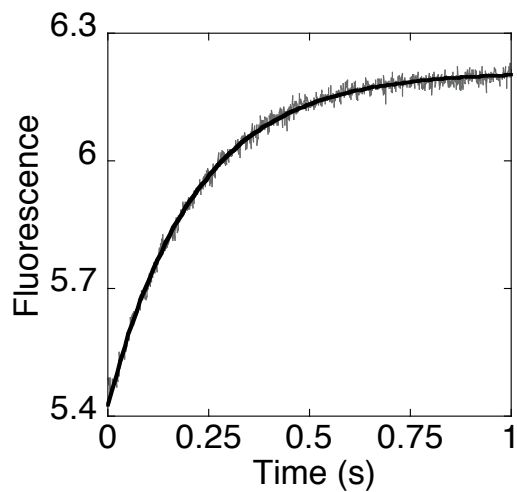
Figure 2.4 Formation of dissociated PPi during FTase reaction

Stopped-flow measurement of diphosphate dissociation from the transiently formed FTase•PPi•farnesylated peptide complex using the peptide GCVLS. The reaction was initiated by mixing the FTase•FPP complex with GCVLS, PPiase, and MDCC-PBP. Samples were excited at 430 nm, and fluorescence emission was measured at more than 450 nm. Final solutions contained 800 nM FTase, 200 nM FPP, 100 μM GCVLS, 34 units ml^{-1} PPiase , and 5 μM MDCC-PBP in 50 mM Heppso, pH 7.8, 5 mM MgCl$_2$, and 2 mM TCEP. The trace represents an average of five measurements. A single exponential is fit to the data.

fluorescence is observed that can be attributed to the slow binding of PPi by MDCC-PBP (data not shown). When the "Pi mop" is included in assays, a slow decrease in fluorescence is observed over longer time intervals (with an observed rate constant of 0.007 s^{-1}). The "Pi mop" was therefore omitted for slower reactions. As described in the Experimental Procedures, MDCC-PBP with no bound phosphate can be obtained by dialyzing MDCC-PBP against the "Pi mop," and subsequent removal of the "Pi mop" by ultrafiltration.

The rate constant for PPi release from the FTase•product complex has previously not been measured. Here we demonstrate that PPi dissociation is faster than the rate constant for the farnesylation of peptide. This assay can therefore be used to measure the single turnover rate constant for FTase in real time, a significant advantage compared to the radiometric assay which is currently used to measure the single turnover rate constant for prenyltransferases.

To further investigate the peptide specificity of FTase, this assay was used to measure the single turnover rate constant of farnesylation for a variety of peptides corresponding to the C-terminal sequence of the K-Ras4b template with varying X groups, including TKCVIS (6.3 ± 0.1 s^{-1}) and TKCVIL (0.11 ± 0.01 s^{-1}) (Table 2.1). The values for k_{obs} are similar (within a factor of 2) to those determined using the radiometric assay (Table 2.1), and demonstrate that the identity of the X group significantly influences the reactivity of peptides with FTase. This assay has also been applied to measure geranylgeranylation catalyzed by GGTase I, as well as prenylation using isoprenyl diphosphate substrate analogs which lack a radiolabel (*24, 77, 151*). Although Mg^{2+} is a required cofactor for PPiase, the Mg^{2+} concentration in this assay can be decreased to 0.01 mM without significantly compromising the activity of PPiase. Therefore, this assay can also be used to investigate the Mg^{2+} dependence of the FTase single turnover rate constant (*77*).

Continuous assay to measure k_{cat}/K_M for prenyltransferases

The MDCC-PBP/PPiase assay was further extended for use as a high throughput assay to measure steady-state turnover catalyzed by FTase. Under multiple turnover

Table 2.1 Single turnover rate constants catalyzed by FTase for varying peptide sequences [a]

Peptide	k_{obs} (s^{-1})	
	MDCC-PBP/PPiase assay	Radiometric assay
GCVLS	4.7 ± 0.1	4.5 ± 0.5
TKCVIS	6.3 ± 0.1	6 ± 1^{b}
TKCVIL	0.11 ± 0.01	0.07 ± 0.01^{b}

[a] Final solutions contained 800 nM FTase, 200 nM FPP, 100 μM peptide, 34 units mL^{-1} PPiase, and 5 μM MDCC-PBP in 50 mM Heppso, pH 7.8, 5 mM MgCl$_2$, and 2 mM TCEP. All assays were conducted at 25 ^{0}C.
[b] Data taken from ref. (*24*).

conditions, a linear increase in fluorescence was observed with an initial velocity that is dependent on the concentration of the peptide TKCVIM (Figure 2.5). The change in fluorescence is converted to the concentration of diphosphate formed by using a standard curve measuring fluorescence change as a function of [NaPPi] (Figure 2.6). The slope of the standard curve was used to convert the change in fluorescence to the change in concentration of product. The initial rate in [product]/time was plotted as a function of peptide concentration to determine the $k_{cat}/K_M^{peptide}$ value of 100 ± 30 mM^{-1}s^{-1}, using the Michaelis-Menten equation (Figure 2.7). As a control, FPP was varied (0-20 μM) at a fixed, saturating concentration of peptide to confirm that 10 μM FPP was saturating (data not shown). To verify the ability of the MDCC-PBP/PPiase assay to accurately measure $k_{cat}/K_M^{peptide}$ for FTase, steady-state turnover was also measured on the stopped-flow spectrometer to compare with results from the platereader assay. Conditions were identical to those used on the platereader, and the results confirm a linear increase in fluorescence, with a $k_{cat}/K_M^{peptide}$ value (120 ± 50 mM^{-1}s^{-1} for TKCVIM) comparable to that obtained on the platereader (Table 2.2).

The steady-state assay described here may be used in a high throughput format to screen a large number of substrates. Peptides with a broad range of specificity constants (TKCVIM, TKCVLA, and TKCVIF) were tested using this assay and were compared with the values measured using the radiometric assay or with dansylated peptides (Table 2.2). Values for k_{cat} were also determined by fitting the Michaelis-Menten equation to the data for each peptide (0.10 ± 0.01 s^{-1} for TKCVIM, 0.08 ± 0.02 s^{-1} for TKCVLA, and 0.0025 ± 0.0003 s^{-1} for TKCVIF). This assay is comparable to the radioactive assay, with a k_{cat}/K_M value for TKCVIM that is slightly higher (100 ± 30 mM^{-1}s^{1} versus 70 ± 20 mM^{-1}s^{-1}) but within error. In general, the values for $k_{cat}/K_M^{peptide}$ measured by the MDCC-PBP/PPiase assay are slightly higher ($\leq$ 2-fold) than the values measured using the dansylated peptide assay. These differences could be due to the dansyl group on the peptides which may decrease the reactivity of these peptides with FTase. This discrepancy may also be explained by slight inhibition by PPi for the radioactive and dansylated peptide assay, which would not occur for the MDCC-PBP/PPiase assay where PPi is removed. Overall, these data demonstrate that the MDCC-PBP/PPiase assay can accurately measure steady-state turnover for peptides with a wide range of rate constants.
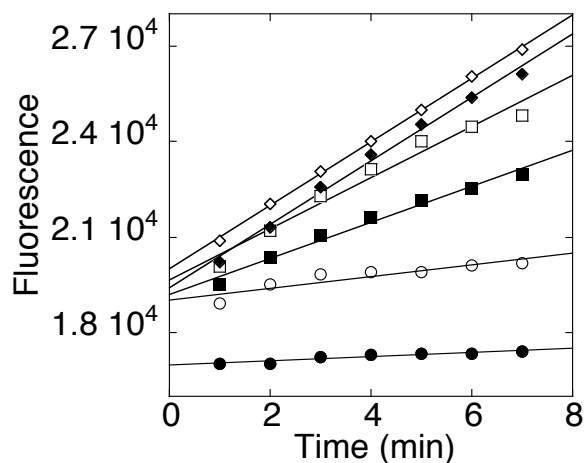
Figure 2.5 Initial velocity for TKCVIM

Initial rates of farnesylation of the peptide TKCVIM measured using the MDCC-PBP/PPiase assay at varying concentrations of peptide: ● 0 μM; ○ 0.5 μM; ■ 0.8 μM; □ 1 μM; ◆ 2 μM; and ◇ 7μM. Fluorescence was measured in 96-well plates, using an excitation wavelength of 430 nm and an emission filter of 450 nm. Final solutions contained 50 nM FTase, 10 μM FPP, 34 units mL^{-1} PPiase, and 5 μM MDCC-PBP in 50 mM Heppso, pH 7.8, 5 mM MgCl$_2$, and 2 mM TCEP.
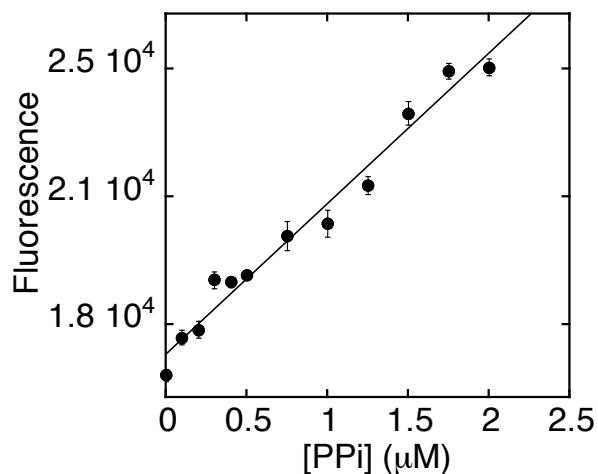
Figure 2.6 PPi standard curve

Standard curve measuring fluorescence change of MDCC-PBP as a function of PPi concentration. Fluorescence was measured in 96-well plates, using an excitation wavelength of 430 nm and an emission filter of 450 nm. Final solutions contained 5 μM MDCC-PBP, 34 units mL^{-1} PPiase, 50 mM Heppso, pH 7.8, 5 mM MgCl$_2$, and 2 mM TCEP.

53
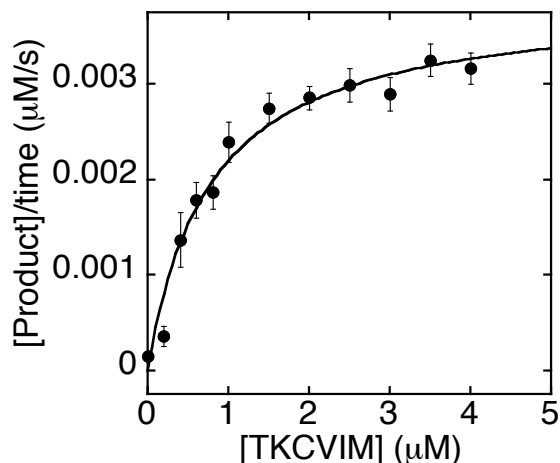
Figure 2.7 Michaelis-Menten plot for TKCVIM

Measurement of farnesylation of TKCVIM catalyzed by FTase under multiple turnover concentrations, under the same conditions as described in Figure 2.5. Initial velocities were determined from a linear fit to the first 10% of the FTase reaction, and converted from fluorescence to product concentration by the Pi and PPi standard curves. The Michaelis-Menten equation was fit to the data to calculate k_{cat} and k_{cat}/K_M.

Table 2.2 Multiple turnover rate constants for peptides catalyzed by FTase [a]

Peptide	k_{cat}/K_M (mM^{-1}s^{-1})		
	MDCC-PBP/PPiase assay	Dansylated peptide assay [c]	Radiometric assay
TKCVIM	100 ± 30 [d] 120 ± 50 [e]	41 ± 3 [b]	70 ± 20
TKCVLA	40 ± 20 [d]	24 ± 2	ND
TKCVIF	2 ± 1 [d]	1.4 ± 0.1	ND

[a] Final solutions contained 50 nM FTase, 10 μM FPP, varying peptide (0-10 μM), 34 units mL^{-1} PPiase, and 5 μM MDCC-PBP in 50 mM Heppso, pH 7.8, 5 mM MgCl$_2$, and 2 mM TCEP. All assays were conducted at 25 ^{0}C.
[b] Data taken from ref. (*77*).
[c] Measurements were taken for the dansylated peptide form.
[d] Measured in fluorescence platereader.
[e] Measured in stopped-flow fluorimeter.
ND = not determined.

Discussion

The dissociation of the farnesylated product has previously been determined to be rate-limiting for steady state turnover catalyzed by FTase, and the binding of additional FPP is required for release of farnesylated product (*89, 92*). However, the timing and rate constant of PPi dissociation in the kinetic pathway has been unclear. The crystal structure of FTase complexed with farnesylated peptide and an additional FPP molecule does not contain bound PPi (*21*). Release of PPi may therefore be required to allow the farnesylated peptide to move into the exit groove and an additional FPP molecule to bind. The fluorescent assay to measure Pi binding by MDCC-PBP, developed by Brune et al. (*141*), has been applied here to measure the rate constant of PPi release by prenyltransferases. These data clearly indicate that PPi dissociation is rapid relative to the formation and dissociation of farnesylated product, contributing little to the steady-state turnover rate constant. Therefore, PPi is released rapidly after the formation of farnesylated peptide and does not bind tightly to the product complex, consistent with the crystal structure (*21*).

Previous methods used to measure prenyltransferase activity have several limitations. The radiometric assay is non-continuous, time-consuming, not amenable to a high throughput assay, and limited by the radiochemical purity of [1-^{3}H]-FPP. High throughput assays have been developed using dansylated peptides; however, these experiments require the synthesis of dansylated peptide libraries which are both expensive and time-consuming, and cannot be used to measure farnesylation of proteins. Both dansyl and biotinyl modifications may also affect binding as well as catalysis for these peptides. The MDCC-PBP/PPiase assay can be used to measure both single and multiple turnover assays rapidly and easily for both peptide and protein substrates. However, the high concentrations of phosphate and diphosphate compounds in cell homogenates complicates the use of this assay for measuring activity in these complex mixtures.

The MDCC-PBP/PPiase assay has been used to measure the single turnover kinetics of GGTase I (*24, 77*). GGTase I is a slower enzyme ($k_{chem} = 0.18$ s^{-1}), and the assay has been used to measure kinetics using GGPP analogs as substrates in addition to

GGPP (Hartman, H.L., and Fierke, C.A., unpublished data). The assay presented here is currently the most comprehensive and general method to assay prenyltransferase activity. It can be applied to a wide range of peptides and even potentially full length proteins as well as substrate analogs, without requiring a radiolabel or any other type of modification. The steady-state assay developed here may greatly facilitate high throughput screening of peptide libraries to identify novel prenyltransferase substrates, as well as inhibitor screens and studies to identify inhibitor targets. In addition, this assay should be readily amenable to the assay of other diphosphate releasing enzymes such as polymerases, ligases, and aminoacyl tRNA synthetases. For example, a general assay to measure diphosphate release using MDCC-PBP coupled with PPiase could potentially be applied to *in vitro* drug screening for replication enzymes of viral pathogens that utilize nucleotide substrates and release diphosphate.

CHAPTER 3
DISSOCIATION OF FARNESYLATED PRODUCT FROM PROTEIN FARNESYLTRANSFERASE [1]

An unusual feature of the reaction mechanism of FTase is that the enzyme rarely exists in its free, unbound form during the catalytic cycle. The kinetic mechanism of FTase is functionally ordered, meaning that either FPP or peptide can bind to the free enzyme, but the reaction only proceeds efficiently if FPP binds first (*83, 92*). The active site zinc ion directly coordinates the cysteine thiolate upon peptide binding to form an unreactive ternary complex. On the basis of structural and mutagenesis studies, a model has been proposed in which the first two isoprene units of FPP rotate to bring the C1 of FPP within reacting distance (2.4 Å) of the peptide thiolate to form a reactive substrate conformation (*88, 94*). After the farnesylated product is formed in the active site, it dissociates very slowly unless a second molecule of substrate binds to stimulate product release. Both FPP and peptide can enhance product dissociation, but FPP is more efficient (*89*). The crystal structure of the FTase•product complex in the absence of Mg^{2+} has been determined, in which the farnesylated product KKKSKTKCVIM lies in an extended conformation in the FTase active site (Figure 3.1A) (*21*). The structure of the FTase•product•FPP complex has also been solved, showing that the product adopts a type I β-turn and the farnesyl group swings out of the active site into the "exit groove," a shallow solvent-accessible hydrophobic groove that extends from the active site to the rim of the β subunit (Figure 3.1B) (*21*). While these crystal structures provide valuable information about the structure of the intermediates in FTase-catalyzed product dissociation, very few kinetic studies have been done to delineate the mechanism of this

---

[1] June Pais wrote this chapter, performed the described experiments, and analyzed the data, with the exception of the kinetic studies of Analogs 5-13, which were performed and analyzed by Yuta Suzuki. All FPP analogs were provided by Thangaiah Subramanian and H. Peter Spielmann at the University of Kentucky.
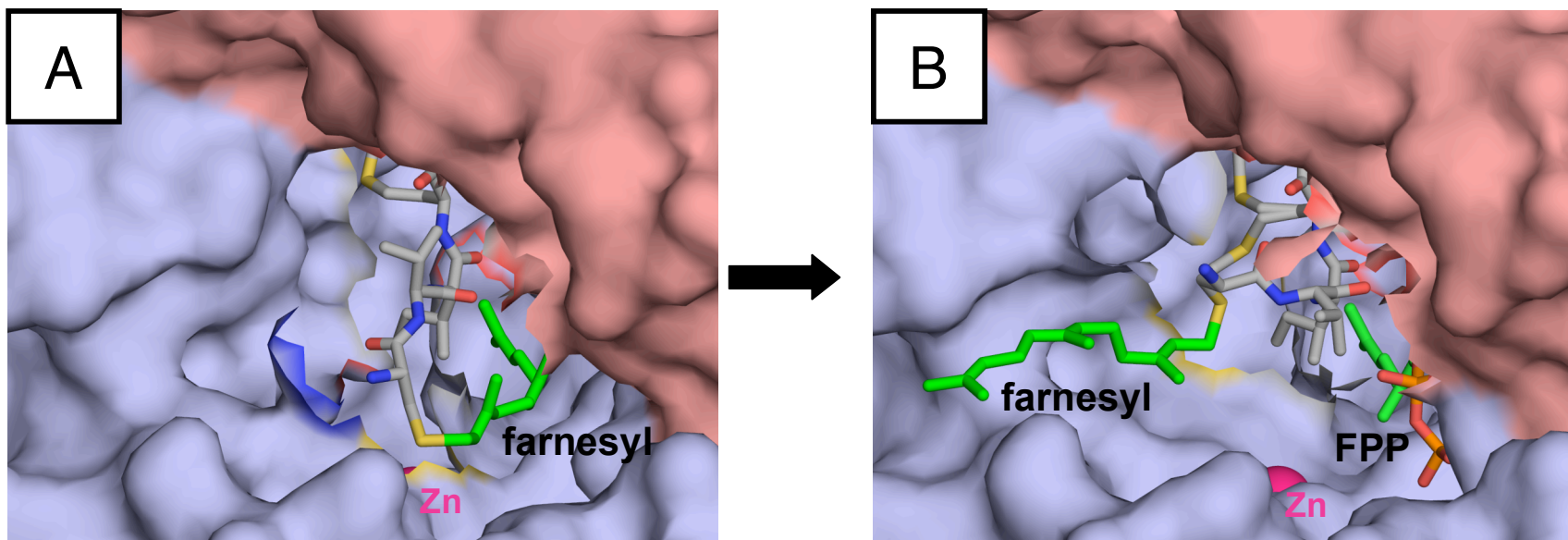
Figure 3.1 FPP-catalyzed product dissociation
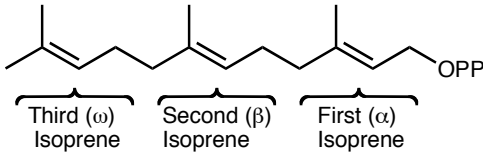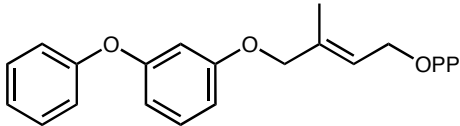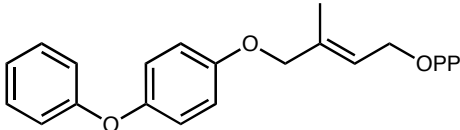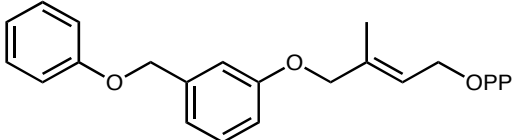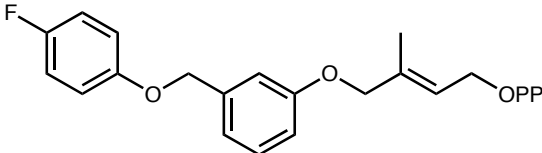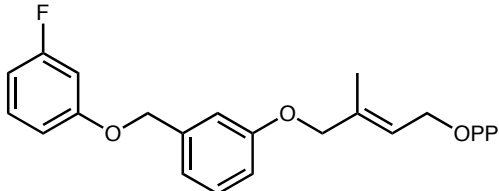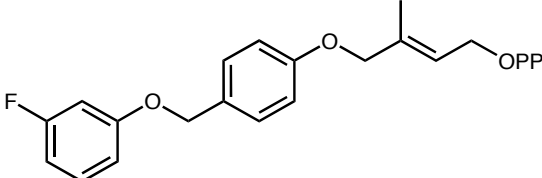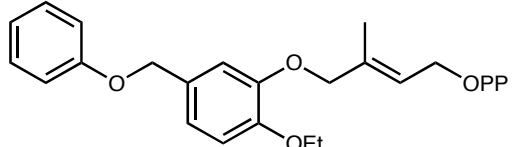
X-ray crystal structure of the FTase active site for (A) the FTase•product complex, formed with FPP and KKKSKTKCVIM (Protein Data Bank code: 1KZP (*21*)); and (B) the FTase•product•FPP complex, where additional FPP has been added to the product complex formed in (A) (Protein Data Bank code: 1KZO (*21*)).   For clarity, the FTase residue K164α is omitted, and only the four terminal amino acids of the peptide substrate are shown.

step which is so crucial for multiple turnovers.

Since FPP is capable of binding to the free enzyme, the FTase•peptide complex and the FTase•product complex, a better understanding of the binding interactions of the active site with FPP is needed and is of particular interest for designing FPP-competitive inhibitors. To further understand the molecular recognition of FPP and the role of the structure of the isoprenoid substrate in facilitating catalysis, a series of FPP analogs was developed by Professor H. Peter Spielmann and coworkers at the University of Kentucky. These compounds are listed in Table 3.1, and vary in the size and electrostatic properties of one, two, or all three isoprene groups. Analogs 1-8 contain aryl substitutions in the second and third isoprene units. The first two isoprene units are thought to undergo a rotational change to form the active substrate conformation during the FTase reaction (*88*). These molecules were therefore designed to probe the conformational rearrangement of FPP and test the steric constraints of the FTase mechanism by varying such things as the addition of fluorine or alkyl substituents, as well as the position of these substituents. In analogs 9 and 10, the first isoprene is replaced by a phenyl moiety, testing the importance of this first isoprene unit in facilitating the FPP conformational change as predicted by crystal structures (*21, 88*). Analog 11 is an analog of anilinogeranyl diphosphate, an efficient FTase substrate, where the terminal isoprene is replaced with a substituted aromatic moiety. Similarly, analog 12 is substituted with a fluorinated phenyl group at the third isoprene while the first two isoprene chains of the FPP structure are retained. The bulkiest compound is analog 13, in which all three isoprenes have been replaced by aryl units. Analog 14 is longer than the other FPP analogs, and was designed as a potential analog of the 20-carbon geranylgeranyl diphosphate (GGPP).
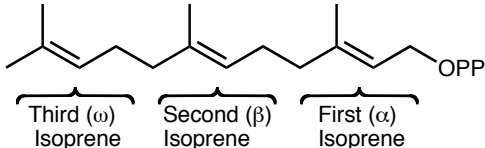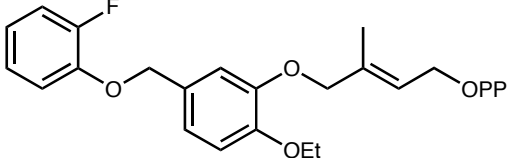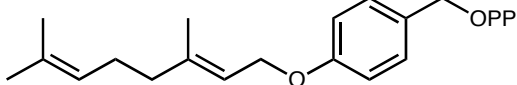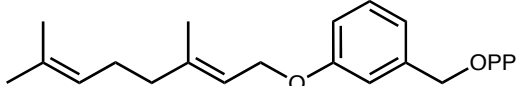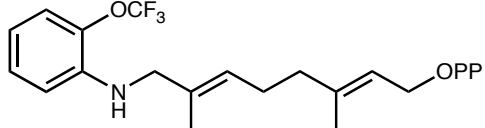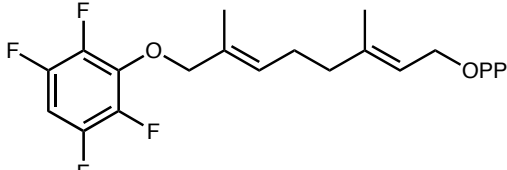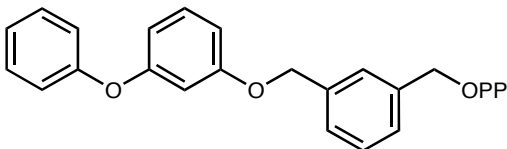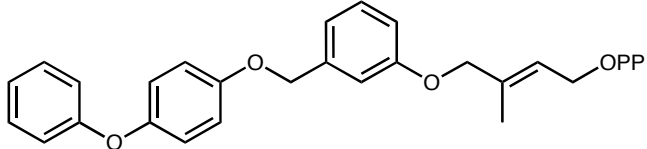
We have characterized the kinetic properties of these analogs and describe unexpected results regarding their effect on catalysis. The steady-state data show that while some analogs are fairly good substrates of FTase, others have reduced k_{cat}/K_M values up to 475–fold. However, the interpretation of steady-state kinetic studies is complicated by the fact that product release is the rate-limiting step at saturating substrate concentrations (*92*). In addition, FPP binds to three species: free FTase, FTase•peptide and FTase•product, the latter of which may be the species that builds up under

Table 3.1 Structures of FPP analogs [a]

Analog	Structure
FPP	
1	
2	
3	
4	
5	
6	
7	

[a] All compounds were synthesized by Thangaiah Subramanian in the laboratory of H. Peter Spielmann at the University of Kentucky.

Table 3.1 (*continued*)   Structures of FPP analogs [a]

Analog	Structure
FPP	
8	
9	
10	
11	
12	
13	
14	

[a] All compounds were synthesized by Thangaiah Subramanian in the laboratory of H. Peter Spielmann at the University of Kentucky.

physiological conditions (*89*). To delineate the different steps of the FTase reaction, we use single turnover kinetics to measure the FPP conformational rearrangement and the chemical step. Unexpectedly, the single turnover rate constant is the same as FPP for all analogs tested. This suggests that the decreased steady-state turnover rate for the analogs most likely reflects the product dissociation step. To directly test this hypothesis, we developed a fluorescent assay to measure FPP-catalyzed product dissociation, which shows that this step is dependent on FPP and Mg^{2+} concentrations. All analogs tested catalyze product dissociation extremely slowly; in contrast, the products formed with these analogs dissociate rapidly when FPP is bound to the E•product complex. These results suggest that the binding of a second molecule of FPP to the FTase•product complex is an essential step in catalysis that may regulate substrate selectivity.

Experimental Procedures

Materials

The peptides TKCVIM, GCVLS and dansylated GCVLS were synthesized and purified by high-pressure liquid chromatography to more than 90% purity by Sigma-Genosys (The Woodlands, TX), and the molecular masses of peptides were confirmed by electrospray mass spectrometry. 7-Diethylamino-3-(((2-maleimidyl)ethyl)amino) carbonyl)coumarin (MDCC) was purchased from Molecular Probes (Eugene, OR). FPP analogs were synthesized in the laboratory of H. Peter Spielmann at the University of Kentucky as previously described (*152, 153*). Farnesyl diphosphate (FPP), purine nucleoside phosphorylase (PNPase), 7-methylguanosine (MEG), and inorganic pyrophosphatase from bakers' yeast (PPiase) were purchased from Sigma-Aldrich (St. Louis, MO). All other chemicals used were reagent grade.

Preparation of MDCC-PBP

The purification and labeling of the A197C phosphate binding protein (PBP) with the coumarin fluorophore MDCC is performed as described in Chapter 2. The final

MDCC-labeled PBP is dialyzed against 50 mM Hepes, pH 7.8, 2 mM TCEP, 0.5 units mL^{-1} purine nucleoside phosphorylase, and 15 μM 7-methylguanosine to form ribose-1-phosphate from any residual phosphate. The low molecular weight species of the "Pi mop" are removed by exchanging the buffer to 50 mM Hepes, pH 7.8, and 2 mM TCEP using Amicon Ultra centrifugal filter devices (10,000 MWCO). The purity of the labeled protein is confirmed by SDS-PAGE. Protein concentration and yield are determined by absorbance at 280 nm using a molecular weight of 35276 g mol^{-1} and a calculated extinction coefficient of 64200 M^{-1}cm^{-1} (*147*), and protein stocks are stored at –80 ^{0}C.

Preparation of WT FTase

Recombinant rat protein FTase expression and purification are carried out in *E. coli* BL21(DE3) FPT/pET23a cells as described previously (*90, 148*). The purified FTase was determined by SDS-PAGE to be >90% pure. The protein is dialyzed at 4 ^{0}C against 50 mM Hepes, pH 7.8, and 2 mM TCEP, and stored at –80 °C. The concentration of FTase is determined by active site titration as previously described (*90*).

Single turnover kinetics

The single turnover rate constant is determined by measuring the release of diphosphate (PPi) using a fluorescently labeled phosphate binding protein (MDCC-PBP) coupled with PPi cleavage by inorganic pyrophosphatase (PPiase), as described in Chapter 2. FTase is preincubated with FPP or analog for >15 minutes at room temperature, and then rapidly mixed with a peptide solution containing MDCC-PBP and PPiase. The final concentrations used are 800 nM FTase, 200 nM FPP/analog, 25 μM peptide, 5 μM MDCC-PBP, 34 units mL^{-1} PPiase, 50 mM Heppso, pH 7.8, 5 mM MgCl$_2$ and 2 mM TCEP. Experiments are conducted at 25 ^{0}C using a KinTek model SF-2001 stopped-flow apparatus (KinTek Corporation, Austin, TX) to detect an increase in fluorescence upon binding of inorganic phosphate to MDCC-PBP (λ_{ex} = 430 nm, λ_{em} = 450 nm Corion LL-450-F cutoff filter). The stopped-flow syringes and mixing chamber are preincubated prior to experiments in buffer containing a "Pi mop" (50 mM Heppso,

pH 7.8, 5 mM MgCl$_2$, 2 mM TCEP, 0.5 units mL^{-1} PNPase and 15 μM MEG). At least five kinetic traces are averaged and the single turnover rate constant (k_{obs}) is determined by fitting Eq. 1 to the data, where Fl is the observed fluorescence at <450 nm at time t, ΔFl is the amplitude, and Fl$_{max}$ is the fluorescence endpoint.

$$Fl = \Delta Fl * e^{-k_{obs}t} + Fl_{max} \qquad \text{Eq. (1)}$$

Steady-state kinetics

The steady-state kinetic parameters k_{cat}, K_M and k_{cat}/K_M are determined from the dependence of the initial velocity on the concentration of FPP or analog at saturating dansylated peptide (dns-GCVLS) concentration. The initial velocity is measured from the time-dependent increase in fluorescence intensity (λ_{ex} = 340 nm, λ_{em} = 520 nm) upon farnesylation of dansylated GCVLS, as described previously (*139, 140, 152*). Reactions are initiated by the addition of FTase (25 nM final concentration) to solutions containing 5 μM dns-GCVLS, varying (1-20 μM) FPP/analog, 50 mM Heppso, pH 7.8, 5 mM MgCl$_2$, and 2 mM TCEP at 25 ^{o}C. The fluorescence intensity over time is measured for the first 10% of the reaction, using a Polarstar Galaxy fluorescence plate reader (BMG Laboratory Technologies, Durham, NC).   The initial velocity of the reaction in fluorescence units s^{-1} (R) is converted to the velocity of the product formed in μM s^{-1} (v) using Eq. 2, where P is the concentration of the limiting substrate and F$_{max}$ is the amplitude in fluorescence measured from the endpoint of each experiment (*152*).

$$v = \frac{R * P}{F_{max}} \qquad \text{Eq. (2)}$$

The values of the steady-state kinetic parameters k_{cat}, K_M, and k_{cat}/K_M are calculated from a fit of the Michaelis-Menten equation to the initial v versus [S] data.

Product dissociation kinetics

A product complex (FTase•farnesyl/analog-dns-GCVLS) is formed by preincubation of equimolar concentrations of FTase (5 μM) and FPP/analog (5 μM) for 15 minutes at 25 ^{o}C followed by addition of an equal concentration of dns-GCVLS (5

µM) and incubation for 1 hour at 25 °C in 50 mM Heppso, pH 7.8, 2 mM TCEP, and 5 mM MgCl$_2$. Measurement of the rate constant for product dissociation is initiated by simultaneous 250-fold dilution and addition of excess FPP/analog (0-200 µM) to stimulate dissociation of product, and unlabeled GCVLS (10 µM) to ensure that FTase does not reassociate with the released dansylated product. The increase in fluorescence intensity (λ_{ex} = 340 nm, λ_{em} = 475 nm) due to dissociation of the dansylated product is monitored as a function of time, using an SLM-Aminco Bowman series 2 luminescence spectrometer with a 1 cm path length. The observed rate constant for product dissociation, k_{pr}, is determined by fitting Eq. 3 to the data where P_t is the fluorescence at time t, and P_∞ is the fluorescence endpoint, which varied from 3-10 (PMT = 700V).

$$\frac{P_t}{P_\infty} = 1 - e^{-k_{pr}*t} \qquad\qquad \text{Eq. (3)}$$

Unlabeled GCVLS at this concentration does not stimulate product dissociation, so that k_{pr} is dependent on the concentration of FPP and a weighted fit of these data to Eq. 4 is used to determine $K_{1/2}^{FPP}$ and $k_{pr}{}^{max}$, the product dissociation rate constant at saturating concentrations of FPP.

$$k_{pr} = \frac{k_{pr}{}^{max}*\left[FPP\right]}{K_{1/2}^{FPP} + \left[FPP\right]} \qquad\qquad \text{Eq. (4)}$$

The magnesium dependence of the product dissociation step was determined by measuring the k_{pr} as a function of Mg^{2+} concentration, maintaining the ionic strength at 0.2 M with NaCl. A weighted fit of Eq. 5 to these data was used to determine the apparent dissociation constant (K_{Mg}), the rate constant for product dissociation at saturating Mg^{2+} concentrations ($k_{max}{}^{Mg}$) and the rate constant for product dissociation in the absence of magnesium (k_0).

$$k_{pr} = \frac{k_{max}{}^{Mg}}{1 + K_{Mg}/\left[Mg^{2+}\right]} + k_0 \qquad\qquad \text{Eq. (5)}$$

Results

Reactivity of FPP substrate analogs

The FPP analogs depicted in Table 3.1 introduce a number of different alterations in the structure and functionality of the FPP molecule. To determine the effect of these substitutions on the chemistry of the FTase reaction, we measured the single turnover rate constant using the MDCC-PBP/PPiase fluorescent assay described in Chapter 2. Surprisingly, the observed rate constant under single turnover conditions (k_{obs}) for all of the FPP analogs is very similar to that measured with FPP (Table 3.2). Kinetic isotope effects experiments (described in Chapter 5) have demonstrated that both the chemical farnesylation step and the FPP rotational rearrangement to form the active substrate conformation can contribute to the observed single turnover rate constant. To delineate the rate constants for these two steps, reactivity was measured for two peptides, GCVLS and TKCVIM, where the rate-limiting step changes from the conformational rearrangement (GCVLS) to farnesylation (TKCVIM), as described in Chapter 5. The observed single turnover rate constants are the same as FPP for both peptides, indicating that these analogs affect neither the conformational change nor the chemical steps (Table 3.2). Additional experiments measuring reactivity for several of these analogs with TKCVIF, a peptide that is farnesylated slowly (k_{obs} = 0.27 s^{-1}), confirm that the single turnover rate constant is unchanged for a variety of peptide substrates (Table 3.2).

To determine the effect of the FPP analog substitutions on multiple turnover kinetics catalyzed by FTase, the steady-state kinetic parameters for reaction of all of the analogs with dansylated GCVLS (dns-GCVLS) were measured using a fluorescent assay (*139, 140, 152*). Representative Michaelis-Menten plots for FPP, a moderate substrate (analog 6), and a poor substrate (analog 8) are shown in Figure 3.2. The k_{cat}/K_M value for each of these compounds is 1.9 x 10^5 M^{-1}s^{-1}, 3 x 10^4 M^{-1}s^{-1}, and 4 x 10^2 M^{-1}s^{-1}, respectively. Unlike the single turnover kinetics, these studies reveal a wide range of reactivity for the group of analogs studied (Table 3.2). The steady-state rate constant k_{cat}/K_M is termed the "specificity constant" and can be used to determine how efficiently the FPP analog is transferred to the peptide. For this group of analogs, the value of k_{cat}/K_M decreases up to 475-fold, much more than the changes observed in the single

Table 3.2 Kinetic constants of FPP analogs [a]

Analog	k_{cat} (s^{-1}) [b]	K_M (µM) [b]	k_{cat}/K_M (M^{-1}s^{-1}) [b]	k_{obs} (s^{-1}) [c]		
				GCVLS	TKCVIM	TKCVIF
FPP	0.287 ± 0.008	1.5 ± 0.2	$(1.9 \pm 0.3) \times 10^5$	3.4 ± 0.01	6.5 ± 0.01	0.26 ± 0.01
1	0.030 ± 0.002 [d]	0.8 ± 0.08 [d]	$(4.3 \pm 0.5) \times 10^4$ [d]	3.3 ± 0.01	5.6 ± 0.01	0.21 ± 0.01
2	0.200 ± 0.008 [d]	2.3 ± 0.1 [d]	$(4.3 \pm 0.3) \times 10^4$ [d]	2.7 ± 0.01	4.7 ± 0.01	0.22 ± 0.01
3	0.0167 ± 0.0003	0.55 ± 0.09	$(3.0 \pm 0.5) \times 10^4$	3.7 ± 0.01	6.0 ± 0.01	0.28 ± 0.01
4	0.05 ± 0.01 [d]	9.2 ± 0.3 [d]	$(5 \pm 1) \times 10^3$ [d]	2.6 ± 0.01	4.3 ± 0.01	0.24 ± 0.01
5	0.22 ± 0.04	5 ± 2	$(4 \pm 2) \times 10^4$	3.4 ± 0.01	5.3 ± 0.01	ND
6	0.12 ± 0.01	5 ± 2	$(3 \pm 1) \times 10^4$	3.5 ± 0.01	5.2 ± 0.01	ND
7	> 0.05 [e]	> 15 [e]	$(1.4 \pm 0.2) \times 10^3$	3.9 ± 0.01	6.2 ± 0.01	ND

[a] Data for analogs 5-13 were collected and analyzed by Yuta Suzuki.
[b] Unless otherwise noted, steady-state experiments were done by Yuta Suzuki using the dansylated peptide assay. Final solutions contained 25 nM FTase, 5 µM dns-GCVLS, varying (1-20 µM) FPP/analog, 50 mM Heppso, pH 7.8, 5 mM MgCl$_2$, and 2 mM TCEP. Assays were conducted at 25 ^{0}C.
[c] Single turnover rate constant, measured using MDCC-PBP/PPiase assay on stopped-flow fluorimeter. Final solutions contained 400 nM FTase, 100 nM FPP/analog, 25 µM peptide, 5 µM MDCC-PBP, 34 units mL^{-1} PPiase, 50 mM Heppso, pH 7.8, 5 mM MgCl$_2$, and 2 mM TCEP. Assays were conducted at 25 ^{0}C.
[d] Measured by H.P. Spielmann and coworkers.
[e] Michaelis-Menten plot was linear up to 20 µM analog, so k_{cat}/K_M was calculated from the slope of the line.
ND = not determined.

Table 3.2 *(continued)* Kinetic constants of FPP analogs [a]

Analog	k_{cat} (s^{-1}) [b]	K_M (μM) [b]	k_{cat}/K_M (M^{-1}s^{-1}) [b]	k_{obs} (s^{-1}) [c]		
				GCVLS	TKCVIM	TKCVIF
FPP	0.287 ± 0.008	1.5 ± 0.2	(1.9 ± 0.3) x 10^5	3.39 ± 0.01	6.48 ± 0.02	0.26 ± 0.01
8	0.00130 ± 0.00009	3.1 ± 0.8	(4 ± 1) x 10^2	3.88 ± 0.01	6.13 ± 0.02	ND
9	0.053 ± 0.002	0.5 ± 0.1	(1.1 ± 0.2) x 10^5	3.85 ± 0.01	5.75 ± 0.02	ND
10	0.0031 ± 0.0001	0.2 ± 0.1	(1.5 ± 0.8) x 10^4	3.73 ± 0.01	6.21 ± 0.02	ND
11	0.00215 ± 0.00005	0.49 ± 0.08	(4.3 ± 0.7) x 10^3	3.84 ± 0.01	5.98 ± 0.02	ND
12	0.43 ± 0.01	6.0 ± 0.7	(7.2 ± 0.9) x 10^4	3.70 ± 0.01	5.21 ± 0.02	ND
13	0.049 ± 0.001	0.2 ± 0.1	(3 ± 1) x 10^5	3.92 ± 0.02	6.21 ± 0.02	ND
14	ND [d,e]	ND [d,e]	ND [d,e]	3.72 ± 0.01	6.16 ± 0.02	0.29 ± 0.01

[a] Data for analogs 5-13 were collected and analyzed by Yuta Suzuki.
[b] Unless otherwise noted, steady-state experiments were done by Yuta Suzuki using the dansylated peptide assay. Final solutions contained 25 nM FTase, 5 μM dns-GCVLS, varying (1-20 μM) FPP/analog, 50 mM Heppso, pH 7.8, 5 mM MgCl$_2$, and 2 mM TCEP. Assays were conducted at 25 ^{0}C.
[c] Single turnover rate constant, measured using MDCC-PBP/PPiase assay on stopped-flow fluorimeter. Final solutions contained 400 nM FTase, 100 nM FPP/analog, 25 μM peptide, 5 μM MDCC-PBP, 34 units mL^{-1} PPiase, 50 mM Heppso, pH 7.8, 5 mM MgCl$_2$, and 2 mM TCEP. Assays were conducted at 25 ^{0}C.
[d] Measured by H.P. Spielmann and coworkers.
[e] Reaction was too slow to measure by steady-state assay.
ND = not determined;
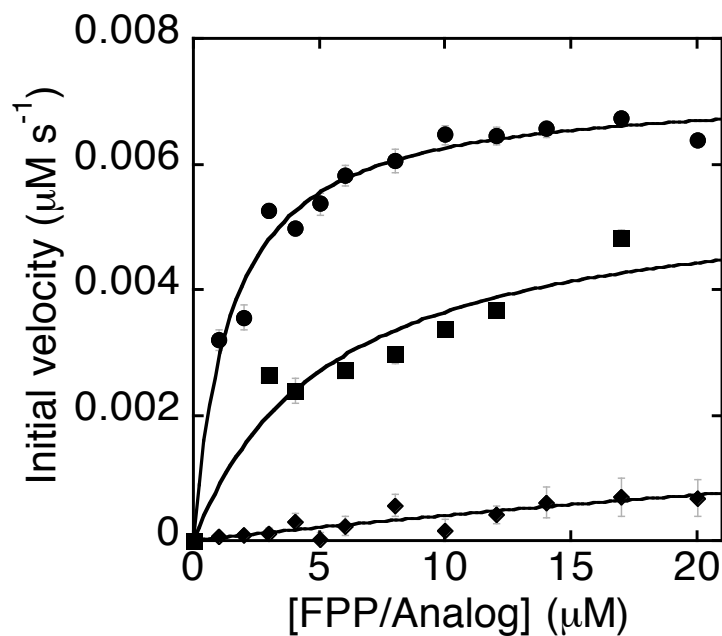
Figure 3.2 Steady-state turnover for FPP analogs

The initial velocity for the reaction of dns-GCVLS with FPP (●), analog 6 (■) and analog 8 (◆) was measured from the time dependent change in fluorescence (λ_{ex} = 340 nm; λ_{em} = 520 nm). Final reactions contained 25 nM FTase, 5 μM dns-GCVLS, varying (1-20 μM) FPP/analog, 50 mM Heppso, pH 7.8, 5 mM $MgCl_2$ and 2 mM TCEP. The Michaelis-Menten equation was fit to the data to determine k_{cat}, K_M and k_{cat}/K_M, listed in Table 3.2. Data were collected and analyzed by Yuta Suzuki.

turnover rate constant. An analysis of the steady-state parameters k_{cat} and K_M reveals that k_{cat} decreases for all analogs, 1.3- to 220-fold, while the value of K_M varies from 0.2-9.2 μM, which are within a 7.5-fold difference from FPP ($K_M = 1.5 \mu$M). The decreases in k_{cat} roughly follow the same trends observed for k_{cat}/K_M.

Analogs 9, 12 and 13 are surprisingly very good substrates, with values of k_{cat}/K_M (1.1×10^5 M^{-1}s^{-1}, 7.2×10^4 M^{-1}s^{-1}, and 3×10^5 M^{-1}s^{-1}, respectively) that are within a factor of 3 of the value for FPP (1.9×10^5 M^{-1}s^{-1}). Most analogs show a moderate (~ 4-13 fold) decrease in k_{cat}/K_M values, ranging from 1.5×10^4 M^{-1}s^{-1} to 5×10^4 M^{-1}s^{-1}. These include analogs 1-3, 5, 6 and 10. The compounds that show the most dramatic decreases in k_{cat}/K_M are analogs 4, 11, 7 and 8, with respective values of 5.0×10^3 M^{-1}s^{-1}, 4.3×10^3 M^{-1}s^{-1}, 1.4×10^3 M^{-1}s^{-1}, and 4×10^2 M^{-1}s^{-1}, corresponding to 38-, 44-, 135- and 475-fold reductions when compared with FPP. Analog 14 reacts very slowly and its steady-state parameters could not be determined (data from Spielmann lab, not shown).

Product dissociation assay

Under multiple turnover conditions for FTase, k_{cat} is proposed to reflect product release (*92*). To verify that the FPP analogs alter the rate constant for product dissociation, we developed a fluorescent assay to directly measure FPP-catalyzed product dissociation from the FTase•product complex. The E•product complex is formed by reacting equimolar concentrations of FTase, FPP, and dansylated GCVLS, and then diluted into an assay containing excess FPP to stimulate product dissociation, and unlabeled peptide to ensure that FTase does not reassociate with the released dansylated product. The increase in fluorescent intensity due to dissociation of the dansylated, farnesylated peptide is monitored as a function of time (Figure 3.3A). In the absence of added FPP, the dissociation rate constant is not measurable using this assay (Figure 3.3A). However, addition of FPP increases the apparent dissociation rate constant to a maximum value (k_{pr}^{max}) of 0.004 ± 0.001 s^{-1}, with a $K_{1/2}^{FPP}$ of 22.3 ± 0.2 μM for WT FTase at 25 ^{0}C (Figure 3.3B). These data are consistent with previous work showing that FPP can enhance product release with a k_{off} value of 0.002 s^{-1} at 10 μM FPP and 10 ^{0}C (*89*). However, this value for the product dissociation rate constant is much lower than the
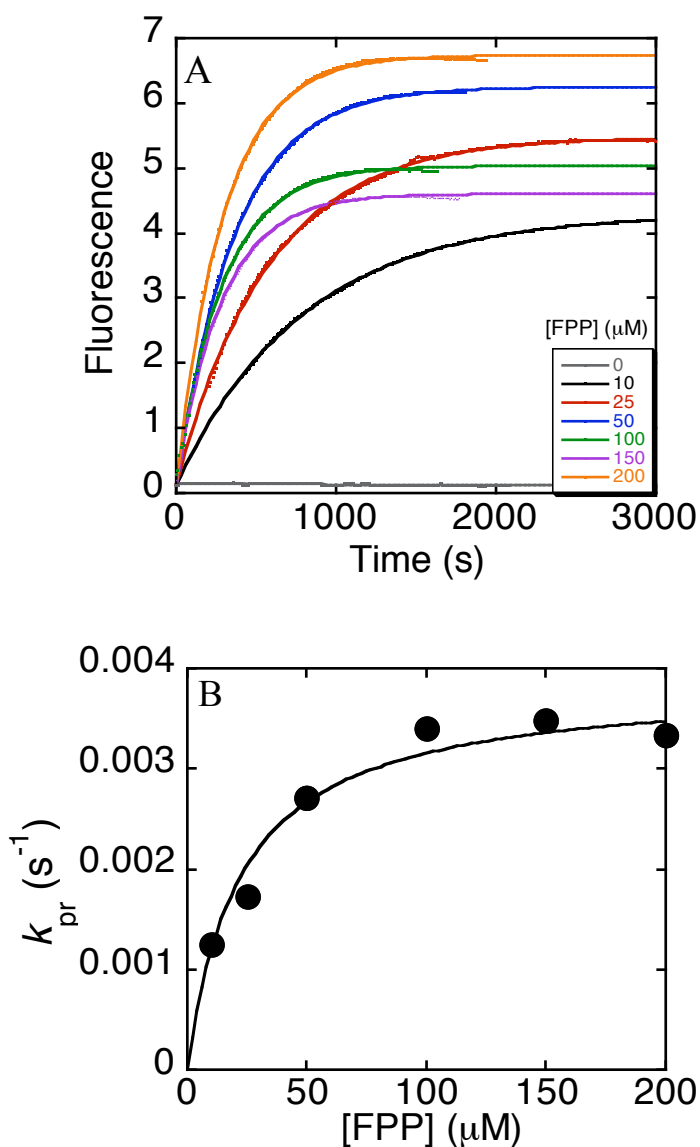
Figure 3.3 FPP-catalyzed product dissociation

(A)The product dissociation rate constant was measured for the E•product complex (FTase•F-dns-GCVLS) after mixing with additional FPP from an increase in fluorescence as described in the Experimental Procedures. The E•product complex was formed by incubating 20 nM FTase, 20 nM FPP, and 20 nM dns-GCVLS in 50 mM Heppso, pH 7.8, 2 mM TCEP, and 5 mM MgCl$_2$ at 25 ^{0}C for 1 hour. Product dissociation was initiated by subsequent dilution (250-fold) into buffer containing FPP (0-200 μM) and 10 μM unlabeled GCVLS. Eq. 3 was fit to the data to determine k_{pr}, the rate constant for product dissociation. (B) The dependence of k_{pr} on [FPP] was measured and Eq. 4 was fit to the data to determine a $K_{1/2}^{FPP}$ of 22.3 ± 0.2 μM and a k_{pr}^{max} of 0.004 ± 0.001 s^{-1}.

value for k_{cat} measured by the steady-state assay with dansylated peptide (Table 3.2), suggesting significant differences between these two assays that affect the observed rate constant for product release.

The dependence of the product dissociation rate constant on Mg^{2+} has also been measured (Figure 3.4). Eq. 5 was fit to these data and a K_{Mg} value of 0.5 ± 0.01 mM was calculated. The rate constant for product dissociation in the absence of Mg^{2+} (k_0) is $(9.0 \pm 0.3) \times 10^{-4}$ s^{-1}, and the rate constant at saturating Mg^{2+} ($k_{max}{}^{Mg}$) is 0.0142 ± 0.0001 s^{-1}. Thus product dissociation is enhanced 15-fold by saturating Mg^{2+} concentrations. Mg^{2+} ions could either facilitate the binding of FPP to the E•product complex or enhance the rate constant for the farnesyl moiety of the product moving from the catalytic groove to the exit groove. Similar to the K_M for FPP, which probably reflects the binding of FPP to the E•product complex, the apparent K_{Mg} of 2 mM measured under steady-state turnover reflects Mg^{2+} binding to both the E•product and the E•FPP complexes (*106*).

Product dissociation of FPP analogs

We next analyzed the dissociation rate constant for the farnesylated product in the presence of the FPP analogs, and observed no change in fluorescence consistent with product dissociation during a two hour incubation (Table 3.3). The only fluorescence increase was observed for the addition of analog 2 at a concentration of 100 μM, and the observed rate constant was still 10-fold lower than what was observed for FPP at only 50 μM (Table 3.3). Therefore, the E•product complexes formed are very stable and the product is released extremely slowly. This result indicates that alteration of the FPP structure could increase the affinity of FTase for the product, hinder the movement of the product into the exit groove and its subsequent release, or affect the binding of the second substrate molecule to the E•product complex to catalyze product dissociation. To distinguish between these possibilities, the E•product complex was formed with the analog, and FPP was added to see if product dissociation could be observed. The dissociation of product from the E•product complexes formed with analogs can be stimulated by the addition of 50 μM FPP with a rate constant similar to that measured for the E•product complex formed with FPP. These data imply that the slow observed
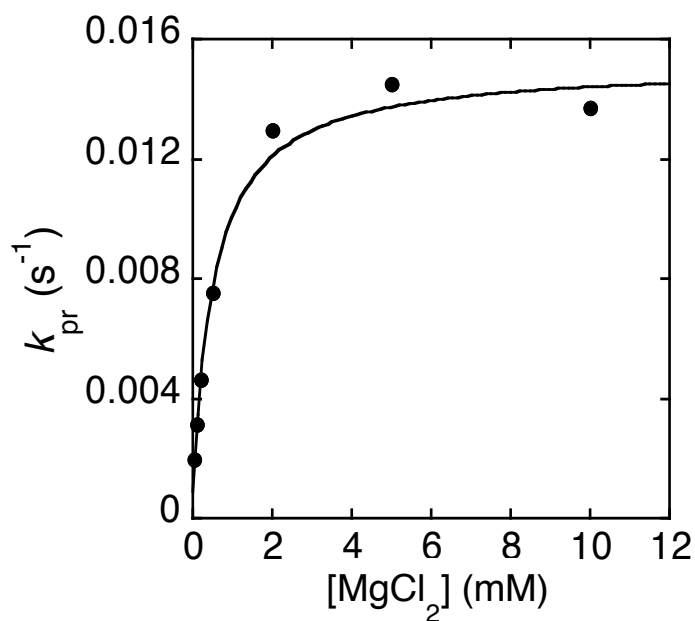
Figure 3.4 Effect of Mg^{2+} on the product dissociation rate constant

The product dissociation rate constant was measured as described in the legend of Figure 3.3 at varying (0-10 mM) MgCl$_2$ concentrations. Final solutions contained 20 nM FTase•F-dns-GCVLS, 150 μM FPP, and 10 μM unlabeled GCVLS in 50 mM Heppso, pH 7.8 and 2 mM TCEP. The ionic strength was maintained at 0.2 M with NaCl. A weighted fit of Eq. 5 to the data was used to determine a K_{Mg} value of 0.55 ± 0.01 mM, a k_0 value of $(9.0 \pm 0.3) \times 10^{-4}$ s^{-1}, and a k_{max}^{Mg} value of 0.0142 ± 0.0001 s^{-1}.

product dissociation for the analogs is due to the inability of the FPP analogs to bind to the E•product complex and facilitate product dissociation (Table 3.3). Figure 3.5 compares the ability of analog 2 and FPP to catalyze product dissociation. When 50 μM analog 2 is added to the E•product complex formed with analog 2, no fluorescence increase is observed. However, the addition of 50 μM FPP to the same product complex results in product dissociation with an observed rate constant (0.0026 s^{-1}) identical to that observed for the E•product complex formed with FPP (Figure 3.5).   Similar results were observed for all analogs tested (analogs 1-4 and 14), where the product dissociation was "rescued" by the addition of FPP to the E•product complex (Table 3.3).

Discussion

FPP-catalyzed product dissociation

The farnesylated product dissociates from FTase extremely slowly unless additional substrate is available to bind to the product complex (*89, 92*). However, the binding affinity of the farnesylated product for FTase ($K_D^{product} = 0.78$ μM) is weaker than either of the substrates for FTase ($K_D^{peptide} = 4$ μM; $K_D^{FPP} = 10$ nM) (*89*). These data suggest that product dissociations require two steps: a slow conformational change and a diffusion-controlled release of product from FTase (Scheme 3.1). The conformational rearrangement of the product in the active site has been confirmed by the crystal structures of the FTase•product and the FTase•product•FPP complexes, in which the product rotates into a hydrophobic "exit groove" when additional FPP is bound in the catalytic site (Figure 4.1) (*21*).   We propose that the favored conformation of the farnesylated product in the absence of additional FPP is in the catalytic site. The binding of FPP in the catalytic site "captures" the product in the exit groove, thereby facilitating subsequent product dissociation (Scheme 3.1).

The analogs in this study introduce many alterations into the FPP structure, but are still efficient single turnover substrates for FTase. Because farnesylation is not altered for these analogs, it is likely that they bind to the catalytic site of FTase in a similar manner to FPP for the first turnover. Therefore, the different reactivities

Table 3.3 Product dissociation kinetics for FPP analogs

Analog	k_{pr} (min^{-1}) [a] 50 μM analog	k_{pr} (s^{-1}) [b] 50 μM FPP
FPP	0.0026 ± 0.0001	0.0026 ± 0.0001
1	[c]	0.0037 ± 0.0001
2	~0.00012 [c,d]	0.0026 ± 0.0001
3	[c]	0.0054 ± 0.0001
4	[c]	0.0044 ± 0.0001
14	[c]	0.0034 ± 0.0001

[a] Measured using dansylated product dissociation assay at 25 ^{0}C. A 1 mL solution containing the pre-formed product complex, FTase•analog•dns-GCVLS (5 μM, in a 1:1:1 ratio), in 50 mM Heppso, pH 7.8, 5 mM MgCl$_2$, and 2 mM TCEP was incubated for 1 hr at 25 ^{0}C and then 4 μL of a solution containing FPP analog (50 μM final concentration) and GCVLS (10 μM final concentration) in the same buffer was added.
[b] Measured using dansylated product dissociation assay as described above, except that 50 μM FPP was added rather than FPP analog to catalyze dissociation of pre-formed product. Eq. 3 was fit to the data to determine k_{pr}.
[c] No fluorescence increase was observed after 2 hours.
[d] The k_{pr} value measured at 100 μM analog 2 was 0.00023 ± 0.00001 s^{-1}.
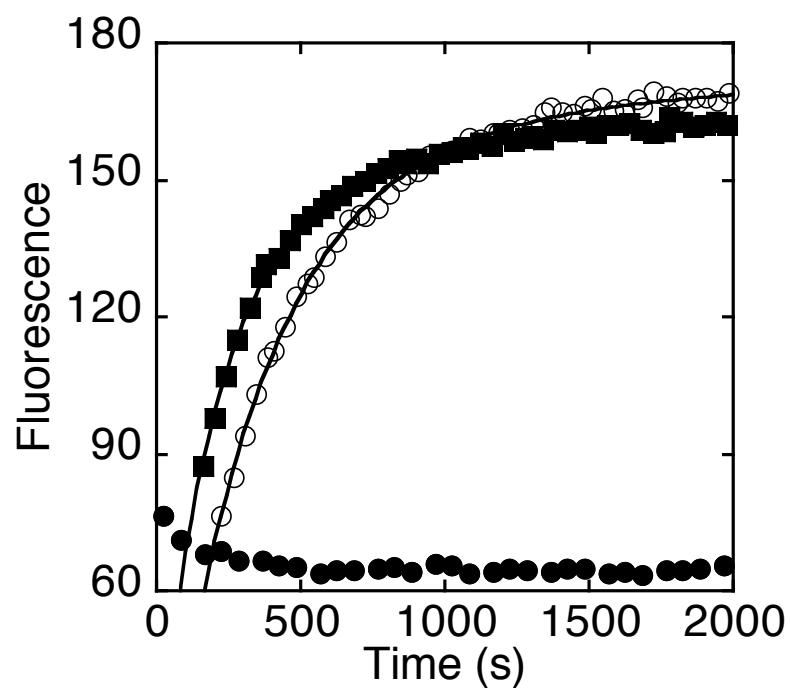
Figure 3.5 Product dissociation of analog 2

Dissociation of dansylated product, as measured by a fluorescent increase as described in the legend of Figure 3.2, from an FTase•F-dns-GCVLS product complex catalyzed by 50 μM FPP (■), and an FTase•analog 2-dns-GCVLS product complex catalyzed by 50 μM analog 2 (●) or 50 μM FPP (○). Final solutions contained 5 μM FTase•FPP/analog-dns-GCVLS (1:1:1), 50 μM FPP/analog, 10 μM unlabeled GCVLS, 50 mM Heppso, pH 7.8, 5 mM MgCl$_2$, and 2 mM TCEP. Eq. 3 is fit to the curves to obtain k_{pr}, the observed rate constant for product dissociation.
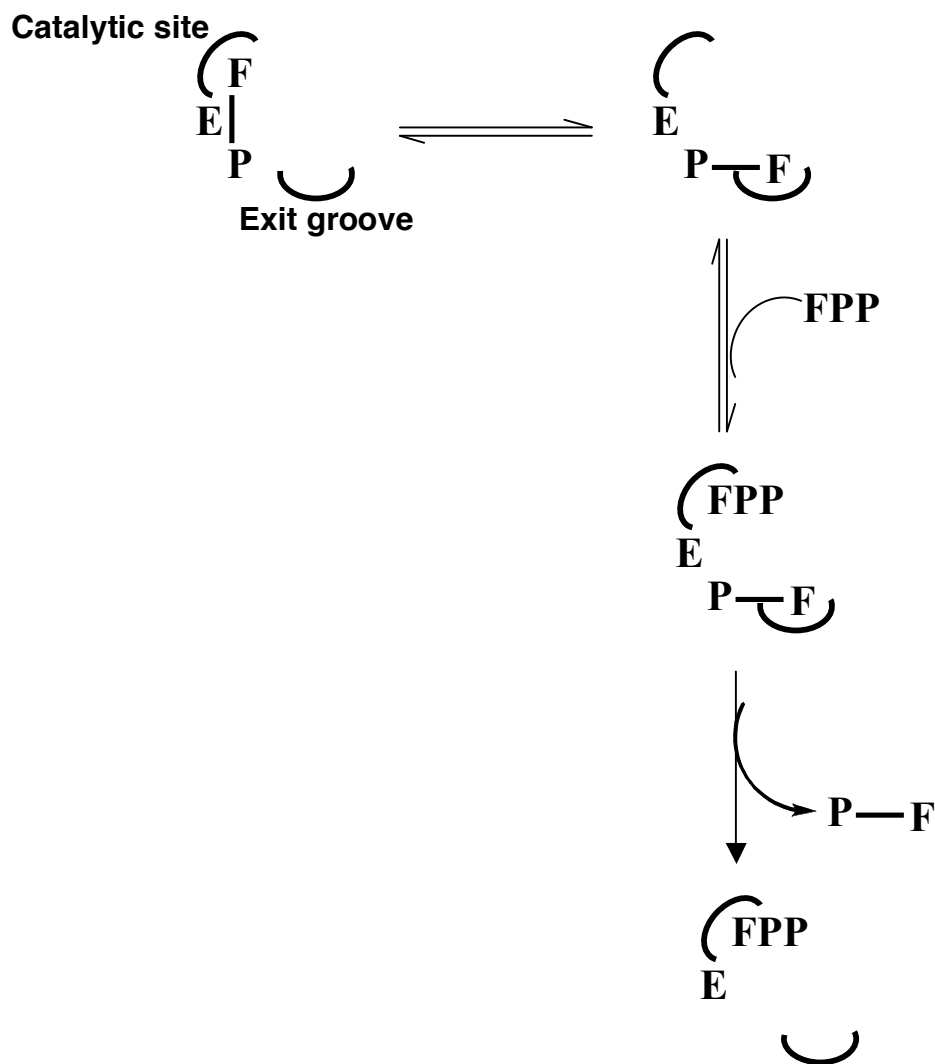
Scheme 3.1 Product dissociation mechanism for FTase

In the E•product complex, the farnesyl group (F) of the product (P-F) can bind in either the catalytic site or the exit groove, but the product is only released when it is bound in the exit groove. FPP competes with the product for the catalytic site and captures the product in the exit groove, thereby facilitating the dissociation of product.

measured under multiple turnovers is most likely due to the ability of the second substrate molecule to bind FTase and release product. The product dissociation data presented here suggest that the analogs bind to the E•product complex in a site other than the catalytic FPP-binding site. The simplest model is that they bind preferentially to the exit groove, thereby trapping the product in the catalytic site (Scheme 3.2). This model suggests that FPP has a higher affinity for the catalytic site of the E•product complex, while the FPP analogs have a higher affinity for the exit groove.

It is also possible that FPP binds first in a separate site and then the product rearranges to its observed position in the exit groove, followed by movement of the FPP to the binding site observed in the crystal structure. In this scenario, FTase catalyzes transfer of each of these analogs to peptide substrates efficiently during the first turnover, and the product is released from the enzyme when FPP binds to this alternate site. The binding of the analogs to this alternate site is adversely affected by alterations in the isoprenoid structure, explaining the differences in reactivity for the FPP analogs observed in multiple turnover and product dissociation studies. However, this model requires a third binding site and suggests additional conformational rearrangements.

FPP analogs

Many of the compounds synthesized in this study were designed to see how sensitive the FPP binding site and the FTase reaction are to alterations in structure, particularly at the second isoprene. Unexpectedly, the enzyme does not appear to be very selective and catalyzes the reaction for all substrates tested, regardless of steric constraints. The conformational rearrangement of FPP prior to farnesylation is proposed to involve rotation of the first two isoprene units of FPP (*88*), and it was therefore surprising that the substitutions introduced into the molecule do not appear to hinder this movement. The catalytic step that does exhibit selectivity, rather, is the binding of the isoprenoid to the E•product complex to facilitate product dissociation.

Some features of the FPP molecule that are important to this step of catalysis are illuminated by comparing the values for k_{cat}/K_M, the "specificity constant," for these analogs. The most striking results are the k_{cat}/K_M values for analogs 7 and 8, which are

Catalytic site

F
E|
P

Exit groove

Analog (APP)

F
E|
P   APP

E

P—F

FPP

FPP
E

P—F

P—F

FPP
E
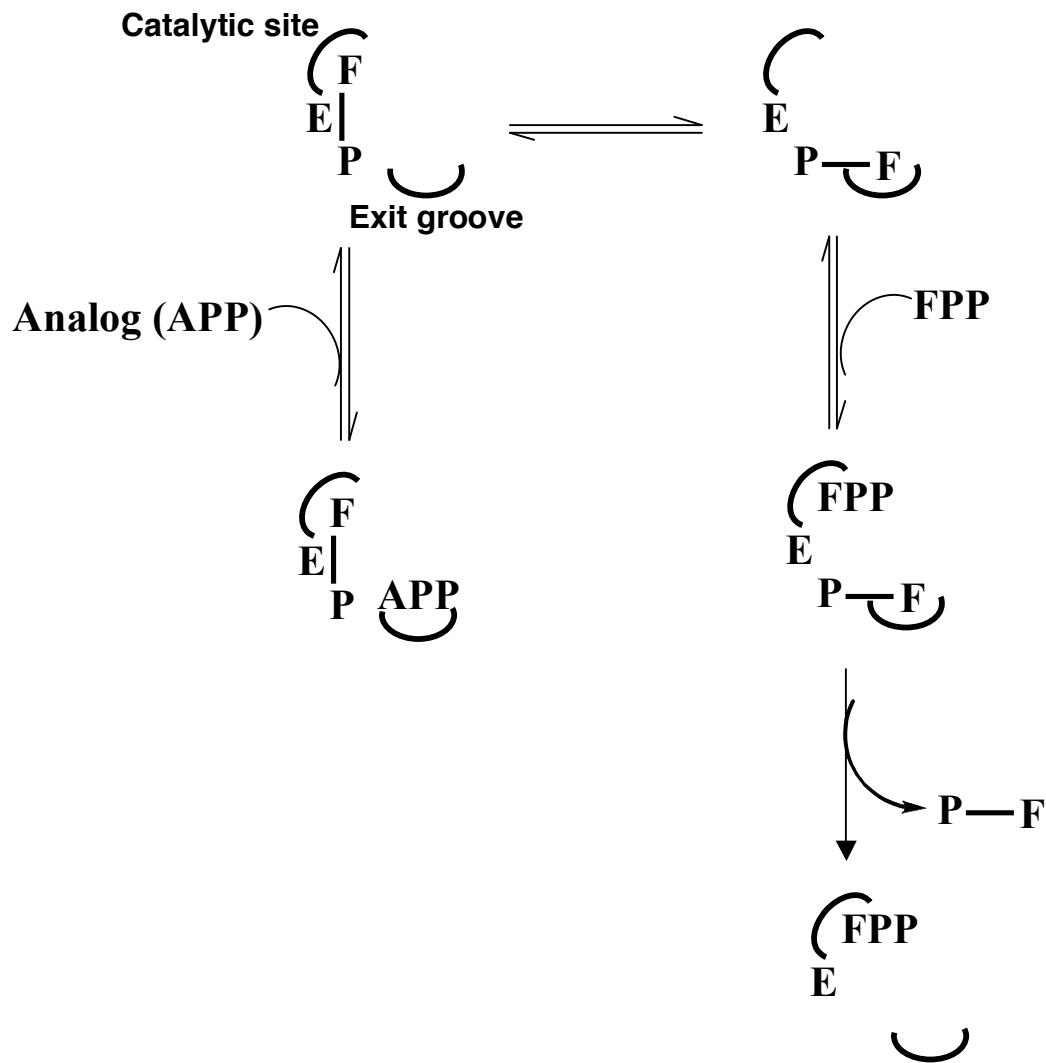
Scheme 3.2 Inhibition of product dissociation by FPP analogs

As described in Scheme 3.1, FPP preferentially binds to the catalytic site of the E•product complex, where the farnesyl group is in the exit groove and product dissociation is favored. The FPP analogs (APP), on the other hand, preferentially bind to the exit groove, trapping the product in the catalytic site and inhibiting product dissociation.

decreased 135 and 475-fold, respectively, compared to FPP. Both analogs contain an ethoxy substituent on the aryl ring at the second isoprene of the molecule, identifying this region as the site of a potentially important interaction between the FPP molecule and the active site of FTase. The addition of an electron-withdrawing fluorine atom on the phenyl ring at the third isoprene in analog 8 further reduces the reactivity relative to analog 7, indicating that this site of the molecule may also be important. The development of additional analogs which introduce different functional groups at these particular positions will shed light on whether this is primarily a steric, hydrophobic or electrostatic effect.

A comparison of analogs 9 and 10 indicate the importance of the correct positioning of the diphosphate group. Analog 9, in which the PPi is *para* to the isoprenyl ether substituent, is a very good substrate, with k_{cat}/K_M values almost the same as FPP. The PPi is in the *meta* position in analog 10, resulting in a 13-fold decrease in k_{cat}/K_M. In Chapter 5, we describe how the PPi moiety is important in facilitating the conformational rearrangement of FPP (*88, 90*). Here we show that the diphosphate must also be involved in FPP-catalyzed product dissociation by making important interactions with the E•product complex. Studies of FPP analogs with modified diphosphate moieties have demonstrated that the diphosphate bridging oxygen of FPP, and the oxygen bound to the C1 of the FPP substrate are both important for enhancing the dissociation rate constant for the farnesylated peptide (*151*). The single turnover rate constant and the binding affinity of these analogs were unchanged, while the rate constants for product release were significantly slower than FPP. Together, these results suggest that interactions of the diphosphate moiety of the second FPP molecule are important for FPP-catalyzed product dissociation.

Analogs 13 and 14 are the two largest molecules tested, but yield very different results. Analog 13 is surprisingly a very good substrate, despite containing phenyl substitutions instead of three isoprene units. Analog 14, on the other hand, is such a slow substrate that its reactivity cannot be measured under multiple turnover conditions. This analog, designed as a GGPP analog, is longer than the other substrates and it is probably the added length which prevents product dissociation. Interestingly, analog 14 is still a good single turnover substrate, indicating that the position of the C1 of the analog must

be in a similar position to the C1 of FPP. FTase binds GGPP and GPP almost as tightly as FPP, but transfers the prenyl group much more slowly to peptides under multiple turnover conditions (*71, 83*). It will be interesting to determine the effect of isoprenoid length on the single turnover rate constant and on product dissociation by comparing reactivity for GGPP (a 20-carbon isoprenyl diphosphate), geranyl diphosphate (10 carbons), and isopentenyl diphosphate (5 carbons). A comparison of the steady-state kinetics for these substrates with the single turnover kinetics and direct product dissociation measurements described here may provide interesting information regarding the mechanism of isoprenoid substrate selectivity for FTase.

While the product dissociation step does discriminate between these different compounds, many analogs were surprisingly good substrates, even under multiple turnover conditions. FTase, then, is fairly tolerant in the structure of the substrates that it will transfer to peptides. For example, analog 13 contains three phenyl moieties in place of the isoprene units, and is still transferred efficiently to peptide substrates. While this may seem surprising at first, many compounds designed as inhibitors of FTase have unexpectedly turned out to be substrates for FTase (*117*). Many of these studies suggest that the crystal structures of FPP illustrating interactions in the inactive ternary complexes cannot be used to predict reactivity of FPP analogs. For example, a series of analogs containing substitutions in the 7-position of FPP were predicted to interact with the a_2 position of the Ca_1a_2X peptide and modulate substrate specificity (*129*). While these compounds do exhibit differences in sequence specificity, the results do not correlate with the a_2 position (*129*). The crystal structure of the E•product complex may be more helpful than ternary complexes in making predictions about the substrate specificity of FTase (*21*). The determination of the crystal structure with an inhibitor bound to the E•product complex would be most valuable, and would confirm the binding site of the second substrate molecule for compounds that may bind in the exit groove.

Implications for substrate specificity and cellular regulation

The role of product dissociation in modulating specificity for the isoprenoid substrate may have implications for specificity in a cellular context. While the enzyme

does not seem to discriminate when binding and transferring alkyl groups to peptide substrates, the tight binding of product may regulate the farnesylation and transport of FTase substrates. FPP-stimulated product dissociation has been observed for a farnesylated full-length Ras protein, and there is substantial evidence to suggest that this phenomenon is physiologically relevant (*89*). Crystallographers have reported that the FTase•product•FPP complex is quite stable under crystallizing conditions and requires additional peptide to release the farnesylated product from the enzyme, suggesting that additional cellular factors may be required for delivery and release of the farnesylated protein product *in vivo* (*21*). Recent studies of FTase reactivity with a peptide library have identified ~60 peptides for which single turnover, but not multiple turnover, is observed (*25*). No FPP-stimulated product dissociation was observed for these peptides, indicating that they bind tightly in the E•product complex (*25*). Three of these peptides correspond to full-length proteins that are known to be farnesylated *in vivo*, and may represent a class of proteins for which additional cellular factor(s) are required to facilitate product dissociation.

A possible regulatory mechanism is that the release of farnesylated product from FTase is stimulated by other proteins. Possible candidates include the subsequent enzyme that processes prenylated proteins, the CaaX protease Rce1, but there may also be unidentified protein(s) responsible for escorting farnesylated proteins to the ER membrane and which may bind to FTase to facilitate the release of product from the enzyme. While peptide-catalyzed product dissociation has been previously observed, its mechanism is poorly understood (*89*). In the FTase•product•FPP complex, the three C-terminal amino acids of the CaaX peptide make extensive van der Waals contacts with the new FPP molecule, and the sequence of the peptide product has therefore been proposed to modulate product release (*21*). Previous data have suggested that peptides of one sequence can catalyze dissociation of tightly bound products of a different sequence from FTase, although this mechanism has not been well characterized (*24*). Further studies of the factors that facilitate product dissociation may provide information about structural and chemical features of the peptide substrate that influence the release of prenylated product from the active site of FTase.

Product dissociation may also be stimulated by other factors *in vivo*. We show here that product dissociation is enhanced by Mg^{2+}, and it is possible that intracellular concentrations of Mg^{2+} may regulate the transfer and delivery of farnesylated proteins. Substrate-mediated product release may be coupled to the delivery of the farnesylated product to a specific site, such as a compartment of the ER membrane rich in FPP or FPP synthase. In addition to regulating the proper transport of farnesylated proteins, this mechanism may provide a means of protecting FTase in the cellular environment, by preventing aggregation or mislocalization of the protein in the cytoplasm.

Implications for inhibitor design

In vivo, FTase probably never exists as a free unliganded species, so that many FTase inhibitors actually target an enzyme complex rather than the free enzyme. Crystallographic studies suggest that several binding modes can be considered in the design of Ca_1a_2X-competitive FTIs (*120*). Many inhibitors mimic the displaced, type I β-turn conformation adopted by the farnesylated peptide product when an additional FPP molecule is bound in the active site. Not surprisingly, bisubstrate inhibitors also adopt this β-turn conformation and mimic the binding of the farnesylated product in the exit groove of the FTase active site. While these crystallographic studies have aided the design of inhibitors, they may not capture the binding mode essential to the inhibition of product dissociation, a phenomenon which is discussed further in Chapter 4. Potential inhibitors blocking this mechanism could either slow the rearrangement of the product complex prior to product dissociation, or trap the enzyme in this product complex.

An inhibitory mechanism that functions by slowing the product release step is demonstrated in Chapter 4. A somewhat similar type of inhibition has been observed for the enzyme serine acetyltransferase, which uses a product inhibition mechanism wherein the product binds to the enzyme, inducing a conformational change that prevents substrate binding (*154*). Moreover, product dissociation is rate-limiting for many enzymes, including dihydrofolate reductase, serine acetyltransferase, and the majority of DNA methyltransferases (*154-156*); interestingly, product dissociation is also activated by substrate binding for dihydrofolate reductase (*155, 157*). The findings presented here

are consistent with a similar type of inhibitory mechanism, which is a novel discovery for FTase. Further defining the features of the enzyme and substrates that contribute to product release will enhance our understanding and utilization of this type of inhibitory mechanism.

CHAPTER 4
INHIBITION OF PRODUCT DISSOCIATION REVEALS DISTINCT
MECHANISM FOR FARNESYLDIPHOSPHATE-COMPETITIVE INHIBITORS
OF PROTEIN FARNESYLTRANSFERASE [1]

The last decade has witnessed a large effort to design potent inhibitors of FTase that could attenuate aberrant signaling pathways leading to human cancers. *In vitro* and *in vivo* research has demonstrated the effectiveness of FTase inhibitors to block cell proliferation and tumor formation in both cultured human cell lines and transgenic animal models (*158*). Although the direct correlation between FTase inhibition and the cellular events leading to tumor regression and stasis remains elusive (*159*), the effectiveness of FTase inhibitors to control certain malignancies in combination therapies is being demonstrated in human clinical trials (*158, 160*). The search for inhibitors of FTase has resulted in the synthesis of mimetics of the CaaX motif and FPP, as well as product and transition-state analogs, that demonstrate variable levels of potency, ranging from micromolar to subnanomolar IC_{50} values (*158*).

The precise mechanism of inhibition of FTase has remained unclear, and an enhanced understanding of this inhibition would provide invaluable insight for rational drug design. To further probe the inhibitory mechanism, we have studied the effects of a specific class of FPP-competitive inhibitors that was initially discovered by a random screen of compounds (*161*). These compounds are competitive inhibitors against FPP for wild-type (WT) FTase, and are thought to interact primarily in or near the FPP binding pocket of FTase (*125*). We have probed the position of the inhibitor binding site using mutagenesis coupled with IC_{50} and K_i measurements, determined from steady-state kinetics. The crystal structure of the ternary complex with bound FPP and CVFM, a slow

---

[1] June Pais wrote this chapter, performed the described experiments, and analyzed the data, with the following exceptions. Site-directed mutagenesis and purification of FTase mutants were performed by Katherine Bowers and Jennifer Pickett; all IC_{50} and K_i experiments were performed, analyzed and described in writing by Katherine Bowers.

peptide substrate, demonstrates that the FPP binding site contains two distinct regions: a region of mainly hydrophobic residues that interact with the nonpolar isoprenoid portion of the substrate (W303β, W102β, Y251β, etc.), and a region of charged residues (K164α, R291β, K294β, H248β and Y300β), termed the PPi binding pocket (Figure 4.1A) (*162*). The FTase residues that interact with the peptide substrate CVFM are illustrated in Figure 4.1B. In addition to crucial interactions with active site residues, the cysteine thiolate of the CaaX peptide coordinates the active site zinc, an interaction that is paramount for catalysis of thioether formation (*82, 163*). The remainder of the CaaX binding site arises from both the hydrophobic surface of the FPP isoprenoid moiety and predominantly aromatic FTase active site residues (Figure 4.1B) (*162*).

Mutations in the PPi binding pocket, R291G and K294A, and to a lesser extent Y300F, dramatically decrease the IC_{50} values of FPP-competitive inhibitors, indicating that these side chains have a repulsive interaction with the inhibitors. Previously it was shown for WT FTase that addition of exogenous phosphate ions enhances the potency of these inhibitors by as much as 170-fold (*164, 165*). By comparing the effect of mutations located in the peptide binding pocket (W102β and W106β) with mutations in the diphosphate binding pocket (Y300β, R291β and K294β), we determined that the phosphate synergy effect is primarily restricted to the PPi binding pocket. For R291G and K294A FTase, inhibitor potency is not enhanced by phosphate anions. These data suggest that phosphate anions enhance inhibitor potency in wild-type FTase by interacting with the positive charge of R291β and K294β to decrease the repulsive interaction with these inhibitors.

While steady-state analysis of the inhibition of WT and mutant FTase determined K_i values in the μM range, a direct measurement of the binding affinity of the free WT enzyme for these inhibitors reveals a dissociation constant in the nM range, comparable to the binding affinity for FPP. Furthermore, there is little synergy in the binding of peptide and these FPP-competitive inhibitors. The $K_D^{peptide}$ is comparable for binding the peptide to both E and E•I. Unexpectedly, these inhibitors bind to the E•product complex and decrease the product dissociation rate constant. Inhibitor binding to the E•product complex is competitive with FPP, with a K_i^{pr} of 25 nM . A comprehensive analysis of the data indicates a unique mode of inhibition, where these inhibitors function by competing
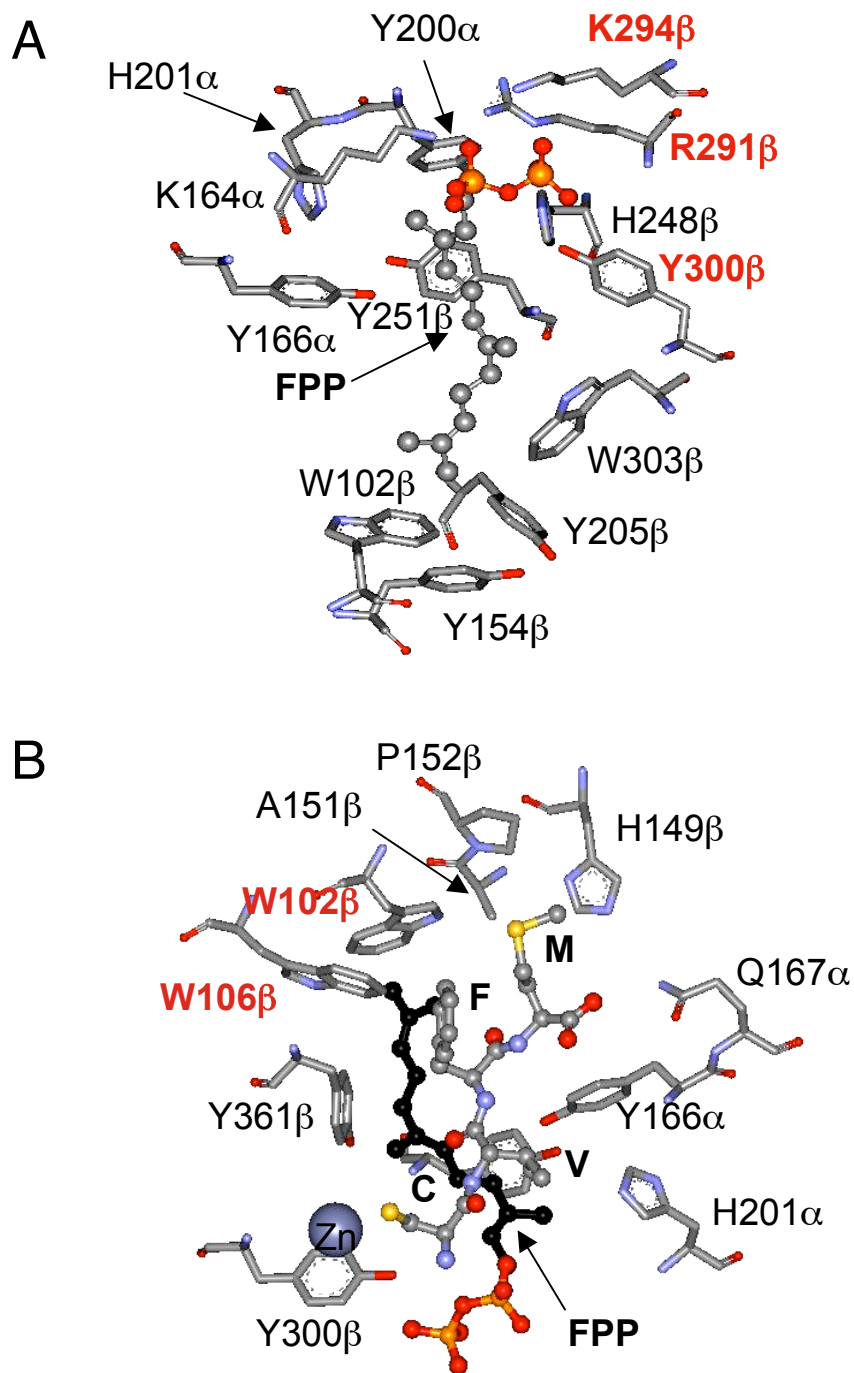
Figure 4.1 Key interactions with FPP and peptide

Substrate binding in the E•FPP•CVFM ternary complex (*162*). (A) Amino acid side chains that interact with FPP (shown in CPK representation); (B) Amino acid side chains that interact with CVFM. FPP is shown as a ball-and-stick representation. The catalytic zinc atom (gray CPK representation) is also shown. The residues studied by mutagenesis in this work are shown in red.

with FPP for binding to the E•product complex and inhibiting turnover by blocking product dissociation. These results offer insight into enzyme-inhibitor interactions that could describe the mechanism of other current FTase inhibitors, and could be exploited to further refine potent inhibitors.

Experimental Procedures

Materials

[1-^{3}H]-FPP and Scintillation Proximity Assay^{TM} (SPA) beads were purchased from GE Healthcare (formerly Amersham Biosciences, Piscataway, NJ). The peptide substrate, biotin-(7-aminoheptanoic acid)-Thr-Lys-Cys-Val-Ile-Met (abbreviated biotin-TKCVIM), was made by solid-state peptide synthesis as described (*166, 167*). The peptides GCVLS and dansylated GCVLS were synthesized and purified by high-pressure liquid chromatography to more than 90% purity by Sigma-Genosys (The Woodlands, TX). FTase inhibitors PD 0152440, PD 0161956, PD 0169451, and PD 0151824 were synthesized as described (*168, 169*) at Parke-Davis Pharmaceuticals, division of Warner-Lambert (currently Pfizer Global Research and Development). FPT inhibitor II (I2) {(*E,E*)-2-[2-oxo-2-[[(3,7,11-trimethyl-2,6,10-dodecatrienyl)oxy]amino]ethyl] phosphonic acid, sodium} was purchased from Calbiochem (San Diego, CA). PE SIL G TLC plates were purchased from Whatman Ltd. (Maidstone, Kent, England). FPP was purchased from Sigma-Aldrich (St. Louis, MO). All other chemicals used were reagent grade.

FTase mutagenesis

The QuikChange^{TM} mutagenesis kit by Stratagene (La Jolla, CA) was utilized to construct FTase mutant genes in the FPTpET23a vector (*148*). Overlapping sets of DNA primers were purchased from Life Technologies (Rockville, MD). DNA sequencing was conducted in the Sequencing Core at Parke-Davis Pharmaceuticals to confirm the presence of the desired mutations. For protein expression, plasmids were transformed

into competent BL21(DE3) *E. coli* cells purchased from Gibco BRL/Life Technologies (Rockville, MD).

Preparation of WT and mutant FTase enzymes

Recombinant WT FTase and mutants were expressed as described (*170*). Cell pellets from a 2 L cell growth were resuspended in buffer containing 20 mM Tris-HCl (pH 8.0), 1 mM EDTA, 1 mM dithiothreitol (DTT) and 10 µg mL^{-1} phenylmethylsulfonyl fluoride (PMSF). Cells were lysed using a French Press at 1200 psi. The lysate was clarified by centrifugation, followed by the addition of a 10% (w:v) solution of streptomycin sulfate to a final concentration of 1%. The lysate was again clarified by centrifugation, followed by the addition of ammonium sulfate to 55% (w:v) saturation to precipitate FTase. The protein was pelleted by centrifugation and the pellet was resuspended in 50 mM Tris-HCl, pH 7.8, 1 mM DTT, and 20 µM ZnCl$_2$. All steps in the protein extraction procedure were carried out at 4°C. The suspension was dialyzed against the same buffer, then mixed with 10% (v:v) glycerol and stored at -20 °C. These crude protein stocks (~10% pure) were utilized in IC$_{50}$ and K_i experiments without further purification.

For K_D^I, $K_D^{peptide}$, and product dissociation studies, FTase was expressed and purified to > 90% homogeneity as determined by SDS-PAGE, as previously described (*90, 170*). The protein was dialyzed at 4 ^{0}C against 50 mM Heppso, pH 7.8, and 2 mM TCEP and stored at -80 ^{0}C. Protein concentrations were determined by active site titrations as previously described (*90*).

IC$_{50}$ determinations

Inhibitor IC$_{50}$ values were determined using the Scintillation Proximity Assay^{TM} (SPA; GE Healthcare, formerly Amersham Biosciences, Piscataway, NJ). Assays, described previously for measuring FTase activity (*164*), were performed in a 96-well plate format. Activity was assayed in buffer containing 50 mM Hepes, 5 mM MgCl$_2$, 0.1% PEG 8000, 20 µM ZnCl$_2$, pH 7.45, with 5 mM DTT (buffer A). For phosphate

synergy experiments, a 12-16 mM concentration of monophosphate anions, in the form of potassium phosphate, was added to the buffer prior to adjusting the pH. In earlier studies of phosphate synergy, a phosphate concentration of 5 mM was utilized (*165*). Control experiments designed to test the effect of phosphate ion concentration on the calculated IC_{50} value indicated no significant alteration in the range of 5-16 mM monophosphate (not shown).

Inhibitor stocks were dissolved in 100% dimethylsulfoxide (DMSO) and the final concentration of DMSO in each assay was 5% (v:v). A 5 µL aliquot of 20 different concentrations of inhibitor in DMSO was added to a 70 µL solution containing 200 nM $[1-^3H]$-FPP and 800 nM biotin-TKCVIM in buffer A or buffer A containing 12-16 mM potassium monophosphate (pH 7.45). The reaction was initiated with the addition of 25 µL of crude FTase. Control experiments were done varying the volume of crude protein to ensure that this concentration of enzyme is well below the K_M for FPP (data not shown). Reactions were allowed to run for 30 minutes at 37 ^{0}C, and were then quenched with the addition of 150 µL stop reagent, which was prepared by diluting a 20 mg mL^{-1} SPA bead solution 1:10 with buffer containing 1.5 M magnesium acetate, 200 mM H_3PO_4, and 0.5% bovine serum albumin, pH 4.0. The 20 mg mL^{-1} stock of SPA beads was made by resuspending dry beads in phosphate buffered saline with 5% sodium azide. The $[^3H]$-labeled farnesylated peptide product was quantified on a Wallac Microbeta 1450 scintillation counter. The average scintillation counts per minute (CPM) of the controls (no inhibitor, 5% DMSO) were set as 100% product, and were used to obtain the percentage of product formed at each concentration of inhibitor. The percent product was plotted against inhibitor concentration and Eq. 1 was fit to the data using the KaleidaGraph software package (Synergy Software).

$$\% \text{ product} = \frac{Y_{max}}{1 + \left(\dfrac{[I]}{IC_{50}}\right)^m} \qquad \text{Eq. (1)}$$

In Eq. 1, Y_{max} represents 100% product, [I] is the inhibitor concentration and m represents the slope of the transition (~1). For the fits, Y_{max} was allowed to float.

K_i determinations

K_i measurements were performed using the SPA assay described above. Time-dependent inhibition studies were initially carried out to test if any of the inhibitor/mutant pairs exhibited effects consistent with slow binding or nonreversible inhibitors. A fixed concentration of protein was combined with an inhibitor concentration equal to its IC_{50} value (in buffer A). The E•I complex was allowed to incubate for various times ranging from 0 to 30 minutes at 37 °C. At a given time interval, turnover was initiated by adding $[1\text{-}^3H]$-FPP and biotin-TKCVIM peptide at saturating concentrations. The reaction was allowed to proceed for 30 minutes at 37 °C, followed by the addition of 150 μl of SPA stop reagent. Product amounts, as a function of E•I incubation time, were quantified by scintillation counting. Inhibitor/mutant combinations that demonstrated a significant (>20%) decrease in the product counts after preincubating for 30 minutes (compared to 1 min) were considered to have slow binding characteristics. Longer incubations did not lead to additional loss in activity.

K_i determinations (versus FPP) were carried out in the following manner. A 96-well plate was set up with samples (75 μL) that contained varying concentrations of inhibitor (0-3 μM), varying concentrations of $[1\text{-}^3H]$-FPP (5-300 nM) and a saturating concentration of biotin-TKCVIM. Turnover was initiated by the addition of 25 μL of a fixed concentration of FTase. Reactions were allowed to proceed for 30 minutes at 37 °C. Reactions were quenched with the addition of 150 μL of SPA stop reagent. The amount of $[1\text{-}^3H]$-labeled product formed was then quantified by scintillation counting. The CPM values at 30 minutes, taken as the initial velocity, were plotted as a function of $[1\text{-}^3H]$-FPP concentration at the various inhibitor levels. Initially, each data set was fit locally to the Michaelis-Menten steady-state equation to determine the effect of increasing inhibitor concentrations on the magnitude of V_{max} and K_M, allowing for a first approximation of the mode of inhibition. The equations below were then fit globally to the entire data set for each mutant/inhibitor pair using the Systat software version 5.2 (SYSTAT Intelligent Software, Evanston, IL). Equations 2, 3, 4, and 5 represent models for competitive, noncompetitive, uncompetitive and mixed noncompetitive modes of inhibition, respectively.

$$v = \frac{V_{max}[S]}{[S] + K_M \alpha} \qquad\qquad \text{Eq. (2)}$$

$$v = \frac{V_{max}[S]/\alpha}{[S] + K_M} \qquad\qquad \text{Eq. (3)}$$

$$v = \frac{V_{max}[S]/\alpha}{[S] + K_M/\alpha} \qquad\qquad \text{Eq. (4)}$$

$$v = \frac{V_{max}[S]}{[S]\left(1 + [I]/K_i\beta\right) + K_M \alpha} \qquad\qquad \text{Eq. (5)}$$

In these equations, $\alpha = (1 + [I]/K_i)$. For the global fits, the values of V_{max}, K_M, K_i and $K_i\beta$ (uncompetitive K_i) were allowed to float.

$K_D{}^I$ determinations

Based on the IC_{50} and K_i results, compound 3 was chosen for further study as a representative FPP-competitive inhibitor. The binding affinity of FTase for compound 3 was measured by competition with $[1-^3H]$-FPP using equilibrium dialysis. A 500 μL solution containing 20-40 nM FTase was preincubated with 60 nM $[1-^3H]$-FPP and 0-500 nM inhibitor for 2 hours at room temperature in buffer (50 mM Heppso, pH 7.8, 2 mM TCEP, 5 mM MgCl$_2$). This solution was then dialyzed against 500 μL of the same buffer containing 60 nM $[1-^3H]$-FPP and the same concentration of inhibitor using a 25,000 molecular weight cutoff dialysis membrane (Spectra/Por 7, Spectrum Laboratories, Rancho Dominguez, CA). For experiments with phosphate, 12 mM KPi (pH 7.8) was used in the buffer on both sides of the membrane. After ~20 hours, the radioactivity in samples (50 μL) from both sides of the membrane was quantified in triplicate by scintillation counting. The fraction of $[1-^3H]$-FPP bound to FTase, $[E\bullet FPP]/[FPP]_{total}$, was determined by subtracting the counts on the buffer side from the counts on the enzyme side, and dividing the difference by the total counts. The concentration of E•FPP

was calculated by multiplying [E•FPP]/[FPP]$_{total}$ by the initial [1-^{3}H]-FPP concentration, [FPP]$_{total}$ (60 nM). The assumption was made that the change in [FPP]$_{free}$ ([FPP]$_{total}$-[E•FPP]) would equal the concentration of inhibitor bound to FTase, [E•I]. Control experiments were done to determine that [E]$_{free}$ was negligible under these conditions, with over 90% of the enzyme bound (data not shown). The concentration of free inhibitor ([I]$_{free}$) was calculated by subtracting the concentration of E•I from the initial inhibitor concentration, [I]$_{total}$ (0-500 nM). The dissociation constant (K_D^I) was then determined by fitting Eq. 6 to the data, where Y$_{max}$ is the maximum concentration of [E•FPP]. For these fits, the K_D^{FPP} for WT and K294A FTase is 10 nM and 51 nM, respectively, as measured previously (*90*).

$$[E \bullet FPP] = \frac{Y_{max}}{1 + \dfrac{K_D^{FPP}}{[FPP]_{total}}\left(1 + \dfrac{[I]_{free}}{K_D^I}\right)}$$ Eq. (6)

$K_D^{peptide}$ determinations

The affinity of the E•I complex for the dansylated peptide substrate was measured by fluorescence anisotropy, as described previously (*24, 108*). A 1.5 mL solution containing 2 nM dansylated GCVLS (dns-GCVLS) in buffer (50 mM Heppso, pH 7.8, 2 mM TCEP, 5 mM MgCl$_2$) was titrated with an equimolar solution of FTase and compound 3 (0-500 nM) in the same buffer. For experiments with phosphate, 12 mM KPi (pH 7.8) was included in the buffer. The samples were incubated for three minutes prior to each measurement at 25 ^{0}C. Measurements were made on an SLM-Aminco Bowman series 2 luminescence spectrometer using a 1 cm path length, where the dansyl group of the peptide was excited at 340 nm (bandpass = 16 nm) and the emission was monitored at 496 nm (bandpass = 16 nm). The dissociation constant for dns-GCVLS, $K_D^{peptide}$, was determined by a weighted fit of Eq. 7 to the data, where ΔA is the observed fluorescence anisotropy, EP is the fluorescence anisotropy endpoint, and IF is the initial fluorescence anisotropy.

$$\Delta A = \frac{EP}{1 + \dfrac{K_D^{peptide}}{[E]}} + IF \tag{7}$$

Product Dissociation Kinetics

The effect of compound 3 on the product dissociation of FTase was measured using a direct fluorescent assay (described in Chapter 3). The E•product complex was formed by preincubation of equimolar concentrations of FTase (5 μM) and FPP (5 μM) for 15 minutes at 25 ^{0}C followed by addition of dns-GCVLS (5 μM) and incubation for 1 hour at 25 ^{0}C in 50 mM Heppso, pH 7.8, 2 mM TCEP, and 5 mM MgCl$_2$. The E•product complex was then incubated with compound 3 (0-800 nM) for 30 min. Product dissociation from the complex was initiated by dilution (250-fold) into the same buffer, containing excess FPP (150 μM) to stimulate dissociation of product, and unlabeled GCVLS (10 μM) to ensure that FTase did not reassociate with the released dansylated product. The increase in fluorescence intensity (λ_{ex} = 340 nm, λ_{em} = 475 nm) due to dissociation of the dansylated, farnesylated peptide product was monitored as a function of time. Measurements were made on an SLM-Aminco Bowman series 2 luminescence spectrometer using a 1 cm path length. The observed rate constant for product dissociation (k_{pr}) was determined by fitting Eq. 8 to the data where P_t is the fluorescence at time t, and P_∞ is the fluorescence endpoint which varied from 3-10 (PMT = 700V).

$$\frac{P_t}{P_\infty} = 1 - e^{-k_{pr}*t} \tag{Eq. (8)}$$

The $K_{1/2}^{FPP}$ for activation of product dissociation for WT FTase has been measured as 22.3 ± 0.2 μM using the assay described above at varying concentrations of FPP in the absence of any inhibitor (Chapter 3). K_i^{pr}, the inhibition constant for product dissociation, was measured for WT FTase by varying the concentration of inhibitor at a fixed value of FPP (150 μM). A weighted fit of Eq. 9 to the data, which corresponds to a competitive mechanism in which the inhibitor competes with FPP for activating product dissociation (Scheme 4.1), was used to determine K_i^{pr}, where $k_{off,1}$ and $k_{off,2}$ are the rate constants for product dissociation (Scheme 4.1), [E]$_{total}$ was fixed at 20 nM, [FPP] was

fixed at 150 μM, and $K_{1/2}^{\text{FPP}}$ was fixed at 22.3 μM.

$$k_{pr} = \frac{k_{\text{off,1}}[\text{E}]_{\text{total}}}{1 + \dfrac{K_{1/2}^{\text{FPP}}}{[\text{FPP}]}\left(1 + \dfrac{[\text{I}]}{K_{\text{i}}^{\text{pr}}}\right)} + \frac{k_{\text{off,2}}[\text{E}]_{\text{total}}[\text{I}]K_{1/2}^{\text{FPP}}}{K_{\text{i}}^{\text{pr}}[\text{FPP}]\left[1 + \dfrac{K_{1/2}^{\text{FPP}}}{[\text{FPP}]}\left(1 + \dfrac{[\text{I}]}{K_{\text{i}}^{\text{pr}}}\right)\right]} \qquad \text{Eq. (9)}$$

To confirm that the mechanism is competitive with respect to FPP, K_{i}^{pr} was measured at a different concentration of FPP (25 μM). A global, weighted fit of Eq. 9 to the entire data set was done using GraphPad Prism Software (San Diego, CA, USA).

Results

Inhibitors

Four compounds, synthesized to serve as product mimetics, were chosen for this study (*164, 165, 168, 169*). The structures of PD 0152440 (1), PD 0161956 (2), PD 0169451 (3) and PD 0151824 (4) are illustrated in Table 4.1. This series of inhibitors including 1, 2 and 3, was initially discovered by a random screen of compounds for FTase inhibitors (*161, 168*). The removal of the polarizable oxygen ether linkage to the terminal benzene ring in 1 to form compound 2 decreases the IC_{50} value from 9.3 μM to 4.0 μM against WT FTase (see Table 4.2). Addition of two methyl groups at this position, resulting in compound 3, further reduces the IC_{50} value to 1.0 μM. These three compounds are hypothesized to interact primarily in or near the FPP binding pocket of FTase, since they are competitive inhibitors against FPP for the WT enzyme (*165*). In addition, the presence of 5 mM phosphate anions decreases the IC_{50} value as much as 170-fold (*165*). Therefore, mutations in the FPP binding pocket are predicted to alter the affinity of these inhibitors. Compound 4 has an IC_{50} value of 0.39 μM and is uncompetitive with respect to FPP, but competitive with respect to peptide in the WT enzyme (data not shown). Mutations in the peptide binding cleft are predicted to alter the affinity of compound 4, with little alteration in the affinity of the FPP-competitive inhibitors (compounds 1-3).
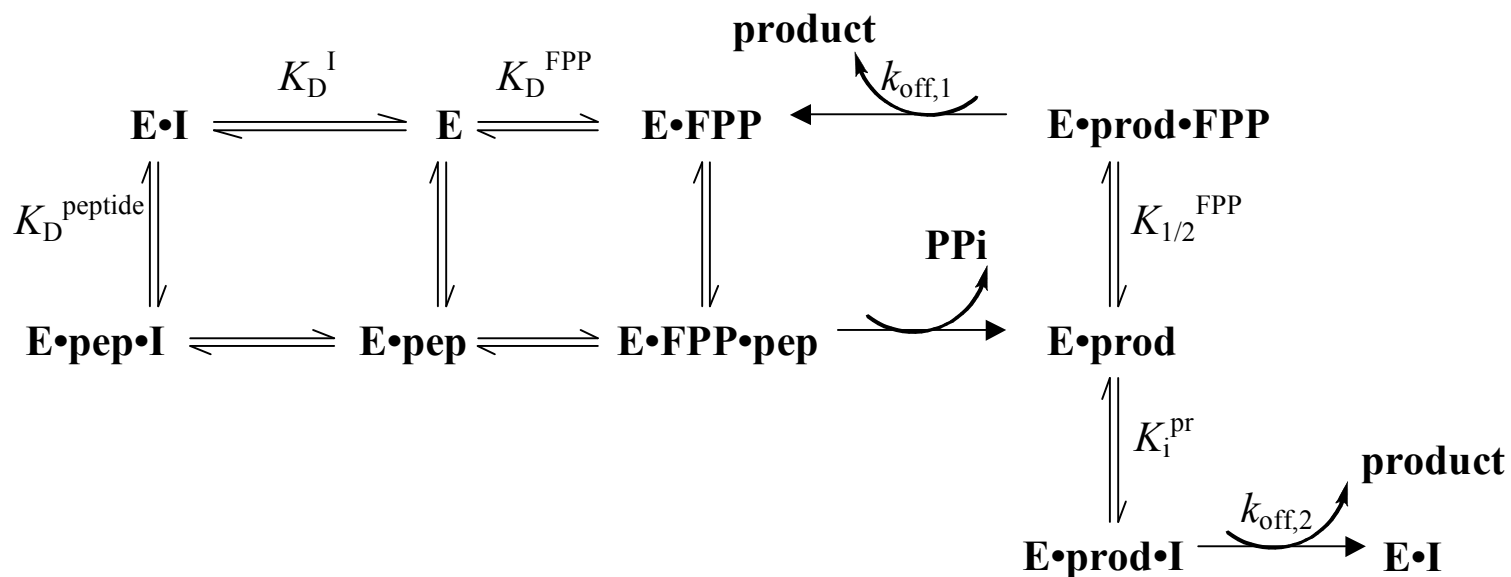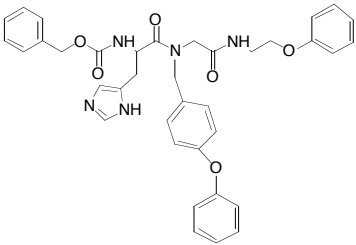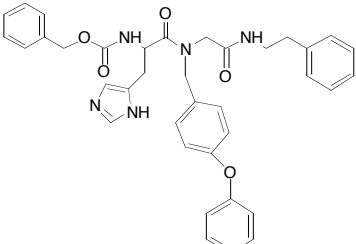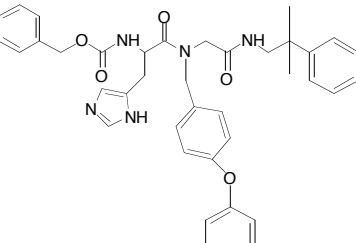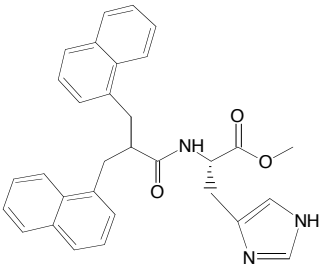
Scheme 4.1 Proposed kinetic mechanism for inhibition of FTase

Proposed mechanism of action for inhibitors (I) listed in Table 4.1 (PD 0152440, PD 0161956, PD 0169451 and PD 0151824). The parameters measured in this study are indicated.

Table 4.1 Inhibitor structures (*164, 165, 168, 169*)

Compound Identification	Structure
1 (PD 0152440 [a])	
2 (PD 0161956 [b])	
3 (PD 0169451 [c])	
4 (PD 0151824 [d])	

[a] [1-{(4-Benzyloxy-benzyl)-[(2-benzyloxy-ethylcarbamoyl)-methyl]-carbamoyl}-2-(1H-imidazol-4-yl)-ethyl]-carbamic acid benzyl ester

[b] [1-{(4-Benzyloxy-benzyl)-(phenethylcarbamoyl-methyl)-carbamoyl}-2-(3H-imidazol-4-yl)-ethyl]-carbamic acid benzyl ester

[c] [1-{(4-Benzyloxy-benzyl)-[(2-methyl-2-phenyl-propylcarbamoyl)-methyl]-carbamoyl}-2-(3H-imidazol-4-yl)-ethyl]-carbamic acid benzyl ester

[d] 3-(1H-imidazol-4-yl)-2-(3-naphthalen-1-yl-2-naphthalen-1-ylmethyl-propionylamino)-propionic acid methyl ester

Mutant selection

To examine interactions between FTase and these inhibitors, we prepared and analyzed FTase mutants in the substrate binding regions of FTase. Figure 4.1A illustrates the amino acid residues that interact directly with FPP in the ternary complex of FPP and the slow peptide substrate CVFM (*162*). Due to the synergy with phosphate, we chose to investigate the role of three residues in the PPi binding pocket, R291β, K294β and Y300β, in determining inhibitor potency by studying the inhibition of the R291G, K294A and Y300F FTase mutants. Figure 4.1B illustrates those amino acid residues that interact with the peptide CVFM (*162*). Of these residues, we chose to investigate the importance of interactions with W102β and W106β by analyzing the inhibition of the W102A and W106A FTase mutants. K356A FTase was analyzed as a control to test the effect of a mutation located at the periphery of the PPi binding pocket on inhibitor binding (location not shown).

IC$_{50}$ Data

We first determined IC$_{50}$ values from the effect of inhibition on enzyme activity, to test the effect of mutations on inhibitor potency and phosphate synergy. Eq. 1 was fit to these data and the resulting IC$_{50}$ values are listed in Table 4.2. The values are a result of a single determination for each mutant/inhibitor combination, with standard errors given.

In the absence of phosphate anions, mutations that decrease the positive charge in the PPi binding pocket of FTase (R291G and K294A) dramatically decrease the IC$_{50}$ values for compounds 1, 2 and 3, with marginal effects on compound 4. The R291G mutation decreases the IC$_{50}$ value 233-fold for compound 1 (0.04 $\pm$ 0.01 μM), 400-fold for compound 2 (0.01 $\pm$ 0.002 μM) and 100-fold for compound 3 (0.01 $\pm$ 0.001 μM) with respect to the WT values. The K294A mutation decreases the IC$_{50}$ value 58-fold for compound 1 (0.16 $\pm$ 0.01 μM), 200-fold for compound 2 (0.02 $\pm$0.004 μM) and 100-fold for compound 3 (0.01 $\pm$ 0.001 μM). A third mutation in the PPi binding pocket, Y300F,

Table 4.2 IC$_{50}$ values [a]

Cmpd.	1		2		3		4	
Pi [b]	—	+	—	+	—	+	—	+
WT	9.3 (1.5)	0.36 (0.03)	4.0 (0.5)	0.10 (0.01)	1.0 (0.1)	0.006 (0.001)	0.39 (0.05)	0.25 (0.03)
R291G	0.04 (0.01)	0.01 (0.002)	0.01 (0.002)	0.003 (0.001)	0.01 (0.001)	0.005 (0.001)	2.4 (0.4)	2.0 (0.3)
K294A	0.16 (0.01)	0.03 (0.01)	0.02 (0.004)	0.003 (.001)	0.01 (0.001)	0.006 (0.001)	1.8 (0.2)	1.3 (0.2)
Y300F	0.73 (0.06)	0.09 (0.01)	0.49 (0.06)	0.01 (0.001)	0.05 (0.006)	0.006 (0.001)	4.9 (0.9)	2.3 (0.4)
K356A	28 (10)	0.33 (0.06)	3.5 (0.5)	0.07 (0.01)	0.24 (0.05)	0.01 (.001)	1.2 (0.2)	0.9 (0.2)
W102A	2.1 (0.4)	0.3 (0.1)	4.2 (0.8)	0.21 (0.06)	3.6 (0.8)	0.02 (0.01)	4.2 (1.0)	3.5 (0.7)
W106A	8.1 (0.9)	1.0 (0.1)	6.3 (0.8)	0.06 (0.02)	0.73 (0.07)	0.02 (0.001)	0.35 (0.08)	0.14 (0.07)

[a] Values, in units of μM, are determined from fitting titration curves of % product vs. inhibitor concentration with Eq. 1. Results are from a single determination for each inhibitor/mutant pair with errors given in parentheses, using the SPA assay as described in the Experimental Procedures. Final solutions contained 25 μL crude FTase, 200 nM [1-^{3}H]-FPP, 800 nM biotin-TKCVIM, and varying inhibitor concentrations in 50 mM Hepes, pH 7.45, 5 mM MgCl$_2$, 0.1% PEG 8000, 20 μM ZnCl$_2$ and 5mM DTT. All assays were conducted at 25 ^{0}C. Data were collected and analyzed by Katherine Bowers.
[b] 12-16 mM KPi (pH 7.45) was used for experiments with Pi.

also decreases the IC_{50} values but the effect is smaller; the IC_{50} values decrease 13-fold for compound 1 (0.73 ± 0.06 μM), 8-fold for compound 2 (0.49 ± 0.06 μM) and 20-fold for compound 3 (0.05 ± 0.006 μM). These data demonstrate that the side chains of the PPi binding pocket interfere with the inhibition by (and likely the binding affinity of) compounds 1, 2 and 3. In contrast, the R291G and K294A mutations modestly increase the IC_{50} value of the peptide competitive inhibitor, compound 4, by 6-fold for R291G (2.4 ± 0.4 μM) and 5-fold for K294A (1.8 ± 0.2 μM). The Y300F mutation has a larger effect on the IC_{50} value for compound 4, resulting in a 13-fold increase (4.9 ± 0.9 μM). These data indicate that these residues provide a small, positive contribution to the apparent affinity of compound 4.

Mutations in the active site also serve as probes to discern what residues are involved in modulating the phosphate ion synergy effect on inhibitor efficacy (*165*). For WT FTase, the addition of phosphate anions decreases the IC_{50} values for compounds 1, 2 and 3 by 26-, 40- and 167-fold, respectively (Figure 4.2, Table 4.2). Strikingly, the R291G and K294A mutations completely abrogate the phosphate synergy effect; the IC_{50} values for compounds 1, 2 and 3 are lowered only modestly (2-8 fold) upon addition of phosphate for these two mutants (Figure 4.2, Table 4.2). Nonetheless, the IC_{50} values for these mutants in the presence of phosphate ions are still lower than the WT values. Therefore, the main effect of the R291G and K294A mutations is to increase the inhibitor affinity significantly in the absence of phosphate, suggesting that phosphate anions and deletion of the positively charged side chains may have a similar effect on inhibitor potency. The last mutation in the PPi binding pocket, Y300F, shows a similar trend in increasing inhibitor potency and decreasing phosphate synergy, albeit with a smaller magnitude (Figure 4.2 and Table 4.2). This mutation lowers the IC_{50} values to a smaller extent (8-20 fold versus 60-400 fold for R291G and K294A), while the enhancement in affinity upon addition of phosphate is 8-20 fold, intermediate between WT FTase and the R291G and K294A mutations.

This observed effect on phosphate synergy is localized to compounds that bind in the FPP binding site. For the peptide competitive inhibitor (compound 4), addition of exogenous phosphate ions decreases the IC_{50} values by < 2.5-fold for WT and all of the mutants (Table 4.2). Furthermore, the large effect of removing the positively charged
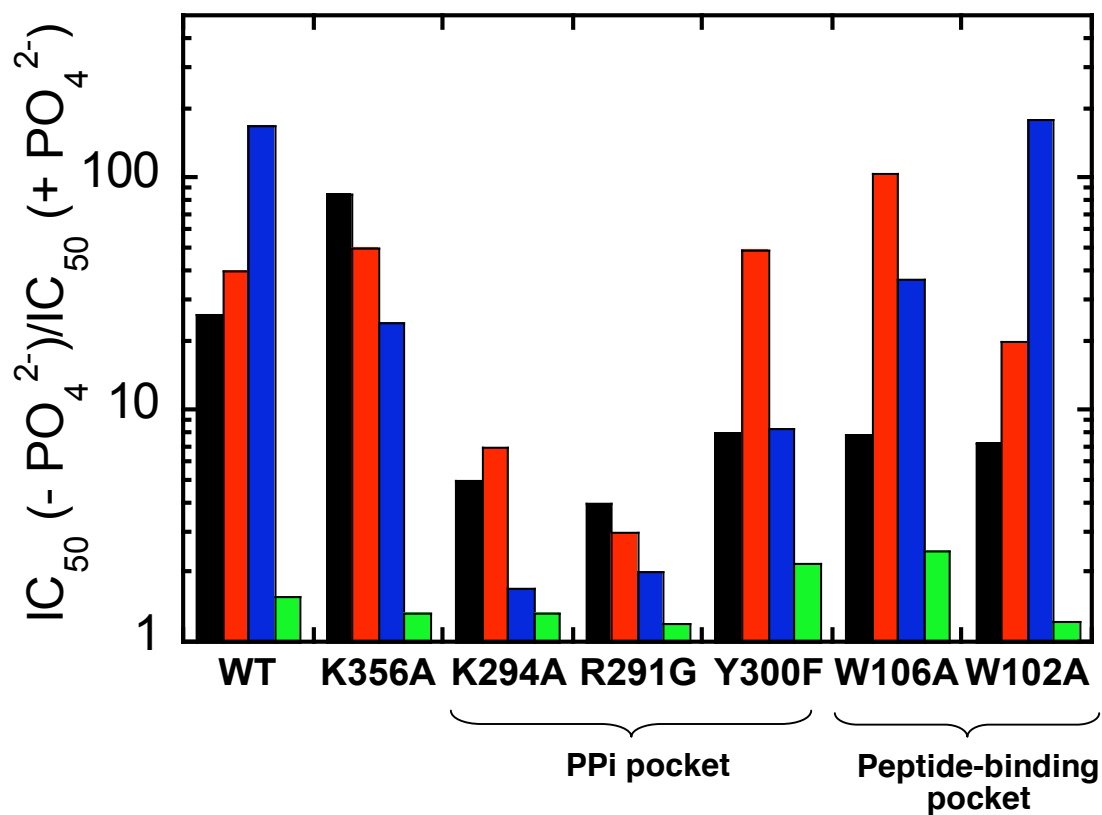
Figure 4.2 Magnitude of the phosphate ion synergy effect

The magnitude is calculated by dividing the IC_{50} value in the absence of phosphate ions by the IC_{50} value in the presence of 12-16 mM phosphate ions; ■ compound **1**; ■ compound **2**; ■ compound **3**; ■ compound **4**. IC_{50} values are listed in Table 4.2. Data were collected and analyzed by Katherine Bowers.

side chains of either R291β or K294β is not simply due to a decrease in the positively charged surface of the protein. The K356A mutation, located on the periphery of the PPi binding pocket, has only small effects on IC_{50} values for all four compounds, while maintaining the phosphate synergy effect. Relative to WT, this mutation lowers the IC_{50} value 4-fold for compound 3 (0.24 ± 0.05 μM), while increasing this value 3-fold for compound 1 (28 ± 10 μM) and compound 4 (1.2 ± 0.2 μM). The IC_{50} value for compound 2 remains unchanged relative to WT (3.5 ± 0.5 μM). In the presence of phosphate ions, the IC_{50} values with this mutation for compounds 1, 2 and 3 decrease 85-, 50- and 24-fold, respectively, which are unchanged relative to WT.

The W102A and W106A mutations in FTase have variable effects on the IC_{50} values for the inhibitors examined. Relative to WT, the IC_{50} value measured for W102A FTase decreases 4-fold for compound 1 (2.1 ± 0.4 μM), and increases almost 4-fold for compound 3 (3.6 ± 0.8 μM) and 11-fold for compound 4 (4.2 ± 1.0 μM). Alteration in the affinity of compound 4 with this mutation was expected owing to the fact that W102β lies in the peptide binding cleft and is proposed to interact with this peptide-competitive inhibitor. The W106A mutation alters the IC_{50} values very little with respect to WT, demonstrating a < 2-fold increase or decrease in these values for all four compounds (Table 4.2). Mutations at W102β and W106β were observed to both modestly increase and decrease the magnitude of the phosphate ion synergy effect. However, a distinct trend was not observed. Owing to the fact that W102β and W106β contribute to the isoprenoid binding cleft for FPP (Figure 4.1), slight variations in inhibitor orientation upon mutation could translate into slight alterations of the phosphate ion synergy effect.

K_i determinations

To determine whether inhibition of FTase by these compounds is competitive with FPP, and to assess the effects of mutations in the PPi binding pocket of FTase on inhibition, we next measured inhibition constants (K_i) using standard steady-state kinetic analyses for compounds 3 and 4 with R291G, K294A, K356A, and WT. For R291G and K294A, time-dependent studies of inhibition suggest that compound 3 has some characteristics of a slow binding inhibitor. Time-dependent experiments were carried out

by varying the incubation time of the E•I complex prior to initiation of the reaction with FPP and peptide. In these experiments, the amount of inhibition increased modestly (~60%) after 30 minutes of preincubation of E•I compared to 1 minute (not shown). For K_i determinations, inhibitors were incubated 1 to 30 min as needed to form the E•I complex. The K_i data are analyzed by Michaelis-Menten kinetics that presume a fast equilibration between E and I. Therefore, the resulting K_i values for compound 3 with R291G and K294A FTase represent an upper limit.

Figure 4.3 illustrates representative double-reciprocal plots for the dependence of steady-state turnover as a function of both FPP and inhibitor concentrations, for WT and mutant FTase. The inhibition of the activity of WT and R291G FTase by compound 3 is competitive with FPP (Figures 4.3A and 4.3B). However, the inhibition of WT and K294A FTase activity by compound 4 is best described as uncompetitive and noncompetitive, respectively (Figures 4.3C and 4.3D). K_i values for WT and mutants are listed in Table 4.3. For compound 3, K_i values for all mutations are decreased as compared to the value for WT FTase (0.12 ± 0.03 μM). Mutants R291G, K294A and K356A reduce the K_i value 30-, 30- and 6-fold, respectively. These data are consistent with the lower IC_{50} values shown in Table 4.2. For compound 4, mutants R291G and K294A increase the K_i value 3-fold relative to WT (0.64 ± 0.05), illustrating a modest effect of the mutations on the binding of this peptide-competitive inhibitor.

Table 4.3 lists the mode of inhibition, with respect to FPP, determined from the analysis of the data by Michaelis-Menten steady-state inhibition models. Compound 3 is competitive against FPP in WT FTase, a characteristic retained in the R291G, K294A, and K356A mutants. Compound 4 is uncompetitive with respect to FPP in WT FTase, a characteristic retained in the R291G and K356A mutants. K294A demonstrated apparent noncompetitive inhibition with this compound. The determination of a noncompetitive versus an uncompetitive model for this inhibitor/mutant pair was based upon the effects of inhibition on V_{max} and K_M determined by fitting inhibition equations (Eq. 2-5) to these data (not shown). Fitting of the data to the uncompetitive equation (Eq. 4) yields a similar K_i of 1.1 ± 0.1 μM (not shown).
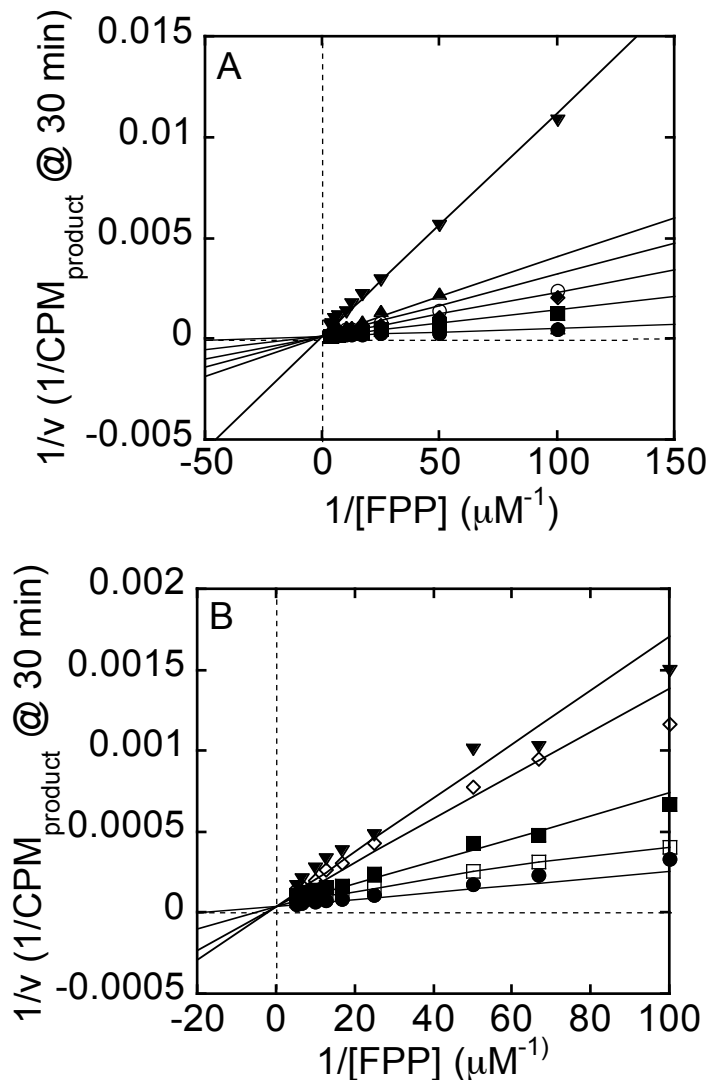
Figure 4.3 Double reciprocal plots

Representative double reciprocal plots of the dependence of initial velocity (v) for formation of product under steady-state conditions as a function of FPP and inhibitor concentration; (A) WT activity at the following concentrations of compound **3**: 0 μM (●), 0.25 μM (■), 0.5 μM (♦), 0.75 μM (○), 1 μM (▲) and 3 μM (▼). Eq. 2 (competitive) is fit to all of the data simultaneously; (B) R291G activity at the following concentrations of compound **3**: 0 μM (●), 0.003 μM (□), 0.005 μM (■), 0.007 μM (◊) and 0.009 μM (▼). Eq. 2 (competitive) is fit to all of the data simultaneously. K_i values are listed in Table 4.3 and were determined using the SPA assay after 30 min of incubation, as described in the Experimental Procedures. Final solutions contained 25 μL crude FTase, 800 nM biotin-TKCVIM, varying (5-300 nM) [1-^{3}H]-FPP concentrations, and varying (0-3 μM) inhibitor concentrations in 50 mM Hepes, pH 7.45, 5 mM MgCl$_2$, 0.1% PEG-8000, 20 μM ZnCl$_2$ and 5 mM DTT. All assays were conducted at 37 ^{0}C. Data were collected and analyzed by Katherine Bowers.

Figure 4.3 *(continued)* **Double reciprocal plots**

Representative double reciprocal plots of the dependence of initial velocity (v) for formation of product under steady-state conditions as a function of FPP and inhibitor concentration; (C) WT activity at the following concentrations of compound **4**: 0 μM (●), 0.1 μM (○), 0.2 μM (■), 0.4 μM (□), and 0.6 μM (▲). Eq. 4 (uncompetitive) is fit to all of the data simultaneously; (D) K294A activity at the following concentrations of compound **4**: 0 μM (●), 0.4 μM (○), 0.8 μM (■), 1.2 μM (□), 1.5 μM (▲). Eq. 3 (noncompetitive) is fit to all of the data simultaneously. K_i values are listed in Table 4.3 and were determined using the SPA assay after 30 min of incubation, as described in the Experimental Procedures. Final solutions contained 25 μL crude FTase, 800 nM biotin-TKCVIM, varying (5-300 nM) [1-^{3}H]-FPP concentrations, and varying (0-3 μM) inhibitor concentrations in 50 mM Hepes, pH 7.45, 5 mM MgCl$_2$, 0.1% PEG-8000, 20 μM ZnCl$_2$ and 5 mM DTT. All assays were conducted at 37 [0]C. Data were collected and analyzed by Katherine Bowers.

Table 4.3 K_i values for select inhibitor/mutant pairs [a]

Mutant	K_i Cmpd. 3 (μM)	K_i Cmpd. 4 (μM)
WT	0.12 ± 0.03 competitive	0.64 ± 0.05 uncompetitive
R291G	0.001 ± 0.000002 competitive [b]	1.9 ± 0.3 uncompetitive
K294A	0.001 ± 0.000002 competitive [b]	1.9 ± 0.2 noncompetitive
K356A	0.02 ± 0.003 competitive	0.67 ± 0.11 uncompetitive

[a] Data, as in Figure 4.3, were fitted with Equations 2-5, as indicated in the text, using the Systat software. Results are from a single determination for each mutant/inhibitor pair and standard errors from the global fit of the data are given. K_i values were determined using the SPA assay after 30 min of incubation, as described in the Experimental Procedures. Final solutions contained 25 μL crude FTase, 800 nM biotin-TKCVIM, varying $[1-^3H]$-FPP concentrations (5-300 nM), and varying inhibitor concentrations (0-3 μM) in 50 mM Hepes, pH 7.45, 5 mM $MgCl_2$, 0.1% PEG 8000, 20 μM $ZnCl_2$ and 5mM DTT. All assays were conducted at 37 ^{0}C. Data were collected and analyzed by Katherine Bowers.
[b] Inhibitors demonstrated a modest time-dependent increase in inhibition over a 30 min duration.

K_D^I determinations

For FTase, K_i determinations measured under steady-state conditions do not necessarily reflect the affinity of the inhibitor for either the free enzyme or the E•peptide complex, since FPP also binds to the E•product complex to accelerate product dissociation (*89*). Steady-state kinetic analysis is further complicated by the slow binding characteristics of compound 3 with R291G and K294A FTase. Therefore, the binding affinity of compound 3 for the free enzyme was determined by a direct binding asssay. Competitive equilibrium dialysis versus FPP was used to measure K_D^I values for compound 3 with both WT and K294A FTase, in the presence and absence of 12 mM phosphate. The inhibitor binds tightly to both WT and K294A, yielding a K_D^I of 7 ± 1 nM and 42 ± 14 nM, respectively (Figure 4.4, Table 4.4). These numbers are comparable to the binding affinity of free FTase for FPP (K_D^{FPP}= 10 nM for WT and 51 nM for K294A) (Table 4.4) (*90*). The K294A mutation modestly reduces the affinity of the enzyme for the inhibitor by 6-fold, similar to the decrease in K_D^{FPP} for this mutant (*90*). The K_D^I values are essentially unchanged by the addition of phosphate (Figure 4.4, Table 4.4). The K_D^I values are 8 ± 4 nM for WT and 33 ± 11 nM for K294A in the presence of 12 mM phosphate, which is within error of the values measured in the absence of phosphate (Figure 4.4, Table 4.4). It is important to note that both the K_D^{FPP} and K_D^I values are much tighter than the K_i values for WT and mutant FTase, suggesting that the inhibition observed in steady-state kinetic experiments is not a result of the inhibitor binding to the free enzyme, but to some other complex.

$K_D^{peptide}$ determinations

The affinity constant of FTase for the peptide substrate was measured for dansylated GCVLS (dns-GCVLS) binding to a preformed E•I complex, where I is compound 3. A fluorescence anisotropy assay was used, which has been previously used to measure peptide affinity constants using a commercial FPP-competitive inhibitor, FPT inhibitor II (I2) (*24*). The affinity constant for dns-GCVLS binding to E•I is 19 ± 3 nM, ~3-fold tighter than the value measured for dns-GCVLS binding to FTase•I2 (*82*) (Figure
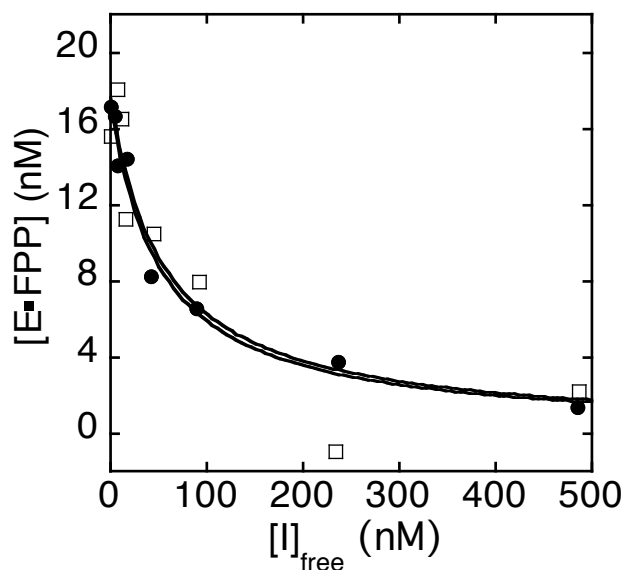
Figure 4.4 K_D^I **determination**

K_D^I plot of WT FTase in the absence (●) and presence (□) of 12 mM KPi (pH 7.8). The plot represents the concentration of E•FPP measured as a function of the concentration of I_{free} by competitive equilibrium dialysis, as described in the Experimental Procedures. A solution containing enzyme with [^{3}H]-FPP and inhibitor is separated by a 25,0000 molecular weight cutoff dialysis membrane from a solution containing [^{3}H]-FPP and inhibitor alone. Final solutions contained 20 nM FTase, 60 nM [1-^{3}H]-FPP, and varying concentrations (0-500 nM) of compound 3 in 50 mM Heppso, pH 7.8, 5 mM MgCl$_2$, and 2 mM TCEP. Assays were conducted at 25 ^{0}C. The radioactivity on either side of the membrane is counted to determine the amount of FPP bound to FTase, which varied as a function of inhibitor concentration. Eq. 6 is fit to the data and K_D^I values are listed in Table 4.4.

Table 4.4 Dissociation constants for WT and K294A FTase with compound 3

Mutant	K_D^{FPP} (nM) [a]	K_D^{I} (nM) [b]		$K_D^{peptide}$ (nM) [c]	
Pi [d]	—	—	+	—	+
WT	10 ± 2	7 ± 1	8 ± 4	19 ± 3	16 ± 2
K294A	51 ± 10	42 ± 14	33 ± 11	17 ± 1	35 ± 2

[a] Measure of the affinity of FTase for FPP. Data taken from ref. (*90*).
[b] Measure of the affinity of FTase for compound 3, using competitive equilibrium dialysis as described in the Experimental Proecdures. Final solutions contained 20 nM FTase, 60 nM [1-^{3}H]-FPP, and varying concentrations (0-500 nM) of compound 3 in 50 mM Heppso, pH 7.8, 5 mM MgCl$_2$, and 2 mM TCEP. Assays were conducted at 25 ^{0}C. Eq. 6 was fit to the data to determine K_D^{I}.
[c] Measure of the affinity of the FTase•compound 3 complex for dns-GCVLS, using fluorescence anisotropy as described in the Experimental Procedures. Final solutions contained varying concentrations (0-500 nM) of an equimolar FTase•compound 3 complex, 2 nM dns-GCVLS, 50 mM Heppso, pH 7.8, 5 mM MgCl$_2$ and 2 mM TCEP. Assays were conducted at 25 ^{0}C. Eq. 7 was fit to the data to determine $K_D^{peptide}$.
[d] 12 mM KPi (pH 7.8) was used for experiments with Pi.
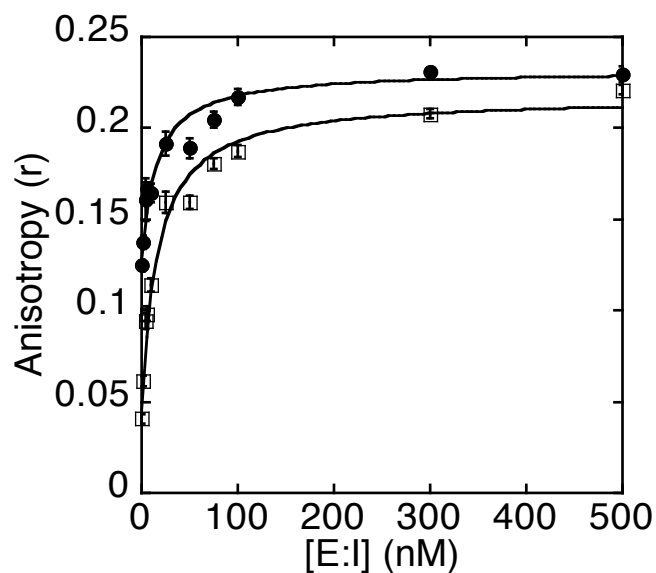
Figure 4.5 $K_D^{peptide}$ determination

$K_D^{peptide}$ plot for WT (●) and K294A (□). The plot represents the fluorescence anisotropy measured as a function of the concentration of E•I using compound 3, as described in the Experimental Procedures.   A weighted fit of Eq. 7 to the data yields the dissociation constants for dansylated GCVLS, listed in Table 4.4. Final solutions contained varying concentrations (0-500 nM) of an equimolar FTase•compound 3 complex, 2 nM dns-GCVLS, 50 mM Heppso, pH 7.8, 5 mM $MgCl_2$ and 2 mM TCEP. Assays were conducted at 25 ^{0}C.

4.5, Table 4.4). The affinity constant did not change when 12 mM phosphate was added to the assay ($K_D^{peptide}$ = 16 ± 2 nM) or when the experiment was repeated for the K294A mutant ($K_D^{peptide}$ = 17 ± 1 nM). A slightly weaker peptide affinity was observed for K294A in the presence of 12 mM Pi, with a $K_D^{peptide}$ of 35 ± 2 nM (Figure 4.5, Table 4.4).

Product dissociation kinetics

One model consistent with the previous data is that compound 3 inhibits steady-state turnover by competing with FPP to bind to the E•product complex to facilitate product dissociation (Scheme 4.1). To examine this hypothesis, we used a fluorescent assay (described in Chapter 3) to directly measure product dissociation from a preformed 1:1 E•product complex, using a constant FPP concentration and varying inhibitor concentrations.   The dependence of the dissociation rate constant on inhibitor concentration allows the calculation of an apparent inhibition constant, K_i^{pr}, using Equations 8 and 9 (Figure 4.6, Table 4.5). To confirm competitive binding, K_i^{pr} was measured at two FPP concentrations (25 µM and 150 µM) for WT FTase, and Eq. 9 was fit to the data at both FPP concentrations. A K_i^{pr} of 21 ± 5 nM was measured for WT FTase (Figure 4.6, Table 4.5), which is an inhibition constant for product association that is lower than the steady-state K_i and comparable to the K_D^I for binding compound 3 to FTase (Tables 4.3 and 4.4). The apparent inhibition constant was also measured for K294A FTase to determine the effect of removing positive charge on the product dissociation step. The value of K_i^{pr} was only slightly decreased (2-fold) for K294A relative to WT FTase, suggesting that the steady-state kinetic effects from this mutation are the result of other steps in catalysis.   Overall, the effect of inhibition on product dissociation indicates that the IC$_{50}$ and K_i values measured under steady-state conditions may reflect inhibition of the product dissociation step in the overall reaction mechanism. A commercially available FPP-competitive inhibitor, FPT inhibitor II (I2), was tested as a control and was found to have no effect on product dissociation at µM levels (data not shown).
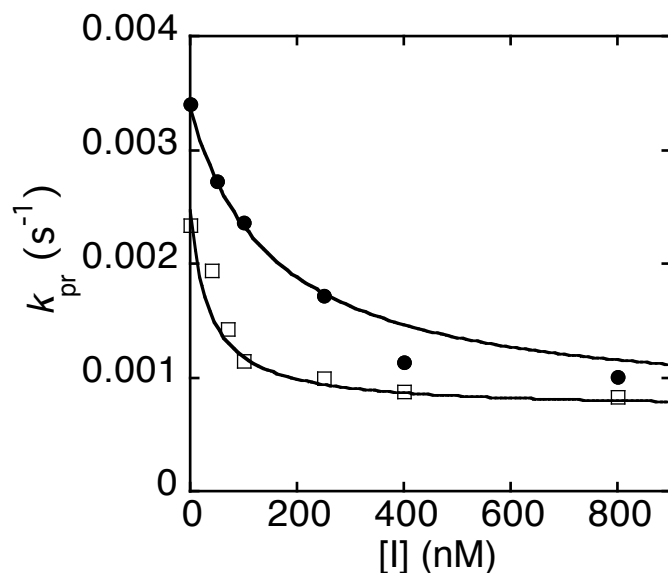
Figure 4.6 Plot of K_i^{pr} for WT FTase

The observed rate constant for product dissociation as a function of the concentration of compound 3 is measured by mixing the E•product•I complex with 25 μM (□) or 150 μM (●) FPP, measuring the time-dependent increase in fluorescence (λ_{ex} = 340 nm, λ_{em} = 475 nm) and fitting Equations 8 and 9 to the data to determine k_{pr} and K_i^{pr} values, listed in Table 4.5.   Final solutions contained 20 nM E•product (FTase preincubated with FPP and dns-GCVLS in a 1:1:1 complex for 1 hour), varying concentrations (0-800 nM) of compound 3 (preincubated with E•product complex for 30 min), 25 or 150 μM FPP, 10 μM GCVLS, 50 mM Heppso, pH 7.8, 5 mM MgCl$_2$, and 2 mM TCEP. Assays were conducted at 25 ^{0}C.

112

Table 4.5 Rate and equilibrium constants for dissociation of farnesylated peptide product from WT and K294A FTase [a]

Enzyme	$K_{1/2}^{\text{FPP}}$ (μM)	K_{i}^{pr} (nM)	$k_{\text{off, 1}}$ (min^{-1})	$k_{\text{off, 2}}$ (min^{-1})
WT	22.3 ± 0.2	21 ± 5	0.013 ± 0.001	0.0024 ± 0.0004
K294A	22.1 ± 0.3	12 ± 2	0.013 ± 0.001	0

[a] Product dissociation rate constants were detemined using a fluorescent assay described in Chapter 3. Final solutions contained 20 nM E•product (FTase preincubated with FPP and dns-GCVLS in a 1:1:1 complex), varying concentrations (0-800 nM) of compound 3, 150 μM FPP, 10 μM GCVLS, 50 mM Heppso, pH 7.8, 5 mM MgCl$_2$, and 2 mM TCEP. Assays were conducted at 25 ^{0}C. Eq. 8 was initially fit to the data to determine the rate constant for product dissociation, k_{pr}, and then Eq. 9 was used to determine K_{i}^{pr}, $k_{\text{off,1}}$, and $k_{\text{off, 2}}$ (see Scheme 4.1).

Discussion

Effect of mutations on FPP-competitive inhibitors

Unexpectedly, mutations in the PPi binding pocket (R291G, K294A and Y300F) significantly increase the potency, lowering the values of both IC_{50} and K_i, of the FPP-competitive inhibitors, compounds 1, 2 and 3 (Tables 4.2 and 4.3). K356A, located on the periphery of the FPP binding pocket, was included as a control to test the effect of removal of a positive charge located outside the active site on inhibitor potency. The effect of the K356A mutation, as well as mutations in the peptide-binding pocket, on both the IC_{50} and K_i values for compound 3 is small when compared to the PPi binding pocket mutants. These results indicate that residues that interact directly with the PPi moiety of FPP are important modulators of the potency of the FPP-competitive inhibitors. These three residues are implicated in making electrostatic and hydrogen bonding interactions with the PPi moiety of FPP in both the inactive and active substrate conformations. In the inactive ternary complex FTase•FPP•CVFM, R291β interacts primarily with the α-phosphate of FPP, while Y300β and K294β interact with the β-phosphate (Figure 4.1A) (*85*). In the proposed active substrate conformation, R291β makes a bidentate interaction with two of the nonbridging oxygen atoms of the PPi group, while Y300β forms a hydrogen bond with the phosphate oxygen bound to C1 of FPP and K294β interacts with the terminal oxygen atom on the β-phosphate (*88, 90, 115*).

The inhibition data indicate that removal of the positive charge in the R291G and K294A mutants provides the most favorable environment for inhibition, while the Y300F mutant causes a smaller increase in potency. The effect of these mutations on the IC_{50} and K_i values is most likely due to the removal of unfavorable charge-charge or steric interactions between the positively charged PPi binding pocket and the inhibitors. Other possibilities include a gain of new favorable interactions with the inhibitor in the active site of the mutant FTase, or a change in the mechanism whereby the inhibitor binds in an alternate site. Several other mutations at position R291β, such as Val, Ala and Glu, similarly decrease the IC_{50} values for compounds 1, 2 and 3 (data not shown). These results highlight the importance of the positive charge of R291β as being the main

modulator of inhibitor potency, as opposed to steric and/or hydrophobic repulsions. These results are most adventitious to drug design since the unfavorable interactions with side chains in the WT protein could be exploited to design inhibitors that could overcome these repulsions by inclusion of charge and/or changes in van der Waals volume and hydrophobicity.

Effect of mutations on peptide-competitive inhibitors

Compound 4, a peptide-competitive inhibitor, was affected quite differently from the other compounds by the mutations in this study. Examining the IC_{50} data, the greatest effect on the IC_{50} value occurred with Y300F, causing a 13-fold decrease in the potency of this compound. Y300F interacts with both the FPP and peptide substrates (close to the CaaX cysteine residue) in the crystal structure (Figure 4.1). Given the intimate nature of the substrate binding regions of FTase, it is not unlikely that alterations to $Y300\beta$ could bring about changes in the peptide binding pocket, either directly or indirectly, resulting in altered binding of compound 4. W102A also affected the potency of compound 4, causing an 11-fold decrease in potency as compared to the WT protein. Owing to the fact that this residue constitutes a portion of the peptide binding cleft (Figure 4.1B), alterations in the interaction with compound 4 are reasonable. Unexpectedly, the W106A mutation has little effect on the IC_{50} value as compared to WT. This residue is proposed to interact with the N-terminus of the peptide substrate (*171*), but may not directly contact compound 4. R291G, K294A and K356A mutations had smaller effects, ranging from a 3- to 6-fold reduction in inhibitor potency as measured by IC_{50} and K_i values. These mutations must be altering the E•FPP complex conformation and/or the binding surface for compound 4 to some degree and affecting potency and affinity. Without further structural information, it would be difficult to estimate the structural distortions occurring upon mutation. However, the close proximity of the FPP and peptide binding pockets in FTase makes it likely that these mutations could translate into alterations of the binding capabilities of this peptide-competitive inhibitor. These results indicate that other amino acid side chains outside of the predicted binding surface for this compound can affect inhibitor affinity.

Effect of mutations on phosphate synergy effect

The comparison of the magnitude of the decrease in IC_{50} values in the absence and presence of 12-16 mM phosphate ions for compound 3 (Figure 4.2, Table 4.2) indicates that the greatest loss of the phosphate ion synergy effect occurs with the R291G and K294A mutations. These data suggest that the phosphate synergy effect is due to interactions located primarily in the PPi binding pocket, as opposed to arising from allosteric effects or other interactions. One reasonable model is that the phosphate ions would bind to the positively charged residues in the PPi binding pocket in the presence of inhibitors to mimic the PPi moiety of the natural FPP substrate. This effect would neutralize the ionic environment of the PPi binding pocket residues and perhaps also alter the position of the hydrophobic side chains, resulting in more favorable interactions with bound inhibitors. Since the affinity of these mutants for the FPP-competitive inhibitors is higher than with WT FTase, deletion of these side chains both decreases the protein-inhibitor repulsions and removes the requirement for phosphate ions to interact with these residues.

The phosphate synergy effect demonstrated by the IC_{50} data clearly supports earlier observations related to the ability of phosphate anions to increase the potency of FPP-competitive inhibitors. Scholten *et al.* have suggested that the phosphate synergy effect is restricted to the active site of FTase, rather than anions being purely allosteric effector molecules (*165*). The mutational data presented in this study further develop the argument that the phosphate synergy effect is, more specifically, restricted mainly to the PPi binding pocket in the active site of FTase. These data support the hypothesis that the role of phosphate ions in increasing the potency of FPP-competitive inhibitors is to mask the unfavorable interactions of the inhibitors with the electrostatic environment of the PPi binding pocket.

Dissociation constants for inhibitors

K_i values normally reflect the affinity of a competitive inhibitor for E_{free}. For FTase, however, steady-state kinetic analyses are complicated by the fact that FPP also

binds to the E•product complex to accelerate product release (*21, 89*). Therefore, a direct binding analysis was needed to determine the affinity of the inhibitor for the free enzyme. Compound 3 binds tightly to WT FTase with a K_D^I of 7 nM, similar to the 10 nM K_D^{FPP} (Table 4.4) (*90*). The mutation of K294β to alanine in FTase only reduces the affinity of the enzyme for both the inhibitor and FPP 5 to 6-fold. The presence of 12 mM Pi does not affect the K_D^I values for WT or K294A FTase, indicating that the phosphate synergy observed in the IC$_{50}$ studies is not a factor in the affinity of the free enzyme for the inhibitor. Additionally, both the K_D^{FPP} and the K_D^I values are much tighter (nM) than the K_i values (μM) for WT FTase, demonstrating that the observed effects of inhibition cannot be solely explained by a simple mechanism in which the inhibitor competes with FPP for binding to the free enzyme.

In addition to FPP binding, the effect of compound 3 on peptide binding was also measured by a fluorescence anisotropy assay that directly measures the binding of a dansylated peptide to the E•I complex. The affinity constant for dns-GCVLS ($K_D^{peptide}$ = 19 nM) is ~ 3-fold tighter for compound 3 with both WT and K294A than for the commercial inhibitor I2, which is commonly used to measure peptide affinity constants (*82*). The presence of phosphate did not affect the $K_D^{peptide}$ value for WT, and only slightly increased the $K_D^{peptide}$ value for K294A, further indicating that the peptide binding step is not significantly altered in the overall inhibitory mechanism for WT or K294A FTase. However, the affinity of the E•peptide complex for the inhibitor can be calculated from the affinity of FTase for peptide alone (K_D = 0.35 μM) (*82*) and the affinity of FTase for the inhibitor alone (K_D = 7 nM), and indicates an extremely tight binding (K_D = 0.4 nM). Therefore, the binding of the inhibitor to the E•peptide complex represents a possible mode of inhibition in the FTase mechanism.

Revised model for FTase inhibitory mechanism

To test the hypothesis that the inhibitor also competes with FPP for binding to the product complex, the dissociation of product from the E•product complex was directly measured using a fluorescent assay. Interestingly, compound 3 inhibits product dissociation for WT FTase in an FPP-competitive manner. The inhibition constant for

product dissociation for WT FTase is 21 ± 5 nM, reflecting a tight inhibition constant the same order of magnitude as the K_D^{FPP} and K_D^I values, and significantly lower than the K_i values measured under steady-state conditions. A commercial FTase inhibitor, FPT inhibitor II (I2), did not inhibit product dissociation, indicating multiple modes for the inhibition of FTase (data not shown).

We propose that these inhibition studies can be combined with previous kinetic studies to establish a unique mechanism for FTase inhibition whereby FPP-competitive inhibition is mediated by three different enzyme forms: binding of the inhibitor to the free enzyme, the E•peptide complex, and the E•product complex (Scheme 4.1). The binding affinities of the all three complexes for the inhibitor are tight, indicating that any one of these binding modes represents a possible mode of inhibition. The kinetic mechanism of FTase is functionally ordered, where FPP is thought to bind before peptide, and additional FPP is required for product release so that the enzyme does not exist in an unbound form throughout the catalytic cycle (*83, 92*). Therefore, the functional inhibitory mechanism is to prevent product dissociation. However, the complex kinetic mechanism given in Scheme 4.1 makes a prediction of the steady-state data difficult. For example, it remains unclear why the K_i values for WT are much larger than any of the inhibitor dissociation constants measured in this study. The effect is likely a kinetic effect, rather than a thermodynamic effect, and may involve a rate-limiting conformational change such as the flipping of the FPP molecule to form an active substrate conformation prior to catalysis. A more detailed computational analysis of the available data is needed to predict the steady-state kinetic data for this enzyme.

The inhibition of product dissociation of FTase may be a novel mechanism by which proteins can regulate their own activity *in vivo*. Indeed, a number of peptide sequences have been identified for FTase that undergo a single turnover but not multiple turnovers (*24, 25*). These peptides bind tightly to the enzyme upon farnesylation and are not released in the presence of FPP (*25*), but their dissociation may be stimulated by other cellular factors. For example, studies have indicated that other peptides may catalyze product dissociation for these peptide products (*24*). If this is indeed the case, the inhibitory mechanism described here may be applicable to peptidomimetic inhibitors as

well, which compete for the peptide binding site and may thereby inhibit peptide-catalyzed product dissociation.

This phenomenon of inhibition of product release may be applicable to a broad range of enzymes for which product dissociation is the rate-limiting step, such as dihydrofolate reductase (*155*), many members of the GNAT superfamily of acetyltransferases (*172*), and the majority of DNA methyltransferases (*156*) and RNA polymerases. Many of these enzymes are targets in the development of a variety of anti-cancer, antibacterial, or antivirulent inhibitors and have been studied extensively toward these purposes. The current wealth of structural information for these proteins may aid in the design of compounds that target the E•product complex, representing a unique strategy in the development of potent inhibitors.

Implications for drug development

As demonstrated by this study of inhibitor interactions with mammalian FTase, the ability of mutagenesis to pinpoint residues that are involved in modulating inhibitor potency offers one tool in determining inhibitor orientations within the active site and key interactions that could be exploited to improve on inhibitor potency. Mutagenesis is a quicker but less exhaustive means of gaining information concerning protein/inhibitor interactions compared to X-ray crystallography. Although precise orientations of the inhibitor in the active site cannot be determined, vital information about key interactions can still be obtained. By examining the effect of selective mutations on inhibitor potency, one can further narrow the search for what attractive or repulsive forces would be the most advantageous to address for improving inhibitor efficacy. From this work on FTase, it is clear that the interactions of the inhibitors with the residues located in the PPi binding pocket are unfavorable and can be modulated with mutagenesis. Interactions with the positively charged residues of the PPi pocket should be addressed when designing inhibitors for FTase. Given the fact that charged moieties on inhibitors can translate into poor bioavailability, alterations to limit the interaction of inhibitors with the PPi binding pocket (i.e. size or hydrophobicity) would be a more advantageous route to improved potency.

In addition to the information obtained through mutagenesis in this work, our current understanding of FTase inhibitors must be redefined by the mechanism presented in Scheme 4.1. As suggested by the analog data presented in Chapter 3, the inhibition of product dissociation is an important inhibitory mechanism which should be considered when performing inhibitor screens and characterizations. Future compounds may also be developed to modulate product release to design more suitable inhibitors. With the available structural information, especially the structures of the ternary E•product and E•product•FPP complexes (*21*), the importansce of an inhibitor binding to these complexes can be elucidated. Many inhibitors adopt a β-turn conformation in the active site of FTase, corresponding to the position of the farnesylated peptide product in the "exit groove" of the active site, suggesting a possible conformation by which product release may be inhibited (*120*). An E•product•I complex would be particularly useful in determining important structural interactions that enable the inhibitor to bind to the E•product complex and inhibit product dissociation. Such a structure would provide useful mechanistic insight into this unique mode of inhibition.

CHAPTER 5
KINETIC ISOTOPE EFFECT STUDIES OF THE PROTEIN FARNESYLTRANSFERASE REACTION [1,2]

FTase and GGTase I are the newest members of the class of zinc metalloenzymes that catalyze sulfur alkylation. Other members of this class of enzymes include methionine synthases, human betaine-homocysteine methyltransferase, and methanol:coenzyme M methyltransferases (*101, 102*). Despite the extensive structural and kinetic data obtained for FTase, however, the structure of the chemical transition state for the reaction catalyzed by FTase or any other member of this class of enzymes has yet to be clearly defined. A concerted mechanism has been supported by direct zinc ion coordination of the cysteine thiol which lowers the pK_a of the thiolate nucleophile, as well as by inversion of stereochemistry during the FTase reaction (*82, 98*). Substitution of Cd^{2+} for Zn^{2+} in the active site of FTase enhances peptide affinity and decreases the observed single turnover rate constant, further supporting a concerted associative mechanism with metal-thiolate coordination in the transition state (*95*). However, substitution of electron-withdrawing fluorine atoms at the C4 methyl position of FPP leads to a decrease in the rate constant proportional to the number of fluorines added, indicating that there is substantial positive charge in the transition state of FTase (*95, 99*).

An increased knowledge of the geometry and electrostatic features of the chemical transition state of FTase may provide a blueprint for the design of potent FTase inhibitors. Given the sensitivity of transition state energies to structural perturbations, the

---

best method for investigating the structure of the transition state in FTase is the measurement of heavy atom kinetic isotope effects (KIEs) (*133*). KIEs are defined by the ratio k_{normal}/k_{heavy} and are a vibrational phenomenon that results from changes in atomic vibrational states between the ground state and transition state (Scheme 5.1). When the mass of a substrate is changed by isotopic substitution, the vibrational frequency of the substrate is changed, both in the ground and transition states but by different relative magnitudes (Scheme 5.1). This results in a difference in activation energies between the normal and heavy substrates, which is experimentally measured as a difference in reaction rates. For most reactions, the bonding environment in the transition state is less constrained than in the ground state and the rate constant for the normal substrate is faster than the rate constant for the heavy substrate (Scheme 5.1A). Thus the KIE will be "normal," or greater than 1. For "inverse" KIEs, which are less than 1, the bonding environment in the transition state is more constrained, and the rate constant for the normal substrate is slower than the rate constant for the heavy substrate (Scheme 5.1B).

For FTase, a purely associative reaction would exhibit a decreased bond order for C1, wherein C1 becomes less constrained as the geometry changes from tetrahedral to trigonal bipyramidal in the transition state (Scheme 5.2A). This would result in a large primary ^{14}C KIE (~10%), while the α-secondary ^{3}H KIE would be near unity due to little change in the bonding environment of the α-secondary hydrogen atoms (*133, 173*). In contrast, for a purely dissociative reaction, C1 would form a carbocation and become more constrained in the transition state resulting in a small or inverse primary ^{14}C KIE (Scheme 5.2B). Additionally, the increased vibrational freedom of the α-hydrogen atoms in a carbocation intermediate, as they change from an sp^3 hybridization in the ground state to an sp^2 hybridization in the transition state, would result in a large α-secondary ^{3}H KIE (~20%) (*133, 174*).

Traditionally, KIEs for enzyme-catalyzed reactions are measured under steady-state turnover conditions; however, this requires a reaction with a single rate-limiting step and a low commitment to catalysis (*175*). The α-secondary ^{2}H KIE for yeast FTase was measured under steady-state conditions and determined to be slightly inverse (0.977) (*176*). However, the KIE measured under steady-state conditions is complicated by the rate-limiting product release and high commitment factors for both substrate binding and
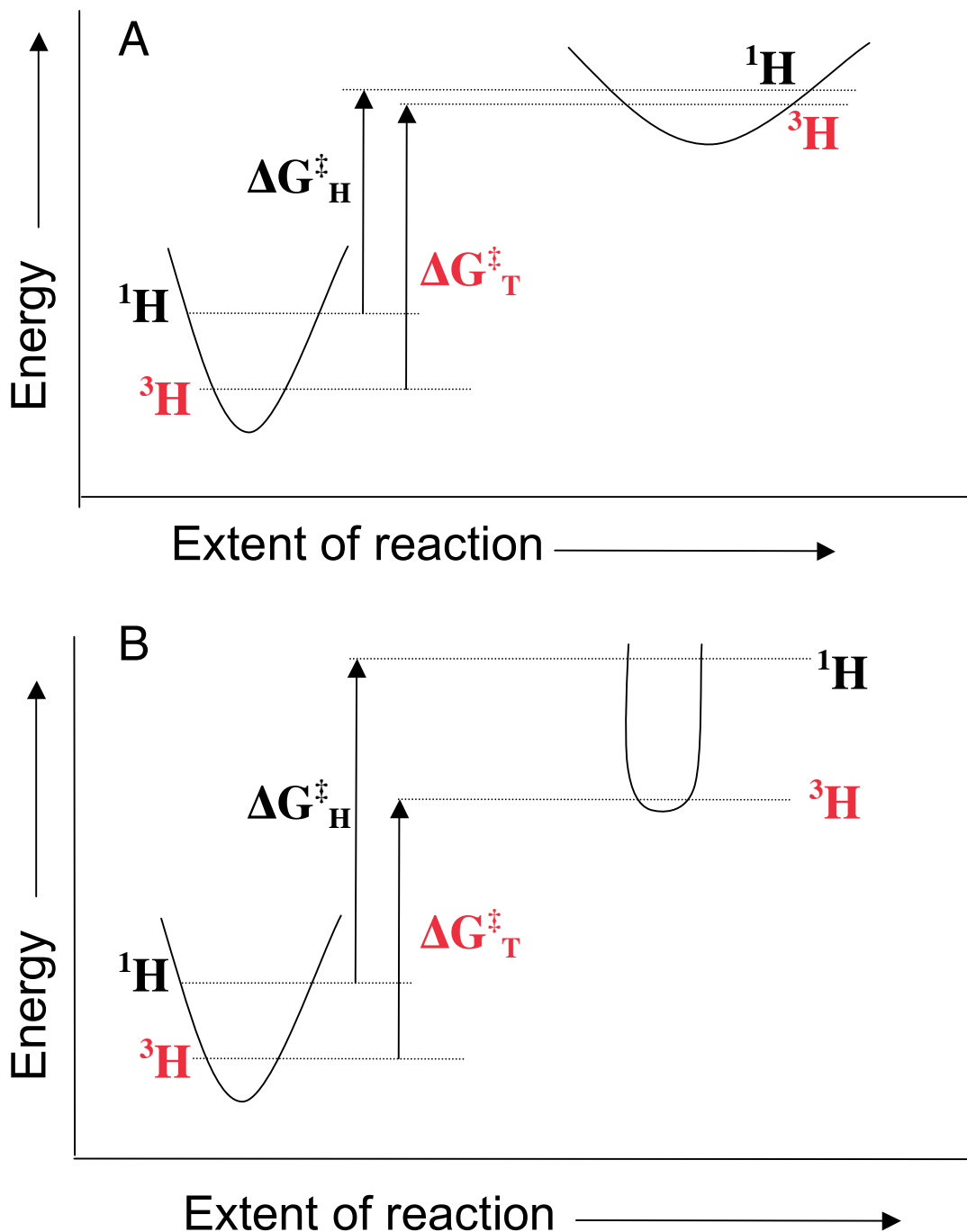
Scheme 5.1 Transition state theory for ^{3}H KIEs

Reaction coordinate diagrams for a ^{3}H KIE experiment illustrating changes in the ground and transition states for two reactions: (A) the bonding environment in the transition state is less constrained, and a normal KIE is observed ($k_H > k_T$); and (B) the bonding environment in the transition state is more constrained, and an inverse KIE is observed ($k_H < k_T$). These diagrams are for illustrative purposes only, and energy values are not to scale.

A
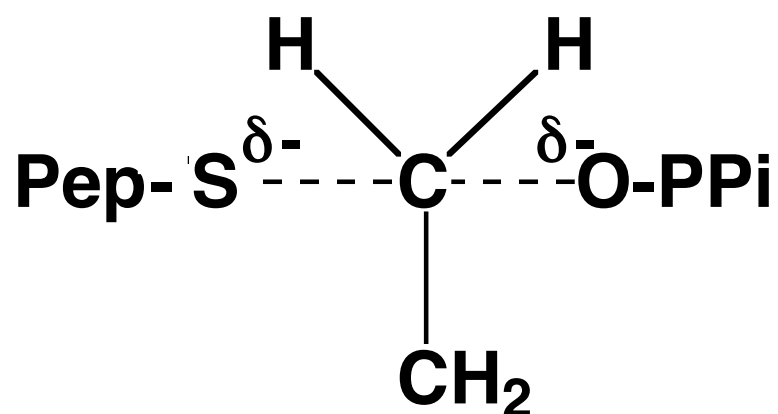
B
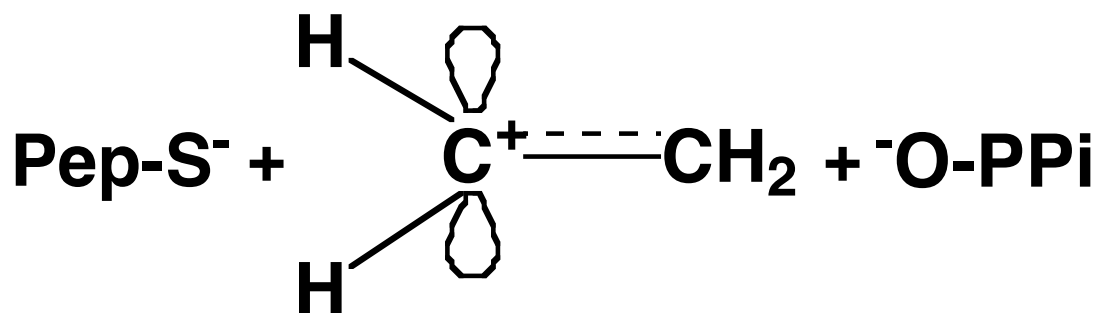
Scheme 5.2 Possible transition states for FTase

Proposed chemical structure of the FTase transition state, centered on the C1 of FPP, for: (A) an associative mechanism, where the C1 is partially bonded with both the thiolate nucleophile and the PPi leaving group in a symmetrical transition state with trigonal bipyramidal geometry; and (B) a dissociative mechanism with carbocation character and sp^2 hybridization.

product formation, and probably does not reflect the intrinsic KIE for either the rat or yeast FTases (*83, 92, 95, 96*). Therefore, we have measured the intrinsic KIEs in rat FTase under single turnover conditions of limiting FPP and excess enzyme, which acts as a stoichiometric reactant, so that the step that undergoes isotopic discrimination, the chemical step, is the main rate-limiting step (Scheme 5.3) (*177, 178*). A combination of the competitive method for KIE measurement and transient kinetics has been used previously to measure the intrinsic KIEs for purine nucleoside phosphorylase and glutamate mutase (*179, 180*).

Crystal structures for FTase have been solved in a number of inactive complexes, including a ternary substrate complex (E•FPP•CVFM), a product complex (E•F-KKKSKTKCVIM), and a ternary product complex (E•F-KKKSKTKCVIM•FPP) in the absence of Mg^{2+} (*21, 85*). Ternary complex structures place the two reactive atoms, the sulfur of the peptide cysteine and the C1 of FPP, greater than 7 Å apart (Figure 5.1) (*84, 85, 87*). In order for catalysis to occur, there must be a conformational rearrangement of one or both of the substrates, since little change in the active site of FTase itself is observed between the ternary and the product complexes (*21*). On the basis of structural and mutagenesis studies, a model has been proposed in which the first two isoprene units of FPP rotate to bring the C1 of FPP within reacting distance (2.42 Å) of the peptide thiolate (*88*). Furthermore, the diphosphate moiety rearranges such that Mg^{2+} coordinates the diphosphate oxygens of FPP and two carboxylate oxygens of D352β (Figure 5.2) (*107*). Therefore, while transient kinetics are used to isolate the farnesylation step from the product release step, the observed rate constant under single turnover conditions of limiting FPP (relative to [E]) includes both this conformational rearrangement and the farnesylation step (Scheme 5.4) (*95, 96*).

Here we measure the intrinsic primary ^{14}C and α-secondary ^{3}H KIEs for FTase, under a variety of conditions, to provide information about the sensitivity of the transition state structure to changes in the stability of the ground and transition states. The intrinsic α-secondary ^{3}H KIE for WT FTase is determined to be 1.20 ± 0.01. This ^{3}H KIE, together with a small observed primary ^{14}C KIE of 1.03, is consistent with a concerted transition state with dissociative character. We further explore the contribution of the Zn^{2+} metal ion to the chemical transition state of FTase by measuring the α-secondary

isotopically sensitive step

$$E + FPP + \mathbf{FPP^{*}} \rightleftharpoons E^{FPP} + E^{\mathbf{FPP^{*}}} + pep \rightleftharpoons E^{FPP}_{pep} + E^{\mathbf{FPP^{*}}}_{pep} \longrightarrow E_{product} + E_{\mathbf{product^{*}}}$$
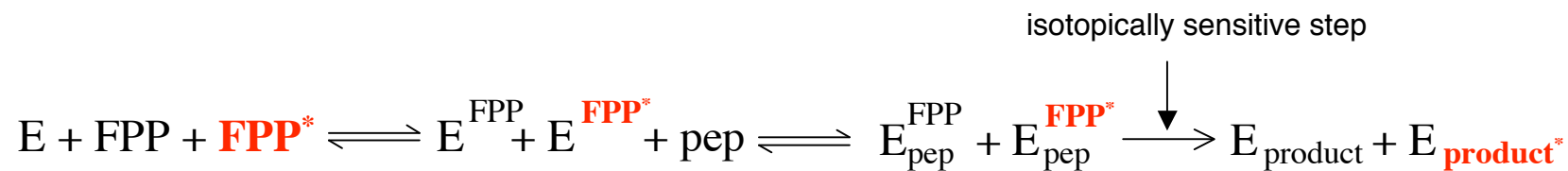
Scheme 5.3 Measurement of single turnover KIEs for FTase

A single turnover KIE experiment is done by preincubating excess FTase with a mixture of FPP radiolabeled at a remote (FPP) and sensitive (**FPP***) position. The reaction is initiated by addition of excess peptide, which binds rapidly so that the formation of product where isotopic discrimination occurs can be measured.
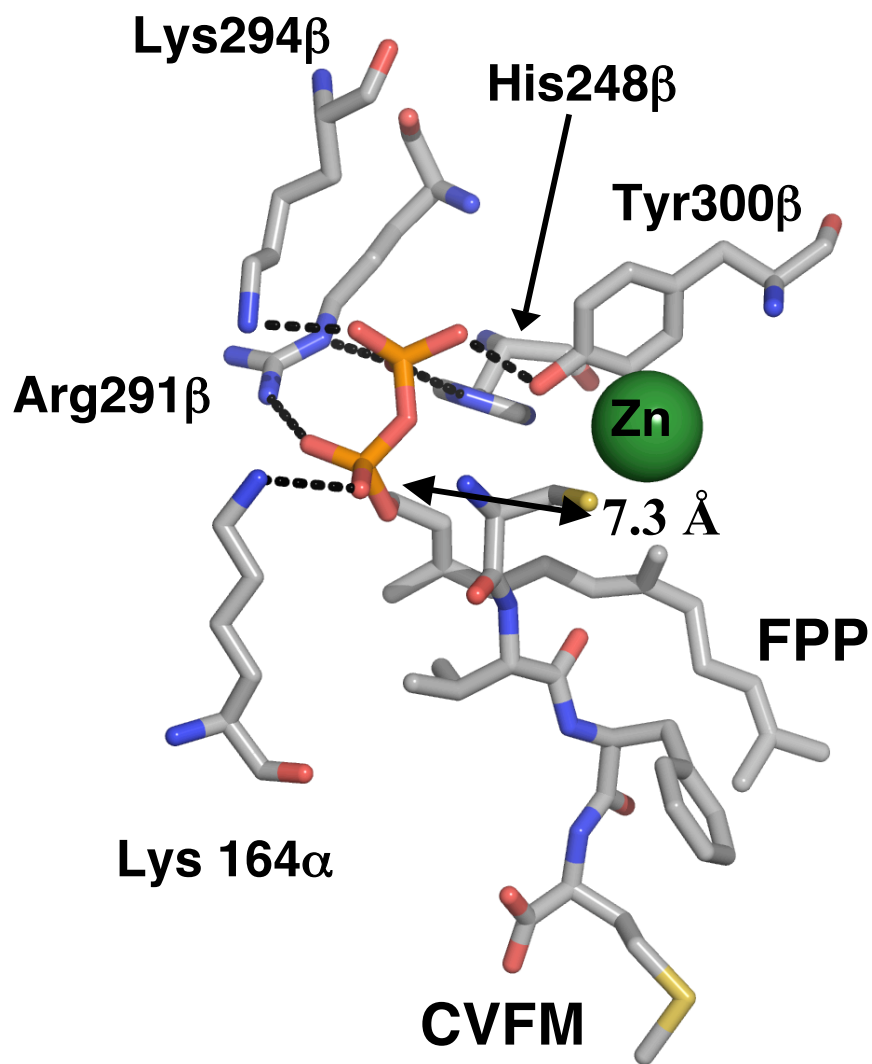
Figure 5.1 Ternary complex of FTase

X-ray crystal structure of the inactive ternary complex with a slow peptide substrate, FTase•FPP•CVFM. The conserved residues K164α, H248β, R291β, K294β and Y300β are shown interacting with the diphosphate moiety of FPP, and the zinc ion is coordinated to the peptide thiolate. Protein Data Bank code: 1JCR (*85*).
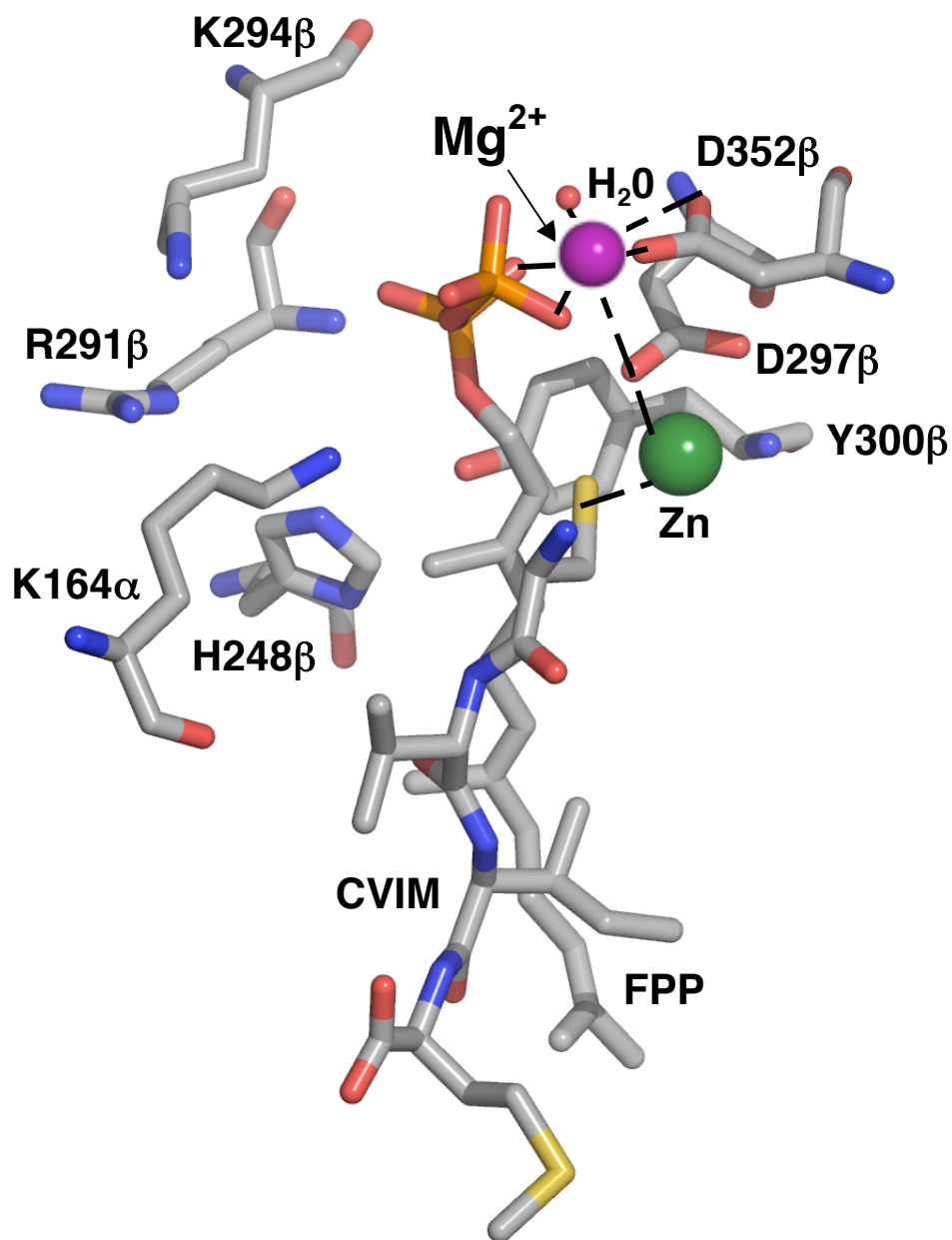
Figure 5.2 Proposed Mg^{2+} binding site in active substrate conformation

Model for the proposed Mg^{2+} binding site formed in the active ternary complex (*107*), based on mutagenesis and crystallographic data (PDB ID 1JCQ (*85*) and 1D8D (*84*)). The octahedral binding site consists of two nonbridging oxygens of the FPP diphosphate, two carboxylate oxygens of D352β, a water molecule, and one carboxylate oxygen of D297β.

128

$$E^{FPP} \xrightleftharpoons[0.06\ s^{-1}]{1 \times 10^6\ M^{-1}s^{-1}} E^{FPP}_{pep} \xrightleftharpoons[k_{-1}]{k_1} E^{FPP*}_{pep} \xrightarrow{k_2} E_{F\text{-}pep}$$

PPi
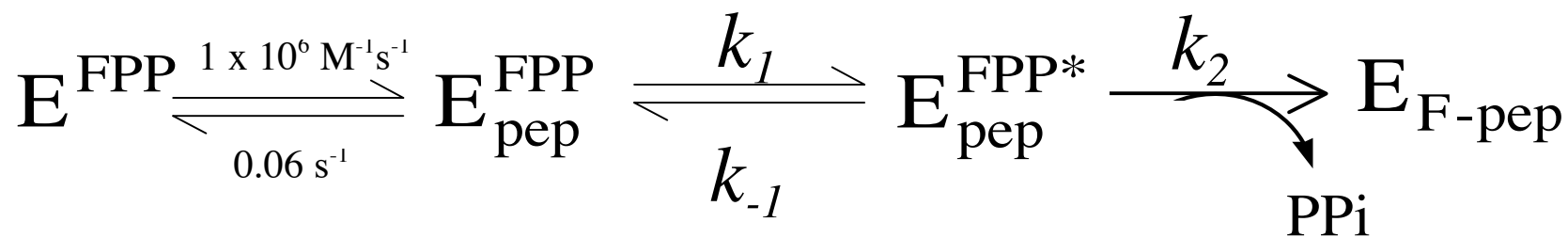
Scheme 5.4 Kinetic mechanism for FTase single turnover reaction

KIE for FTase substituted with Cd^{2+}, which is determined to be 1.24 ± 0.01 and is consistent with a more dissociative transition state.

Unexpectedly, the α-secondary KIE is masked for the pentapeptide GCVLS, which corresponds to the C-terminal sequence of H-Ras, a well-characterized substrate for FTase. A decreased KIE indicates that the FPP conformational rearrangement, rather than the farnesylation step, is at least partially rate-limiting for this peptide. Thus KIEs provide a way to study the kinetics and mechanism of the conformational rearrangement of FPP, which had previously only been inferred from crystallographic and mutagenesis studies. We report α-secondary KIEs for WT FTase at varying concentrations of Mg^{2+}, as well as for mutants in the PPi binding pocket of FTase, to further investigate the contribution of the diphosphate leaving group to catalysis. Surprisingly, changing Mg^{2+} concentrations or removing positive charge from the PPi binding pocket did not change the observed KIE, although both affect the observed farnesylation rate constant and therefore have been proposed to stabilize the diphosphate leaving group of FPP in the chemical transition state. These results implicate both Mg^{2+} as well as the positively charged residues in the PPi binding pocket in facilitating the conformational rearrangement of the FPP substrate as well as stabilizing the farnesylation transition state. In addition, here we show that the structure of the peptide substrate affects the equilibrium of this conformational change, as well as the chemical farnesylation step. Therefore, this FPP conformational change is an important determinant of substrate specificity for FTase, and possibly GGTase I as well. The data lead to a detailed kinetic mechanism for the farnesylation of several peptides and the conformational rearrangement of FPP.

Experimental Procedures

Materials

Radiolabeled isopentenyl diphosphate (IPP) and dimethyallyl diphosphate (DMAPP) were purchased from American Radiolabeled Chemicals (St. Louis, MO). Unlabeled IPP and geranyl diphosphate (GPP), dithiothreitol (DTT), N-acetyl-cysteine

(NAC), and glutathione (GSH) were purchased from Sigma-Aldrich (St. Louis, MO). 2-mercaptoethanol (βME) was purchased from Fisher. Peptides were synthesized and purified by high-pressure liquid chromatography to > 90% purity as follows: TKCVIF by American Peptide Company (Sunnyvale, CA), TKCVIM, TGCVIM, and SKTKCVIM by Bethyl Laboratories (Montgomery, TX) and GCVLS, GCVIM, and TKCVLS by Sigma-Genosys (The Woodlands, TX). The molecular masses of peptides were confirmed by electrospray mass spectrometry. Peptides and thiols were dissolved and stored in 5 mM Tris, pH 8, and 2 mM TCEP. Concentrations were determined by reaction of the cysteine with 5,5'-dithiobis-(2-nitrobenzoic acid) using an extinction coefficient of 14,150 $M^{-1}cm^{-1}$ (*181*). DNA primers were purchased from Invitrogen. All other chemicals used were reagent grade. Thin layer chromatography (TLC) plates were purchased from Whatman Ltd. (Maidstone, Kent, England) and pre-run in 100% acetone.

Cloning of the FPP synthase gene

DNA encoding the wild-type FPP synthase gene was generated by polymerase chain reaction (PCR) amplification of the *ispA* gene from the *E. coli* strain DH5α genomic DNA with two sets of primers: 5'-ATGCATATGGACTTTCCGCAGCAACTC GAAGCCTGC-3' and 5'-GTGGTGCTCGAGTTTATTACGCTGGATGATGTAGTC-3'. Each PCR amplification reaction was catalyzed by *pfu*-turbo DNA polymerase (Stratagene). The resulting fragments were purified using a 1% agarose gel and then cloned into a pCR-Blunt II-TOPO vector and transformed into OneShot TOP10 chemically competent *E. coli* cells (Invitrogen). The purified TOPO plasmid containing the insert was digested with *Nsi*I and *Xho*I, and the fragments were gel purified and then ligated into the pET31b(+) vector (Novagen) digested with the same restriction enzymes. The final gene contains a C-terminal 6X histidine tag. The plasmid pET31b-ispA was transformed into *E. coli* BL21(DE3) cells, and the cells were grown in LB medium containing 100 mg L^{-1} ampicillin. The plasmid was purified using a Plasmid Midi Kit (Qiagen). The sequence of the entire gene was confirmed by DNA sequencing (University of Michigan DNA Sequencing Core, Ann Arbor, MI).

Preparation of FPP synthase

FPP synthase is overexpressed in *E. coli* BL21(DE3) pET31b-ispA cells, grown at 37 ^{0}C to an OD$_{600}$ of 0.7 in LB medium containing 100 mg L^{-1} ampicillin. Protein expression is induced by the addition of 1 mM isopropyl β-D-1-thiogalactopyranoside (IPTG) and 5 mM MgCl$_2$, and incubated at 25 ^{0}C for 14-16 hours. The harvested cells are resuspended in 50 mM Hepes, pH 8.5, 50 mM KCl, and 10 μg mL^{-1} phenylmethylsulfonyl fluoride (PMSF), and lysed by a single pass through a microfluidizer (Microfluidics, Newton, MA). The supernatant is clarified by centrifugation and nucleic acids are precipitated with 1% (w/v) streptomycin sulfate at 4 ^{0}C. The supernatant, 32 mg of total protein per run, is loaded onto a 7.8 mL Ni^{2+}-charged POROS Metal Chromatography Affinity column (Applied Biosystems, Foster City, CA), washed in 50 mM Hepes, pH 8.5, 50 mM KCl buffer, and eluted with a 0-400 mM imidazole gradient. The enzyme elutes at ~ 50 mM imidazole. Fractions containing pure FPP synthase are pooled and concentrated using Amicon Ultra centrifugal filter devices with a 10,000 molecular weight cutoff (MWCO) filter (Millipore, Billerica, MA), and then dialyzed at 25 ^{0}C against 50 mM Tris, pH 8, 50 mM KCl, and 0.125 mM dithiothreitol. Protein concentration and yield are determined by absorbance at 280 nm using a molecular weight of 31356 g mol^{-1} and a calculated extinction coefficient of 7680 M^{-1}cm^{-1} (*147*). A typical yield of approximately 330 mg of > 95% pure FPP synthase, as determined by SDS-PAGE analysis, is obtained from a 1 L growth of cells. The protein is stored in 10% glycerol at -80 ^{0}C.

Enzymatic synthesis of radiolabeled FPP

The selective incorporation of radiolabels into the first and third isoprene units by FPP synthase using the precursors isopentenyl diphosphate (IPP), dimethylallyl diphosphate (DMAPP), and geranyl diphosphate (GPP) has been established by NMR (Scheme 5.5) (*178*). To make FPP labeled in the sensitive (C1) position, radiolabeled IPP and unlabeled GPP are used as precursors; to make FPP labeled in the remote (C11) position, radiolabeled DMAPP and unlabeled IPP are used (Schemes 5.5 and 5.6). The
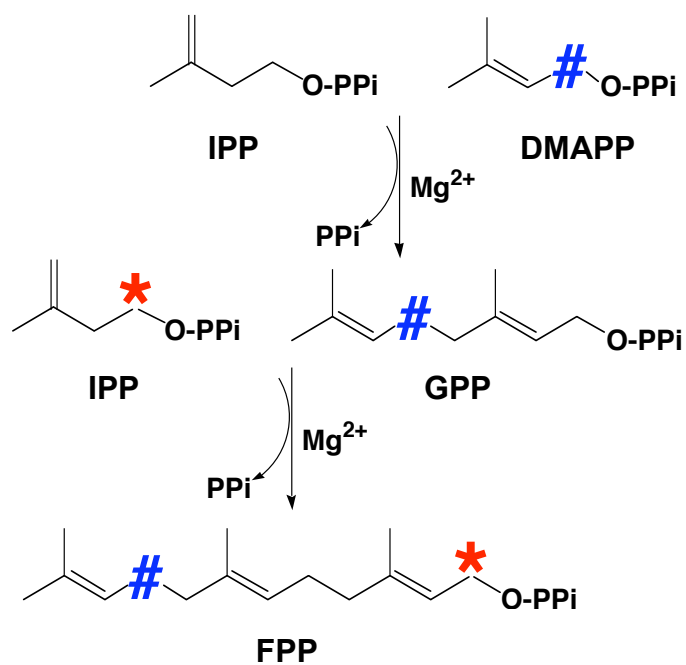
Scheme 5.5 FPP synthase reaction

Reaction catalyzed by FPP synthase, where the positions of the sensitive and remote labels are denoted by "*" and "#", respectively (*178*).

[1-^{14}C] FPP (sensitive, primary)
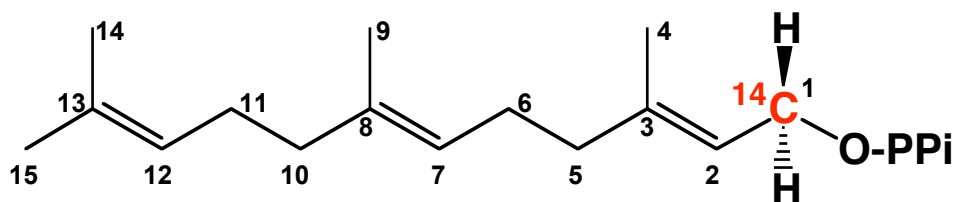
[11-^{3}H] FPP (remote, primary)
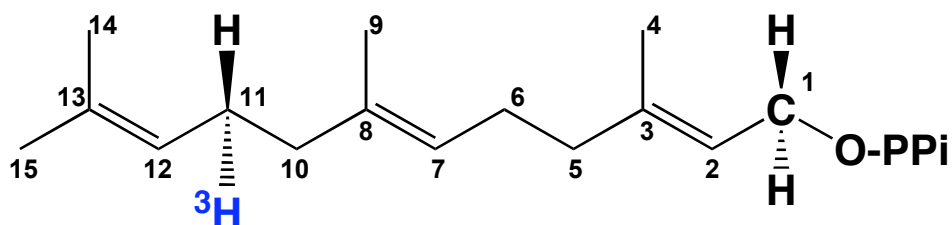
[1-^{3}H] FPP (sensitive, secondary)
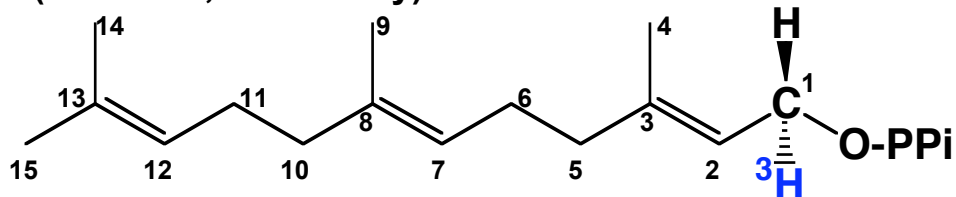
[11-^{14}C] FPP (remote, secondary)
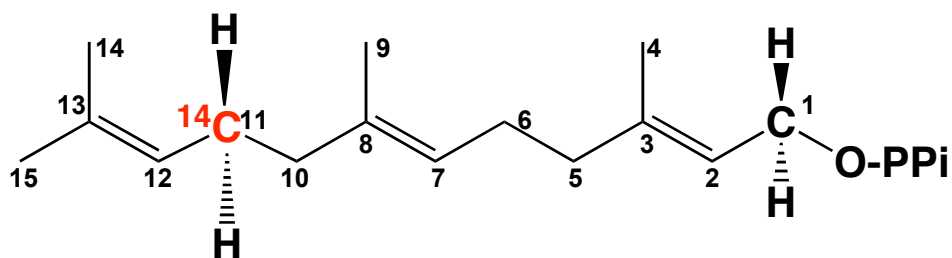
Scheme 5.6 Radiolabeled FPP molecules used to measure primary ^{14}C and α-secondary ^{3}H KIEs

FPP molecules are synthesized from radiolabeled precursors DMAPP and IPP by FPP synthase, as illustrated in Scheme 5.5. The specific incorporation of radiolabels is not stereospecific.

enzymatic reactions are incubated for 6 hours at 37 ^{0}C using 20 μM FPP synthase in 10 mM potassium phosphate buffer, pH 7.3, 10 mM MgCl$_2$, 50 mM KCl, and 10 mM 2-mercaptoethanol. The volumes and concentrations of the precursor molecules are adjusted such that the concentration is ~150 μM FPP and the product forms a white precipitate as the reaction proceeds. The solution is clarified by centrifugation for 30 minutes at 14000 rpm after completion of the reaction. The pellet is dissolved in 1 mL containing 25 mM NH$_4$HCO$_3$, pH 8, and 8.2 mM EDTA, and then purified by reversed-phase HPLC using a Vydac 259VHP54 column with a 300 Å particle size. Reversed-phase HPLC has previously been used to separate phosphorylated isoprenoids on a preparative scale (*182*). A linear, 30 minute gradient of 0-70% acetonitrile in 25 mM NH$_4$HCO$_3$, pH 8, is used at a flow rate of 0.5 mL min^{-1} and the absorbance is monitored at 214 nm. Samples are collected every minute and counted. Fractions corresponding to the radioactive peak are dried, dissolved in 70% ethanol and 50 mM NH$_4$HCO$_3$, pH 8, and stored at -20 ^{0}C. The concentration is determined by scintillation counting, based on a standard curve. Typical yields for FPP are ~ 45% of the limiting, radiolabeled starting material. For ^{3}H-labeled FPP, the specific radioactivity is decreased 10-fold by the addition of cold FPP to 2000 Ci mol^{-1}, while the specific radioactivity of ^{14}C-labeled FPP is maintained at 55 Ci mol^{-1}.

The purity and identity of FPP was confirmed by TLC analysis as follows. To separate FPP from farnesol and farnesyl monophosphate, samples were loaded directly onto Whatman PE SIL G thin layer chromatography (TLC) plates and run in a 7:2:1 2-propanol/NH$_4$OH/H$_2$O mobile phase (*106*). To separate IPP, DMAPP, GPP, and FPP, samples were first dephosphorylated using alkaline phosphatase (*183*). The subsequent alcohols were extracted into pentane and loaded onto Absorbosil RP-18 HPTLC plates which were run in a 1:2:1 50 mM NH$_4$HCO$_3$ (pH 8)/2-propanol/acetonitrile mobile phase. For radioactive samples, plates were visualized by autoradiography and the samples were compared with standards to confirm that the purified reaction products were FPP. Non-radioactive reactions were also run to confirm the identity and purity of FPP at higher concentrations, and plates were visualized by phosphomolybdic acid staining followed by heating.

Preparation of FTase

Recombinant expression and purification of wild-type (WT) FTase and mutants are carried out in *E. coli* BL21(DE3) FPT/pET23a cells as described previously (*90, 148*). The cloning and purification of FTase mutants H248βA, K164βA, K294βA, R291βG, and Y300βF have previously been described (*88, 90*). The purified FTase was determined by SDS-PAGE to be >90% pure. The protein is dialyzed at 4 ^{0}C against 50 mM Hepes, pH 7.8, and 2 mM TCEP, and stored at −80 °C. Protein concentrations are determined by active site titrations as previously described (*90*).

Preparation of Cd-FTase

To reconstitute FTase with Cd^{2+}, apo-FTase is first prepared as described previously (*95, 103*). The active site Zn^{2+} and other metals are removed from FTase by dialysis of the protein against 5 mM EDTA in 50 mM Hepes, pH 7.8 and 2 mM TCEP for 24 hours at 4 ^{0}C, followed by three changes against 500 mL of 50 mM Hepes, pH 7.8, and 2 mM TCEP with 25 g of Chelex (BioRad). The apo-protein is then concentrated to 100 μM using Amicon Ultra centrifugal filter devices (10,000 MWCO) and incubated with 1 equivalent atomic absorption grade Cd^{2+} (Aldrich, Milwaukee, WI) for 12 hours at 4 ^{0}C. Excess, unbound metals are removed by exchanging the buffer several (>5) times to 50 mM Hepes, pH 7.8, and 2 mM TCEP using Amicon Ultra centrifugal filter devices (10,000 MWCO) and then concentrated to ~300 μM. The metal concentration of the protein sample is determined by inductively coupled plasma-mass spectrometry (ICP-MS) at the Keck Elemental Geochemistry Laboratory (University of Michigan, Ann Arbor, MI). Protein concentrations are determined by active site titrations as previously described (*90*).

Measurement of kinetic isotope effects

The single turnover rate constant is measured at 25 ^{0}C as previously described (*90, 95*). To measure primary and α-secondary KIEs, FTase, preincubated for >15

minutes with a mixture of FPP radiolabeled in the sensitive or remote position in buffer (50 mM Heppso, pH 7.8, 2 mM TCEP, 5 mM MgCl$_2$), was rapidly mixed with peptide in the same buffer to give final concentrations of 4 μM FTase, 1 μM FPP, and 100 μM peptide (30 μL reaction volume). A ^{14}C:^{3}H molar ratio of 9:1 was used to give approximately equal counts. For Cd-FTase, 5 mM MgCl$_2$ was preincubated with peptide immediately prior to reaction initiation. For nonpeptidic thiol substrates (GSH, NAC, DTT, and βME), the final reaction conditions were 4 μM FTase, 1 μM FPP, 5 mM thiol, 50 mM Heppso, pH 7.8, 50 mM MgCl$_2$, and 2 mM TCEP. Reactions were quenched at varying times by the addition of 90 μL of 80% 2-propanol and 20% acetic acid (v:v) and placed on ice. Reactions with single turnover rate constants less than 0.1 s^{-1} were performed manually, while reactions with rate constants faster than 0.1 s^{-1} were carried out using a KinTek rapid quench apparatus (KinTek Corporation, Austin, TX). The farnesylated product was separated from unreacted FPP on Whatman PE SIL G TLC plates in an 8:1:1 (v:v:v) 2-propanol/NH$_4$OH/H$_2$O mobile phase (*90*). Corresponding bands were cut from TLC plates and radioactivity was quantified by dual-label liquid scintillation counting using a Beckman LS 6500 liquid scintillation counter. Counts were measured in disintegrations per minute (DPM), and repeated multiple times in 30 minute cycles to minimize the error, which was calculated using standard propagation analysis. The observed first order single turnover rate constant (k_{obs}) is calculated from a single exponential fit of the fraction product (P$_t$) formed at time t defined by Eq. 1, where P$_\infty$ is the calculated reaction endpoint, which varied from 60-90% of the total FPP (*90*).

$$\frac{P_t}{P_\infty} = 1 - e^{-k_{obs}*t}$$

<div align="right">Eq. (1)</div>

An approximate KIE is obtained by calculating the ratio of the observed rate constants for ^{14}C and ^{3}H. To determine the actual observed KIE to a high precision, sets of 12 identical reactions are measured at 20-50% completion and compared with reactions measured at 100% completion (Eq. 2) (*173*). This apparent KIE is then corrected for the extent of conversion using Eq. 3 to obtain the actual observed KIE (*184*). Alternatively, full time courses are done and the ^{14}C:^{3}H ratio at each time point (KIE$_{apparent}$) is calculated and plotted as a function of extent reaction (*f*), according to Eq. 3 (*184*).

$$\text{KIE}_{\text{apparent}} = \frac{\left([\text{product}]_{\text{normal}}/[\text{product}]_{\text{heavy}}\right)_{20\text{-}50\%}}{\left([\text{product}]_{\text{normal}}/[\text{product}]_{\text{heavy}}\right)_{100\%}} \qquad \text{Eq. (2)}$$

$$\text{KIE}_{\text{obs}} = \frac{\ln\left(1 - f * \text{KIE}_{\text{apparent}}\right)}{\ln\left(1 - f\right)} \qquad \text{Eq. (3)}$$

Computational analysis and simulations

The kinetic mechanism for FTase (Scheme 5.4) was used to determine approximate values for k_1, k_{-1}, and k_2. Eq. 4 reflects the obscurement of the intrinsic kinetic isotope effect (KIE_{int}) by the forward commitment factor (C_f), which is defined as the ratio between the forward farnesylation rate constant, k_2, and the reverse rate constant for the conformational step, k_{-1} (Eq. 5). The observed rate constant measured under single turnover conditions, k_{obs}, is described by Eq. 6, derived from a two-step reversible reaction.

$$\text{KIE}_{\text{obs}} = \frac{\text{KIE}_{\text{int}} + C_f}{1 + C_f} \qquad \text{Eq. (4)}$$

$$C_f = \frac{k_2}{k_{-1}} \qquad \text{Eq. (5)}$$

$$k_{\text{obs}} = \frac{k_1 k_2}{k_1 + k_{-1} + k_2} \qquad \text{Eq. (6)}$$

Using these equations and the experimentally determined values for KIE_{obs} and k_{obs}, the data were globally fit using the Solver tool from Microsoft Excel to determine the best solutions for k_1, k_{-1}, and k_2. The relative error, defined by Eq. 7, was calculated for each value of k_{obs} and KIE_{obs}.

$$\text{relative error} = \frac{\left(\text{experimental - calculated}\right)^2}{\text{experimental}} \qquad \text{Eq. (7)}$$

The sum of relative errors, or the total error, was then minimized to globally solve for each constant. To determine the error for each calculated value, a range in values was generated from the experimental errors for k_{obs} and KIE_{obs}. For experiments with Cd-FTase, the value for KIE_{int} was approximately the same and was solved at a fixed value of 1.24 ± 0.01. Similarly, for all peptides and thiol substrates, KIE_{int} was found to be

approximately the same and was solved at a fixed value of 1.20 ± 0.01. This value for KIE_{int} was subsequently fixed as a constant for KIE experiments with FTase mutants in the PPi binding pocket, where the KIE_{int} did not appear to change. For varying Mg^{2+} concentrations with the peptide TKCVIF, KIE_{int} and k_2 were unchanged and so were fixed as constants to solve for k_1 and k_{-1}.

Simulations were done on Berkeley Madonna using the calculated values for k_1, k_{-1}, and k_2 described above. An example of a simulated single turnover experiment for WT FTase with TKCVIM is shown in Figure 5.3. The equilibration of FTase with [1-^{3}H]- and [11-^{14}C]-FPP was first simulated to mimic experimental conditions (Figure 5.3A). The final concentrations of E•FPP were then used as initial concentrations in the simulated single turnover KIE experiment (Figures 5.3B and 5.3C). The raw simulated data for product formation as a function of time were then analyzed exactly the same as the experimental data (described above), and calculated values for k_{obs} and KIE_{obs} from these simulated experiments were directly compared with experimental values.

Reaction coordinate diagrams for the FTase single turnover reaction were generated by calculating the activation energy for each step, E_a, according to the Arrhenius equation (Eq. 8), where k is the microscopic forward or reverse first order or pseudo first order rate constant, A is the frequency factor 10^{12} s^{-1}, R is the gas constant 8.31 J•K^{-1}mol^{-1}, and T is the temperature (298 K).

$$k = Ae^{-E_a/RT}$$
<div align="right">Eq. (8)</div>

The activation energy for each step was plotted, starting with the E•FPP species which is formed prior to the initiation of the reaction, and ending with the E•product complex because FPP is limiting and cannot catalyze product dissociation (Scheme 5.4). For the peptide binding step, the experimental concentrations of peptide (100 μM) were used as well as the previously measured forward and reverse rate constants for peptide binding, given in Scheme 5.4 (*92, 95*). Peptide sequence does not greatly affect binding affinity, and therefore the same rate constants were used for each peptide (*24*).
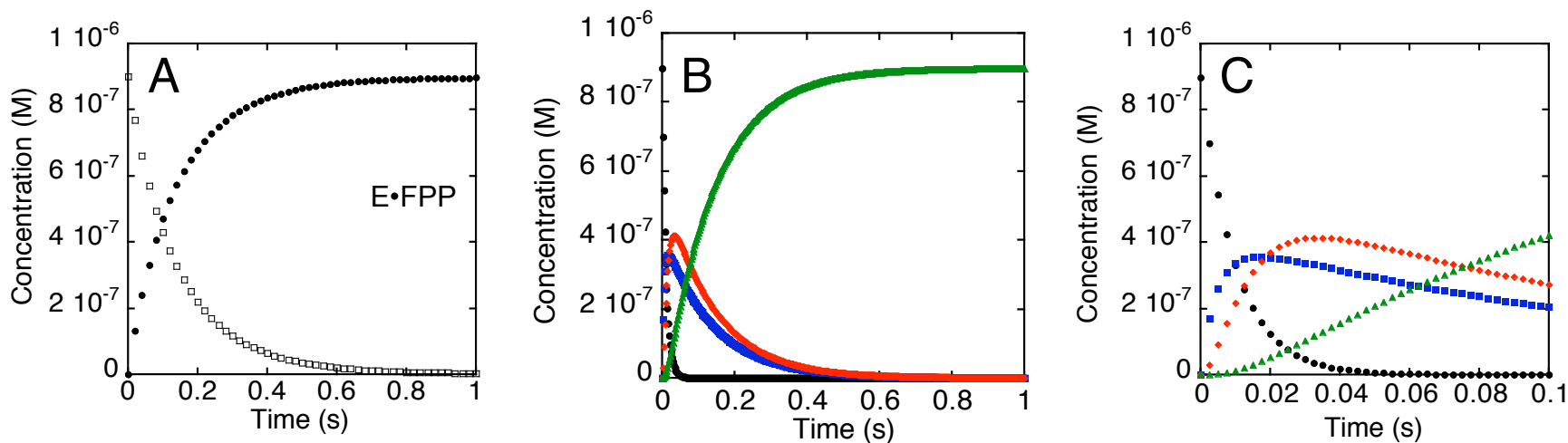
Figure 5.3 Simulated single turnover KIE experiment for FTase

Simulated experiment for WT FTase with TKCVIM, according to Scheme 5.4. (A) Equilibration of 4 μM WT FTase with 1 μM FPP (900 nM [11-^{14}C]-FPP, 100 nM [1-^{3}H]-FPP) to form FTase•FPP, using the microscopic rate constants given in Scheme 5.4. The concentration of FPP is denoted by squares (□), and the concentration of the binary complex FTase•FPP is denoted by circles (●). Only the data for [11-^{14}C]-FPP are shown here, for clarity. (B) Simulated single turnover experiment, using the final concentrations from the equilibration experiment in (A) for the initial concentration of FTase•FPP, 100 μM TKCVIM and the reaction steps including the microscopic rate constants given in Scheme 5.4 and Table 5.1. The formation of the binary complex FTase•FPP (●), inactive ternary complex FTase•FPP•TKCVIM, (■), active ternary complex [FTase•FPP•peptide]*(◆), and product complex FTase•product (▲) are shown. (C) First 0.1 s of the simulated experiment shown in (B).

Results

Synthesis and purification of radiolabeled FPP

FPP with radiolabels at either the sensitive (C1) or remote (C11) positions were synthesized using the precursors isopentenyl diphosphate and geranyl diphosphate or dimethylallyl diphosphate labeled in the appropriate positions, as dictated by the FPP synthase reaction (Schemes 5.5 and 5.6) (*178*). The synthesized FPP was purified by reversed-phase HPLC, and chromatograms measuring both the absorbance at 214 nm as well as radioactive counts showed a single peak corresponding to FPP (Figure 5.4). The purity and identity of the synthesized FPP was confirmed by TLC analysis (Figure 5.5).

Primary and secondary kinetic isotope effects for FTase

Primary ^{14}C and α-secondary ^{3}H KIEs were measured for WT FTase with TKCVIF, a peptide with a slow single turnover rate constant of 0.27 s^{-1} at saturating (5 mM) Mg^{2+}. The primary ^{14}C KIE was small (1.03 ± 0.03) and difficult to distinguish from unity when the high error was taken into account (Figure 5.6). Therefore, the remainder of the KIE experiments have been done measuring only the α-secondary ^{3}H KIE, which is large enough to measure to a high degree of precision and compare under different experimental conditions. For WT FTase, the α-secondary KIE was measured as 1.154 ± 0.006 for TKCVIF (Figure 5.7). This is a signifcant secondary KIE, and together with a small primary KIE, is consistent with a concerted mechanism with dissociative character.

The peptide TKCVIF was initially chosen to characterize the chemical transition state of FTase because the α-secondary ^{3}H KIE measured for GCVLS, a well-characterized substrate for FTase, was near unity (1.04 ± 0.01), indicating that another step besides the chemical step is most likely obscuring measurement of the intrinsic KIE for this peptide under these conditions. Diphosphate release is rapid relative to the farnesylation rate constant (Chapter 2). As a control, inorganic pyrophosphatase was added to the single turnover reaction to rapidly hydrolyze the diphosphate product; the
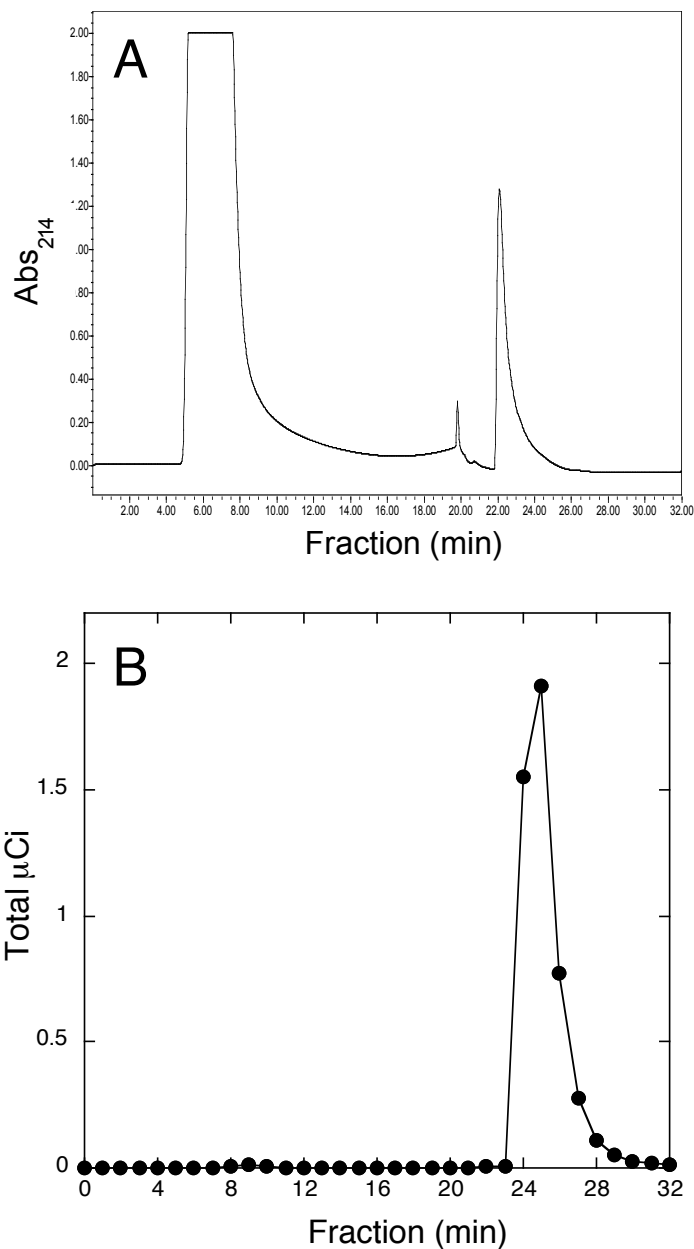
Figure 5.4 HPLC purification of FPP

HPLC chromatograms of [11-^{14}C]-FPP measuring (A) absorbance at 214 nm, and (B) radioactive counts, converted from CPM to μCi with a standard curve. A Vydac 259VHP54 column with a 300 Å particle size was loaded with 1 mL of the FPP synthase reaction, in 25 mM NH_4HCO_3, pH 8, and 8.2 mM EDTA. The first large peak in (A) corresponds to EDTA, and the second peak corresponds to the radioactive peak in (B), which is confirmed by TLC analysis to be [11-^{14}C]-FPP. There is a 2-minute delay between the detector and the fraction collector, leading to an offset of the peaks in A and B.

IPP   GPP   FPP   reaction product
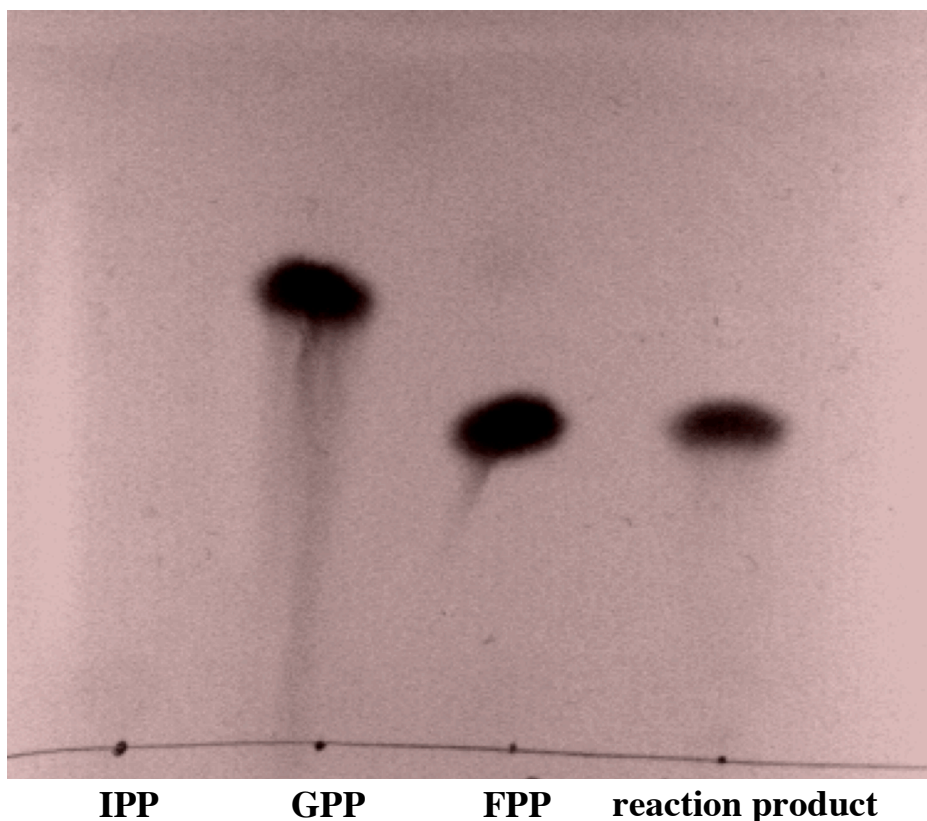
Figure 5.5 TLC analysis of synthesized FPP

Samples were dephosphorylated to alcohols using alkaline phosphatase, then extracted into pentane and loaded onto Absorbosil RP-18 HPTLC plates, and run in a 1:2:1 50 mM NH_4HCO_3 (pH 8)/2-propanol/acetonitrile mobile phase. Radioactive plates were visualized by autoradiography; shown here are results from a nonradioactive FPP synthase reaction to confirm the identity of the reaction product. Bands were detected with phosphomolybdic acid for the commercial standards GPP and FPP, but IPP did not extract into pentane. Based on the number of carbons in IPP (5) compared to GPP (10) and FPP (15), IPP is expected to run higher than GPP on the TLC plate. Therefore, the band for the reaction product corresponds to FPP.
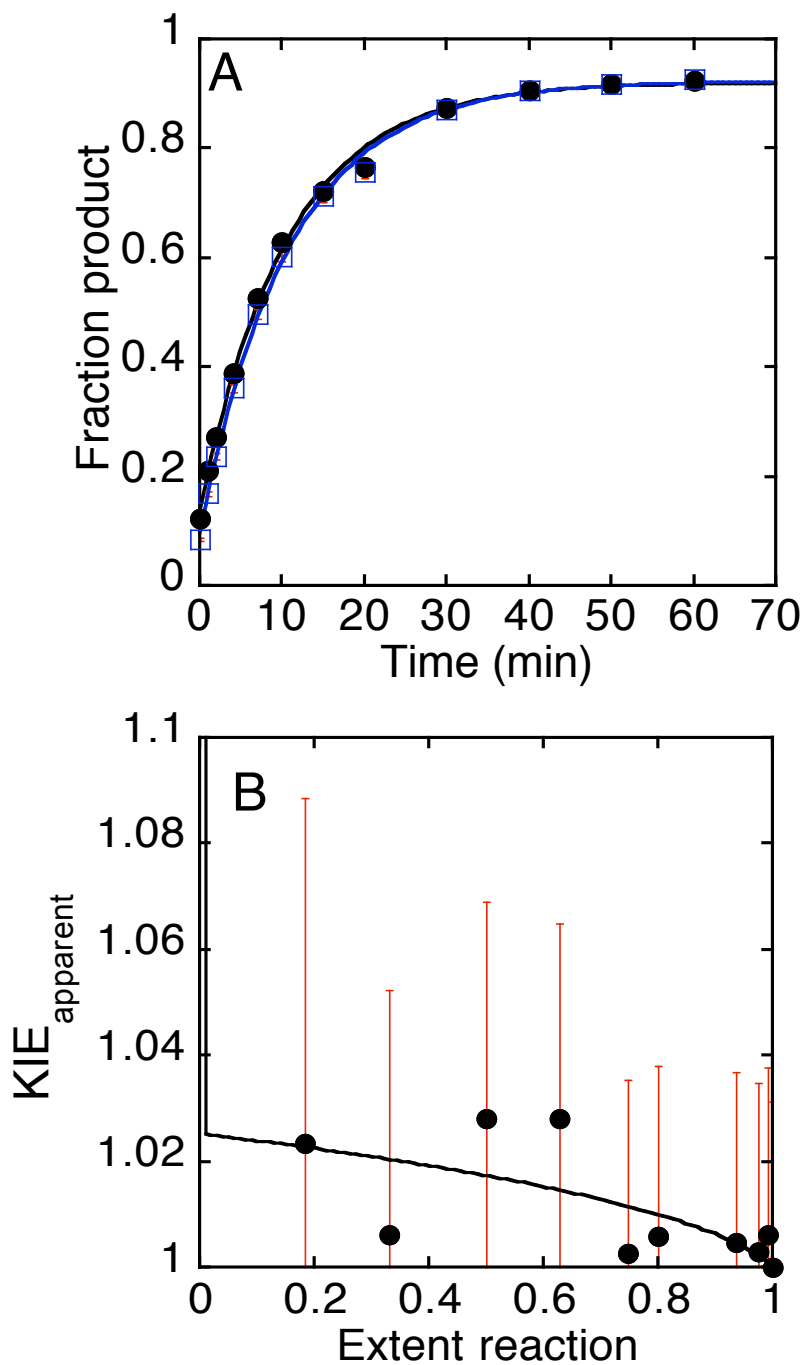
Figure 5.6 Measurement of the 1^0 ^{14}C KIE for WT FTase with TKCVIF

Single turnover reactions were run as described in Experimental Procedures. Final solutions contained 4 μM FTase, 1 μM FPP (900 nM [1-^{14}C]-FPP, 100 nM [11-^{3}H]-FPP), 100 μM TKCVIF, 50 mM Heppso, pH 7.8, and 2 mM TCEP. (A) Fraction product measured by ^{3}H (●) and ^{14}C (▢) counts, and fit to Eq. 1; (B) KIE$_{apparent}$, calculated as the ^{14}C:^{3}H ratio, plotted as a function of extent reaction and fit to Eq. 3 to obtain KIE$_{obs}$ = 1.03 ± 0.03.
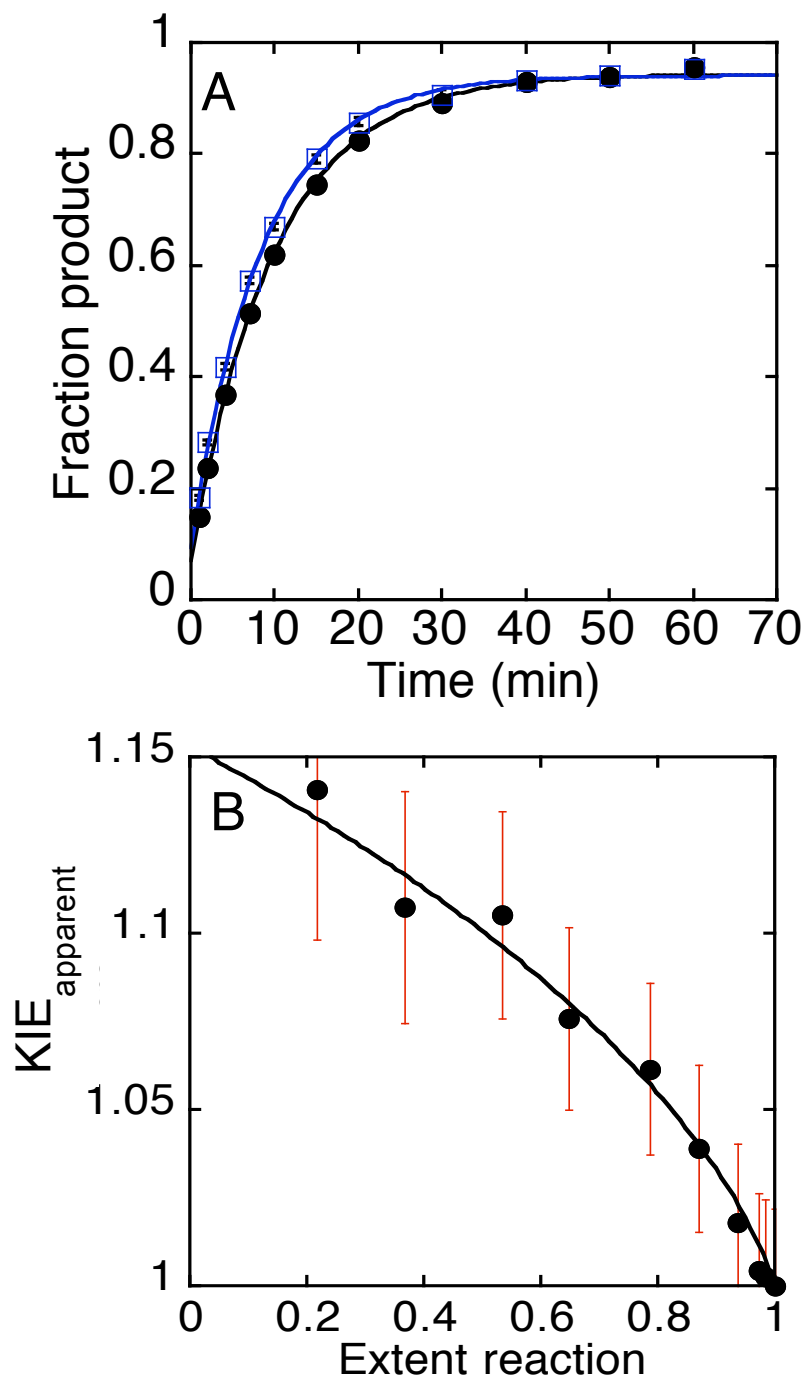
Figure 5.7 Measurement of α-secondary ^{3}H KIE for WT FTase with TKCVIF

Single turnover reactions were run as described in Experimental Procedures. Final reactions contained 4 μM FTase, 1 μM FPP (900 nM [11-^{14}C]-FPP, 100 nM [1-^{3}H]-FPP), 100 μM TKCVIF, 50 mM Heppso, pH 7.8, and 2 mM TCEP. (A) Fraction product measured by ^{3}H (●) and ^{14}C (□) counts, and fit to Eq. 1; (B) KIE$_{apparent}$, calculated as the ^{14}C:^{3}H ratio, plotted as a function of extent reaction and fit to Eq. 3 to obtain KIE$_{obs}$ = 1.154 ± 0.006.

observed KIE was not altered, thereby eliminating the possibility of a reversible reaction or a high reverse commitment factor (data not shown). These data suggest that the rate-limiting step for farnesylation of GCVLS is the conformational rearrangement of FPP prior to the chemical step that obscures the intrinsic KIE. As described later, the kinetics of the conformational rearrangement is dependent on peptide structure, and the collection of data for different peptides with varying commitment factors and observed rate constants allowed a global fit of the data to solve for a common intrinsic α-secondary ^{3}H KIE for WT FTase of 1.20 ± 0.01. This calculated value for the intrinsic KIE for WT FTase is based on the assumption that peptide structure does not change the intrinsic KIE, which agreed with all of the available data. The value of 1.20 is higher than any of the observed KIEs, which are obscured by varying commitment factors, and reflects a transition state with strong dissociative character.

Kinetic mechanism of FTase

In addition to determining the intrinsic KIE, the measurement of observed KIEs combined with single turnover rate constants were used to solve for the microscopic rate constants k_1, k_{-1} and k_2 (Scheme 5.4). This provides the first kinetic information obtained for the conformational rearrangement of FPP, a step which has previously only been inferred from crystallographic and mutagenesis studies (*21, 88*). While the solutions provided in Tables 5.1-5.5 do not represent unique solutions for k_1, k_{-1} and k_2, they are consistent with all of the data obtained thus far, and are in good agreement with experimental data when used in simulated experiments. The calculated and experimental rate constants, as given in Scheme 5.4, were plotted on reaction coordinate diagrams to illustrate the changes in commitment factors and kinetic energy barriers that occur upon different experimental conditions.

Secondary kinetic isotope effects for Cd-FTase

To further explore the contribution of Zn^{2+} to the catalytic transition state of FTase, α-secondary ^{3}H KIEs were measured for FTase substituted with Cd^{2+}, a larger and

more thiophilic metal. Cd-FTase was made by first preparing apo-FTase and then reconstituting with Cd^{2+}. ICP-MS analysis was done to confirm that the apo-protein had < 20% Zn^{2+} bound, and that the final purified Cd-FTase had ≥ 70% bound Cd^{2+}. Controls were done with excess Cd^{2+} (1.6:1), as well as with reconstituted Zn-FTase (1.3:1), to ensure that the varying metal concentrations did not affect the observed rate constants or KIE values (data not shown).

The observed single turnover kinetic rate constant (k_{obs}) was only modestly decreased (1.1 to 3.6-fold depending on the peptide) by the substitution of Cd^{2+} for Zn^{2+} (Table 5.1). Previous results have shown a greater (6-fold) decrease in the single turnover rate constant for the reaction of FPP and GCVLS catalyzed by Cd-FTase, but this effect was still relatively modest and was not observed in the absence of Mg^{2+} (95). Additionally, substitution with Cd^{2+} had little effect on other steps in the FTase reaction pathway (95). Interestingly, however, the α-secondary ^{3}H KIE was substantially increased, from 1.13 ± 0.01 for TKCVIF to 1.19 ± 0.01 (Figure 5.8, Table 5.1). A similar increase, from 1.179 ± 0.008 to 1.23 ± 0.01, was observed for TKCVIM, another peptide for which chemistry is thought to be rate-limiting; but not for GCVLS, a peptide for which the conformational step is partially rate-limiting (Table 5.1). The latter control was done to confirm that substitution of Cd^{2+} does not change the rate-limiting step in this reaction, and that the change in the observed KIE for the other two peptides is likely a direct result of a change in the structure of the chemical transition state. These results were validated by globally fitting the data and solving for the microscopic rate constants in the kinetic mechanism of FTase, using Equations 4-6 and Scheme 5.4. For the peptides TKCVIF and TKCVIM, the values for k_1 and k_{-1} are changed very little, while k_2 is slightly decreased when Cd^{2+} is substituted for Zn^{2+} (Table 5.1). While only a slight change is observed for the microscopic rate constant for farnesylation (k_2), the intrinsic KIE is solved as 1.24 ± 0.01 to account for the higher observed KIEs for TKCVIF and TKCVIM, but not for GCVLS. These calculated data were simulated and yield very similar results to the experimental data (Figure 5.8). A higher intrinsic α-secondary KIE indicates a more dissociative transition state for Cd-FTase, suggesting an integral role for the metal ion in modulating the reactivity of the thiolate nucleophile in the FTase-catalyzed reaction.

Table 5.1 Kinetic constants for reaction of FPP and various peptides catalyzed by Zn- and Cd-FTase [a]

Peptide	Metal	k_{obs} (s^{-1})	2^0 ^{3}H KIE$_{obs}$	k_1 (s^{-1}) [b]	k_{-1} (s^{-1}) [b]	k_2 (s^{-1}) [b]	C_f [b]
GCVLS	Zn-FTase	4.9 ± 0.8	1.04 ± 0.01	12 ± 2	3 ± 1	10 ± 2	4 ± 1
	Cd-FTase	2.0 ± 0.2	1.03 ± 0.03	2.5 ± 0.9	3 ± 1	20 ± 10	7 ± 4
TKCVIM	Zn-FTase	7.2 ± 0.4	1.179 ± 0.008	138 ± 1	98 ± 1	13 ± 1	0.13 ± 0.01
	Cd-FTase	2.0 ± 0.2	1.23 ± 0.01	63 ± 3	110 ± 20	5.6 ± 0.2	0.05 ± 0.01
TKCVIF	Zn-FTase	0.27 ± 0.01	1.13 ± 0.01	970 ± 10	0.48 ± 0.04	0.27 ± 0.01	0.56 ± 0.06
	Cd-FTase	0.25 ± 0.01	1.19 ± 0.01	1000 ± 10	0.92 ± 0.04	0.25 ± 0.01	0.27 ± 0.01

[a] Final solutions contained 4 μM FTase, 1 μM FPP (900 nM [11-^{14}C]-FPP, 100 nM [1-^{3}H]-FPP), 100 μM TKCVIF, 5 mM MgCl$_2$, 50 mM Heppso, pH 7.8, and 2 mM TCEP. All assays were conducted at 25 ^{0}C.
[b] k_1, k_{-1}, k_2 and C_f are calculated constants given by Scheme 5.4 and Equations 4-6. They were calculated by globally fitting the data for k_{obs} and KIE$_{obs}$ using the Solver tool from Microsoft Excel, which minimized the sum of relative errors for each data set (defined by Eq. 7). To determine the error for each calculated value, a range in values was generated from the experimental errors for k_{obs} and KIE$_{obs}$. The intrinsic KIE (Eq. 4) was solved as 1.24 ± 0.01 for Cd-FTase and 1.20 ± 0.01 for Zn-FTase.
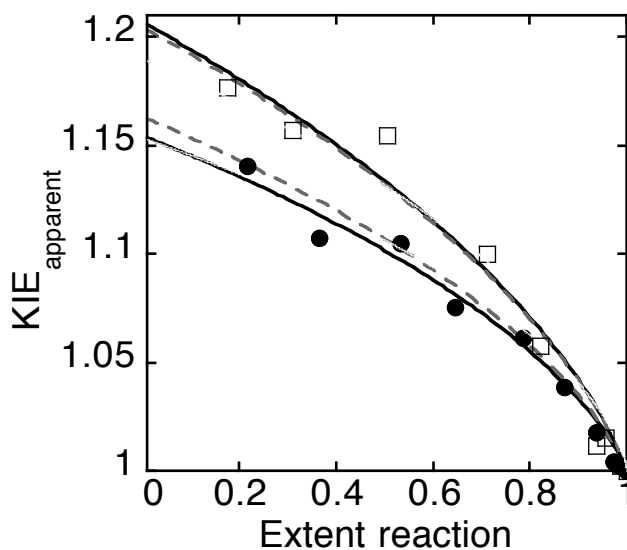
Figure 5.8 Measurement of α-secondary ^{3}H KIE for TKCVIF for Zn-FTase and Cd-FTase

Measurement of α-secondary ^{3}H KIE for TKCVIF for Zn-FTase (●) and Cd-FTase (□). Final reactions contained 4 μM FTase, 1 μM FPP (900 nM [11-^{14}C]-FPP, 100 nM [1-^{3}H]-FPP), 100 μM TKCVIF, 5 mM MgCl$_2$, 50 mM Heppso, pH 7.8, and 2 mM TCEP. The data from simulated experiments using the constants shown in Table 5.1 are shown in dotted lines. Eq. 3 is fit to the data to determine the observed α-secondary ^{3}H KIE, listed in Table 5.1.

Effect of Mg^{2+} on secondary KIE

One important catalytic feature of the proposed chemical transition state of FTase is the development of negative charge on the PPi leaving group (*95*). Mg^{2+} enhances the single turnover rate constant catalyzed by FTase up to 700-fold for GCVLS, and has been proposed to stabilize the transition state by coordinating to and stabilizing the formation of the PPi leaving group (*95, 96, 106*). Mg^{2+} has also been proposed to stabilize the conformational rearrangement of FPP by forming a high affinity Mg^{2+} binding site in this conformation (Figure 5.2) (*107*). Therefore, Mg^{2+} could affect the rate constant for either the conformational change (k_1, k_{-1}) or farnesylation (k_2). Consistent with a catalytic role, Mg^{2+} enhances the single turnover rate constant for TKCVIF approximately 100-fold but the α-secondary ^{3}H KIE is not greatly altered (Table 5.2). An unchanged KIE could mean that the transition state structure is unchanged; however, the effect on the observed single turnover rate constant suggests that Mg^{2+} decreases the activation energy for the conformational step, leading to a change in the relative energies between the ground and transition states for the active substrate conformaton. The data were simulated to solve for the microscopic rate constants in Scheme 5.4, listed in Table 5.2. The forward rate constant for the conformational change, k_1, is greatly increased by Mg^{2+}, while k_{-1} and k_2 are changed very little, consistent with Mg^{2+} equally stabilizing the transition states for both the conformational change and farnesylation (Table 5.2).

Secondary KIEs for FTase PPi binding pocket mutants

In addition to Mg^{2+}, the positively charged residues in the PPi binding pocket interact with the PPi group when FPP is bound in the inactive conformation (Figure 5.1). The role of these residues in the stabilization of the PPi leaving group in the chemical transition state and the FPP conformational change was therefore examined by measuring the α-secondary ^{3}H KIEs for mutants of FTase in the PPi binding pocket. The specific mutants chosen for this study (H248A, K164A, K294A, R291G and Y300F) have previously been characterized using steady-state and single turnover kinetics, and exhibit significantly decreased catalytic activity (Table 5.3) (*88, 90*). Surprisingly, the α-

Table 5.2 Effect of Mg^{2+} on α-secondary ^3H KIE for reaction with TKCVIF [a]

[MgCl$_2$]	k_{obs} (s^{-1})	2^0 ^3H KIE$_{obs}$	k_1 (s^{-1}) [b]	k_{-1} (s^{-1}) [b]	k_2 (s^{-1}) [b]	C$_f$ [b]
0	0.0026 ± 0.0001	1.154 ± 0.006	0.011 ± 0.002	0.9 ± 0.1	0.27 ± 0.01	0.32 ± 0.05
0.1 mM	0.016 ± 0.001	1.14 ± 0.01	0.05 ± 0.01	0.6 ± 0.1	0.27 ± 0.01	0.4 ± 0.1
5 mM	0.27 ± 0.01	1.13 ± 0.01	970 ± 10	0.48 ± 0.04	0.27 ± 0.01	0.56 ± 0.06

[a] Final solutions contained 4 μM FTase, 1 μM FPP (900 nM [11-^{14}C]-FPP, 100 nM [1-^{3}H]-FPP), 100 μM TKCVIF, 0-5 mM MgCl$_2$, 50 mM Heppso, pH 7.8, and 2 mM TCEP. All assays were conducted at 25 ^{0}C.

[b] k_1, k_{-1}, k_2 and C$_f$ are calculated constants given by Scheme 5.4 and Equations 4-6. They were calculated by globally fitting the data for k_{obs} and KIE$_{obs}$ using the Solver tool from Microsoft Excel, which minimized the sum of relative errors for each data set (defined by Eq. 7). To determine the error for each calculated value, a range in values was generated from the experimental errors for k_{obs} and KIE$_{obs}$. The intrinsic KIE (Eq. 4) and k_2 were unchanged for all of the data and were solved as 1.20 ± 0.01 and 0.27 s^{-1}, respectively.

Table 5.3 Kinetic constants of FTase PPi pocket mutants [a]

FTase mutant	k_{obs} (s^{-1})	2^0H KIE$_{obs}$	k_1 (s^{-1}) [b]	k_{-1} (s^{-1}) [b]	k_2 (s^{-1}) [b]	C_f [b]
WT	7.2 ± 0.4	1.179 ± 0.008	138	98	13	0.133
H248A	0.70 ± 0.04	1.16 ± 0.01	4.5	9.7	2.6	0.27
K164A	0.20 ± 0.02	1.19 ± 0.01	3.3	82	5.5	0.067
K294A	0.20 ± 0.01	1.20 ± 0.02	15	390	5.5	0.014
R291G	0.048 ± 0.001	1.179 ± 0.004	0.42	24	3.1	0.13
Y300F	0.0149 ± 0.0003	1.20 ± 0.02	1.1	29	0.41	0.014

[a] Final solutions contained 4 μM FTase, 1 μM FPP (900 nM [11-^{14}C]-FPP, 100 nM [1-^{3}H]-FPP), 100 μM TKCVIM, 5 mM MgCl$_2$, 50 mM Heppso, pH 7.8, and 2 mM TCEP. All assays were conducted at 25 ^{0}C.
[b] k_1, k_{-1}, k_2 and C_f are calculated constants given by Scheme 5.4 and Equations 4-6. They were calculated by globally fitting the data for k_{obs} and KIE$_{obs}$ using the Solver tool from Microsoft Excel, which minimized the sum of relative errors for each data set (defined by Eq. 7). The intrinsic KIE (Eq. 4) was unchanged for all of the data and was solved as 1.20 ± 0.01.

secondary ^{3}H KIE changes very little for all mutations in the PPi binding pocket (Table 5.3). Like Mg^{2+}, then, these positively charged residues appear to stabilize the transition state for the formation of the active substrate conformation as well as the farnesylation step (Figure 5.2). The KIEs for the mutants for the $-$Mg^{2+} reaction were also unchanged, indicating that Mg^{2+} does not change the transition state energies in the absence of any of these positively charged residues (data not shown). Alterations in the kinetics are further examined by fitting the kinetic mechanism of FTase to the KIE$_{obs}$ and k_{obs} data (Scheme 5.4); each of these residues greatly affects k_1, while having little effect on the other rate constants (Table 5.3). One exception is Y300F, which has a much slower observed rate constant than the other mutants, as well as a decreased calculated value for k_2. This results in a very low commitment factor (0.01) and a high observed KIE of 1.20 ± 0.02.

Effect of thiol structure on observed secondary KIE

The α-secondary KIE is significantly different for the reaction of FTase•FPP with TKCVIM (1.179) and GCVLS (1.04) (Table 5.1), suggesting that the peptide structure may affect the equilibrium of the FPP conformational rearrangement. To further investigate the effect of the structure of the peptide substrate on reactivity, we examined the KIE for the FTase reaction with small, nonpeptidic thiol substrates (Scheme 5.7). These molecules are all smaller in size than the peptide substrate GCVLS, but have previously been shown to be FTase substrates (*181*). However, they not only have much slower rate constants, but also bind Mg^{2+} with an apparent weaker affinity than peptide substrates (*181*). These data suggest that the small thiols may alter the FPP conformational change and key interactions of FPP with Mg^{2+}.

KIE experiments were done at the subsaturating substrate concentrations of 5 mM thiol and 50 mM Mg^{2+}. These conditions were used to minimize the inhibition observed at higher concentrations of thiol and/or Mg^{2+} (data not shown). The observed rate constants, therefore, are smaller than those previously reported at saturating concentrations (*181*). The Mg^{2+} concentration has little effect on the α-secondary ^{3}H KIE for peptide substrates (Table 5.2), and similarly should not change the observed KIE for
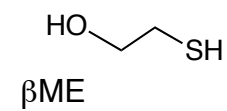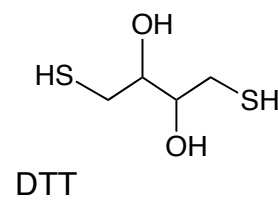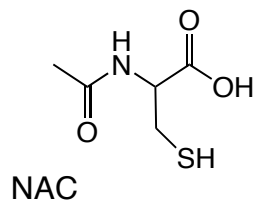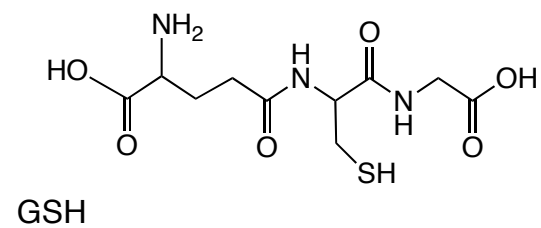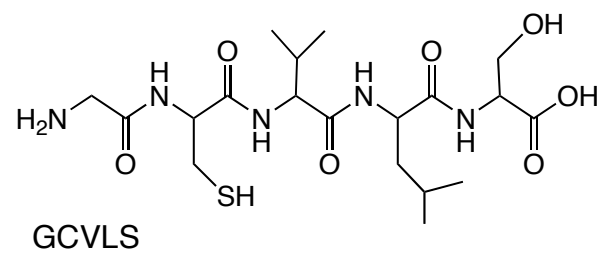
Scheme 5.7 Structures of nonpeptidic thiol substrates used in this study (*181*)

GCVLS

GSH

NAC

DTT

βME

nonpeptidic thiols. Although the thiol concentrations are subsaturating, the observed KIE most likely reflects a step after thiol binding, since the thiols bind and dissociate rapidly and thus the commitment for binding is low (*181*).

The α-secondary KIEs for WT FTase with the small nonpeptidic thiols GSH, NAC, DTT and βME are near unity, within error (Table 5.4). A smaller KIE, indicative of a larger commitment factor, and a smaller observed rate constant indicate that the transition state for the conformational change is destabilized more than the transition state for farnesylation for these substrates, and therefore the FPP conformational step is rate-limiting. Indeed, when these data are globally fit, the step that is most affected is k_1, which is slowed down so drastically that k_{obs} is essentially equal to k_1 (Table 5.4). The reverse rate constant for the conformational step, k_{-1}, is also slowed relative to k_2 so that the commitment factor is very high and the observed KIE is unity (Equations 4 and 5). Thus the FPP conformational change is sensitive to the structure of the peptide, and the decrease in size for the nonpeptidic thiols most likely removes important interactions that the peptide substrate makes with both FPP and the active site of FTase.

Dependence of peptide sequence on observed secondary KIE

To further understand the interactions between E•FPP and thiol substrates that enhance the conformational change, we next investigated how peptide sequence affects the kinetic mechanism of FTase. Important determinants of peptide specificity that affect reactivity include the X group of the CaaX region and the region of polybasic residues located upstream of the CaaX box (*24, 77*). The α-secondary KIE was measured for several peptides with differing X residues as well as peptides that contain an upstream lysine residue (Table 5.5). A global fit of the data for all peptide substrates yields the same intrinsic KIE (1.20 ± 0.01). This suggests that the structure of the peptide substrate does not change the structure of the chemical transition state. This is not surprising since the basicity, and therefore nucleophilicity, of these compounds is similar. The large differences in the observed KIE, on the other hand, reflect different commitment factors for each peptide (Table 5.5).

Table 5.4 Kinetic constants of WT FTase with small nonpeptidic thiol substrates [a]

Substrate	k_{obs} (s^{-1})	2^0 ^{3}H KIE$_{obs}$	k_1 (s^{-1}) [b]
GCVLS	4.9 ± 0.8	1.04 ± 0.01	12 ± 2
GSH	0.0014 ± 0.0001	1.01 ± 0.03	0.0016 ± 0.0004
NAC	0.00054 ± 0.00005	1.05 ± 0.09	0.0007 ± 0.0004
DTT	0.0028 ± 0.0002	1.03 ± 0.02	0.0035 ± 0.0005
βME	0.0005 ± 0.0001	1.00 ± 0.03	NA

[a] Final solutions contained 4 μM FTase, 1 μM FPP (900 nM [11-^{14}C]-FPP, 100 nM [1-^{3}H]-FPP), 5 mM thiol, 50 mM MgCl$_2$, 50 mM Heppso, pH 7.8, and 2 mM TCEP. All assays were conducted at 25 ^{0}C.

[b] k_1 is the calculated rate constant for the conformational change (Scheme 5.4). The values for k_1, k_{-1}, k_2 and C$_f$ were calculated by globally fitting the data for k_{obs} and KIE$_{obs}$ using the Solver tool from Microsoft Excel, which minimized the sum of relative errors for each data set (defined by Eq. 7). To determine the error for k_1, a range in values was generated from the experimental errors for k_{obs} and KIE$_{obs}$. The intrinsic KIE (Eq. 4) was unchanged for all of the data and was solved as 1.20 ± 0.01. Because $k_1$ is very small and represents the rate-determining rate constant, the values for k_{-1} and k_2 are not well defined. The value for C$_f$ is also not well defined, but is large for all thiol substrates (≥ 4-20).

NA = not applicable; since the observed KIE was 1.00 for βME, the commitment factor and rate constants could not be calculated. Considering the error associated with the observed KIEs for all thiols, the calculated values for βME are probably similar to the other compounds.

Table 5.5 Kinetic constants of WT FTase with different peptides [a]

Peptide	k_{obs} (s^{-1})	2^0 ^{3}H KIE$_{obs}$	k_1 (s^{-1}) [b]	k_{-1} (s^{-1}) [b]	k_2 (s^{-1}) [b]	C_f [b]
TKCVIM	7.2 ± 0.4	1.179 ± 0.008	138 ± 1	98 ± 1	12.9 ± 0.8	0.133 ± 0.008
TKCVLS	4.0 ± 0.2	1.16 ± 0.01	27.6 ± 0.4	48 ± 1	12.8 ± 0.7	0.27 ± 0.01
TKCVIF	0.27 ± 0.01	1.13 ± 0.01	970 ± 10	0.48 ± 0.04	0.27 ± 0.01	0.56 ± 0.06
TGCVIM	4.2 ± 0.9	1.095 ± 0.004	13 ± 3	10 ± 1	11 ± 2	1.1 ± 0.3
SKTKCVIM	0.92 ± 0.09	1.087 ± 0.005	1.8 ± 0.2	8.5 ± 0.2	11.3 ± 0.1	1.33 ± 0.04
GCVLS	4.9 ± 0.8	1.04 ± 0.01	12 ± 2	3 ± 1	10 ± 2	4 ± 1

[a] Final solutions contained 4 μM FTase, 1 μM FPP (900 nM [11-^{14}C]-FPP, 100 nM [1-^{3}H]-FPP), 100 μM peptide, 5 mM MgCl$_2$, 50 mM Heppso, pH 7.8, and 2 mM TCEP. All assays were conducted at 25 ^{0}C.
[b] k_1, k_{-1}, k_2 and C_f are calculated constants given by Scheme 5.4 and Equations 4-6. They were calculated by globally fitting the data for k_{obs} and KIE$_{obs}$ using the Solver tool from Microsoft Excel, which minimized the sum of relative errors for each data set (defined by Eq. 7). To determine the error for each calculated value, a range in values was generated from the experimental errors for k_{obs} and KIE$_{obs}$. The intrinsic KIE (Eq. 4) was unchanged for all of the data and was solved as 1.20 ± 0.01.

Surprisingly, the identity of the X residue makes little difference in the observed KIE, despite drastically affecting the reactivity of FTase, as measured by both steady-state kinetic constants as well as the single turnover rate constant (Table 5.5) (*24*). For example, two peptides differing only in the identity of the X residue, TKCVIM and TKCVIF, have similar α-secondary KIEs (1.179 and 1.13, respectively) even though TKCVIF is a much slower substrate (0.27 s^{-1} compared to 7.2 s^{-1} for TKCVIM) (Figure 5.9, Table 5.5). Similar KIEs between these two peptides reflect similar commitment factors (within a 5-fold difference), and therefore the ratio of k_2/k_{-1} is changed little (Equations 4 and 5). To explain the small change in KIE but the great difference in the observed rate constants, a decrease in k_2 for the slower peptide, TKCVIF, must be accompanied by a corresponding decrease in k_{-1}. Thus the stability of the ground state of the active substrate conformation is greatly affected by the identity of the X group. When these data are fit to determine the individual rate constants, k_2 is ~10 s^{-1} when X = M or S, whereas when X = F, k_2 is reduced to ~ 0.3 s^{-1} (Table 5.5). The value for k_{-1} changes accordingly so that the commitment factor does not depend greatly on the X residue, while there is a modest effect on the value of k_1 (Table 5.5). The calculated kinetic constants for TKCVIM and TKCVIF were used in a simulated experiment and are in good agreement with the experimental data (Figure 5.9).

In contrast to the X residue of the CaaX sequence, the presence of a lysine one residue upstream of the reactive cysteine, present in the K-Ras4B template TKCVIM, greatly affects the forward equilibrium constant for the conformational change. There is a significant increase in the observed KIE when an upstream lysine is present; for example, the α-secondary ^{3}H KIEs for TKCVLS and GCVLS are 1.16 $\pm$ 0.01 and 1.04 $\pm$ 0.01, respectively, while the observed rate constants for these peptides are quite similar (Figure 5.10, Table 5.5). These data are consistent with the upstream lysine residue stabilizing the transition state for the FPP conformational step, while the farnesylation step is unchanged. Fitting individual rate constants to these data suggests that the upstream lysine residue significantly increases the values of k_1 and k_{-1} relative to k_2, by stabilizing the transition state for formation of the active substrate conformation. Because k_2 is unchanged, this leads to a smaller C_f and a larger observed KIE. However, when more than one lysine residue is present, as in SKTKCVIM, the observed KIE is
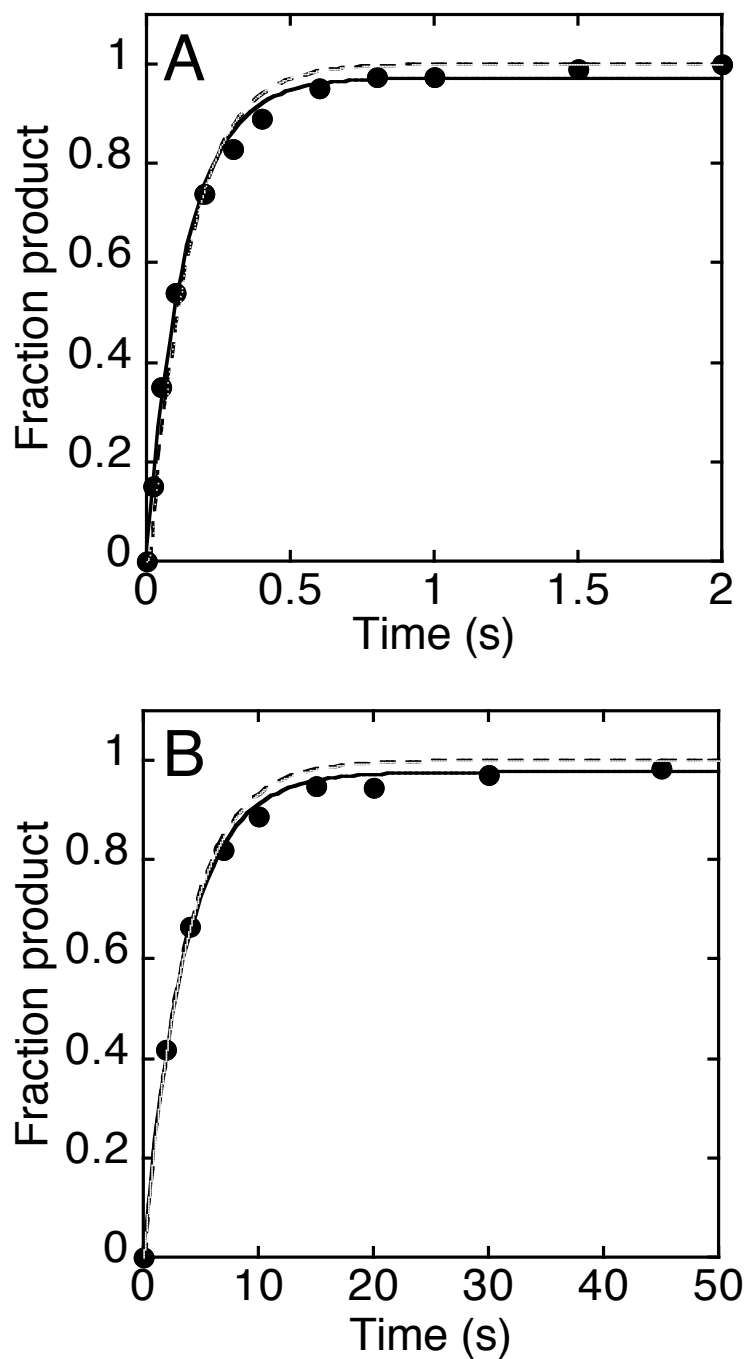
Figure 5.9 Time course for TKCVIM and TKCVIF

Single turnover experiment for WT FTase with (A) TKCVIM and (B) TKCVIF. Final reactions contained 4 μM FTase, 900 nM $[11\text{-}^{14}C]$-FPP, 100 μM peptide, 50 mM Heppso, pH 7.8, 2 mM TCEP, and 5 mM $MgCl_2$. Eq. 1 is fit to the data to determine k_{obs}, the single turnover rate constant. The data from simulated experiments are shown in dotted lines.
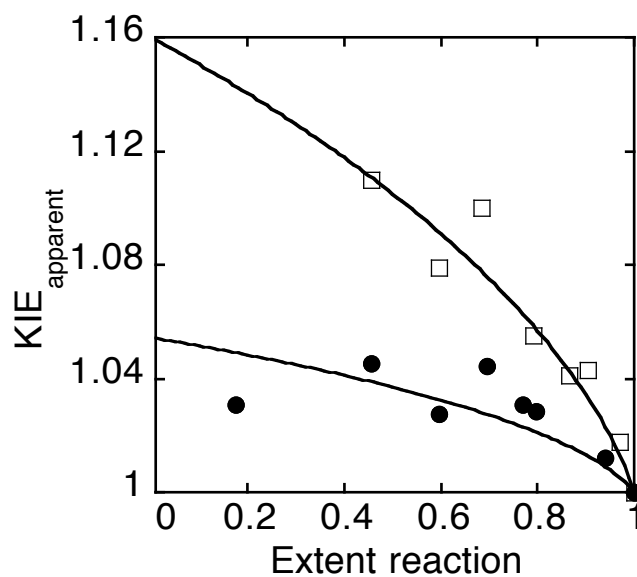
Figure 5.10 Measurement of α-secondary ^{3}H KIE for GCVLS and TKCVLS

Measurement of α-secondary ^{3}H KIE for GCVLS ($\bullet$) and TKCVLS ($\square$). Final reactions contained 4 μM FTase, 1 μM FPP (900 nM [11-^{14}C]-FPP, 100 nM [1-^{3}H]-FPP), 100 μM peptide, 50 mM Heppso, pH 7.8, 2 mM TCEP, and 5 mM MgCl$_2$. Eq. 3 is fit to the data to determine the observed α-secondary ^{3}H KIE.

smaller (1.087 ± 0.005), indicating that C_f increases. Peptides containing multiple lysine residues have a weaker apparent affinity for Mg^{2+} (*77*), which may partially explain the decrease in the rate constants for the conformational step, k_1 and k_{-1}, as well as the higher commitment factor for SKTKCVIM (Table 5.5). These results highlight the importance of the peptide sequence in determining the kinetics of the conformational change, which may be a significant factor in the substrate specificity of FTase.

Discussion

Chemical transition state of FTase

Isotope experiments have identified concerted mechanisms with dissociative character for many enzymes. The α-secondary ³H KIE measured here is comparable to the α-secondary ³H KIEs for pertussis and diphtheria toxins and orotate phosphoribosyl-transferase (1.199, 1.194, and 1.200, respectively), for which dissociative mechanisms with oxocarbenium-ion-like character in the transition state have been described (*174, 177, 185*). The reaction of pertussis toxin, like FTase, has an attacking cysteine thiolate as a nucleophile with a primary ¹⁴C KIE of 1.049 ± 0.003 and an α-secondary ³H KIE of 1.199 ± 0.009 (*177*). A transition state structure analysis of pertussis toxin reveals a transition state with oxocarbenium ion character due to accumulation of positive charge on the ribosyl ring of NAD^+ (*177*). For FTase, the intrinsic α-secondary ³H KIE of 1.20 ± 0.01 is consistent with a concerted mechanism with dissociative character (Scheme 5.8), since it is significantly less than the theoretical equilibrium isotope effect for the formation of a fully dissociated carbocation in the transition state (1.4-1.5) (*186, 187*). A primary ¹⁴C KIE of 1.03 ± 0.03 is consistent with this proposed transition state structure, in which the bond to the PPi leaving group is nearly broken, while the bond to the incoming thiolate nucleophile is barely formed (Scheme 5.8).

The measurement of KIEs using transient kinetics is a powerful technique to overcome large commitments in complex enzymatic reactions, but has only been used for a limited number of systems thus far. In the case of FTase, measurement of intrinsic KIEs are complicated using steady-state analysis, and the α-secondary ³H KIE

Scheme 5.8 Transition state model for rat FTase (*95*).

measurement reported here provides the first direct evidence of a transition state with dissociative character for this class of enzymes that catalyzes zinc-dependent sulfur alkylation. This value is larger than the experimental α-secondary ^{2}H KIE of 1.068 (corresponding to a ^{3}H KIE of 1.100) reported for yeast FTase with the unnatural substrate GPP using steady-state kinetic analysis, and probably reflects either a difference in the mechanism between these two enzymes or substrates used, or an obscurement of the intrinsic KIE for GPP despite a lower commitment factor than was measured for FPP (*176, 188*).

Role of zinc ion in chemical transition state of FTase

The prenyltransferases FTase and GGTase I are the newest members of the class of enzymes that catalyze zinc-dependent sulfur alkylation, which include methionine synthases, human betaine-homocysteine methyltransferase, and methanol:coenzyme M methyltransferases (*101, 102*). Members of this class are characterized by a thiolate nucleophile directly coordinated to Zn^{2+} in a catalytic metal site. With the exception of prenyltransferases, these enzyme mechanisms are characterized by poor leaving groups and are proposed to proceed via associative mechanisms. FTase is the first enzyme in this class for which there is evidence for dissociative character in the transition state (*95, 99, 102*). Nonetheless, the zinc ion is proposed to enhance catalysis in FTase by lowering the pK_a of the sulfur to create a more potent zinc-thiolate nucleophile (*82*). This is supported by structural and kinetic evidence which point to the importance of zinc in coordinating to the peptide substrate in a concerted catalytic transition state (*78-80, 82, 95, 98, 189*).

The increased intrinsic α-secondary ^{3}H KIE of 1.24 ± 0.01 for Cd-FTase indicates a more dissociative transition state when Cd^{2+} is substituted for Zn^{2+}. This result can be explained by the fact that Cd^{2+} is significantly larger (99 pm compared to 88 pm), more polarizable and more thiophilic than Zn^{2+}, with Cd-FTase binding 5-fold more tightly to the peptide (*95*). While it has been proposed that the metal-thiolate distance controls the nucleophilicity of the FTase reaction, there is no direct evidence for this since structural studies are unable to capture the active substrate conformation (*103*). The KIE data

presented here are consistent with the role of Zn^{2+} in being essential to the nucleophilic participation of the thiolate in the chemical transition state (Scheme 5.8). The ambiguous effect of Cd^{2+} substitution on the observed single turnover rate constant measured here and elsewhere (Table 5.1) (*95*) may be explained by the fact that the observed single turnover rate constant does not necessarily reflect the farnesylation step, as previously thought. Thus the determination of the α-secondary KIE provides more direct information regarding the effect of Cd^{2+} on the chemical transition state.

Role of diphosphate leaving group

An important feature of the dissociative transition state model stabilized by FTase is the buildup of charge on the diphosphate leaving group, because the bond with the oxygen atom is nearly broken (Scheme 5.8) (*95*). The diphosphate moiety in many enzymes is important for catalysis as a leaving group, a characteristic which is facilitated by coordination of the diphosphate by Mg^{2+}. In addition, for FTase a high affinity Mg^{2+} binding site is crucial for formation of the active substrate conformation (Figure 5.2). This site consists of the two nonbridging oxygens of the diphosphate, the two carboxylate oxygens of D352β, a water molecule, and one carboxylate oxygen of D297β (shared with Zn^{2+}) (*107*). It had been suggested from these studies that the binding site for Mg^{2+} is not created until the bound FPP rearranges into the active substrate conformation. Here we show that Mg^{2+} equally stabilizes the transition states for both the conformational change and the chemical farnesylation step, as well as the ground state for the active substrate conformation (Table 5.2, Figure 5.11). The net effect is an apparent increase in k_1, which leads to an increase in the observed single turnover rate constant but no change in the observed KIE.

While less is known about the mechanism of GGTase I, this enzyme is generally thought to proceed via a similar catalytic and kinetic mechanism as FTase, with the notable exception that Mg^{2+} does not accelerate catalysis for GGTase I (*12, 108*). The FTase aspartate residue, D352β, is changed in GGTase I to a lysine, which is thought to replace Mg^{2+} in the FTase active site (*107, 108*). Thus it seems likely that for GGTase I, the conformational rearrangement of geranylgeranyl diphosphate is not accelerated by
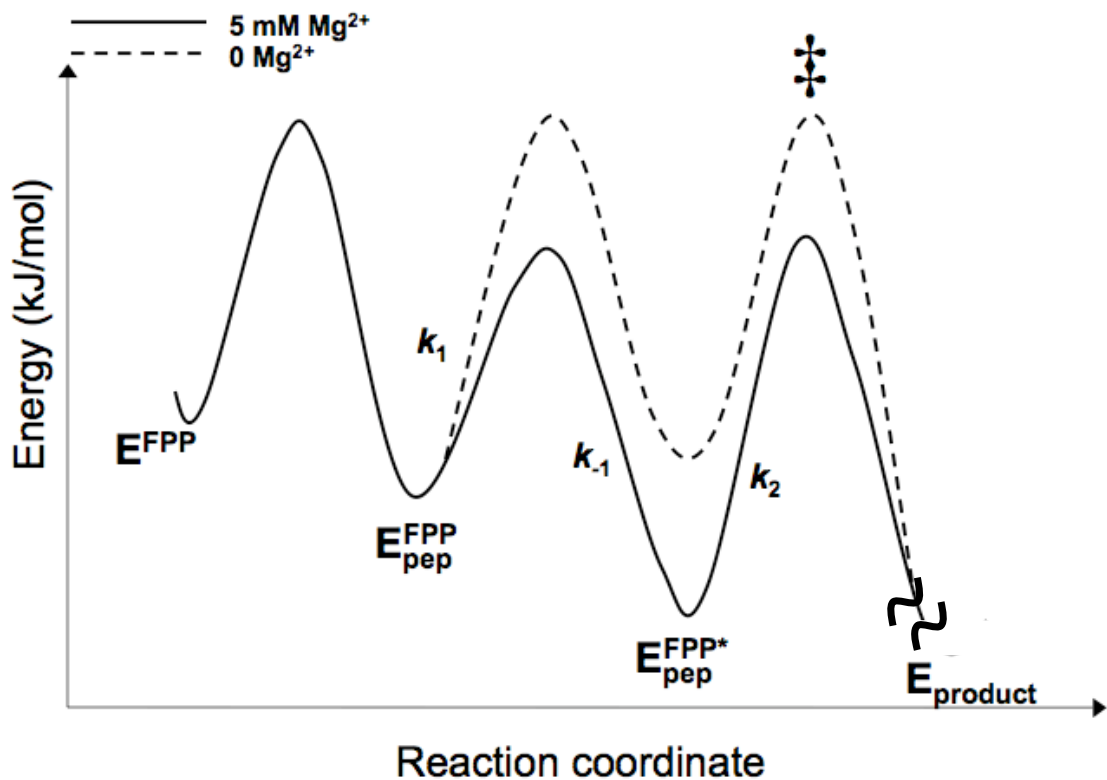
Figure 5.11 Effect of Mg^{2+} on the reaction pathway of FTase

Reaction coordinate diagram following the FTase reaction pathway during a single turnover experiment, illustrating how the conformational rearrangement and chemical steps are affected by magnesium. Free energies were calculated from the kinetic rate constants given in Scheme 5.4 and Table 5.2, using Eq. 8, for WT FTase with 100 µM TKCVIF at 5 mM MgCl$_2$ (solid line) and 0 mM MgCl$_2$ (dashed line). Concentrations used are the same as experimental conditions (see Experimental Procedures).

Mg^{2+} because there is no high affinity Mg^{2+} binding site present in the active substrate conformation for GGTase I. Given that the formation of the active substrate conformation is dependent on the structure of the peptide substrate, this difference between the two prenyltransferases may partially explain some key differences in their peptide substrate specificities.

The interactions of the positively charged residues in the PPi binding pocket with the diphosphate of FPP in the inactive ternary conformations have been determined from crystallographic studies (*84, 85, 87*), while interactions with the diphosphate in the active substrate conformation are inferred from structural modeling and mutagenesis studies (*88, 90*). In the inactive ternary complex FTase•FPP•CVFM, K164α and R291β interact primarily with the α-phosphate of FPP, while Y300β, H248β, and K294β interact with the β-phosphate (Figure 5.1) (*85*). In the proposed active substrate conformation, on the other hand, K164α forms a hydrogen bond with the β-phosphate and R291β makes a bidentate interaction with two of the nonbridging oxygen atoms of the PPi group, while Y300β forms a hydrogen bond with the phosphate oxygen bound to C1 of FPP, H248β interacts with the diphosphate bridging oxygen, and K294β interacts with the terminal oxygen atom on the β-phosphate (Figure 5.2) (*88, 90, 115*). Like Mg^{2+}, then, these residues have been proposed to be important in catalysis by stabilizing the diphosphate leaving group as well as correctly orienting the PPi group in the active substrate conformation (*88, 90*).

The KIEs measured for the PPi binding pocket mutants H248βA, K164βA, K294βA, R291βG, and Y300βF are not changed, despite the fact that the reactivity is drastically affected (Table 5.3). These data mirror the results for Mg^{2+}, and indicate that interactions with the PPi group mediated by both Mg^{2+} and positively charged residues in the PPi binding pocket are involved in the structural rearrangement of the FPP substrate prior to farnesylation as well as stabilizing the transition state for farnesylation. While this had previously been inferred from structural studies, the kinetic studies presented here confirm the importance of the FPP conformational rearrangement in the catalytic cycle of FTase.

FPP conformational rearrangement is dependent on peptide structure

The conformational rearrangement of FPP has indirectly been studied by crystal structures, site-directed mutagenesis and substrate analogs (*21, 88, 90, 107*). The use of kinetic isotope effects provides information about this conformational step that is not available from crystal structures, and may identify interactions that are important but not observed in the inactive conformation illustrated in crystal structures. Here we see that the peptide structure has a great influence on the conformational rearrangement of FPP. Nonpeptidic thiols are extremely slow substrates with α-secondary KIEs near unity, suggesting that the conformational change of FPP is slow (Table 5.4). While these molecules are FTase substrates, their small size most likely prevents them from properly activating the FPP substrate molecule. It is also possible that key side chain interactions are lacking when peptide/protein substrates are substituted with nonpeptidic thiols. This may be due to the loss of interactions of the X residue of the peptide substrate with the FTase active site, or the loss of direct interactions between the peptide and the FPP molecule.

The hydrophobicity or volume of the "X" residue is an important determinant of peptide specificity, and is proposed to alter the prenylation step, as well as an additional kinetic step (*24*). From crystal structures, the identity of the X residue affects both the position of this side chain in the binding pocket of FTase as well as the conformation of the backbone of the peptide substrate in the active site (*23*). Thus the X residue has been suggested to affect the equilibrium between the active and inactive conformers of the FPP substrate, by differentially orienting the peptide substrate in the active site and affecting side chain interactions that optimally induce rotations about the C1 of FPP during the formation of the active ternary complex (*23, 24*). The KIE studies here indicate that the X group significantly affects the stability of the active substrate conformation ground state relative to the transition states for both the conformational change and farnesylation (Figure 5.12). These results are consistent with crystallographic studies highlighting the importance of the X residue in the formation of the active substrate conformation.

In addition to a CaaX sequence, many FTase substrates contain an upstream polybasic region, which increases the affinity of the substrate and aids in plasma membrane localization (*74-76*). This region of positively charged residues in the peptide
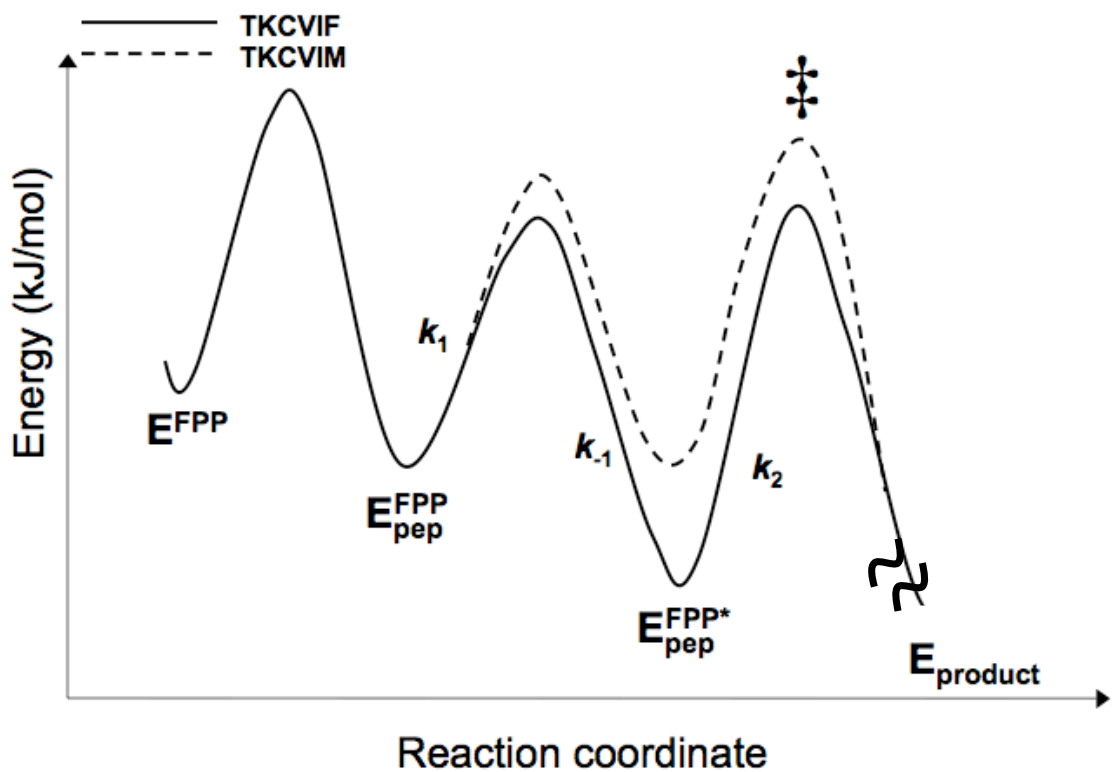
Figure 5.12 Effect of the X residue on the reaction pathway of FTase

Reaction coordinate diagram following the FTase reaction pathway during a single turnover experiment, illustrating how the conformational rearrangement and chemical steps are affected by the X residue. Free energies were calculated from the kinetic rate constants given in Scheme 5.4 and Table 5.5, using Eq. 8, for WT FTase with 100 μM TKCVIF (solid line) and 100 μM TKCVIM (dashed line) at 5 mM MgCl$_2$. Concentrations used are the same as experimental conditions (see Experimental Procedures).

substrate enhances the binding affinity for FTase but decreases the catalytic efficiency, as measured by k_{cat}/K_M, reflecting a decrease in the rate constant for peptide association, prenyl chain rotation, and/or the farnesylation step (*77*). KIE data clearly show the importance of the lysine residue upstream of the CaaX box in lowering the energy barrier for the conformational rearrangement of FPP, while having little effect on the farnesylation step (Table 5.5, Figure 5.13). This lysine residue is thought to interact in both the inactive and active substrate conformations with K164α, a residue in the PPi pocket which is important in the stabilization of the transition states for the conformational change and farnesylation (Table 5.3) (*84, 88*). This interaction may therefore be important in increasing the rate constant for the conformational step, although additional experiments are required to address exactly why the lysine of the peptide substrate has such a significant impact on the conformational rearrangement of FPP. Intriguingly, the presence of more than one lysine residue in the substrate SKTKCVIM appears to slow the conformational change when compared with TKCVIM (Table 5.5). This may be due to the decreased apparent Mg^{2+} affinity observed for substrates with polybasic residues (*77*), and further crystallographic and kinetic studies on the role of these additional lysine residues would shed light on any important interactions with Mg^{2+} that might affect the conformational change for these substrates.

Implications for substrate specificity

The reaction of FTase is extremely complex and offers a variety of mechanisms by which to control substrate specificity. The affinity of different peptides for the FTase•FPP complex is insensitive to the identity of the X group, while the single turnover rate constant for farnesylation depends greatly on the X group structure (*24*). Additionally, other steps in the catalytic cycle may be regulated by the peptide structure. The KIE experiments here demonstrate that both the rate constants for the conformational change and for farnesylation depend on the structure of the thiol substrate. The final step of the catalytic cycle, dissociation of farnesylated product, is another step where the specificity of FTase for certain substrates may be controlled (see Chapter 3) (*24*). Nonetheless, the data presented here provide clear evidence that the substrate specificity
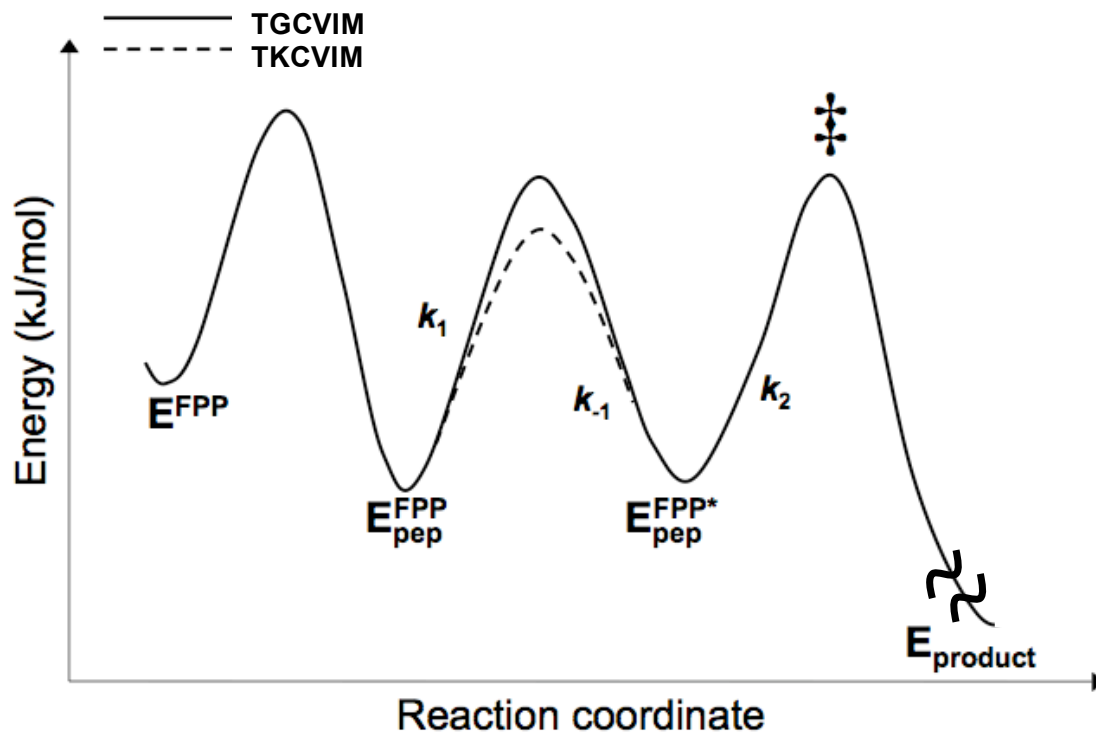
Figure 5.13 Effect of the upsteam lysine residue on the reaction pathway of FTase

Reaction coordinate diagram following the FTase reaction pathway during a single turnover experiment, illustrating how the conformational rearrangement and chemical steps are affected by the upstream lysine residue of the peptide. Free energies were calculated from the kinetic rate constants given in Scheme 5.4 and Table 5.5, using Eq. 8, for WT FTase with 100 μM TGCVIM (solid line) and 100 μM TKCVIM (dashed line) at 5 mM MgCl$_2$. Concentrations used are the same as experimental conditions (see Experimental Procedures).

of FTase can be modulated by the concerted structural dynamics of the substrate conformational change prior to catalysis. This conformational rearrangement may partially explain how farnesylation is regulated in cells. For instance, the nonspecific farnesylation of nonpeptidic thiols, which has been observed *in vitro*, is limited by the slow conformational rearrangement of FPP required for farnesylation. This specificity constraint is potentially an important regulatory mechanism, due to the high cellular concentrations of some of these small molecules, such as GSH and cysteine. The need for a better understanding of the protein substrate specificity of FTase is highlighted by both the uncertainty as to the identity of all of the proteins farnesylated *in vivo* and the unclear mode of action of current inhibitors. Further insights into the mechanism of FTase will provide additional information about the determinants of substrate specificity that may enhance the development and application of FTase inhibitors as well as our understanding of the biological pathways affected by farnesylation in cells.

Transition state inhibitors

There are no direct methods to observe the structure of the transition state for any chemical reaction, which is thought to have a lifetime near 10^{-13} s, the time corresponding to a single bond vibration (*173*). Enzymes function by lowering the activation energy for a given reaction, and transition state mimics bind tightly to enzymes by capturing a fraction of this binding energy. The TS structures for AMP deaminase, nucleoside hydrolase, and purine nucleoside phosphorylase have been estimated from KIE measurements and these data have led to the development of powerful transition state analog inhibitors of these respective enzymes (*133*). Transition state analogs for FTase have been designed to mimic the buildup of positive charge in the transition state (*99*). However, these compounds are very poor inhibitors and suggest that an increased knowledge of the geometry and electrostatic features of the transition state of FTase, as measured by KIEs, may provide a blueprint for the design of potent FTase inhibitors. Unexpectedly, KIEs also provide additional information about the conformational rearrangement of FPP, a step which appears to be an important determinant in substrate specificity and which may therefore also lead to the development of potent, specific

FTase inhibitors. The data presented in this work suggest that key features of the active substrate conformation may represent a novel target for FTase inhibition. Possible potent inhibitors include compounds with restricted mobility in the active site, or compounds that coordinate Mg^{2+} or residues in the PPi binding pocket in the active substrate conformation of FTase.

CHAPTER 6
SUMMARY, CONCLUSIONS AND FUTURE DIRECTIONS

Assay for prenyltransferase activity

The protein prenyltransferases have been the subject of intensive scientific investigation for both biological and pharmaceutical reasons. FTase, in particular, is studied by many research groups investigating various features of the mechanism, substrate specificity, cellular regulation and inhibition of farnesylation. As described in Chapter 2, the development of a continuous, fluorescence-based assay that measures the rate of diphosphate release during the FTase reaction presents several clear advantages over other assays presently used to measure FTase activity. First, the MDCC-PBP/PPiase assay is practical, in terms of both expense and time, and easily amenable to a high-throughput format. Second, the assay is more general than methods that require a radiolabeled FPP or dansylated peptide, and thus can be used to study reactions with inhibitors, substrate analogs and full-length proteins. By using unmodified substrates for FTase, effects of the dansyl group on binding and/or reactivity may also be avoided. Finally and more broadly, this assay can be used to study the enzymatic activity for any reaction where diphosphate is a product, including polymerases, ligases and aminoacyl tRNA synthetases.

While the majority of prenylation research has focused on farnesylation, geranylgeranylation is increasingly recognized as being crucial to the proper function of the majority of prenylated proteins, and GGTase I is proving to be a clinical target with considerable promise in the treatment of a variety of maladies (*40-43*). As a result, mechanistic and structural studies on GGTase I have been carried out recently and provide valuable information about the mechanism and substrate specificity of the CaaX prenyltransferases (*20, 23, 24, 71-73, 77, 108*). While less well studied, GGTase II is

also of interest due to key structural differences and its unique role in vesicular transport by specifically prenylating Rab proteins (*29*). The development of a continuous fluorescent assay for prenyltransferase activity should greatly facilitate studies of both GGTase I and II, to increase our understanding of the important similarities and differences between the three classes of prenyltransferases.

Catalytic and kinetic mechanism of FTase

The kinetic isotope effects studies presented in Chapter 5 provide the first direct measurement of the dissociative character in the chemical transition state of FTase. These results are consistent with previous studies which have suggested an "exploded" transition state for FTase, where the stabilization of develping charge in the transition state is an important catalytic feature (*95*). The KIE studies presented here could aid in the design of powerful transition state inhibitors that combine many features of the chemical transition state. The role of the zinc ion in creating a potent thiolate nucleophile is confirmed by substitution of Zn^{2+} with the more thiophilic cadmium, which increases the α-secondary KIE reflecting a reduction in the associative character of the transiton state.

Unexpectedly, the KIE studies presented in Chapter 5 have also provided information about the rotational movement of FPP that occurs prior to catalysis, which had previously been thought to be rapid compared to farnesylation. This work, however, clearly shows that under certain conditions, this step becomes partially rate-limiting and masks the observed KIE, as well as contributes to the observed rate constant measured under single turnover conditions. This provides the first direct kinetic evidence for a conformational rearrangement, which had previously only been inferred from structural and mutagenesis studies (*21, 88*). Combining KIE measurements with single turnover kinetics, the commitment factors and kinetic energy barriers were calculated under a variety of different experimental conditions, providing a detailed characterization of the kinetic mechanism for FTase. Interestingly, changing Mg^{2+} concentrations or removing positive charge from the PPi binding pocket significantly impact the observed rate constant but do not affect the KIE. Therefore, the stabilization of positive charge on the

diphosphate group appears to be important in both the chemical transition state and the formation of an active substrate conformation prior to catalysis.

The most intriguing result from these KIE studies was the observation that the peptide structure greatly affects the rate constant for the conformational rearrangement of the bound FPP molecule. Small nonpeptidic thiols are substrates, albeit very poor ones; one main effect of these substrates on catalysis is to greatly decrease the forward rate constant for the FPP conformational change. These results may have implications for substrate specificity *in vivo*, as the nonspecific farnesylation of molecules such as glutathione and dithiothrietol may be limited by the kinetic barrier that must be overcome to form the active substrate conformation of FPP. Furthermore, KIE experiments demonstrated that the X residue is important in stabilizing the active substrate conformation, while the lysine one residue upstream of the CaaX sequence is important in lowering the activation energy for the conformational rearrangement of FPP. It is unclear from the crystal structures how these residues might affect these steps, because these structures represent inactive ternary complexes. However, crystallographic and modeling studies have suggested that the upstream lysine residue of the peptide substrate interacts with a lysine residue in the active site of FTase, K164α (*88*). We have shown that K164α is important for catalysis by facilitating the formation of the active substrate conformation of FPP, and thus it is reasonable that this may be an important interaction. The upstream lysine residue has also been proposed to make a third-shell interaction with zinc, through the zinc ligand H362β and the D359β residue (*84*). Further kinetic studies using site-directed mutagenesis and different peptide sequences may address the significance of these interactions and lead to an understanding of the importance of this lysine residue in FTase substrates. Additionally, the importance of the entire upstream polybasic region in catalysis is of great interest, since this region is present in many proteins including K-RasB and RhoB.

These recent observations about the mechanism of FTase raise several important questions regarding geranylgeranylation. While GGTase I and FTase have different substrate requirements, it has been assumed that the reaction pathway proceeds similarly for both enzymes (*20*). However, the role of Mg^{2+} in the isoprenoid conformational change in FTase suggests that there may be differences in this step for GGTase I. Mg^{2+}

does not accelerate the GGTase I-catalyzed reaction (*12-14*). However, the K311β residue that replaces the Mg^{2+} ligand in FTase may serve a similar role for GGTase I as Mg^{2+} does for FTase. KIE measurements for the reaction catalyzed by GGTase I would illuminate differences in the kinetics of the active substrate conformational change between GGTase I and FTase, and may provide a mechanistic basis for key differences in their substrate specificities.

Product dissociation and inhibition of FTase

While it was previously shown that the farnesylated product dissociates very slowly in the absence of additional substrate, very little was known about the kinetic mechanism behind this unusual catalytic feature for FTase. In Chapter 3, we have directly measured product dissociation and shown a dependence on both FPP and Mg^{2+}. Therefore, FTase does not exist in an unbound form throughout the catalytic pathway, and one must be wary when interpreting steady-state kinetics experiments. The apparent K_{Mg} measured under steady-state turnover, for instance, likely reflects Mg^{2+} binding to the E•product complex, as well as to the E•FPP complex. Moreover, the kinetic parameter K_M for FPP includes the step where FPP binds to the E•product complex to enhance product dissociation.

The binding of a second molecule of FPP to the E•product complex appears to be a very important step in the overall turnover of FTase, as well as substrate selectivity. Alterations in the structure of the FPP substrate have very little effect on the conformational rearrangement or the formation of bound farnesylated product, but affect turnover by decreasing the observed rate constant for product dissociation. Interestingly, some FPP analogs affect this step much more significantly than others, and much work remains to delineate the important interactions that facilitate product dissociation. It is clear that the correct orientation of the diphosphate as well as the isoprenoid moiety is important in the product dissociation step, and structural studies of additional product complexes would certainly complement the work described here. One important question that remains is the location of the binding sites for the second FPP and peptide molecules in the product complex. While the crystal structure shows FPP bound in the original FPP

binding site (*21*), it is possible that FPP binds first in a separate site and then the product moves to the exit groove, followed by movement of the FPP to the binding site observed in the crystal structure. In this mechanism, FPP binding catalyzes the conformational rearrangement of the bound product. The other possibility is that the prenyl group of the product moves first to the exit groove and then FPP binds in the FPP-binding site observed in the crystal structure. In this case, the FPP molecule captures the product complex that dissociates more rapidly. Our studies with FPP analogs suggest the latter mechanism and indicate that one possible mode of inhibition is to bind to the exit groove to inhibit product dissociation. Additional structural and mechanistic studies with substrate analogs and inhibitors are needed to further understand the mechanism of product dissociation.

While peptide-catalyzed product dissociation has been observed, it is less well understood than FPP-catalyzed product dissociation (*89*). There are several curious observations that point to the importance of peptide-catalyzed product dissociation as a means of regulating the activity of FTase, or even serving as a determinant of substrate specificity. There are a number of peptide sequences corresponding to farnesylated proteins which undergo a single turnover but not multiple turnovers (*24, 25*). These peptides bind tightly to the enzyme upon farnesylation and are not released in the presence of FPP, indicating that *in vivo* their dissociation may be induced by cellular factors, such as other proteins. It is also possible that product dissociation may be stimulated by the presence of the ER membrane or the CaaX protease Rce1, as a means of regulating the proper transport of farnesylated proteins and/or protecting FTase in the cellular environment.

Studies on the product dissociation step carry many implications for the inhibition of FTase. The data presented in Chapter 4 for a group of FPP-competitive inhibitors have shown that an important inhibitory feature for these compounds is the inhibition of product dissociation. This novel mechanism may describe many current FTIs, and may be exploited in the design of future inhibitors. Given that peptides may also catalyze product dissociation, this inhibitory mechanism may be applicable to peptidomimetic inhibitors as well. A further understanding of the binding mode for inhibitors and key interactions that enable inhibition would therefore aid in the design of not only more

potent inhibitors, but also more specific inhibitors that could be designed to selectively block the farnesylation of specific proteins. These studies would be greatly accelerated by a crystal structure of the inhibitor bound to the product complex, which would provide invaluable information about the inhibitor binding site.

Closing remarks

The work presented here has substantially enhanced our current understanding of the mechanism of FTase. Studies on the kinetic and catalytic mechanism for this enzyme provide valuable information about the catalysis of zinc enzymes and the biochemistry of alkyl transfer. The developed methodology and results of this work may also be used toward the study of prenylation *in vivo*. The identification of prenylated proteins in the cell is of great interest, and a better physiological understanding of prenylation will also lead to a clearer picture of the inhibition of prenyltransferases. FTase inhibitors show significant promise in the treatment of a variety of diseases, especially cancer, and studies on the mechanism, substrate specificity and inhibition of FTase will contribute to the growth of this field and the development of specific and effective inhibitors.

BIBLIOGRAPHY

(1)   Seo, J., and Lee, K. J. (2004) Post-translational modifications and their biological functions: proteomic analysis and systematic approaches. *J Biochem Mol Biol 37*, 35-44.

(2)   Zhang, F. L., and Casey, P. J. (1996) Protein Prenylation: Molecular Mechanisms and Functional Consequences. *Annu. Rev. Biochem. 65*, 241-69.

(3)   Figueroa, C., Taylor, J., and Vojtek, A. B. (2001) Prenylated Rab acceptor protein is a receptor for prenylated small GTPases. *J Biol Chem 276*, 28219-25.

(4)   Kadereit, D., Kuhlmann, J., and Waldmann, H. (2000) Linking the fields--the interplay of organic synthesis, biophysical chemistry, and cell biology in the chemical biology of protein lipidation. *Chembiochem 1*, 144-69.

(5)   Gelb, M. H., Scholten, J. D., and Sebolt-Leopold, J. S. (1998) Protein prenylation: from discovery to prospects for cancer treatment. *Curr Opin Chem Biol 2*, 40-8.

(6)   Tamanoi, F., Gau, C. L., Jiang, C., Edamatsu, H., and Kato-Stankiewicz, J. (2001) Protein farnesylation in mammalian cells: effects of farnesyltransferase inhibitors on cancer cells. *Cell Mol Life Sci 58*, 1636-49.

(7)   Sebti, S. M. (2005) Protein farnesylation: implications for normal physiology, malignant transformation, and cancer therapy. *Cancer Cell 7*, 297-300.

(8)   Boyartchuk, V. L., Ashby, M. N., and Rine, J. (1997) Modulation of Ras and a-factor function by carboxyl-terminal proteolysis. *Science 275*, 1796-800.

(9)   Hancock, J. F., Cadwallader, K., and Marshall, C. J. (1991) Methylation and proteolysis are essential for efficient membrane binding of prenylated p21K-ras(B). *Embo J 10*, 641-6.

(10)   Choy, E., Chiu, V. K., Silletti, J., Feoktistov, M., Morimoto, T., Michaelson, D., Ivanov, I. E., and Philips, M. R. (1999) Endomembrane trafficking of ras: the CAAX motif targets proteins to the ER and Golgi. *Cell 98*, 69-80.

(11)   Reuther, G. W., and Der, C. J. (2000) The Ras branch of small GTPases: Ras family members don't fall far from the tree. *Curr Opin Cell Biol 12*, 157-65.

(12)   Zhang, F. L., and Casey, P. J. (1996) Influence of metal ions on substrate binding and catalytic activity of mammalian protein geranylgeranyltransferase type-I. *Biochem J 320 (Pt 3)*, 925-32.

(13)   Witter, D. J., and Poulter, C. D. (1996) Yeast geranylgeranyltransferase type-II: steady state kinetic studies of the recombinant enzyme. *Biochemistry 35*, 10454-63.

(14)   Moomaw, J. F., and Casey, P. J. (1992) Mammalian protein geranylgeranyltransferase. Subunit composition and metal requirements. *J Biol Chem 267*, 17438-43.

(15)   Casey, P. J., and Seabra, M. C. (1996) Protein prenyltransferases. *J Biol Chem 271*, 5289-92.

(16)   Seabra, M. C., Reiss, Y., Casey, P. J., Brown, M. S., and Goldstein, J. L. (1991) Protein farnesyltransferase and geranylgeranyltransferase share a common alpha subunit. *Cell 65*, 429-34.

(17)   Zhang, F. L., Diehl, R. E., Kohl, N. E., Gibbs, J. B., Giros, B., Casey, P. J., and Omer, C. A. (1994) cDNA cloning and expression of rat and human protein geranylgeranyltransferase Type-I. *J. Biol. Chem. 269*, 3175-3180.

(18)   Chen, W. J., Andres, D. A., Goldstein, J. L., Russell, D. W., and Brown, M. S. (1991) cDNA cloning and expression of the peptide-binding beta subunit of rat p21ras farnesyltransferase, the counterpart of yeast DPR1/RAM1. *Cell 66*, 327-34.

(19)   Omer, C. A., Kral, A. M., Diehl, R. E., Prendergast, G. C., Powers, S., Allen, C. M., Gibbs, J. B., and Kohl, N. E. (1993) Characterization of recombinant human farnesyl-protein transferase: cloning, expression, farnesyl diphosphate binding, and functional homology with yeast prenyl-protein transferases. *Biochemistry 32*, 5167-76.

(20)   Taylor, J. S., Reid, T. S., Terry, K. L., Casey, P. J., and Beese, L. S. (2003) Structure of mammalian protein geranylgeranyltransferase type-I. *Embo J 22*, 5963-74.

(21)   Long, S. B., Casey, P. J., and Beese, L. S. (2002) Reaction path of protein farnesyltransferase at atomic resolution. *Nature 419*, 645-50.

(22)   Casey, P. J., Solski, P. A., Der, C. J., and Buss, J. E. (1989) p21ras is modified by a farnesyl isoprenoid. *Proc Natl Acad Sci U S A 86*, 8323-7.

(23)   Reid, T. S., Terry, K. L., Casey, P. J., and Beese, L. S. (2004) Crystallographic analysis of CaaX prenyltransferases complexed with substrates defines rules of protein substrate selectivity. *J Mol Biol 343*, 417-33.

(24)   Hartman, H. L., Hicks, K. A., and Fierke, C. A. (2005) Peptide Specificity of Protein Prenyltransferases is Determined Mainly by Reactivity Rather than Binding Affinity. *Biochemistry 44*, 15314-15324.

(25)   Hicks, K. A., Hartman, H. L., Janik, L. S., and Fierke, C. A. Identification of Novel Substrates for Proteins Farnesyltransferase and Geranylgeranyltransferase Type I. *manuscript in preparation*.

(26)   Pereira-Leal, J. B., Hume, A. N., and Seabra, M. C. (2001) Prenylation of Rab GTPases: molecular mechanisms and involvement in genetic disease. *FEBS Lett 498*, 197-200.

(27)   Seabra, M. C. (1998) Membrane association and targeting of prenylated Ras-like GTPases. *Cell Signal 10*, 167-72.

(28)   Andres, D. A., Seabra, M. C., Brown, M. S., Armstrong, S. A., Smeland, T. E., Cremers, F. P., and Goldstein, J. L. (1993) cDNA cloning of component A of Rab geranylgeranyl transferase and demonstration of its role as a Rab escort protein. *Cell 73*, 1091-9.

(29)   Zhang, H., Seabra, M. C., and Deisenhofer, J. (2000) Crystal structure of Rab geranylgeranyltransferase at 2.0 A resolution. *Structure Fold Des 8*, 241-51.

(30)   Van Voorhis, W. C., Rivas, K. L., Bendale, P., Nallan, L., Horney, C., Barrett, L. K., Bauer, K. D., Smart, B. P., Ankala, S., Hucke, O., Verlinde, C. L., Chakrabarti, D., Strickland, C., Yokoyama, K., Buckner, F. S., Hamilton, A. D., Williams, D. K., Lombardo, L. J., Floyd, D., and Gelb, M. H. (2007) Tetrahydroquinoline Plasmodium falciparum protein farnesyltransferase inhibitors: Efficacy, pharmacokinetics, and metabolism. *Antimicrob Agents Chemother*.

(31)   Gelb, M. H., Van Voorhis, W. C., Buckner, F. S., Yokoyama, K., Eastman, R., Carpenter, E. P., Panethymitaki, C., Brown, K. A., and Smith, D. F. (2003) Protein farnesyl and N-myristoyl transferases: piggy-back medicinal chemistry targets for the development of antitrypanosomatid and antimalarial therapeutics. *Mol Biochem Parasitol 126*, 155-63.

(32)   Mallampalli, M. P., Huyer, G., Bendale, P., Gelb, M. H., and Michaelis, S. (2005) Inhibiting farnesylation reverses the nuclear morphology defect in a HeLa cell model for Hutchinson-Gilford progeria syndrome. *Proc Natl Acad Sci U S A 102*, 14416-21.

(33)   Barbacid, M. (1987) ras genes. *Annu Rev Biochem 56*, 779-827.

(34)   Cox, A. D., and Der, C. J. (1997) Farnesyltransferase inhibitors and cancer treatment: targeting simply Ras? *Biochimica et Biophysica Acta 1333*, F51-71.

(35)   Basso, A. D., Kirschmeier, P., and Bishop, W. R. (2006) Lipid posttranslational modifications. Farnesyl transferase inhibitors. *J Lipid Res 47*, 15-31.

(36)   Bernhard, E. J., McKenna, W. G., Hamilton, A. D., Sebti, S. M., Qian, Y., Wu, J. M., and Muschel, R. J. (1998) Inhibiting Ras prenylation increases the radiosensitivity of human tumor cell lines with activating mutations of ras oncogenes. *Cancer Res 58*, 1754-61.

(37)   Bernhard, E. J., Kao, G., Cox, A. D., Sebti, S. M., Hamilton, A. D., Muschel, R. J., and McKenna, W. G. (1996) The farnesyltransferase inhibitor FTI-277 radiosensitizes H-ras-transformed rat embryo fibroblasts. *Cancer Res 56*, 1727-30.

(38)   Moasser, M. M., Sepp-Lorenzino, L., Kohl, N. E., Oliff, A., Balog, A., Su, D. S., Danishefsky, S. J., and Rosen, N. (1998) Farnesyl transferase inhibitors cause enhanced mitotic sensitivity to taxol and epothilones. *Proc Natl Acad Sci U S A 95*, 1369-74.

(39)   Liu, M., Bryant, M. S., Chen, J., Lee, S., Yaremko, B., Lipari, P., Malkowski, M., Ferrari, E., Nielsen, L., Prioli, N., Dell, J., Sinha, D., Syed, J., Korfmacher, W. A., Nomeir, A. A., Lin, C. C., Wang, L., Taveras, A. G., Doll, R. J., Njoroge, F. G., Mallams, A. K., Remiszewski, S., Catino, J. J., Girijavallabhan, V. M., Bishop, W. R., and et al. (1998) Antitumor activity of SCH 66336, an orally bioavailable tricyclic inhibitor of farnesyl protein transferase, in human tumor xenograft models and wap-ras transgenic mice. *Cancer Res 58*, 4947-56.

(40)   Chakrabarti, D., Azam, T., DelVecchio, C., Qiu, L., Park, Y. I., and Allen, C. M. (1998) Protein prenyl transferase activities of Plasmodium falciparum. *Mol Biochem Parasitol 94*, 175-84.

(41)   Walters, C. E., Pryce, G., Hankey, D. J., Sebti, S. M., Hamilton, A. D., Baker, D., Greenwood, J., and Adamson, P. (2002) Inhibition of Rho GTPases with protein prenyltransferase inhibitors prevents leukocyte recruitment to the central nervous system and attenuates clinical signs of disease in an animal model of multiple sclerosis. *J Immunol 168*, 4087-94.

(42)   Stark, W. W., Jr., Blaskovich, M. A., Johnson, B. A., Qian, Y., Vasudevan, A., Pitt, B., Hamilton, A. D., Sebti, S. M., and Davies, P. (1998) Inhibiting geranylgeranylation blocks growth and promotes apoptosis in pulmonary vascular smooth muscle cells. *Am J Physiol 275*, L55-63.

(43)   Sebti, S. M., and Hamilton, A. D. (2000) Farnesyltransferase and geranylgeranyltransferase I inhibitors and cancer therapy: lessons from mechanism and bench-to-bedside translational studies. *Oncogene 19*, 6584-93.

(44)   Lackner, M. R., Kindt, R. M., Carroll, P. M., Brown, K., Cancilla, M. R., Chen, C., de Silva, H., Franke, Y., Guan, B., Heuer, T., Hung, T., Keegan, K., Lee, J. M., Manne, V., O'Brien, C., Parry, D., Perez-Villar, J. J., Reddy, R. K., Xiao, H.,

Zhan, H., Cockett, M., Plowman, G., Fitzgerald, K., Costa, M., and Ross-Macdonald, P. (2005) Chemical genetics identifies Rab geranylgeranyl transferase as an apoptotic target of farnesyl transferase inhibitors. *Cancer Cell 7*, 325-36.

(45)   Cox, A. D., Garcia, A. M., Westwick, J. K., Kowalczyk, J. J., Lewis, M. D., Brenner, D. A., and Der, C. J. (1994) The CAAX peptidomimetic compound B581 specifically blocks farnesylated, but not geranylgeranylated or myristylated, oncogenic ras signaling and transformation. *J Biol Chem 269*, 19203-6.

(46)   James, G. L., Goldstein, J. L., Brown, M. S., Rawson, T. E., Somers, T. C., McDowell, R. S., Crowley, C. W., Lucas, B. K., Levinson, A. D., and Marsters, J. C., Jr. (1993) Benzodiazepine peptidomimetics: potent inhibitors of Ras farnesylation in animal cells. *Science 260*, 1937-42.

(47)   Kohl, N. E., Mosser, S. D., deSolms, S. J., Giuliani, E. A., Pompliano, D. L., Graham, S. L., Smith, R. L., Scolnick, E. M., Oliff, A., and Gibbs, J. B. (1993) Selective inhibition of ras-dependent transformation by a farnesyltransferase inhibitor. *Science 260*, 1934-7.

(48)   Oliff, A. (1999) Farnesyltransferase inhibitors: targeting the molecular basis of cancer. *Biochim Biophys Acta 1423*, C19-30.

(49)   Sepp-Lorenzino, L., and Rosen, N. (1998) A farnesyl-protein transferase inhibitor induces p21 expression and G1 block in p53 wild type tumor cells. *J Biol Chem 273*, 20243-51.

(50)   Miquel, K., Pradines, A., Sun, J., Qian, Y., Hamilton, A. D., Sebti, S. M., and Favre, G. (1997) GGTI-298 induces G0-G1 block and apoptosis whereas FTI-277 causes G2-M enrichment in A549 cells. *Cancer Res 57*, 1846-50.

(51)   Crespo, N. C., Ohkanda, J., Yen, T. J., Hamilton, A. D., and Sebti, S. M. (2001) The farnesyltransferase inhibitor, FTI-2153, blocks bipolar spindle formation and chromosome alignment and causes prometaphase accumulation during mitosis of human lung cancer cells. *J Biol Chem 276*, 16161-7.

(52)   Ashar, H. R., James, L., Gray, K., Carr, D., Black, S., Armstrong, L., Bishop, W. R., and Kirschmeier, P. (2000) Farnesyl transferase inhibitors block the farnesylation of CENP-E and CENP-F and alter the association of CENP-E with the microtubules. *J Biol Chem 275*, 30451-7.

(53)   Ura, H., Obara, T., Shudo, R., Itoh, A., Tanno, S., Fujii, T., Nishino, N., and Kohgo, Y. (1998) Selective cytotoxicity of farnesylamine to pancreatic carcinoma cells and Ki-ras-transformed fibroblasts. *Mol Carcinog 21*, 93-9.

(54)   Kainuma, O., Asano, T., Hasegawa, M., and Isono, K. (1996) [Growth inhibition of human pancreatic cancer by farnesyl transferase inhibitor]. *Gan To Kagaku Ryoho 23*, 1657-9.

(55)   Lebowitz, P. F., Sakamuro, D., and Prendergast, G. C. (1997) Farnesyl transferase inhibitors induce apoptosis of Ras-transformed cells denied substratum attachment. *Cancer Res 57*, 708-13.

(56)   Kohl, N. E., Omer, C. A., Conner, M. W., Anthony, N. J., Davide, J. P., deSolms, S. J., Giuliani, E. A., Gomez, R. P., Graham, S. L., Hamilton, K., and et al. (1995) Inhibition of farnesyltransferase induces regression of mammary and salivary carcinomas in ras transgenic mice. *Nat Med 1*, 792-7.

(57)   Mangues, R., Corral, T., Kohl, N. E., Symmans, W. F., Lu, S., Malumbres, M., Gibbs, J. B., Oliff, A., and Pellicer, A. (1998) Antitumor effect of a farnesyl protein transferase inhibitor in mammary and lymphoid tumors overexpressing N-ras in transgenic mice. *Cancer Res 58*, 1253-9.

(58)   Adjei, A. A. (2001) Blocking oncogenic Ras signaling for cancer therapy. *J Natl Cancer Inst 93*, 1062-74.

(59)   Koblan, K. S., Kohl, N. E., Omer, C. A., Anthony, N. J., Conner, M. W., deSolms, S. J., Williams, T. M., Graham, S. L., Hartman, G. D., Oliff, A., and Gibbs, J. B. (1996) Farnesyltransferase inhibitors: a new class of cancer chemotherapeutics. *Biochem Soc Trans 24*, 688-92.

(60)   Sepp-Lorenzino, L., Ma, Z., Rands, E., Kohl, N. E., Gibbs, J. B., Oliff, A., Rosen, N., and Serve, H. (1995) A peptidomimetic inhibitor of farnesyl:protein transferase blocks the anchorage-dependent and -independent growth of human tumor cell lines. *Cancer Res 55*, 5302-9.

(61)   Lebowitz, P. F., Davide, J. P., and Prendergast, G. C. (1995) Evidence that farnesyltransferase inhibitors suppress Ras transformation by interfering with Rho activity. *Mol Cell Biol 15*, 6613-22.

(62)   Prendergast, G. C., Davide, J. P., deSolms, S. J., Giuliani, E. A., Graham, S. L., Gibbs, J. B., Oliff, A., and Kohl, N. E. (1994) Farnesyltransferase inhibition causes morphological reversion of ras-transformed cells by a complex mechanism that involves regulation of the actin cytoskeleton. *Mol Cell Biol 14*, 4193-202.

(63)   Adamson, P. C., Balis, F. M., Feusner, J., Aronson, L., Murphy, R. F., Horowitz, M. E., Reaman, G., Hammond, G. D., Fenton, R. M., and Adamson, P. (1992) Post-translational modifications of p21rho proteins. *J Clin Oncol 10*, 1666-73.

(64)   Sebti, S. M., and Hamilton, A. D. (2001) *Farnesyltransferase Inhibitors in Cancer Therapy*, Vol. 8, Humana Press, Totowa, NJ.

(65)   Rowell, C. A., Kowalczyk, J. J., Lewis, M. D., and Garcia, A. M. (1997) Direct demonstration of geranylgeranylation and farnesylation of Ki-Ras in vivo. *J. Biol. Chem. 272*, 14093-7.

(66) Prendergast, G. C. (2001) Actin' up: RhoB in cancer and apoptosis. *Nat Rev Cancer 1*, 162-8.

(67) Sebti, S. M., and Der, C. J. (2003) Opinion: Searching for the elusive targets of farnesyltransferase inhibitors. *Nat Rev Cancer 3*, 945-51.

(68) Roskoski, R., Jr. (2003) Protein prenylation: a pivotal posttranslational process. *Biochem Biophys Res Commun 303*, 1-7.

(69) Maurer-Stroh, S., and Eisenhaber, F. (2005) Refinement and prediction of protein prenylation motifs. *Genome Biol 6*, R55.

(70) Armstrong, S. A., Hannah, V. C., Goldstein, J. L., and Brown, M. S. (1995) CAAX geranylgeranyl transferase transfers farnesyl as efficiently as geranylgeranyl to RhoB. *J Biol Chem 270*, 7864-8.

(71) Yokoyama, K., Zimmerman, K., Scholten, J., and Gelb, M. H. (1997) Differential prenyl pyrophosphate binding to mammalian protein geranylgeranyltransferase-I and protein farnesyltransferase and its consequence on the specificity of protein prenylation. *J Biol Chem 272*, 3944-52.

(72) Del Villar, K., Mitsuzawa, H., Yang, W., Sattler, I., and Tamanoi, F. (1997) Amino acid substitutions that convert the protein substrate specificity of farnesyltransferase to that of geranylgeranyltransferase type I. *J Biol Chem 272*, 680-7.

(73) Del Villar, K., Urano, J., Guo, L., and Tamanoi, F. (1999) A mutant form of human protein farnesyltransferase exhibits increased resistance to farnesyltransferase inhibitors. *J Biol Chem 274*, 27010-7.

(74) Apolloni, A., Prior, I. A., Lindsay, M., Parton, R. G., and Hancock, J. F. (2000) H-ras but not K-ras traffics to the plasma membrane through the exocytic pathway. *Mol Cell Biol 20*, 2475-87.

(75) James, G. L., Goldstein, J. L., and Brown, M. S. (1995) Polylysine and CVIM sequences of K-RasB dictate specificity of prenylation and confer resistance to benzodiazepine peptidomimetic in vitro. *J Biol Chem 270*, 6221-6.

(76) Fiordalisi, J. J., Johnson, R. L., 2nd, Weinbaum, C. A., Sakabe, K., Chen, Z., Casey, P. J., and Cox, A. D. (2003) High affinity for farnesyltransferase and alternative prenylation contribute individually to K-Ras4B resistance to farnesyltransferase inhibitors. *J Biol Chem 278*, 41718-27.

(77) Hicks, K. A., Hartman, H. L., and Fierke, C. A. (2005) Upstream Polybasic Region in Peptides Enhances Dual Specificity for Prenylation by both Farnesyltransferase and Geranylgeranyltransferase Type I. *Biochemistry 44*, 15325-15333.

(78)   Reiss, Y., Brown, M. S., and Goldstein, J. L. (1992) Divalent cation and prenyl pyrophosphate specificities of the protein farnesyltransferase from rat brain, a zinc metalloenzyme. *J Biol Chem 267*, 6403-8.

(79)   Chen, W. J., Moomaw, J. F., Overton, L., Kost, T. A., and Casey, P. J. (1993) High level expression of mammalian protein farnesyltransferase in a baculovirus system. The purified protein contains zinc. *J Biol Chem 268*, 9675-80.

(80)   Park, H. W., Boduluri, S. R., Moomaw, J. F., Casey, P. J., and Beese, L. S. (1997) Crystal structure of protein farnesyltransferase at 2.25 angstrom resolution. *Science 275*, 1800-4.

(81)   Park, H. W., and Beese, L. S. (1997) Protein farnesyltransferase. *Curr Opin Struct Biol 7*, 873-80.

(82)   Hightower, K. E., Huang, C.-c., Casey, P. J., and Fierke, C. A. (1998) H-Ras and peptide and protein substrates bind protein farnesyltransferase as an ionized thiolate. *Biochemistry 37*, 15555-15562.

(83)   Pompliano, D. L., Schaber, M. D., Mosser, S. D., Omer, C. A., Schafer, J. A., and Gibbs, J. B. (1993) Isoprenoid Diphosphate Utilization by Recombinant Human Farnesyl:Protein Transferase: Interactive Binding between Substrates and a Preferred Kinetic Pathway. *Biochemistry 32*, 8341-8347.

(84)   Long, S. P., Casey, P. J., and Beese, L. S. (2000) The basis for K-Ras4B binding specificity to protein farnesyl-transferase revealed by a 2A resolution ternary complex structures. *Structure 8*, 209-222.

(85)   Long, S. B., Hancock, P. J., Kral, A. M., Hellinga, H. W., and Beese, L. S. (2001) The crystal structure of human protein farnesyltransferase reveals the basis for inhibition by CaaX tetrapeptides and their mimetics. *Proc Natl Acad Sci U S A 98*, 12948-53.

(86)   Long, S. B., Casey, P. J., and Beese, L. S. (1998) Cocrystal structure of protein farnesyltransferase complexed with a farnesyl diphosphate substrate. *Biochemistry 37*, 9612-8.

(87)   Strickland, C. L., Windsor, W. T., Syto, R., Wang, L., Bond, R., Wu, Z., Schwartz, J., Le, H. V., Beese, L. S., and Weber, P. C. (1998) Crystal Structure of Farnesyl Protein Transferase Complexed with a CaaX Peptide and Farnesyl Diphosphate Analogue. *Biochemistry 37*, 16601-16611.

(88)   Pickett, J. S., Bowers, K. E., Hartman, H. L., Fu, H.-W., Embry, A. C., Casey, P. J., and Fierke, C. A. (2003) Kinetic Studies of Protein Farnesyltransferase Mutants Establish Active Site Conformation. *Biochemistry 42*, 9741-8.

(89)   Tschantz, W. R., Furfine, E. S., and Casey, P. J. (1997) Substrate Binding Is
        Required for Release of Product from Mammalian Protein Farnesyltransferase. *J.
        Biol. Chem. 272*, 9989-9993.

(90)   Bowers, K. E., and Fierke, C. A. (2004) Positively charged side chains in protein
        farnesyltransferase enhance catalysis by stabilizing the formation of the
        diphosphate leaving group. *Biochemistry 43*, 5256-65.

(91)   Turek-Etienne, T. C., Strickland, C. L., and Distefano, M. D. (2003) Biochemical
        and structural studies with prenyl diphosphate analogues provide insights into
        isoprenoid recognition by protein farnesyl transferase. *Biochemistry 42*, 3716-24.

(92)   Furfine, E. S., Leban, J. J., Landavazo, A., Moomaw, J. F., and Casey, P. J.
        (1995) Protein Farnesyltransferase: Kinetics of Farnesyl Pyrophosphate Binding
        and Product Release. *Biochemistry 34*, 6857-6862.

(93)   Pompliano, D. L., Rands, E., Schaber, M. D., Mosser, S. D., Anthony, N. J., and
        Gibbs, J. B. (1992) Steady State Kinetic Mechanism of Ras Farnesyl:Protein
        Transferase. *Biochemistry 31*, 3800-3807.

(94)   Huang, C.-c., Casey, P. J., and Fierke, C. A. (1997) Evidence for a Catalytic Role
        of Zinc in Protein Farnesyltransferase. *J. Biol. Chem. 272*, 20-23.

(95)   Huang, C., Hightower, K. E., and Fierke, C. A. (2000) Mechanistic studies of rat
        protein farnesyltransferase indicate an associative transition state. *Biochemistry
        39*, 2593-602.

(96)   Mathis, J. R., and Poulter, C. D. (1997) Yeast protein farnesyltransferase: a pre-
        steady-state kinetic analysis. *Biochemistry 36*, 6367-76.

(97)   Mu, Y., Omer, C. A., and Gibbs, R. A. (1996) On the stereochemical course of
        human protein- farnesyl transferase. *J. Am. Chem. Soc. 118*, 1817-1823.

(98)   Edelstein, R. L., Weller, V. A., Distefano, M. D., and Tung, J. S. (1998)
        Stereochemical analysis of the reaction catalyzed by yeast protein
        farnesyltransferase. *J. Org. Chem. 63*, 5298-5299.

(99)   Dolence, J. M., and Poulter, C. D. (1995) A mechanism for posttranslational
        modifications of proteins by yeast protein farnesyltransferase. *Proc Natl Acad Sci
        U S A 92*, 5008-11.

(100)   Poulter, C. D., and Wiggins, P. L. (1981) Farnesylpyrophosphate Synthetase. A
        Stepwise Mechanism for the 1'-4 Condensation Reaction. *J. Am. Chem. Soc. 103*,
        3926-3927.

(101)   Matthews, R. G., and Goulding, C. W. (1997) Enzyme-catalyzed methyl transfers
        to thiols: the role of zinc. *Curr Opin Chem Biol 1*, 332-9.

(102)   Hightower, K. E., and Fierke, C. A. (1999) Zinc-catalyzed sulfur alkylation: insights from protein farnesyltransferase. *Curr. Op. Chem. Bio. 3*, 176-181.

(103)   Tobin, D. A., Pickett, J. S., Hartman, H. L., Fierke, C. A., and Penner-Hahn, J. E. (2003) Structural Characterization of the Zinc Site in Protein Farnesyltransferase. *J. Am. Chem. Soc. 125*, 9962-9.

(104)   Sousa, S. F., Fernandes, P. A., and Ramos, M. J. (2005) Farnesyltransferase--new insights into the zinc-coordination sphere paradigm: evidence for a carboxylate-shift mechanism. *Biophys J 88*, 483-94.

(105)   Ebel, H., and Gunther, T. (1980) Magnesium metabolism: a review. *J Clin Chem Clin Biochem 18*, 257-70.

(106)   Saderholm, M. J., Hightower, K. E., and Fierke, C. A. (2000) Role of metals in the reaction catalyzed by protein farnesyltransferase. *Biochemistry 39*, 12398-405.

(107)   Pickett, J. S., Bowers, K. E., and Fierke, C. A. (2003) Mutagenesis studies of protein farnesyltransferase implicate aspartate beta 352 as a magnesium ligand. *J Biol Chem 278*, 51243-50.

(108)   Hartman, H. L., Bowers, K. E., and Fierke, C. A. (2004) Lysine beta311 of protein geranylgeranyltransferase type I partially replaces magnesium. *J Biol Chem 279*, 30546-53.

(109)   Tarshis, L. C., Yan, M., Poulter, C. D., and Sacchettini, J. C. (1994) Crystal structure of recombinant farnesyl diphosphate synthase at 2.6-A resolution. *Biochemistry 33*, 10871-7.

(110)   Starks, C. M., Back, K., Chappell, J., and Noel, J. P. (1997) Structural basis for cyclic terpene biosynthesis by tobacco 5-epi-aristolochene synthase. *Science 277*, 1815-20.

(111)   Lesburg, C. A., Zhai, G., Cane, D. E., and Christianson, D. W. (1997) Crystal structure of pentalenene synthase: mechanistic insights on terpenoid cyclization reactions in biology. *Science 277*, 1820-4.

(112)   Wendt, K. U., and Schulz, G. E. (1998) Isoprenoid biosynthesis: manifold chemistry catalyzed by similar enzymes. *Structure 6*, 127-33.

(113)   Wu, Z., Demma, M., Strickland, C. L., Radisky, E. S., Poulter, C. D., Le, H. V., and Windsor, W. T. (1999) Farnesyl protein transferase: identification of K164 alpha and Y300 beta as catalytic residues by mutagenesis and kinetic studies. *Biochemistry 38*, 11239-49.

(114)   Hightower, K. E., De, S., Weinbaum, C., Spence, R. A., and Casey, P. J. (2001) Lysine(164)alpha of protein farnesyltransferase is important for both CaaX substrate binding and catalysis. *Biochem J 360*, 625-31.

(115) Kral, A. M., Diehl, R. E., deSolms, S. J., Williams, T. M., Kohl, N. E., and Omer, C. A. (1997) Mutational analysis of conserved residues of the beta-subunit of human farnesyl:protein transferase. *J Biol Chem 272*, 27319-23.

(116) Andres, D. A., Goldstein, J. L., Ho, Y. K., and Brown, M. S. (1993) Mutational analysis of alpha-subunit of protein farnesyltransferase. Evidence for a catalytic role. *J Biol Chem 268*, 1383-90.

(117) Gibbs, R. A., Zahn, T. J., and Sebolt-Leopold, J. S. (2001) Non-peptidic prenyltransferase inhibitors: diverse structural classes and surprising anti-cancer mechanisms. *Curr Med Chem 8*, 1437-65.

(118) Bell, I. M., Gallicchio, S. N., Abrams, M., Beese, L. S., Beshore, D. C., Bhimnathwala, H., Bogusky, M. J., Buser, C. A., Culberson, J. C., Davide, J., Ellis-Hutchings, M., Fernandes, C., Gibbs, J. B., Graham, S. L., Hamilton, K. A., Hartman, G. D., Heimbrook, D. C., Homnick, C. F., Huber, H. E., Huff, J. R., Kassahun, K., Koblan, K. S., Kohl, N. E., Lobell, R. B., Lynch, J. J., Jr., Robinson, R., Rodrigues, A. D., Taylor, J. S., Walsh, E. S., Williams, T. M., and Zartman, C. B. (2002) 3-Aminopyrrolidinone farnesyltransferase inhibitors: design of macrocyclic compounds with improved pharmacokinetics and excellent cell potency. *J Med Chem 45*, 2388-409.

(119) Reid, T. S., Long, S. B., and Beese, L. S. (2004) Crystallographic analysis reveals that anticancer clinical candidate L-778,123 inhibits protein farnesyltransferase and geranylgeranyltransferase-I by different binding modes. *Biochemistry 43*, 9000-8.

(120) Reid, T. S., and Beese, L. S. (2004) Crystal structures of the anticancer clinical candidates R115777 (Tipifarnib) and BMS-214662 complexed with protein farnesyltransferase suggest a mechanism of FTI selectivity. *Biochemistry 43*, 6877-84.

(121) Strickland, C. L., Weber, P. C., Windsor, W. T., Wu, Z., Le, H. V., Albanese, M. M., Alvarez, C. S., Cesarz, D., del Rosario, J., Deskus, J., Mallams, A. K., Njoroge, F. G., Piwinski, J. J., Remiszewski, S., Rossman, R. R., Taveras, A. G., Vibulbhan, B., Doll, R. J., Girijavallabhan, V. M., and Ganguly, A. K. (1999) Tricyclic farnesyl protein transferase inhibitors: crystallographic and calorimetric studies of structure-activity relationships. *J Med Chem 42*, 2125-35.

(122) Curtin, M. L., Florjancic, A. S., Cohen, J., Gu, W. Z., Frost, D. J., Muchmore, S. W., and Sham, H. L. (2003) Novel and selective imidazole-containing biphenyl inhibitors of protein farnesyltransferase. *Bioorg Med Chem Lett 13*, 1367-71.

(123) Roskoski, R., Jr., and Ritchie, P. A. (2001) Time-dependent inhibition of protein farnesyltransferase by a benzodiazepine peptide mimetic. *Biochemistry 40*, 9329-35.

(124) Leonard, D. M., Shuler, K. R., Poulter, C. J., Eaton, S. R., Sawyer, T. K., Hodges, J. C., Su, T. Z., Scholten, J. D., Gowan, R. C., Sebolt-Leopold, J. S., and Doherty, A. M. (1997) Structure-activity relationships of cysteine-lacking pentapeptide derivatives that inhibit ras farnesyltransferase. *J Med Chem 40*, 192-200.

(125) Scholten, J. D., Zimmerman, K. K., Oxender, M. G., Leonard, D., Sebolt-Leopold, J., Gowan, R., and Hupe, D. J. (1997) Synergy between Anions and farnesyldiphosphate Competitive Inhibitors of Farnesyl:protein Transferase. *J. Biol. Chem. 272*, 18077-18081.

(126) Roberts, M. J., Troutman, J. M., Chehade, K. A., Cha, H. C., Kao, J. P., Huang, X., Zhan, C. G., Peterson, Y. K., Subramanian, T., Kamalakkannan, S., Andres, D. A., and Spielmann, H. P. (2006) Hydrophilic Anilinogeranyl Diphosphate Prenyl Analogues Are Ras Function Inhibitors. *Biochemistry 45*, 15862-15872.

(127) Chehade, K. A., Andres, D. A., Morimoto, H., and Spielmann, H. P. (2000) Design and synthesis of a transferable farnesyl pyrophosphate analogue to Ras by protein farnesyltransferase. *J Org Chem 65*, 3027-33.

(128) Gibbs, B. S., Zahn, T. J., Mu, Y., Sebolt-Leopold, J. S., and Gibbs, R. A. (1999) Novel farnesol and geranylgeraniol analogues: A potential new class of anticancer agents directed against protein prenylation. *J Med Chem 42*, 3800-8.

(129) Krzysiak, A. J., Rawat, D. S., Scott, S. A., Pais, J. E., Handley, M., Harrison, M. L., Fierke, C. A., and Gibbs, R. A. (2007) Combinatorial modulation of protein prenylation. *ACS Chem Biol 2*, 385-9.

(130) Reigard, S. A., Zahn, T. J., Haworth, K. B., Hicks, K. A., Fierke, C. A., and Gibbs, R. A. (2005) Interplay of isoprenoid and peptide substrate specificity in protein farnesyltransferase. *Biochemistry 44*, 11214-23.

(131) Rose, M. W., Xu, J., Kale, T. A., O'Doherty, G., Barany, G., and Distefano, M. D. (2005) Enzymatic incorporation of orthogonally reactive prenylazide groups into peptides using geranylazide diphosphate via protein farnesyltransferase: implications for selective protein labeling. *Biopolymers 80*, 164-71.

(132) Rose, M. W., Rose, N. D., Boggs, J., Lenevich, S., Xu, J., Barany, G., and Distefano, M. D. (2005) Evaluation of geranylazide and farnesylazide diphosphate for incorporation of prenylazides into a CAAX box-containing peptide using protein farnesyltransferase. *J Pept Res 65*, 529-37.

(133) Schramm, V. L. (1999) Enzymatic transition-state analysis and transition-state analogs. *Methods Enzymol 308*, 301-55.

(134) Fu, H. W., Beese, L. S., and Casey, P. J. (1998) Kinetic analysis of zinc ligand mutants of mammalian protein farnesyltransferase. *Biochemistry 37*, 4465-72.

(135) Casey, P. J., Thissen, J. A., and Moomaw, J. F. (1991) Enzymatic modification of proteins with a geranylgeranyl isoprenoid. *Proc Natl Acad Sci U S A 88*, 8631-5.

(136) Reiss, Y., Goldstein, J. L., Seabra, M. C., Casey, P. J., and Brown, M. S. (1990) Inhibition of purified p21ras farnesyl:protein transferase by Cys-AAX tetrapeptides. *Cell 62*, 81-8.

(137) Thissen, J. A., and Casey, P. J. (1996) Kinetics of protein farnesyltransferase: sigmoidal vs hyperbolic behavior as a function of assay conditions. *Anal Biochem 243*, 80-5.

(138) Pompliano, D. L., Gomez, R. P., and Anthony, N. J. (1992) Intramolecular Fluoresence Enhancement: A Continuous Assay of Ras Farnesyl:Protein Transferase. *J. Am. Chem. Soc. 114*, 7946-7948.

(139) Cassidy, P. B., Dolence, J. M., and Poulter, C. D. (1995) Continuous fluorescence assay for protein prenyltransferases. *Methods Enzymol 250*, 30-43.

(140) Pompliano, D. L., Gomez, R. P., and Anthony, N. J. (1992) Intramolecular Fluoresence Enhancement: A Continuous Assay of Ras Farnesyl:Protein Transferase. *J. Am. Chem. Soc. 114*, 7945-7946.

(141) Brune, M., Hunter, J. L., Corrie, J. E., and Webb, M. R. (1994) Direct, real-time measurement of rapid inorganic phosphate release using a novel fluorescent probe and its application to actomyosin subfragment 1 ATPase. *Biochemistry 33*, 8262-71.

(142) Brune, M., Hunter, J. L., Howell, S. A., Martin, S. R., Hazlett, T. L., Corrie, J. E., and Webb, M. R. (1998) Mechanism of inorganic phosphate interaction with phosphate binding protein from Escherichia coli. *Biochemistry 37*, 10370-80.

(143) Hirshberg, M., Henrick, K., Haire, L. L., Vasisht, N., Brune, M., Corrie, J. E., and Webb, M. R. (1998) Crystal structure of phosphate binding protein labeled with a coumarin fluorophore, a probe for inorganic phosphate. *Biochemistry 37*, 10381-5.

(144) White, H. D., Belknap, B., and Webb, M. R. (1997) Kinetics of nucleoside triphosphate cleavage and phosphate release steps by associated rabbit skeletal actomyosin, measured using a novel fluorescent probe for phosphate. *Biochemistry 36*, 11828-36.

(145) Kim, D. E., Narayan, M., and Patel, S. S. (2002) T7 DNA helicase: a molecular motor that processively and unidirectionally translocates along single-stranded DNA. *J Mol Biol 321*, 807-19.

(146) Halonen, P., Baykov, A. A., Goldman, A., Lahti, R., and Cooperman, B. S. (2002) Single-turnover kinetics of Saccharomyces cerevisiae inorganic pyrophosphatase. *Biochemistry 41*, 12025-31.

(147) Gill, S. C., and von Hippel, P. H. (1989) Calculation of protein extinction coefficients from amino acid sequence data. *Anal Biochem 182*, 319-26.

(148) Zimmerman, K. K., Scholten, J. D., Huang, C. C., Fierke, C. A., and Hupe, D. J. (1998) High-level expression of rat farnesyl:protein transferase in Escherichia coli as a translationally coupled heterodimer. *Protein Expr Purif 14*, 395-402.

(149) Baykov, A. A., and Shestakov, A. S. (1992) Two pathways of pyrophosphate hydrolysis and synthesis by yeast inorganic pyrophosphatase. *Eur J Biochem 206*, 463-70.

(150) Baykov, A. A., Fabrichniy, I. P., Pohjanjoki, P., Zyryanov, A. B., and Lahti, R. (2000) Fluoride effects along the reaction pathway of pyrophosphatase: evidence for a second enzyme.pyrophosphate intermediate. *Biochemistry 39*, 11939-47.

(151) Hartman, H. L., Pais, J. E., and Fierke, C. A. Interactions between farnesyltransferase and the diphosphate group of farnesyldiphosphate essential for substrate-assisted product dissociation. *manuscript in preparation*.

(152) Chehade, K. A., Kiegiel, K., Isaacs, R. J., Pickett, J. S., Bowers, K. E., Fierke, C. A., Andres, D. A., and Spielmann, H. P. (2002) Photoaffinity analogues of farnesyl pyrophosphate transferable by protein farnesyl transferase. *J Am Chem Soc 124*, 8206-19.

(153) Subramanian, T., Wang, Z., Troutman, J. M., Andres, D. A., and Spielmann, H. P. (2005) Directed library of anilinogeranyl analogues of farnesyl diphosphate via mixed solid- and solution-phase synthesis. *Org Lett 7*, 2109-12.

(154) Johnson, C. M., Roderick, S. L., and Cook, P. F. (2005) The serine acetyltransferase reaction: acetyl transfer from an acylpantothenyl donor to an alcohol. *Arch Biochem Biophys 433*, 85-95.

(155) Fierke, C. A., Johnson, K. A., and Benkovic, S. J. (1987) Construction and evaluation of the kinetic scheme associated with dihydrofolate reductase from Escherichia coli. *Biochemistry 26*, 4085-92.

(156) Jeltsch, A. (2002) Beyond Watson and Crick: DNA methylation and molecular enzymology of DNA methyltransferases. *Chembiochem 3*, 274-93.

(157) Sawaya, M. R., and Kraut, J. (1997) Loop and subdomain movements in the mechanism of Escherichia coli dihydrofolate reductase: crystallographic evidence. *Biochemistry 36*, 586-603.

(158) Ohkanda, J., Knowles, D. B., Blaskovich, M. A., Sebti, S. M., and Hamilton, A. D. (2002) Inhibitors of protein farnesyltransferase as novel anticancer agents. *Curr Top Med Chem 2*, 303-23.

(159) Cox, A. D., and Der, C. J. (2002) Farnesyltransferase inhibitors: promises and realities. *Curr Opin Pharmacol 2*, 388-93.

(160) Haluska, P., Dy, G. K., and Adjei, A. A. (2002) Farnesyl transferase inhibitors as anticancer agents. *Eur J Cancer 38*, 1685-700.

(161) McNamara, D. J., Dobrusin, E., Leonard, D. M., Shuler, K. R., Kaltenbronn, J. S., Quin, J., 3rd, Bur, S., Thomas, C. E., Doherty, A. M., Scholten, J. D., Zimmerman, K. K., Gibbs, B. S., Gowan, R. C., Latash, M. P., Leopold, W. R., Przybranowski, S. A., and Sebolt-Leopold, J. S. (1997) C-terminal modifications of histidyl-N-benzylglycinamides to give improved inhibition of Ras farnesyltransferase, cellular activity, and anticancer activity in mice. *J Med Chem 40*, 3319-22.

(162) Long, S., Hancock, P., Kral, A., Hellinga, H., and Beese, L. (2001) The crystal structure of human protein farnesyltransferase reveals the basis for inhibition by CaaX tetrapeptides and their mimetics. *Proc Natl Acad Sci U S A 98*, 12948-12953.

(163) Huang, C. C., Casey, P. J., and Fierke, C. A. (1997) Evidence for a catalytic role of zinc in protein farnesyltransferase. Spectroscopy of Co2+-farnesyltransferase indicates metal coordination of the substrate thiolate. *J Biol Chem 272*, 20-3.

(164) Scholten, J., Zimmerman, K., Oxender, M., Sebolt-Leopold, J., Gowan, R., Leonard, D., and Hupe, D. (1996) Inhibitors of farnesyl:protein transferase--a possible cancer chemotherapeutic. *Bioorg Med Chem 4*, 1537-1543.

(165) Scholten, J., Zimmerman, K., Oxender, M., Leonard, D., Sebolt-Leopold, J., Gowan, R., and Hupe, D. (1997) Synergy between anions and farnesyldiphosphate competitive inhibitors of farnesyl:protein transferase. *J Biol Chem 272*, 18077-18081.

(166) Stewart, J., and Young, J. (1984) *Solid phase peptide synthesis*, 2nd ed., Pierce Chemical Co, Rockford, Ill.

(167) Bodanszky, M. (1984) *The practice of peptide synthesis*, Vol. 21, Springer-Verlag, Berlin, New York.

(168) McNamara, D., Dobrusin, E., Leonard, D., Shuler, K., Kaltenbronn, J., Quin, J. r., Bur, S., Thomas, C., Doherty, A., Scholten, J., Zimmerman, K., Gibbs, B., Gowan, R., Latash, M., Leopold, W., Przybranowski, S., and Sebolt-Leopold, J. (1997) C-terminal modifications of histidyl-N-benzylglycinamides to give improved inhibition of Ras farnesyltransferase, cellular activity, and anticancer activity in mice. *J Med Chem 40*, 3319-3322.

(169) Quinn, J., Kaltenbronn, J., Leonard, D., Shuler, K., Sebolt-Leopold, J., Gowan, R., Scholten, J., Zimmerman, K., and Doherty, A. (1997) in *213th ACS National Meeting* pp MEDI-197, American Chemical Society, San Francisco, CA.

(170) Zimmerman, K., Scholten, J., Huang, C., Fierke, C., and Hupe, D. (1998) High-level expression of rat farnesyl:protein transferase in Escherichia coli as a translationally coupled heterodimer. *Protein Expr Purif 14*, 395-402.

(171) Strickland, C., Windsor, W., Syto, R., Wang, L., Bond, R., Wu, Z., Schwartz, J., Le, H., Beese, L., and Weber, P. (1998) Crystal structure of farnesyl protein transferase complexed with a CaaX peptide and farnesyl diphosphate analogue. *Biochemistry 37*, 16601-16611.

(172) Vetting, M. W., LP, S. d. C., Yu, M., Hegde, S. S., Magnet, S., Roderick, S. L., and Blanchard, J. S. (2005) Structure and functions of the GNAT superfamily of acetyltransferases. *Arch Biochem Biophys 433*, 212-26.

(173) Schramm, V. L. (1998) Enzymatic transition states and transition state analog design. *Annu Rev Biochem 67*, 693-720.

(174) Tao, W., Grubmeyer, C., and Blanchard, J. S. (1996) Transition state structure of Salmonella typhimurium orotate phosphoribosyltransferase. *Biochemistry 35*, 14-21.

(175) Berti, P. J. (1999) Determining transition states from kinetic isotope effects. *Methods Enzymol 308*, 355-97.

(176) Weller, V. A., and Distefano, M. D. (1998) Measurement of the a-secondary kinetic isotope effect for a prenyltransferase by MALDI mass spectrometry. *J. Am. Chem. Soc. 120*, 7975-7976.

(177) Scheuring, J., Berti, P. J., and Schramm, V. L. (1998) Transition-state structure for the ADP-ribosylation of recombinant Gialpha1 subunits by pertussis toxin. *Biochemistry 37*, 2748-58.

(178) Christensen, D. J., and Poulter, C. D. (1994) Enzymatic synthesis of isotopically labeled isoprenoid diphosphates. *Bioorg Med Chem 2*, 631-7.

(179) Cheng, M. C., and Marsh, E. N. (2004) Pre-steady-state measurement of intrinsic secondary tritium isotope effects associated with the homolysis of adenosylcobalamin and the formation of 5'-deoxyadensosine in glutamate mutase. *Biochemistry 43*, 2155-8.

(180) Kline, P. C., and Schramm, V. L. (1995) Pre-steady-state transition-state analysis of the hydrolytic reaction catalyzed by purine nucleoside phosphorylase. *Biochemistry 34*, 1153-62.

(181) Hightower, K. E., Casey, P. J., and Fierke, C. A. (2001) Farnesylation of nonpeptidic thiol compounds by protein farnesyltransferase. *Biochemistry 40*, 1002-10.

(182) Zhang, D., and Poulter, C. D. (1993) Analysis and purification of phosphorylated isoprenoids by reversed-phase HPLC. *Anal Biochem 213*, 356-61.

(183) Ohnuma, S., Hirooka, K., Tsuruoka, N., Yano, M., Ohto, C., Nakane, H., and Nishino, T. (1998) A pathway where polyprenyl diphosphate elongates in prenyltransferase. Insight into a common mechanism of chain length determination of prenyltransferases. *J Biol Chem 273*, 26705-13.

(184) Bigeleisen, J., and Wolfsberg, M. (1958) Theoretical and Experimental Aspects of Isotope Effects in Chemical Kinetics. *Advances in Chemical Physics 1*, 15-76.

(185) Parikh, S. L., and Schramm, V. L. (2004) Transition state structure for ADP-ribosylation of eukaryotic elongation factor 2 catalyzed by diphtheria toxin. *Biochemistry 43*, 1204-12.

(186) Cleland, W. W. (1980) Measurement of isotope effects by the equilibrium perturbation technique. *Methods Enzymol 64*, 104-25.

(187) Goitein, R. K., Chelsky, D., and Parsons, S. M. (1978) Primary 14C and alpha secondary 3H substrate kinetic isotope effects for some phosphoribosyltransferases. *J Biol Chem 253*, 2963-71.

(188) Lenevich, S., Xu, J., Hosokawa, A., Cramer, C. J., and Distefano, M. D. (2007) Transition state analysis of model and enzymatic prenylation reactions. *J Am Chem Soc 129*, 5796-7.

(189) Rozema, D. B., and Poulter, C. D. (1999) Yeast protein farnesyltransferase. pKas of peptide substrates bound as zinc thiolates. *Biochemistry 38*, 13138-46.